Speed and Temperature Effects in the Energy Absorption of Axially Crushed Composite Tubes

Quentin Paul Vianney FONTANA

Emmanuel College

University of Cambridge

January 1990

This thesis is submitted in accordance with the regulations of the Faculty of Physics and Chemistry of the University of Cambridge for the degree of Doctor of Philosophy (Ph.D.).

This thesis records the findings of work carried out by the author in the period from 1st October 1986 to 30th September 1989 in the Department of Materials Science and Metallurgy of the University of Cambridge. The work was carried out solely by the author except where credit has been given to others in the text, acknowledgements and references. This thesis does not exceed sixty thousand words.

e-copy note

The original thesis was written in 1989/90 on a Macintosh Plus with a processor at 8 Mhz and 2.5 Mb of RAM; it was written using Micro$oft Word Version 4 for the Macintosh and all of the figures, with the exception of the photographs, were included. Significant changes in computer technology have occurred in the years between the writing and the generation of this electronic copy in 2008, there have been some problems with backward compatibility of the software used, in particular with respect to the graphics handling capability, so there have been some significant problems with the use of old file formats; consequently not all of the figures are as clear as they were when the original was written.

Abstract

Tubes of glass reinforced thermosetting resins have been tested in axial compression between steel platens with one end chamfered to prevent critically high loads causing catastrophic centre failure. By testing in such a manner these tubes crush in a progressive and controlled manner, and are capable of exhibiting high levels of energy absorption, particularly when related to the material mass involved. Polymers are known to display viscoelastic behaviour and polymer composites are similarly sensitive to test speed and temperature. Energy absorption in tube crushing has been shown to be speed and temperature sensitive and the purpose of this project has been to understand the variability of the energy absorption and the associated mechanisms. The main aim has been to show how the two variables interrelate.

The materials used have been produced by hot rolling of pre-preg cloth or by resinjection into closed moulds. Reinforcement has consisted of woven glass cloth or random glass mat; matrix materials have been epoxy and polyester resins.

Trends to higher values of specific energy absorption with increasing speed have been observed for epoxy matrix tubes, while polyester matrix tubes have shown less certain trends and give lower values of specific energy absorption at high speeds. All the tubes have shown a rapid drop in specific energy absorption with increasing temperature above normal room temperature, with changes in crush mode being very apparent. At temperatures in excess of about 100 °C the tubes have failed by centre buckling, the transition temperature from normal crushing to buckling being sensitive to the crush speed.

The interrelation between speed and temperature effects has been examined. Three factors that prevent simple interrelation have been identified; these are inertial effects

of crush debris, residual stresses in the hoop direction of the tube and frictional heating in the crush zone. Speed sensitivity of the energy absorption has been determined over a range of temperatures and various features of these responses related to the responses of the material properties.

Frictional temperature rises have been modelled mathematically and the predictions have been shown to be reasonably consistent with experimental measurements. These temperature rises have been shown to be important in determining the speed sensitive behaviour of the energy absorption levels, particularly for polyester resin matrix tubes tested at high speeds.

to my parents

Contents

Symbols

0°: axial fibres

90°: hoop fibres

a: acceleration

c: constant, load fraction borne by the fronds

d: constant

dy/dt: testing speed

f: tongue deflection, flexural

k: Boltzmann's constant, fraction of load by non frictional mechanisms, thermal conductivity, reaction rate constant

l: tube length, length

l_c: length of crush

m: slope

m/l: mass per unit length

n: element number, number of elements

r: radius

t: wall thickness, glass cloth thickness, thickness

tan(δ): loss tangent

u: initial velocity

v: speed, velocity

v_f: fibre volume fraction

w: wedge width

x: distance

x_c: length of material involved in a crush

A: constant

C_p: specific heat capacity

CSM: chopped-strand-mat

D: tube diameter

DMA: dynamic mechanical analyser

DSC: differential scanning calorimeter

E: Young's modulus, epoxy resin, energy

E_s: specific energy absorption

F: crush load, force

FEM: finite element modelling

Fo: Fourier number

FWP: frond:wedge:platen

G_I: strain energy release rate

Gl: glass fibres

Gr: graphite fibers (carbon fibres)

ILSS: interlaminar shear strength

K: Kevlar fibres

K_I: stress intensity factor

L: longitudinal

M: mass

N: layer number, number of layers

OD: outer diameter

P: local crush load, polyester resin

PET: polyethylene terephthalate

PTFE: polytetrafluoroethylene (Teflon)

R: random glass mat, force, residual, universal gas constant, measure of line fit

R_c: crush ratio

RJ: resinjection

S: constant

SHPB: split Hopkinson pressure bar

SMC: sheet moulding compound

T: transverse, temperature

T_g: glass transition temperature

V: volume

W: tube width

W: woven glass cloth, weave repeat distance

WLF: Williams-Landel-Ferry

XMC: unspecified moulding compound

α: thermal diffusivity

α,β,γ: relaxation peaks

δ: crack opening displacement

δx: movement of the crush platen

ε: strain

$\dot{\varepsilon}$: strain rate

ϕ: specific density, wedge semi angle

γ: shear strain

λ: speed sensitivity

μ: coefficient of friction

ν: Poisson's ratio

θ: winding angle, chamfer angle, wedge semi angle

ρ: density

σ: tensile stress

τ: shear stress, time

Δ: change in property

ΔF: serration of crush trace

ΔH: activation energy

Δt: linear dimension

Δτ: time interval

Σ: specific crush stress

Superscript

': plane strain, polished platen

Subscripts

1,2: as appropriate

2: internal

a: arrest, after, arc

b: bend

bb: bounce back

c: crush, critical, composite, curvature

d: debris

e: external, element

f: frictional, fibre

fp: frond-platen

h: hoop, horizontal

he: hoop external

hi: hoop internal

i: internal, impact, initiation, initial, interface

in: inertial

l: longitudinal, layer

m: mean, non frictional, matrix

n: element number, layer number, number of layers

o: outer

p: time

t: tensile, total, transition

v: vertical

W,w: wedge

wf: wedge-frond

y: yield

EX: external

IN: internal

Brackets

[ ]: reference numbers, fibre lay-up

{ }: figure numbers

( ): all other uses of brackets

Acknowledgements

There are many people that I would like to thank for their help throughout this project, in particular:

Professor D. Hull, for general supervision and advice,

Dr. J.C. Copolla, for general help and encouragement,

Messrs: W.R. Broughton, A.D. Lowe, C.A. Stanford-Beale, D.A. Williams and the misses: T.M. Jennings and X-N Huang for help, encouragement and tolerating my sense of humour,

Mr. D.G. Pafitis for help and toleration and for proof-reading much of this thesis,

Drs. A.H. Fairfull and J.N. Price for their help during the first year of the project,

Dr. M. Kumosa for seemingly unlimited feedback,

Mr. B. Barber for photographic help,

Mr. R. Fella for help with microscopy and relevant preparation,

Mr. M.J. Free for help with material and test-piece preparation,

Mr. T.G. Whitworth for help with testing machines,

the Science and Engineering Research Council for financial support in the form of a Quota award,

Mr. G.L. Skidmore for computing help and advice and constant support,

Miss A. Salway for helping me through a very bad time,

Messrs: P.A. Jackson and G.D. Hine for frequent discussions and encouragement,

Mr. D.G. Hay for tolerating my presence in the same house for three years,

Dr. B.R. Martin of Emmanuel College for allowing a college transfer,

Messrs. E.M. Rowbotham of Ford U.K. and J. Baldwin of the S.E.R.C. for continuing interest throughout the project,

Mr. R. Murchie of Ford U.K. for the introduction of new concepts,

Scott Bader, Tufnol, Fibreglas, Ciba-Geigy, Moore Plastics and Ford Motor Company for suppling test materials,

Apple computers for inventing the Macintosh,

Beryl and Doris for being wonderful,

Ms. B. Rolfe for access to scanning hardware,

Mrs. M. Tissot for printing help and being there to talk to,

all the other members of the Department of Materials Science and Metallurgy of the University of Cambridge and those of Emmanuel College, in particular the EBC,

the students and Union of the Imperial College of Science and Technology, without whom I would probably not have undertaken this research,

and last but by no means least, my family for constant help, support and encouragement throughout my three years in Cambridge and in particular during the time that I have been writing in Portsmouth.

1 Introduction

1.1 Impact Energy Absorption

There are many circumstances in which kinetic energy must be absorbed and many ways of achieving this. These ways can be divided into two main categories, repeated use and once only [1-3][1]. Examples of the former category include: the hydraulic shock absorbers in a car's suspension system, buffers on railway rolling stock and the arrester landing device on aircraft carrier flight decks. Those in the latter category exist as safety devices in case of an unforeseen impact and may be found, for instance, in the front and rear structures of cars and in helicopter sub-floor structures.

Repeated use energy absorbers generally rely on hydraulic damping by forcing a viscous liquid through restricting holes; thus converting the kinetic energy into heat which can be dissipated readily. Pneumatic bag shock absorbers also fall into this category. Once-only energy absorbers rely on structural collapse of a component to absorb energy.

A good example of once only energy absorption is in the front and rear structures of cars. These are designed to collapse under impact, such that the kinetic energy of the vehicle is dissipated, and the passenger compartment is brought to rest without the occupants being subjected to high decelerations which can cause serious internal injury, particularly brain damage {figure 1.1}. Current legislation requires that vehicles should be designed such that, in the event of an impact of the vehicle at speeds up to 30 mph with a solid, immovable object, the occupants of the passenger compartment must survive uninjured. The specific requirement is that the upper thorax of a belted passenger must not experience a net deceleration greater than 600 m s^{-2} or about 60g [4]. Other examples of crashworthiness legislation include those from FISA, motor racing's governing body, where the front end of a car must be able to survive an impact with a 780 kg mass moving at 10 m s^{-1} [5], and US helicopter requirements of safely surviving a descent, under no power, of 15 m s^{-1} [6].

[1]References are listed at the end of chapter 10. In the text they are denoted by numbers in square brackets.

From the laws of motion, to provide a constant level of deceleration of the passenger compartment, there must be a constant level of resisting force exerted on the compartment, thus the ideal energy absorber would collapse with a square wave force-displacement characteristic {figure 1.2}.

1.2 Current Methods

The current method of absorbing impact energy in cars is to design the front and rear metallic structures such that they collapse by progressive folding [1,7]. This form of collapse provides a good level of energy absorption but the form of the force-displacement response is not a close approximation to the ideal square wave form, with large peaks and troughs corresponding to the various stages of the formation and propagation of the folds {figures 1.3 and 1.4}.

1.3 Composite Materials

For some time there has been considerable interest in using fibre reinforced composite materials in many applications where material mass is an important consideration [7,8]. Automotive and aerospace structures are examples of such applications. Composite materials offer several advantages over metals for the automobile designer along with weight reduction, particularly corrosion resistance, near net shape formability of components and part integration, where several metal components that were previously bolted together can be replaced by a single component. These advantages have meant that the amount of composites that have been used in transport applications has greatly increased in recent years, although apparently some car designers have not yet heard of composite materials despite growing public awareness of their existence and properties [9,10]. One estimate of European consumption of composites in land transport applications for 1985 was 152 000 tonnes [11] and predictions for 1995 give a four fold increase in the use of plastics in automotive applications, a large proportion of which will be in the form of fibre reinforced plastics [12]. Another figure for 1985 gave transport as accounting for 17.8% of the U.K. market for glass reinforced polyester resins [13]. There is also considerable interest in using composites in railway rolling stock, particularly in the high speed *Inter-City* trains, which currently incorporate polymer composites that account for about 8% of vehicle weight [14].

While there is much work being carried out looking at directly replacing metal components with composites, potential advances are possible by completely redesigning the components to take advantage of the special properties of composite materials. An example of both approaches is in automotive suspension systems. While direct replacement of metal leaf springs by composites has been achieved for various vehicles [15,16], it has been possible to design systems such that the elastic response of the springs is different in different planes, so that the response of the spring can be tailored to that desired by the system [15].

While composites have many advantages for the designer, they also have several disadvantages such that their universal employment has not been immediate. Current disadvantages of composite materials include: difficulty of incorporation into mass production processes, inferior fire resistance of some composites when compared to metals and difficulties of disposal of components at the end of service life. One of the main current problems is the production time, as current materials and methods call for a process time of about three to four minutes which is at the upper limit of viability for automotive production [8]. Resin chemistry and production methods are being improved to overcome the problems.

The requirement of being able to absorb energy has led to work being carried out in this area with a view to using composites. Early work showed that the amount of energy absorbed per unit mass of material involved for crushed composite tubes, could greatly exceed that for steel components [1,2,8,17]. Composites also have the advantage over metals for energy absorbers that their force-displacement response during crushing gives a better approximation to the ideal square wave of figure 1.2 {figure 1.5}. An example of the ability of composites to provide life saving protection from the effects of a high speed impact, happened in the 1989 San Marino Grand Prix; Gerhard Berger, driving for Ferrari, hit a wall at about 240 kilometres per hour but survived, partly because of the use of composites in the car construction [5]; similarly, Nelson Piquet, then with Williams, survived a crash at the same track in 1987.

1.4 Calculation of Specific Energy Absorption

The specific energy absorption of a component can be defined as the amount of energy absorbed per unit mass of the absorber involved [18]. For buckling metallic

components, the amount of material involved is greater than that contained in the distance over which the energy is absorbed as the metal buckles ahead of the compression front, so the concept of a crush ratio, R_c, must be introduced, being the amount of material involved in absorbing the energy divided by the amount of material contained in the energy absorption distance for an uncrushed component {figure 1.3}. The specific energy absorption, E_s, is then given by:

$$E_s = \frac{F}{R_c(m/l)} \tag{1.1}$$

where F is the mean crush load and m/l the mass per unit length of the energy absorber. For a component of constant mass per unit length, for instance a tube of constant cross-sectional area, the crush ratio can be given by the relative lengths involved. The crush ratio will then be given by:

$$R_c = \frac{x_c}{l_c} \tag{1.2}$$

where x_c is the length of material involved and l_c is the crush distance, as illustrated in figure 1.3. For metallic components the crush ratio is always greater than unity, but for composites it is generally sufficiently close to unity to be disregarded. In most of the composite work, trends in the crush load may be taken to be trends in specific energy absorption, unless the mass per unit length is changing as a function of the variable under consideration, for instance the tube wall thickness or the fibre volume fraction.

One point that should be made concerns compaction of debris within a closed ended tube. If half of the crushed material moves to the inside of the tube and stays as a ring of internal debris, a situation that has been observed frequently, then once half of the tube has crushed, the internal debris will start to compact against the closed end and the crush load will rise. If compaction is to be avoided then the maximum tube length usable will be half of the original tube length, giving a crush ratio of 2 and halving the real value of specific energy absorption. However, most of the work published to date

has ignored this effect and has concentrated on the energy absorption in the crush zone alone. The problem may be overcome using an open ended tube but this could give mounting problems for an in-service component. However, the increase in crush load from internal debris compaction may be advantageous and may be utilised by suitable design; generally, this problem has been disregarded.

Most of this work has involved the utilisation of specific energy absorption in this way, although many of the results obtained have been quoted in terms of the specific crush stress to eliminate the use of the crush ratio. The specific crush stress and the appropriate units are discussed in section 4.1.

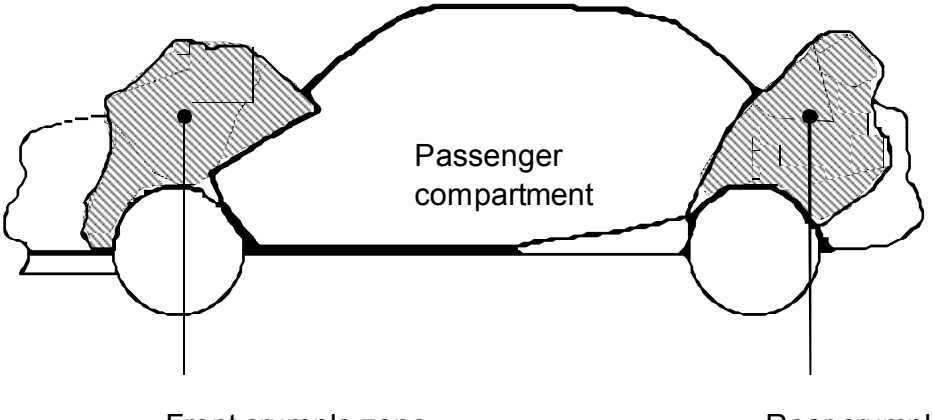

Figure 1.1 Side elevation of a car showing the front and rear crumple zones [1-3].

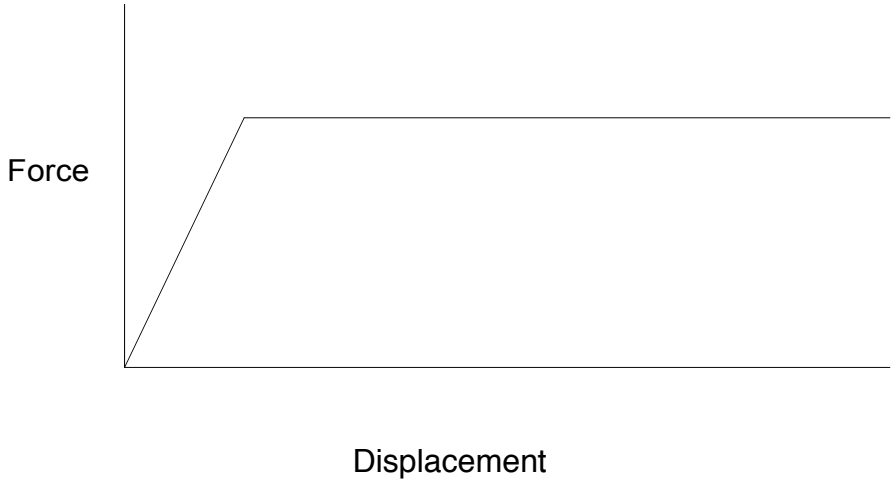

Figure 1.2 Ideal force-displacement characteristic for energy absorption [2].

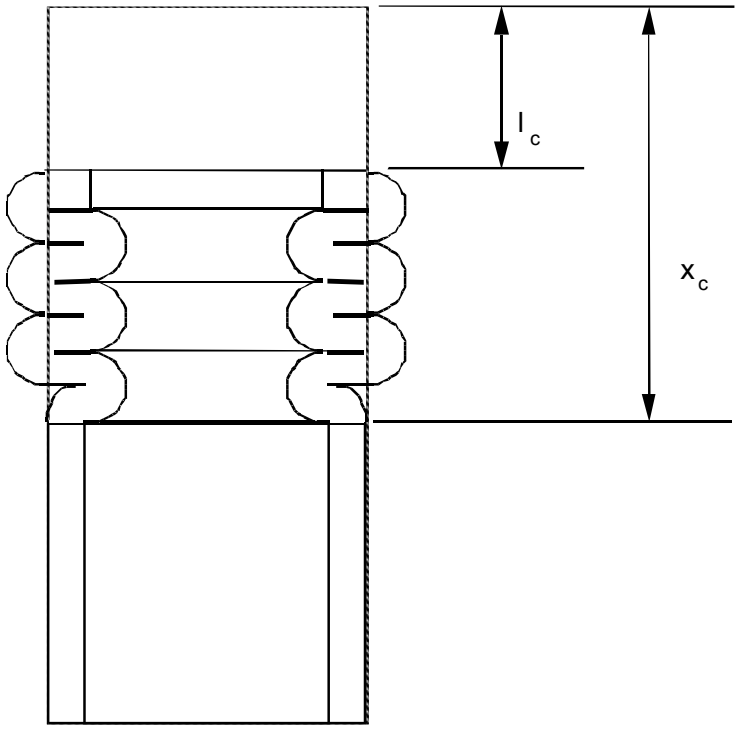

Figure 1.3 Metal tube displaying a buckling collapse mode [1].

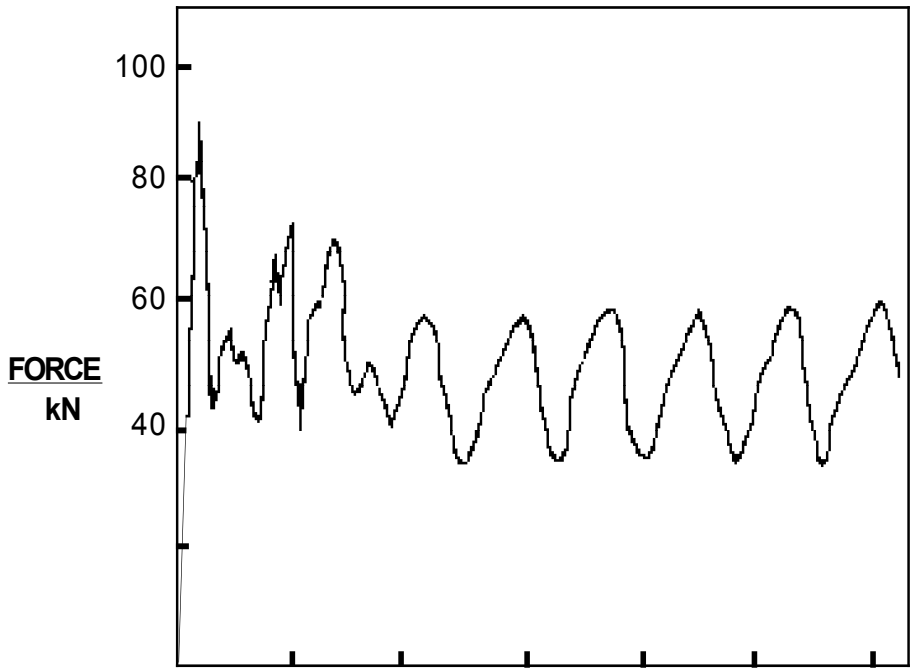

Figure 1.4 Typical force-displacement trace from a buckling metallic component [1].

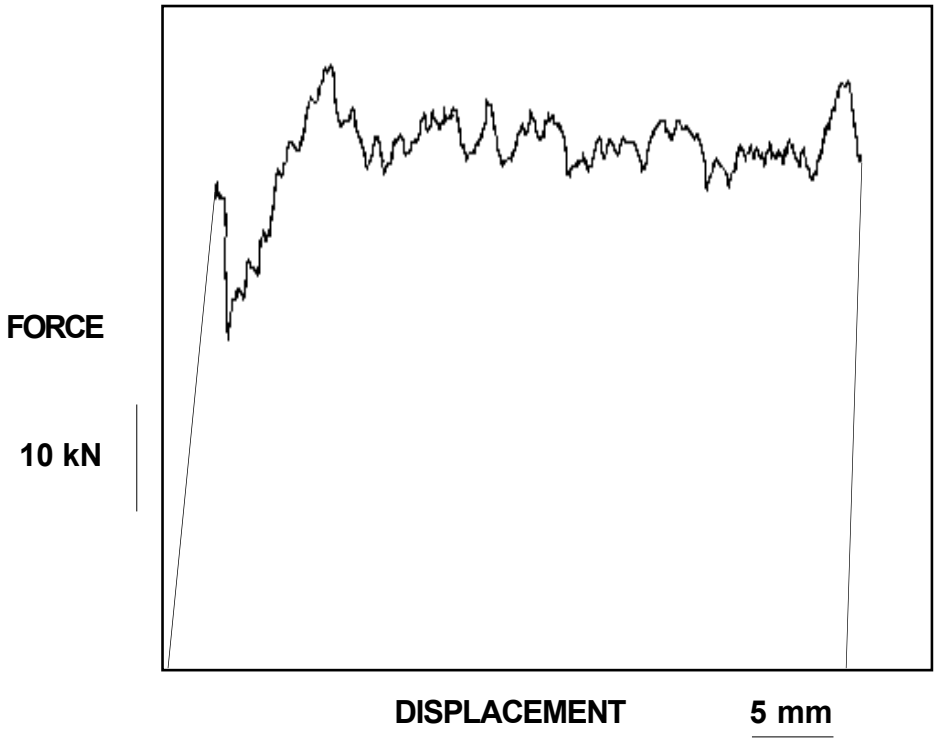

Figure 1.5 Typical force-displacement response for a composite tube subjected to axial crushing.

2 Literature Review

This review has been divided into two main sections, energy absorption and mechanical properties of the materials. There is some overlap, particularly in section 2.1.3.2.2, but this overlap is only where material property work has been carried out in conjunction with the energy absorption work as a direct comparison.

2.1 Energy Absorption

The energy absorption section of the review has been divided into two main sections, the first dealing with general trends in energy absorption levels and the second with the mechanisms of energy absorption.

The calculation of specific energy absorption was discussed in section 1.4; however, the various workers in this field have used different ways of quoting this value, hence the presentation of the results in this review section can appear inconsistent, particularly when considering the figures. There have been three main groups working in this field: Liverpool and Cambridge Universities, under the guidance of Professor D. Hull; Ford Motor Company, Dearborn, Michigan, led by Dr. P.H. Thornton and the National Aeronautics and Space Administration of the U.S.A, led by Mr G.L. Farley. The Liverpool and Cambridge results have been presented as Specific Energy Absorption using the notation E_s and the units kJ kg^{-1}, the Ford results have been presented as simply Specific Energy, using the same units while the NASA results have been presented as the Specific Sustained Crushing Stress with the units of N m g^{-1}, which is the same as kJ kg^{-1}. For the purposes of this review there is no difference between the different presentations of the results.

2.1.1 Centre Failure

Some early work on composite tubes in compression concentrated on avoiding end effects in filament wound glass-polyester tubes by reinforcing the ends of the tubes with extra winds of glass filaments [19,20]. These tubes failed catastrophically by centre failure and interpenetration with a high initial peak load followed by a low post-failure load and, consequently, low energy absorption {figure 2.1}. Work on square-ended pultrusions with no end reinforcement showed similar behaviour.

Work on glass cloth-epoxy tubes showed that tubes without end reinforcement could give a different mode of failure [20]. Rather than centre failure, end failure could occur giving a much higher post failure load carrying capacity, thus a higher energy absorption capability {figure 1.5}. This mode of collapse was not obtained reliably and centre failure could occur unpredictably.

2.1.2 Crushing with a Trigger

At an early stage it was found that it was possible to avoid the high peak loads which led to catastrophic centre failure, by providing a stress concentrator at one end of the tube. Thornton [17] showed that a bevel on one end of the tube provided such a stress concentration and found that the tubes failed by progressive crushing, giving a high level of energy absorption {figure 2.2}. With this type of progressive failure, a good approximation to the ideal square wave for the force-displacement trace could be achieved {figures 1.2 and 1.5}. Tubes made of fibre reinforced composite materials which collapsed in this manner were shown to be capable of absorbing more energy per unit mass than comparable metallic tubes which collapsed by buckling (typically 60 kJ kg^{-1} compared to 25 kJ kg^{-1} for metallic tubes) [8].

2.1.3 Effect of Specimen Variables

Six main specimen variables have been considered, these can be divided into material variables and structural variables. The former category includes the fibre and matrix type, the fibre volume fraction and the fibre arrangement. The latter includes the specimen geometry and size.

2.1.3.1 Fibre Type

Three main types of fibre reinforcement have been studied, these were glass, carbon and Kevlar. Most of the work concentrated on glass fibres in various matrix materials. Carbon and Kevlar fibres have only been studied in epoxy resin matrices. Some other fibres have been studied including nylon, Dyneema and terylene, but little information is available for these tubes [20-23]. Some work has been carried out on hybrid fibre composites but they have not shown any improvement over tubes manufactured using only one type of fibre [22,24,25].

Early work on different fibres was carried out by Thornton [17] and showed that both glass and carbon fibre reinforced tubes when progressively crushed could give a close approximation to the ideal square wave form for energy absorption by progressive crushing {figures 1.1 and 1.5}. Kevlar fibre reinforced tubes were also studied in this investigation and were found to fail by buckling, resulting in an unfavourable force-displacement characteristic {figure 2.3}. This work showed that carbon fibre reinforced epoxy tubes gave the best values for specific energy absorption. Further work by Thornton and Edwards [24] confirmed this observation.

A comparison of Kevlar, carbon and E glass fibres was carried out at the University of Liverpool [25]. Kevlar-epoxy tubes were much less effective in absorbing energy than carbon-epoxy or E-glass-epoxy tubes with similar lay-up, absorbing only 40% of the

energy per unit mass. Differences in behaviour observed between this work and that by Thornton [17] were probably because of differences in the fibre lay-up.

Similar work was performed by Farley [26] who also concluded that the carbon-epoxy system was the most promising with respect to specific energy absorption. This work showed little difference between the energy absorption capability of glass and Kevlar fibre reinforced tubes. This work also showed that the sensitivity of the energy absorption to the fibre arrangement was dependent on the fibre type (see section 2.1.3.3.1, figure 2.11).

A systematic investigation into the effect of different fibre properties was carried out by Farley [27]. This work was performed by testing tubes manufactured using two different types of carbon fibre with different strains to failure, in common epoxy resin matrices. The tubes incorporating the higher strain to failure fibres gave higher values of energy absorption, although this finding appeared sensitive to the fibre arrangement and matrix material {figure 2.4}. A combination of a high strain to failure fibre, combined with a low strain to failure matrix resulted in a low value of energy absorption because of a change in the failure mode.

The effect of the fibre stiffness was studied by Farley [28] for carbon-epoxy tubes. It was found that the energy absorption decreased rapidly with increasing fibre Young's modulus between 200 GPa and about 350 GPa. Above this value of fibre Young's modulus, the energy absorption appeared largely insensitive to the fibre stiffness, although the actual behaviour was dependent on the fibre arrangement {figure 2.5}. The fibres used in this study had very different strains to failure, so an interpretation of the effect of fibre stiffness alone was not valid. A conclusion was reached that

energy absorption was less sensitive to the fibre stiffness than to the fibre strain to failure.

A series of tests on carbon, Kevlar and glass fibres in an epoxy resin matrix was performed by Schmueser and Wickliffe [29]. It was found that the energy absorption of a carbon-epoxy tube was 50% higher than that of a similar Kevlar-epoxy tube while that for a glass-epoxy tube was about 30% lower than for the Kevlar-epoxy tubes. Although not clearly stated, this work appears to have been performed without any trigger on the tubes and failure modes were unclear, hence, these results could be of little consequence for understanding energy absorption behaviour. This lack of a trigger would account for the difference in these observations from those of other workers.

A comparison of two different chopped-strand-mats (CSMs) in the same polyester resin was carried out at the University of Liverpool [30]. The two CSMs were nominally very similar but tubes manufactured using Pilkingtons PB6 absorbed about 20% more energy than tubes manufactured using the same manufacturer's PB8. The differences between the two CSMs were not recorded but it was concluded that the difference in energy absorption was due to differences in the glass size and binder.

Work on different diameter glass fibres was carried out by Thornton [31]. This work was performed using glass-polyester pultrusions with either T-filament rovings with a nominal fibre diameter of 24 μm, or K filament rovings with a nominal fibre diameter of 12 μm. The tubes with the K filament rovings gave consistently lower values of specific energy absorption than those made with T filament rovings. The K filament tubes had a lower fibre volume fraction than those with the T filaments, so that any

effect of fibre diameter might have been masked by a fibre volume fraction effect. However, the effect of fibre volume fraction is, as yet uncertain (see section 2.1.3.4).

The effect of fibre diameter on the crush stress and hence, the energy absorption, of glass:vinylester rods was examined by Tao, Robertson and Thornton [32]. The fibre diameters examined were 13 μm, 17 μm and 23 μm. It was found that the crush stress of the 13 μm fibre diameter rods was about 10% less than for the rods containing the thicker fibres. There was little difference in behaviour between the 17 and 23 μm fibre diameter rods.

The behaviour of tubes reinforced with Dyneema fibres (high density polyethylene fibres with a very high degree of crystal alignment) was studied by van Dingenen [23]. These fibres were incorporated into an epoxy resin matrix but the fibre alignment was not stated. Collapse occurred in a buckling mode and the quoted value of specific energy absorption was comparable to those obtained from similar glass-epoxy tubes. These tubes do not appear to have been triggered for progressive crushing.

2.1.3.1.1 Conclusion of Fibre Type

For the three main fibre types studied, there has been shown to be a progression in specific energy absorption of carbon > glass > Kevlar. Increases in fibre strain to failure and modulus result in increases in specific energy absorption. Larger diameter fibres appear to give better performance than lower diameter fibres. Hybrid fibre tubes have not been shown to give any significant improvement over single fibre type tubes.

2.1.3.2 Matrix Properties

The effect of the matrix properties has been divided into a comparison of different types of resin, for instance epoxies and polyesters, and comparison of the energy

absorption behaviour with matrices that were of similar type but differed in their mechanical properties due to additives.

2.1.3.2.1 Comparison of Different Resins

A comparison was made at the University of Liverpool of tubes made from glass cloth:resin pre-pregs using different types of resin [25]. This work allowed a direct comparison of the behaviour of tubes using a polyester resin matrix, to that of tubes using an epoxy resin matrix with similar reinforcement. An increase in specific energy absorption of about 20% was obtained by the change from polyester to epoxy resin. It was concluded that the resin properties were important in determining the energy absorption capability of the material. The observations were later challenged by work on filament wound tubes with a 0-90° configuration where Scott Bader Crystic 272 polyester tubes were superior to tubes manufactured using Ciba-Geigy MY750/HY917 epoxy resin [33]. This work showed that a comparison of the relative performances of matrix materials must consider the test speed, as the trends in specific energy absorption of tubes with different matrix materials with respect to speed were opposite, since glass-epoxy tubes gave an increase in specific energy absorption with increasing speed while glass-polyester tubes showed a decrease (see sections 2.1.4.1.1). Addition of 50% of CY208, a flexibilising epoxy resin, to the MY750 resulted in the epoxy matrix tubes equalling the performance of the polyester matrix tubes. Similar tubes manufactured using a phenolic resin matrix material gave specific energy absorption values of only about 55% of those obtained for the epoxy and polyester resin matrices. This reduction could be related to the relative brittleness of phenolic resins compared to epoxies and polyesters [7].

Further work [33] compared the behaviour of filament wound tubes made variously with a polyester, an epoxy and a phenolic resin. The low speed properties of the

polyester and epoxy tubes were comparable while at high speeds the epoxy matrix tubes were consistently superior to the polyester matrix tubes. Under all conditions, the phenolic tubes were inferior to both the polyester and the epoxy tubes. The addition of a flexibiliser to the epoxy resin resulted in an increase in specific energy absorption of about 20%.

Work on acrylic resin matrix tubes at the University of Cambridge showed their performance to be comparable to polyesters [35].

The effect of the matrix tensile failure strain in carbon-epoxy tubes was investigated by Farley [27]. These tubes were tested with various fibre orientations and in all cases the tubes with the higher matrix failure strain absorbed more energy than those with the lower matrix failure strain. The actual increase was dependent on the fibre failure strain and the lay-up. Tubes with the fibres aligned closest to the hoop direction were those that were the most sensitive to the matrix maximum strain. For these tubes, an increase of about 60% in specific energy absorption could be achieved by doubling the matrix failure strain.

Further work [36] showed that the trend to higher energy absorption with higher matrix failure strain for carbon-epoxy tubes, was not matched when the reinforcement was Kevlar fibres. The failure mode of Kevlar reinforced tubes was very different to that for carbon fibre reinforced tubes, since the fibres deformed rather than fractured. It was concluded that the decrease in specific energy absorption for these tubes was related to a reduction in stiffness at high stresses.

A comparison of pultrusions of glass fibres in vinylester and polyester resin matrices was made by Thornton [31]. The vinylester resin tubes absorbed about 40% more

energy than the polyester resin tubes at low speeds, but the difference was reduced to about 12% at high speeds {figures 2.6}.

2.1.3.2.1.1 SMC Resins

Variations in the polyester resins used in SMCs were studied at the University of Liverpool [30,37]. A conventional SMC resin, 40-6020, gave the best results for energy absorption while the least favourable results were with a low modulus resin, 40-6003. Results from a high modulus resin, 40-7488, gave little improvement over the 40-6003 results, so that no conclusion could be drawn from the difference in resin modulus.

2.1.3.2.2 Effect of Additives

The effect was studied of additions on the behaviour of filament wound tubes manufactured with Scott Bader Crystic 272 as the base resin [30]. The additions were Crystic 586, a highly flexible polyester resin, and CRC 1080. Addition of less than 40% Crystic 586 had little effect on the specific energy absorption of tubes with a winding configuration of 90°/0°/0°/90°, but above 40% addition, the specific energy absorption decreased. The level of decrease was dependent on the test speed. Tubes with a winding configuration of 55°+/-/+/- tended increasingly to collapse in an unstable manner as the amount of addition increased, resulting in low levels of energy absorption. This collapse mode was most apparent at low testing speeds. The addition of CRC 1080 gave an increase in specific energy absorption for a winding configuration of 90°/0°/0°/90° to about 20% addition, above which level it gave a decrease. Tubes with a winding configuration of 55°+/-/+/- behaved in a similar way to tubes modified with Crystic 586. Addition of up to 30% Crystic 586 had the effect of increasing the tensile strength of the resin from 64.2 MPa to 71.8 MPa, while having negligible effect on the Young's modulus. Above 30% addition, both

properties decreased sharply. Addition of up to 20% CRC 1080 increased the tensile strength, above which level the strength decreased. The Young's Modulus decreased steadily with increasing addition of CRC 1080, from 3.5 GPa for the pure Crystic 272 to 2.7 GPa for an addition of 30%.

Part of this work involved the use of additions to the base polyester resin (Crystic 272) and relating the changes in specific energy absorption to changes in the basic mechanical properties of the resins. For the polyester resin system, the specific energy absorption decreased with increasing resin fracture toughness {figure 2.7}. A good correlation was found between the specific energy absorption and the tensile strength of the matrix {figure 2.8}. No conclusive correlation was found between the specific energy absorption and the Young's modulus of the resin, although it was indicated that the specific energy absorption may increase with increasing resin modulus {figure 2.9}. It was concluded that an interpretation of the way in which specific energy absorption varied with each material property was difficult because it was not possible to vary each property independently and that a trade-off of properties occurred.

2.1.3.2.3 Conclusion of Matrix Properties

Although the effect of each individual resin could be masked by changes in various other properties, generally it was found that epoxies were the best performers for energy absorption. Polyesters were very close in performance to epoxies, although the comparison must consider the test speed. Increasing the flexibility of the resin decreased the energy absorption. The work that has been carried out on vinylesters has shown them to be very promising while the inherent brittleness of phenolics renders them poor contenders. To date there does not appear to have been much, if any, work carried out in this field on thermoplastic matrix tubes.

2.1.3.3 Fibre Arrangement

Many mechanical properties of composite materials are strongly dependent on the fibre arrangement, so much work has been carried out to determine how the specific energy absorption of composite tubes varies with fibre lay-up.

2.1.3.3.1 Filament Wound Tubes

Work on filament wound glass-polyester tubes by Hull [38] showed that a fibre lay-up of 0-90° was 50% more effective in absorbing energy than a helical wind of ±55°[1].

The effect of varying the amount of hoop fibres inside and outside of the tube using a carbon-epoxy system was examined at the University of Liverpool [25]. It was found that the presence of external hoop fibres was crucial in obtaining reasonable values of specific energy absorption while the presence of internal hoop fibres was not crucial. It was concluded that, for maximum energy absorption, good external hoop restraint was required plus some internal hoop restraint. The same workers showed that the dependence of specific energy absorption on winding angle was dependent on the crush speed, since ±55° wound tubes were more sensitive to the crush speed than 90°/0°/0°/90° wound tubes, manufactured using the same fibre-resin system. Further work [30] showed that tubes with a winding angle of ±55° were more sensitive to the presence of resin additives than 90°/0°/0°/90° tubes, because centre failure could occur with various amounts of plasticising agents (see section 2.1.3.2.2). This work showed that the matrix sensitivity of the crush response of the tubes was strongly dependent on the fibre architecture.

---

[1]Various different ways of quoting the lay-up were used in the reports on which much of this review is based. It is believed that more than one notation was used for the same lay-up. The lay-ups quoted here are as they were written in the original report.

Later work [34,39] examined the effect of winding angle, θ, for filament wound tubes over the full range of angles from entirely hoop fibres (0°) to entirely axial fibres (90°), all in the configuration ±/±θ. The specific energy absorption increased with increasing winding angle to a maximum at ±/±65°, above which angle a decrease was observed {figure 2.10}. It was observed that the magnitude of the serrations in the force-displacement trace increased with increasing winding angle. Furthermore, the failure mode changed significantly with changing winding angle. The crush zone of an entirely hoop wound tube consisted of the hoop windings detaching from the tube, with the outer windings failing in tension, the detached fibres breaking into lengths that varied from about 5 mm to 300 mm, compared to a tube diameter of 50 mm. The internal fibres were found to have been subjected to bending, fracture and interpenetration. 85° and 75° wound tubes failed in a similar manner to the 90° wound tubes. 55° and 45° wound tubes failed with large plates being detached from the crush zone; these plates being bent both inwards and outwards. Tubes with entirely axial fibres (90°) failed by the propagation of long axial cracks producing thin struts that bent outwards. Some circumferential cracks were formed by the bending of the struts. This work may be compared to the behaviour of the pultruded tubes tested by Thornton [31].

Thornton and Edwards [24] showed that a carbon-epoxy tube, with a lay-up of $[+45/-45]_n$, gave a value of specific energy absorption that was about 25% lower than for equivalent tubes with a lay-up of $[0/90]_n$. A similar observation was made for glass-epoxy tubes, the difference being a decrease of about 40%.

The effect of fibre orientation for epoxy tubes reinforced with carbon, Kevlar and glass fibres was studied by Farley [26,36]. The fibre angle dependence of the specific

energy absorption was shown to be dependent on the nature of the fibres. For carbon-epoxy tubes, maximum energy absorption was found to occur at low fibre angles, with a steady decrease in specific energy absorption with increasing fibre angle to about 50°, above which the energy absorption was independent of the fibre angle. The value of specific energy absorption for a fibre angle of 15° was more than twice the minimum value for tubes with a fibre angle greater than 50° {figure 2.11} [36]. Kevlar-epoxy tubes behaved differently from carbon and glass reinforced tubes since, for angles between 15° and 45°, the energy absorption was independent of the fibre angle. From 45° to 90°, the energy absorption increased steadily to a value at 90° that was about 30% greater than the minimum value measured. The findings for glass-epoxy tubes were similar to those from the University of Liverpool [34]. For angles between 15° and 45°, there was little sensitivity of the energy absorption to fibre angle. Above 45° the energy absorption increased steadily and reached a maximum at about 75°, of about 52 kJ kg^{-1}, above which angle it decreased to a lower value at 90° of about 45 kJ kg^{-1}. The differences in the behaviour observed by Farley and those observed at Liverpool could be accounted for by the differences between epoxy and polyester resins, particularly the difference in fibre-matrix bond strength [40].

The effect of fibre orientation on the crush stress for flat sections and tube corners, manufactured from glass tape-epoxy was studied by Thornton [41]. For flat sections the crush stress increased with increasing percentage of 0° fibres, although the apparent amount of scatter in the results made the trend uncertain. For similar but curved sections, the mean crush stress increased with an increasing proportion of 0° fibres. This increase was much greater than for the flat sections, increasing about 120% with an increase in the proportion of 0° fibres from 5% to 100%.

2.1.3.3.2 Woven Cloth Reinforcement

The effect of different proportions of axial to hoop fibres in tubes manufactured from woven cloth pre-pregs was studied by Berry [30,39]. The specific energy absorption increased with increasing proportion of axial fibres, with the maximum recorded value being for a hoop:axial ratio of 1:4. A higher proportion of axial fibres resulted in the specific energy absorption decreasing rapidly because of longitudinal splitting, indicating that the presence of hoop restraint was very important. The performance of the 1:4 tubes was somewhat unreliable and it was concluded that the optimum proportion would probably be about 1:3 {figure 2.12}.

Work by Berry [30,39] on plain weave cloth (1:1), varying the angle of lay-up, showed that the specific energy absorption of tubes with the warp and weft directions at 45° to the tube axis was 30% less than for similar tubes with the warp and weft directions parallel to the axial and hoop directions respectively. The debris size from the ±45° tubes was larger than that from the 0°/90° tubes and it was concluded that this was significant in the lower level of energy absorption as less material deformation and fracture had occurred.

2.1.3.3.3 Random Fibres

The other main type of fibre arrangement that has been studied has been that of random fibres. This has been concerned with either chopped-strand-mat or continuous random filament mat. Comparison of tubes made from chopped-strand-mat-polyester with filament wound tubes [30] has shown that the chopped-strand-mat tubes are capable of absorbing as much energy as the filament wound tubes with the most favourable winding angle of 65° with a similar tube geometry.

2.1.3.3.4 Conclusion of Fibre Arrangement

The work on fibre arrangement has given rise to some basic design rules for composite energy absorbers. These are: external hoop restraint is essential to prevent unstable collapse while longitudinal fibres provide most of the energy absorption, these rules applying for both filament wound/pre-preg tape and woven cloth arrangements. 0-90° is better than ±55° and is generally more stable. Random fibre arrangement can be very effective. The effect of fibre arrangement can be affected by other variables, such as the crush speed and the fibre and matrix types.

2.1.3.4 Fibre Volume Fraction

Little systematic work has been carried out on the effect of fibre volume fraction on the specific energy absorption of crushed composite tubes. Many properties of composite materials are dependent on the fibre volume fraction, so it would be expected that energy absorption would be sensitive to it. As the fibre volume fraction increases then, generally, the material density increases[1]; so that, if the specific energy absorption were to increase, then the crush load must increase by an amount that exceeds the increase in material density.

Work on SMCs at the University of Liverpool showed that an increase in fibre volume fraction from 13% to 18% gave an increase in specific energy absorption from 39 to 54 kJ kg^{-1} [30].

An investigation into the effect of fibre volume fraction for carbon-epoxy tubes was carried out by Farley [36]. The effect of fibre volume fraction was dependent on the fibre lay-up, but generally, the specific energy absorption decreased with increasing

[1]Providing that the fibre density is greater than the matrix density.

fibre volume fraction between 40% and 60%. The effect was most marked for carbon-epoxy tubes with a lay-up of $[0/\pm15°]_4$ {figure 2.13}. No work has been published in this area for glass fibre reinforced tubes or for fibre volume fractions less than 40%. Farley [42] has indicated that the reason for the decrease in specific energy absorption with increasing fibre volume fraction was that the inter-fibre distance was reduced.

Random glass mat-polyester tubes produced by resinjection in both square and round cross sections were tested by Price [43]. Tubes with a fibre volume fraction of 28% gave a higher crush load than tubes with a fibre volume fraction of 18%. Although the higher fibre volume fraction resulted in the density of the tubes increasing, the specific energy absorption was still higher than for the tubes with the lower fibre volume fraction. Increasing the fibre volume fraction resulted in increased stability for thin-walled square tubes such that they were less liable to fail catastrophically.

The effect of fibre volume fraction on specific energy absorption has been shown to differ according to the fibre type. The difference in trends has been shown to be opposite to that which would be expected from the increase in material density alone, as glass fibres are denser than carbon and Kevlar fibres [40].

2.1.3.5 Specimen Geometry

Very little work has been carried out on determining the individual effects of the two main geometrical variables of axisymmetric tubes; being the wall thickness t and the mean diameter D. Most of the work has been concerned with the ratio between t and D.

2.1.3.5.1 Effect of t and D

Although the most obvious effect of increasing the tube wall thickness is to increase the crush load, this increase might not have represented an increase in specific energy absorption because of the resultant increase in the mass per unit length.

Thornton [41] showed that the specific energy absorption of square section tubes increased rapidly with increasing wall thickness t, the increase in specific energy absorption being approximately proportional to the increase in t {figure 2.14}.

A trend to higher values of specific energy absorption with higher wall thickness and lower mean diameter was found by Fairfull and Hull [44]. This work was based on varying t/D but it was shown that the effect of t/D was dependent on the values of the individual variables, so that the measured value of specific energy absorption was also dependent on the values of the individual variables. It was shown that the effect of t decreased with increasing D {figure 2.15}.

2.1.3.5.2 Specific Volume and t/D.

Most of the geometrical work that has been carried out has concentrated on the ratio between the major dimensions of t and D. Three different ways of quoting this ratio have been used in the literature; being t/D, D/t and the specific density ϕ which is given by the volume of the solid part of the tube divided by the volume of a solid block with the same external dimensions. For instance, for an axisymmetric tube ϕ is given by:

$$\phi = \frac{(D_o^2 - D_i^2)}{D_o^2} \qquad (2.1)$$

where D_o and D_i are the external and internal diameters respectively [17]. This value is more difficult to use and to visualise than t/D or D/t but it has the advantage that it can be applied to tubes that are not axisymmetric, such as square or rectangular tubes.

Early work on the effect of ϕ was carried out by Thornton [17] on carbon-epoxy, Kevlar-epoxy and glass-polyester tubes. For all the tubes tested, it was found that the specific energy absorption increased with increasing ϕ {figure 2.16}. A linear relationship between the specific energy absorption and ϕ was suggested. Insufficient tubes were available to determine any relationships accurately but it was suggested that the specific energy absorption was less sensitive to ϕ for glass-polyester pultrusions than for carbon-fabric-epoxy tubes. It was also suggested that the cross section was important in determining the effect of ϕ as square section tubes were more sensitive to ϕ than equivalent round section tubes. The reasons were not clarified. If the cross section is important in determining the effect of ϕ, then it appears that there is very little to be gained from using ϕ to compare different sections.

Thornton and Edwards [24] showed that tubes with very low values of ϕ could fail by unstable collapse and that a critical value, ϕ_c, must be exceeded for progressive crushing to be possible. The value of ϕ_c was greater for square section tubes than axisymmetric tubes, implying that these were less stable. For cylindrical carbon-epoxy tubes, if progressive crushing occurred, the value of specific energy absorption was largely independent of ϕ. The value of ϕ_c for glass-polyester pultrusions was greater than that for equivalent carbon-epoxy tubes implying a lower stability.

The crush response of carbon-epoxy and Kevlar-epoxy tubes over a range of D/t ratios was studied by Farley [45]. The specific energy absorption of the carbon-epoxy tubes decreased with increasing D/t {figure 2.17 (a)}. This relationship was non linear and

it was concluded that specific energy absorption was not scalable with D/t. Kevlar-epoxy tubes showed a linear decrease in specific energy absorption with increasing D/t {figure 2.17 (b)}. The relationship between specific energy absorption and D/t was independent of the tube internal diameter for both carbon-epoxy and Kevlar-epoxy tubes. It was concluded that the dependence of the specific energy absorption on D/t was because of changes in the degree of interlaminar cracking.

The effect of the t/D ratio on the crush performance of glass cloth-epoxy tubes was studied by Fairfull and Hull [44,46]. Tubes with thin walls failed by elastic instability, and the failure stress increased with increasing wall thickness up to the stress for progressive crushing. The value of specific energy absorption was strongly dependent on t/D for tubes with a low mean diameter but largely independent of t/D for larger diameter tubes. The mean diameter was defined as being the diameter where the amount of material in the tube wall outside of it equalled the amount of material inside of it. It was given by [47]:

$$D_m = \sqrt{\frac{D_o^2 + D_i^2}{2}} \qquad (2.2)$$

For tubes with a mean diameter of 15.9 mm, the specific energy absorption increased with increasing t/D to a maximum at t/D = 0.2, corresponding to a wall thickness of 3.18 mm, above which thickness the specific energy absorption decreased rapidly. Tubes with a mean diameter of 24.1 mm showed a similar behaviour, but the increase in specific energy absorption was not so pronounced. The maximum value of specific energy absorption was measured at t/D = 0.17 which corresponded to a wall thickness of 4.1 mm. Tubes with larger mean diameters did not show a maximum in the specific energy absorption versus t/D trace. Tubes with a mean diameter of 33.1 mm showed no dependence of specific energy absorption on t/D up to a value of 0.15, above which it decreased {figure 2.15}. Larger diameter tubes were insensitive to t/D within the range tested. Three different modes of crushing were identified depending on the

t/D ratio. These were presented on a mode map {figure 2.18} (see section 2.1.5.1 for a complete description).

The effect of the W/t ratio for square section carbon-epoxy and Kevlar-epoxy tubes, where W was the tube width, was studied by Farley [36]. The specific energy absorption of the carbon-epoxy tubes was found to be a nonlinear function of W/t {figure 2.19 (a)}. Energy absorption increased with increasing W/t to a maximum when W/t was between 20 and 50, above which ratio the energy absorption decreased rapidly. The response of the Kevlar-epoxy tubes was also a nonlinear function of W/t {figure 2.19 (b)}. It was concluded that the observed increase in specific energy absorption with decreasing W/t was related to reduced interlaminar cracking, and was consistent with buckling load characteristics of edge supported plates.

2.1.3.5.3 Section Shape

Two main geometries of tube have been considered, being axisymmetric and square cross section. It had been shown that the value of specific energy absorption measured for a tube was dependent on the tube dimensions, hence a direct comparison of the two geometries was difficult. The concept of specific density was one way of comparing the two geometries, although the validity of this for the crushing of composite tubes has not yet been established and results so far indicate that it's use was probably not valid as a comparison tool.

A comparison of glass-polyester pultrusions of both square and round cross section was made by Thornton [17], who found that, for the same value of specific density, the value of specific energy absorption from the round tubes was consistently greater than that from the square tubes. At low values of ϕ, the specific energy absorption of the round tubes was twice that of the square tubes while at high values of ϕ the value for the round tubes was about 60% greater than for the square tubes.

The behaviour of tubes with round, square and rectangular cross sections was studied by Thornton and Edwards [24]. It was found that, for all sections, there was a critical value of the specific density below which unstable collapse occurred (see section 2.1.3.5.2). This value of ϕ_c was lower for round carbon-epoxy tubes (about 0.025) than for similar tubes with a square or rectangular section (about 0.075) implying a higher stability for round tubes. The values of ϕ_c were found to be independent on the fibre lay-up for 0/90 or 45/45 fabric, the only two arrangements used in this work, although the latter collapsed at lower loads than the 0/90 fabric tubes due to the lower modulus of the material in the axial direction. Later work by Price [43] indicated that the values of ϕ_c are dependent on the specimen length, with shorter tubes having a lower value of ϕ_c. This work concluded that the specific energy absorption was largely independent of ϕ for these tubes if ϕ_c was exceeded. There was little difference in the measured value of specific energy absorption between the square and rectangular tubes. Similar work on glass-epoxy tubes gave similar trends to the carbon-epoxy tubes but the values of ϕ_c were much higher indicating lower stability. For Kevlar-epoxy tubes the value of ϕ_c for the square tubes was similar to that for the round tubes. The value of the specific energy absorption for the square tubes was less than half that for the round tubes.

Thornton *et al.* [7] concluded that there was a progression in the value of specific energy absorption of rectangular < square < round for a given size, presumably the relative density. It was noted that the instability observed at low values of ϕ was dependent on the fibre lay-up and tube length. It was concluded that the corner sections contributed a much higher proportion to the crush load per unit mass of material involved than the flat sections, in a proportion of about 3:1.

A comparison of the responses of square section carbon-epoxy tubes to those of similar tubes with round cross sections was made by Farley [28,36]. The square section tubes exhibited a lower specific energy absorption than round tubes of similar dimensions. These findings were in agreement with earlier published work.

The crush response of random filament glass mat-polyester tubes produced by resinjection with round and square cross sections with various wall thicknesses, was examined by Price [43]. The square tubes had varying corner radii. Two basic failure modes were found, being dependent on the specimen dimensions, cross section profile and specimen length. The failure modes were catastrophic centre failure and progressive crushing. All the tubes with circular cross sections failed by progressive crushing, as did the square section tubes with wall thicknesses of 4 mm and greater. 2 mm wall thickness square tubes failed by either mode depending on the corner radius and specimen length[1]. It was found that increasing the corner radius favoured progressive crushing while increasing the specimen length favoured catastrophic shell failure. The value of specific energy absorption increased with increasing corner radius {figure 2.20}. For tubes with a wall thickness of 4 mm, the specific energy absorption doubled with an increase in corner radius from 10 mm to 40 mm (i.e. circular), the increase being approximately linear with increasing corner radius. This trend was not as clear for tubes of other wall thicknesses. It was observed that the flat sections of the square tubes did not always exhibit the frond-wedge-frond type of crush mode that was commonly observed in circular tubes. The highest values of specific energy absorption were found when the frond-wedge-frond type of crush mode extended around the entire circumference of the tube. The conclusion was

[1]Thornton's work on ϕ_c did not show any length dependence as all the tubes used in that investigation were of the same length.

drawn that the highest values of specific energy absorption were found when the cross-sectional geometry of the tube was closest to being circular.

2.1.3.5.4 Other Geometries

Most of the work on energy absorption has concentrated on tubes with either circular or square cross sections. Whilst these sections are useful from an experimental viewpoint, because of being relatively easily produced and consistent in behaviour, applications for the use of energy absorbing components can demand that other sections are employed. For instance, the structural under-bonnet components in a car required to provide impact energy absorption have space considerations that can restrict the section geometries available to the designer [8]. The under-floor structures of helicopters can also have geometrical restrictions on the shape of energy absorbers [6,28,36,48,49].

The behaviour of bulkhead components made from carbon-epoxy and Kevlar-epoxy composites on a honeycomb stiffener was studied by Sen and Dremann [49]. These bulkheads were essentially flat plates with reinforcing webs in various configurations, but they were not effective in absorbing energy when compared to tubes made from similar materials. The highest value of specific energy absorption obtained in this work was 18 kJ kg^{-1} which was about one third of that obtained from a poor quality, axisymmetric tube.

The behaviour of energy absorbers constructed from various curved and flat components was studied by Farley [28,36]. These components were circular and square tubes; flat plates and sine wave section beams. It was found that the total energy absorption of the whole device was the sum of the energy absorptions of the component parts. The sine wave beams crushed in a progressive manner. If they

consisted of half-tangent circles with an included angle of 180°, then the energy absorption capacity was comparable to that of a tube of circular cross section. If the included angle was less than 180° the energy absorption was much less than for a circular tube.

The energy absorption of a cellular structure manufactured from glass cloth-epoxy pre-preg material was studied by Small and Ansell [50]. Two modes of collapse were found; stable, with a resulting high level of energy absorption; and unstable with a resulting low energy absorption level. Unstable collapse was observed for specimens with a large cell size and low wall thickness. These observations can be compared to the observations made for tubes where tubes with a low value of t/D were found to collapse in an unstable fashion. The specific energy absorption measured for structures that crushed in a stable manner, was a linear function of the ratio of wall thickness to cell diameter, essentially the t/D ratio as measured for tubes. As the maximum inner cell diameter was 11.2 mm, this observation was consistent with the results obtained for tubes by Fairfull (section 2.1.3.5.2) [44,51]. The values of specific energy absorption obtained in this work were high, in some cases exceeding 100 kJ kg^{-1}.

2.1.3.5.5 Length

The effect of tube length on the serrations of the force-displacement curve for glass cloth-epoxy tubes was investigated by Fairfull [51,52]. In that work, the serrations were thought to have resulted from stick-slip crack propagation. The gradient of the rising part of the serrations was determined for different tube lengths, and it was found that the gradient was largely independent of the tube length. This was contrary to that which was expected from normal elastic loading, as the

displacement to reach a certain strain was less for a shorter tube. It was concluded that the crush zone, the appearance of which was independent of the tube length, must have had a characteristic stiffness which related to the elastic loading and unloading. The mean load and the peak to trough height of the serrations were independent of the tube length.

The effect of length on thin-walled, random glass mat-polyester tubes with square cross sections was investigated by Price (see section 2.1.3.5.3) [43]. Long tubes failed by catastrophic centre failure instead of stable crushing. For each tube configuration studied there was a critical length, l_c, below which stable crushing occurred while above it, centre failure occurred. This value of critical length increased with increasing wall thickness, fibre volume fraction and corner radius.

2.1.3.5.6 Sections

The crush performance of tube sections and slotted tubes was studied by Price [53] to try to understand the effect of hoop stresses. No significant drop in energy absorption was observed resulting from the slotting of the tubes. Quarter section tubes were less effective in absorbing energy than axisymmetric tubes. There was little difference in the performance of half and three quarter section tubes from that of axisymmetric tubes. This work implied that the presence of absolute hoop restraint was not crucial for good energy absorption.

A comparison of the crush response of flat and curved sections was made by Thornton [41]. The curved sections exhibited a stable crush over much greater distances than the flat sections, whilst there appeared to be little difference in the peak crush stress between the flat and the curved sections. It was also shown that the mean crush stress increased with decreasing radius of curvature for the curved sections.

The combined findings of Price and Thornton indicated that local curvature was important for energy absorption.

2.1.3.5.7 Conclusion on Specimen Geometry

It has been found that, for optimum energy absorption, tubes should be as close as possible to circular in cross section. Specific energy absorption increases with increasing wall thickness and decreasing tube diameter. Generally, a certain level of wall thickness must be exceeded to prevent catastrophic failure. Length has no effect on the energy absorption if catastrophic failure is avoided.

2.1.3.6 The Trigger

Much interest has been shown regarding the trigger used to prevent centre failure and promote progressive crushing. Both the nature and the geometry of the trigger have been studied [34,54-58]. For the purposes of this work it is enough to note that the chamfer trigger which consists of a bevel machined at one end of the tube, was effective in promoting progressive crushing and preventing catastrophic centre failure. It has been shown that the geometry of this type of trigger affects the beginning of the force-displacement trace but does not affect the measured crush load. The use of a 45° chamfer has been shown to prevent an initial peak load before progressive crushing proceeds. Although other types of trigger have been studied, these have not been considered in this work[1].

2.1.4 Effect of Testing Variables

The main testing variables that have been considered are the crush speed and the tube temperature. The effect of the nature of the crush platen has also been investigated.

---

[1]Another trigger of note is the "Tulip" type of trigger employed by Thornton and co workers, although the benefits to be gained from this type of trigger appear to be limited to square section pultrusions.

2.1.4.1 Effect of Speed

Most of the work that has been carried out on crushing of tubes has employed constant speed crushing as a simulation of an impact. During an impact the speed must decrease from the initial impact speed to rest as the energy absorber performs it's function. Hence, constant speed crushing may not be a true simulation of crash conditions. Polymers are known to be sensitive to the strain rate during testing, so composites incorporating polymers in the matrix or fibres may also be strain rate sensitive (see section 2.2). If the crush behaviour of composite tubes is sensitive to the crush speed, then constant speed crushing will not be a true simulation of crash conditions. To this end, much work has been carried out on the speed sensitivity of the specific energy absorption of crushed composite tubes.

2.1.4.1.1 Glass Fibre Reinforcement

Work has been carried out examining the speed effects on energy absorption by tubes reinforced with glass fibres in various matrix materials. The main types of matrices studied have been polyester and epoxy resins, although phenolic, acrylic and vinylester resins have also been examined.

2.1.4.1.1.1 Polyester Resin Matrices

Most of the work on speed effects on polyester matrix tubes was carried out at the University of Liverpool. This work concentrated on filament wound tubes and random fibre reinforcement. Early work [59] showed that, for filament wound tubes with a fibre arrangement of ±55°, there was little significant sensitivity to speed. Later work [25] on tubes with a fibre arrangement of 55°/0°/0°/55° {given as ±55° in figure 2.21} displayed a definite decrease in energy absorption with increasing crush speed with a value of about 70 kJ kg^{-1} at 0.005 m s^{-1} compared to about 50 kJ kg^{-1} at 5 m s^{-1}.

Tubes made with the same glass-resin system but with a fibre arrangement of 90°/0°/0°/90° {0/90° in figure 2.21} displayed much less speed sensitivity, showing that the speed sensitivity depends on the fibre arrangement. Further work [30] incorporating additions of a plasticising agent (Crystic 586) to the basic resin, gave significant reductions in energy absorption with increasing speed {figure 2.22}. Additions of a vinyl terminated rubber (CRC 1080) gave a substantial speed sensitivity to 90°/0°/0°/90° tubes with a decrease in specific energy absorption from about 75 kJ kg^{-1} at 0.005 m s^{-1} to about 60 kJ kg^{-1} at 5 m s^{-1} {figure 2.23}. Additions of an agent that had a strengthening effect on the base resin, decreased the speed sensitivity of 90°/0°/0°/90° lay-up tubes while having little effect on the speed sensitivity of 55°+/-/+/- tubes. The basic resin used in this work was Scott Bader Crystic 272. This work showed that the effect of the fibre lay up on the speed sensitivity was complicated, but that a 0/90° lay up was less speed sensitive than ±55°.

Work performed using Scott Bader Crystic 272 polyester resin showed that the fracture toughness of the polyester resin matrix increased with increasing test speed {figure 2.24} [33]. This can be compared to the observation in section 2.1.3.2.2 that the specific energy absorption decreased with increasing fracture toughness {figure 2.7}. These trends were consistent with the observation that specific energy absorption decreased with increasing test speed for a polyester resin matrix.

Early work at Liverpool on chopped-strand-mat-polyester tubes [21] showed that the reduction in energy absorption with increasing speed observed for filament wound tubes was also present with this type of reinforcement. With this work; however, there was a lack of dimensional control, so that the trends observed must be treated with caution {figure 2.25}.

Work on SMCs with various resin formulations [30,59], showed probable trends to lower energy absorption at higher speeds, however the scatter was too great to be able to draw firm conclusions.

Tubes manufactured by resinjection with random filament glass reinforcement in Crystic 272 were examined by Price [43]. It was found that the speed sensitivity of energy absorption was dependent on the wall thickness. Tubes with 4 mm thick walls showed a decrease in energy absorption with increasing speed while those with 8 mm thick walls appeared relatively insensitive to speed {figure 2.26}.

Work on glass-polyester pultrusions by Thornton [31] showed that higher speeds gave higher values of energy absorption {figures 2.6 (a) and 2.27}. It appears that the high speed tests might have been subject to a degree of debris compaction, so that the levels of energy absorption might have been artificially high for these tests. These pultruded tubes had a very high proportion of axial fibres and much of the hoop restraint was provided by the matrix. Crushing in these tubes consisted of splaying of the axial fibres with resin fracture being a major contributor to energy absorption. It has been shown that the fracture toughness of polyester resins increases with increasing speed [33], hence these observations are not inconsistent with the observations of other workers that the specific energy absorption of glass-polyester tubes decreases with increasing crush speed.

2.1.4.1.1.2 Epoxy Resin Matrices

Most of the work that has been carried out to date on speed effects in glass-epoxy tubes has been performed on tubes reinforced with woven cloth. Thornton [17] showed that the energy absorption of glass cloth-epoxy tubes increased with

increasing crush speed. These results gave a linear increase with log speed and a formula was proposed of the type

$$E_s = c \log_{10} (v_c) + d \qquad (2.3)$$

where c and d were empirically determined constants. The author suggested values of $c = 1.49\ kJ\ kg^{-1}$ and $d = 53.2\ kJ\ kg^{-1}$ {figure 2.28}. The logarithmic dependence of specific energy absorption was later confirmed by Berry and Hull [60], although the later values of c and d were 3.74 and 57.9 $kJ\ kg^{-1}$ respectively {figure 2.29}. These differences could be accounted for in the differences between the test-pieces used by the workers. Berry and Hull examined some debris using an SEM from tubes tested at high and low speed and found distinct differences as resin flow appeared to have occurred at low speed and brittle resin fracture at high speed.

Some work on speed effects in filament wound glass-epoxy tubes was carried out at the University of Liverpool [33]. Small increases in energy absorption with increasing speed were found {figure 2.30}. However, the fibre arrangement was 0–90° and this was known to be a lay-up that is relatively insensitive to the matrix properties (see Section 2.1.3.3.1).

The speed dependence of specific energy absorption of a cellular structure made from glass cloth-epoxy pre-preg was studied by Small and Ansell [50]. It was found that the measured value of specific energy absorption increased sharply from 0.1 $mm\ s^{-1}$ to 1 $mm\ s^{-1}$, but that the increase was not sustained when tested at 1 $m\ s^{-1}$. It was observed that testing at high speeds increased the incidence of unstable collapse of the cells. The cells were not triggered for progressive crushing {figure 2.31}.

2.1.4.1.1.3 Other Matrix Materials

Very little work has been carried out on the crush behaviour of tubes manufactured using matrix materials other than epoxies or polyesters. The behaviour of filament

wound tubes manufactured with a phenolic resin matrix was examined at the University of Liverpool [33]. These tubes showed no speed sensitivity for their energy absorption capability {figure 2.32}. The lay-up was however 0–90°, a lay-up that has been shown to be relatively insensitive to the matrix properties (see section 2.1.3.3.1). These results may thus have little significance with respect to the speed sensitivity of other lay-ups. Some work on phenolic-cotton tubes suggested there was little speed sensitivity of the post failure crush load.

Work on acrylic resin matrix tubes at the University of Cambridge showed that a negative speed dependence was present [35]. These tubes were made using glass mat in two different acrylic resins. For one system (ICI MDR 804) a 26% decrease in the specific energy absorption was observed over the speed range 4 mm s^{-1} to 4 m s^{-1}. Another system, ICI MDR 835, displayed a 23% drop over the same speed range {figure 2.33}.

Tests on glass-vinylester pultrusions were performed by Thornton [31]. Little speed sensitivity was found, any trends being apparently masked by scatter in the results. The suggestion was however, made that there was a negative speed sensitivity of energy absorption for some of these tubes and a positive speed dependency for others {figure 2.6 (b) and 2.34}.

Some tests on filament wound glass-vinylester tubes with a winding angle of $(\pm 45°)_3$ were performed by Burtin and Hamelin [61]. Contradictory trends as functions of speed were found for apparently identical tubes, since one set of tubes displayed a negative speed dependence of specific energy absorption while two other batches displayed a positive dependence. No indication was given of the number of tests carried out. The values given for specific energy absorption were much lower than

those quoted by other workers, despite the tube dimensions being comparable, probably because of the fibre arrangement used in this work. Translation problems appear to have masked the value of this paper's contribution to the field.

2.1.4.1.2 Carbon Fibre Reinforcement

Thornton [17] showed that, for carbon-epoxy tubes, the energy absorption capability increased slightly with increasing speed {figure 2.28}. These results showed a linear relationship of the form shown in equation 2.3. The value of c, the gradient of the line, was a measure of the speed sensitivity and the author found a value of 0.631 kJ kg^{-1} for carbon-epoxy tubes, compared to 1.49 kJ kg^{-1} for similar glass-epoxy tubes, showing that the carbon-epoxy tubes were less rate sensitive than the glass-epoxy tubes. The author noted that the level of serration of the force-displacement curve increased with increasing speed. Thornton *et al.* [7] appear to have re-presented the same results but concluded that the rate dependence of carbon-epoxy tubes was only 10% of that of glass-epoxy instead of 42%, although there did not appear to have been any more data collected. No reasons were given for this apparent contradiction.

A positive speed dependence for 0-90° lay-up carbon-epoxy tubes with a ratio of hoop to axial fibres of 1:3 but a negative speed dependence for similar tubes with a ratio of 1:5 {figure 2.35}, was found by workers at the University of Liverpool [25].

Quasi-static and impact rate tests on carbon-epoxy tubes were performed by Farley [26]. It was concluded that the results agreed to within 20% of each other but gave no indication of any trend. The same author [36] later performed tests on the effect of varying the fibre lay-up on the speed sensitivity of carbon-epoxy tubes and found that, as the ply orientation angle increased from 15° to 75°, the sensitivity to speed of the energy absorption increased. Farley concluded that the reason that the speed

sensitivity varied with ply angle, was that, as the ply angle increased, the contribution to energy absorption of the matrix material increased.

2.1.4.1.3 Conclusion of Speed Effects

This work has shown that the specific energy absorption for the composite tubes tested was, to some degree, sensitive to the crush speed. The direction of speed sensitivity has been found to depend on the matrix material, with polyester and acrylic resin matrix tubes showing a negative speed dependence while epoxy resin matrix tubes showed a positive speed dependence. The degree of speed dependence was shown to be strongly dependent on the fibre type and arrangement.

2.1.4.2 Temperature Effects

Thornton [17] showed there was little variation of energy absorption with varying temperature below 25 °C, for glass-epoxy and carbon-epoxy tubes {figure 2.36}. At temperatures above 25 °C, the energy absorption of the glass-epoxy tubes was found to decrease rapidly with increasing temperature. The author concluded that this decrease started at about -100 °C but the figure presented in this paper suggested that this observation could be because of experimental scatter instead of any true effect. The carbon-epoxy system maintained a reasonable level of energy absorption with increasing temperature up to about 150 °C, before it started to decrease. The energy absorption of glass-polyester pultrusions decreased rapidly with increasing temperature above room temperature. All systems displayed a greater level of serration in the force-displacement trace at low temperatures. At high temperatures the tubes were observed to remain intact, rather than to display the high degree of fragmentation that was found at low temperatures. A later presentation of these results

by Thornton and Jeryan [62] concluded that the glass-epoxy tubes gave a significant increase in energy absorption with a reduction in temperature below ambient.

A filament wound glass-polyester system was examined by workers at the University of Liverpool [25]. It was found that, within the range -20 to 60 °C, there was no significant temperature dependence of the energy absorption {figure 2.37}. The lay-up in these tubes was 0-90°, a lay-up that has been shown to be relatively insensitive to speed (section 2.1.3.3.1), so these observations suggest that the crush properties of this lay-up are relatively insensitive to the matrix properties.

Berry and Hull [60] showed that a glass cloth-epoxy tube tested at -20 °C gave a higher value of energy absorption than a similar tube tested at room temperature at the same speed. The authors suggested that it might be possible to obtain a simulation of very high speed crushing by testing at low temperatures.

2.1.4.3 Nature of the Crush Platen

Specific energy absorption cannot be regarded as being purely a property of the test piece, as the nature and condition of the crush platen can affect the values obtained.

The effect of platen roughness on the crush load was examined by Fairfull and Hull [63]. A polished steel platen gave a crush load that was about 7% less than for the normally used ground surface. Surfaces that were rougher than a polished finish did not appear to display any surface condition sensitivity of the crush load. It was concluded that friction between the crush platen and the debris fronds played an important part in energy absorption.

2.1.5 Mechanisms

So far this review has concentrated on the trends in the observed values of specific energy absorption with each individual variable with no reference to the mechanisms of crush. However, work has been carried out into trying to understand the mechanisms of crush.

2.1.5.1 Crush Zone Morphology

The crush mechanisms of glass cloth-epoxy tubes, crushed over a wide range of t/D ratios, were examined by Fairfull and Hull [44,51]. All the tubes considered in this study were triggered for progressive crushing and three basic types of crush zone morphology were found depending on the tube scale if catastrophic shell failure was avoided.

Type I crushing occurred for tubes with a t/D ratio of less than 0.1 and consisted of an annular wedge of tightly compacted material that forced the material in the tube wall to flow into the centre of the tube and outside of the tube {figure 2.38 (a)}. A centre wall mode I crack[1] was formed and propagated by the opening forces applied by the wedge. These forces caused the formation of debris fronds.

Type II crushing occurred for a wide range of tube dimensions up to a t/D ratio of about 0.2 {figure 2.38 (b)}. This mode was largely independent of the tube diameter; being mainly dependent on the wall thickness. This mode featured a smaller debris wedge than type I crushing with no evidence of the mode I centre wall crack, the apex of the wedge being displaced to the inside of the tube.

---

[1]Although generally referred to as a mode I crack, hoop restraints on the crack must have meant that it it was not purely mode I and should be referred to as a modified mode I crack. However, the original author used the terminology mode I so it is also used here.

Type III crushing occurred for the tubes with the highest values of t/D {figure 2.38 (c)}. In this mode, a cone of debris formed in the centre of the tube forcing the material to flow to the outside of the tube with no flow to the inside. All three types of crushing involved extensive delamination of the tube wall.

Type III crushing was less efficient as an energy absorbing mechanism than types I and II, resulting in the decrease in specific energy absorption that was observed for high values of t/D with small bore tubes {figure 2.15}. In figure 2.38 (c), the depth of the external frond has been given as 0.95t. As described, this was very unlikely to have been the true depth for reasons of conservation of matter. For this type of crushing, once the crush zone was established and the wedge formed, all the material in the tube wall had to flow away from the crush zone as the external frond, thus it was very improbable that the depth of the frond was less than the wall thickness.

2.1.5.2 Energy Absorbing Mechanisms

Eight different mechanisms that contributed to the energy absorbed in the crushing of glass cloth-epoxy tubes were identified by Fairfull [51]. These mechanisms were identified for type I crushing, but they were also applicable to types II and III crushing, although some of the mechanisms might not have been active. These mechanisms were:

1. Propagation of mode I crack at the apex of the debris wedge,
2. Friction between the wedge and the debris fronds,
3. Delamination of the fronds,
4. Flexural damage of the fronds at the limits of delamination,
5. Friction between the laminae of the fronds after delamination,
6. Friction between the fronds and the crush platen,
7. Propagation of axial splits between fronds,

8. Transverse flattening of the fronds.

Consideration of the three types of crush zone showed that the first mechanism was only present in type I crushing while the other mechanisms all operated for all three modes. However, it was unlikely that type II crushing could have occurred without a mode I intra-wall crack as the wedge would not then have been able to move down the tube wall. It must be assumed that in this type of crushing the crack was not visible but was present and that the first mechanism was operational. The eight modes that were identified are divisible into five fracture modes (1,3,4,7,8) and three frictional modes (2,5,6).

The levels of contribution to the energy absorption of each of the mechanisms were dependent on the testing conditions and the material properties. Some dependence of the levels of contribution on the specimen geometry was identified. The contribution of mechanism 6 was dependent on the crush platen and was not a true material property (see sections 2.1.4.3 and 7.1).

Another crush mode for glass cloth-epoxy tubes with a t/D ratio of about 0.04 was identified by Berry and Hull [60]. This mode was very different from those identified by Fairfull since the debris wedge was not present and most of the energy absorption appeared to be due to micro-fracture processes {figure 2.39}. It was unclear in either work what determined the nature of the crush mode between the type I mode observed by Fairfull and that observed by Berry and Hull, as the tubes used appear to have been very similar. It was probable that the differences were in the resin used as the pre-preg suppliers were different.

2.1.5.3 Load distribution

To estimate the level of contribution of some of the mechanisms, Fairfull [51] determined the different contributions of the wedge and fronds to the crush load. The results were for tubes with a t/D ratio of 0.05 and might not be directly applicable to other tube geometries. The crush mode for these tubes was type I where the debris wedge took 67% of the crush load, the internal fronds 13% and the external fronds 20%. The findings of this work are discussed in depth in section 7.1.

2.1.5.4 Friction

The force distribution within the crush zone was defined by Fairfull as shown in figure 2.40[1] [51,63]. P_{IN}, P_W and P_{EX} having been determined, μ_1 was determined by measuring the radial frictional force. μ_1 was found to be 0.25 - 0.45. From this work it was possible to estimate the contribution of friction between the fronds and the crush platen to the total energy absorbed (see section 7.1).

The coefficient of friction between the crush front and the crush platen for different platen surface conditions was determined by Fairfull and Hull [63] by rotating the crush zone against the platen and measuring the frictional resistance to torsion. A polished steel platen surface gave a significantly lower coefficient of friction than for a ground surface (0.26 to 0.30 as opposed to 0.35 to 0.39). A sand blasted surface gave a slightly higher value than the ground surface (0.38 to 0.41) while a cross-milled platen gave much higher values (0.65 to 0.70). The values for the ground and sandblasted surfaces were towards the high range of the values obtained by Fairfull in

[1]The forces as drawn were show the forces on the wedge as being on the fronds, eg. P_1 etc. Compare figure 2.40 to figure 7.1.

previous work [51]. This work measured the coefficient of friction between the entire crush zone and the platen instead of just the fronds and the platen as would be the case for axial crushing. The presence of the debris wedge sliding against the platen in these experiments might have had an effect on the values measured.

Some work on determining the frictional contribution at the wedge-frond interface was carried out by Fairfull [51] by introducing a PET film to reduce the friction at the interfaces. The film had the effect of reducing the crush load by 23% without seriously affecting the appearance of the crush zone. It was concluded that wedge-frond interface friction was a very important contributor to the energy absorption. The level of serration of the force-displacement trace was much less for the tubes incorporating the PET film and it was concluded that the serrations were largely caused by stick-slip friction. This conclusion was contrary to that reached by the same author, as stated in section 2.1.3.5.5, that the serrations were caused by stick-slip crack propagation. However, this work was later than that carried out on the length effects, so that the conclusion of stick-slip friction probably represents a state of better understanding of the crush process.

2.1.6 Conclusions

This work has shown that composites are capable of absorbing large amounts of energy per unit mass if the correct design is used. Energy absorption is dependent on many variables which can be grouped into material, geometrical and testing variables. Trends of energy absorption with each individual variable were difficult to quantify as there was a great deal of interaction of variables, for instance the sensitivity of the specific energy absorption to speed depends on the matrix material, fibre type and fibre arrangement. Nonetheless, some general trends have been observed.

1. Carbon fibres are superior to glass which are superior to Kevlar.
2. Hybrid fibre tubes give no significant improvement over single fibre type tubes.
3. 0-90° is a better fibre arrangement than ±55°.
4. The optimum ratio of axial to hoop fibres is about 3:1.
5. Woven cloth and random fibres are both effective types of reinforcement.
6. Epoxy resins are the best matrix materials although polyester, vinylester and acrylic resins are very close in performance.
7. Specific energy absorption is dependent on the specimen geometry.
8. Circular tubes are the most effective energy absorbers.
9. The levels of energy absorption are dependent on the crushing speed, although the sensitivity to speed is dependent on the fibre and matrix types and fibre arrangement.
10. Energy absorption decreases with increasing temperature for all the matrix materials studied.
11. Energy absorption is dependent on the platen condition and is not purely a material property.

2.2 Material Properties

Work has been performed on the basic mechanical properties of thermosetting resins, particularly epoxy resins, and composite materials incorporating these resins as matrix materials. This section gives an outline of the way the strength, stiffness and fracture properties vary with the test speed and temperature for both the monolithic matrix material and the resins when reinforced with glass fibres.

2.2.1 Resin Properties

Most of the work on the properties of thermosetting polymers has been carried out on epoxy resins, although a limited amount of work concerning polyester resins has also

been performed. As these were the only two types of resin used in the experimental part of this project, this review section is only concerned with these types.

2.2.1.1 Epoxy Resins

Work has been carried out on the strength, stiffness and fracture properties of a range of epoxy resins. Strain rate and temperature responses have been examined.

2.2.1.1.1 Strength and Stiffness

Deformation of an epoxide resin at temperatures below the T_g was examined by Pink and Campbell [64]. Stress-strain curves showed that the response at low temperatures was strictly linear elastic, while at higher temperatures deviations from linearity were very apparent {figure 2.41}. At these temperatures, about 250 K to 390 K (-23 °C to 117 °C), deformation was found to be a combination of linear and nonlinear elastic with an increasing degree of plasticity as the temperature rose. Increasing temperatures resulted in increasing strains to failure at decreasing failure stresses. A strain rate sensitivity, λ, of the tensile stress σ, was defined as:

$$\lambda = \frac{\Delta\sigma}{\ln\left(\frac{\dot{\varepsilon}_2}{\dot{\varepsilon}_1}\right)} \qquad (2.4)$$

where $\Delta\sigma$ was the change in the tensile stress for a strain rate variation from $\dot{\varepsilon}_1$ to $\dot{\varepsilon}_2$. The value of λ was found to vary with temperature and was approximately zero at temperatures up to about 170 K (-103 °C), above which temperature it rose rapidly to a maximum at about 200 K (-73 °C). Between 200 K and 350 K (77 °C), λ decreased linearly with increasing temperature to zero. Above 350 K, λ rose sharply with increasing temperature {figure 2.42}. The T_g of the resin was given as 423 K (150 °C). The actual values of λ that were measured were found to be dependent on the strain employed in the test, λ increasing with increasing strain. The observations made in

this work divided the deformation into three regions which were deduced to be due to different mechanisms. Each mechanism was associated with an activation energy and estimates of the energies were given. The regions were defined as being: below 180 K (-93 °C), 180 K to 320 K (47 °C) and above about 350 K (77 °C). The region between 320 K and 350 K was not defined. The activation energies associated with each mechanism were: 1 eV, 2-3 eV and 4-6 eV respectively. There was no qualitative description of the mechanisms.

Mechanical properties of a series of epoxy resins as functions of the testing rate and the temperature were studied by Yamini and Young [65-67]. For each of the resins investigated, the Young's modulus displayed a slight increase with an increase in test speed of two orders of magnitude. The Young's moduli of the resins were found to decrease linearly with increasing temperature over most of the range investigated, however, the decrease was found to be greatest as the T_g was approached {figure 2.43}. Measurements of the yield stress as a function of the testing variables showed similar variations to those found for the Young's modulus, in that a slight increase was observed with increasing speed and a decrease with increasing temperature {figure 2.44}. The observed percentage decrease in yield stress with increasing temperature was much greater than the percentage decrease in the Young's modulus. The shear yield stress was found to decrease linearly with increasing temperature in the range -60 °C to 80 °C for an epoxy resin with a T_g of 110 °C {figure 2.45}.

The effects of temperature and strain rate on the strength and stiffness of an epoxy resin were studied by Kinloch *et al.* [68]. The compressive yield strength was found to increase logarithmically with the strain rate, the gradient of the σ_y versus $\log(\dot{\varepsilon})$ line being apparently independent of the test temperature. The yield strength decreased rapidly with increasing temperature from -60 °C to 20 °C, but temperature increases above 20 °C had a much lower effect. Similar trends were found for the compressive

modulus. The crack opening displacement, δ, was examined as a function of the test variables. Crack opening displacement is a quantity that relates the fracture toughness, K_{Ic}, to the yield strength, σ_y, and yield strain, ε_y, of the material. It is given by:

$$\delta = \left(\frac{K_{Ic}}{\sigma_y}\right)^2 \quad \varepsilon_y \qquad (2.5)$$

δ increased slightly from -90 °C to about -20 °C, above which temperature it increased rapidly as the temperature was increased. The actual increase was found to be dependent on the strain rate, lower strain rates favouring a more rapid increase in δ with increasing temperature. From equation 2.5, it is clear that trends in δ can be related to a combination of trends in K_{Ic}, σ_y and ε_y. This work showed the compressive modulus and yield strength to increase with increasing strain rate, the apparent increases being greatest at -60 °C. From -40 °C to 60 °C there did not appear to be any temperature sensitivity of the speed sensitivity of either quantity. The increases were linear with log. strain rate.

The properties of an epoxy resin at 77K (-196 °C) were compared with those at room temperature by Egusa *et al.* using a three point bend test [69-71]. An increase in the Young's modulus of about 120% occurred on cooling the resin from room temperature to 77 K. This increase was accompanied by an increase in the ultimate bend strength of about 25%, while the ultimate strain decreased by about 50%. The authors showed that the temperature sensitivity of the mechanical properties of the resin was dependent on the state of the resin. The basic purpose of the work was to examine the effects of irradiation on the properties of the resin and it was found that the degree of irradiation affected the temperature sensitivity of the resin properties.

The dynamic mechanical behaviour of epoxide resins was studied by Mikolajczak *et al.* [72]. This work was carried out on a dynamic mechanical analyser (DMA) and showed that there were three relaxation peaks in the tan(δ) versus temperature curve

at a frequency of 1 Hz, over a temperature range of 125 K to 475 K (-148 °C to 202 °C). Tan(δ), known as the loss tangent, is a viscoelastic property of a material that is related to the inherent structure of the polymer matrix. Each of the peaks that were observed were related to α, β and γ relaxations in the material {figure 2.46}. The temperatures at which these relaxations occurred were generally independent of the cure state of the resin. Similar work was performed by Kinloch *et al.* although only the α and β peaks were detected [73].

2.2.1.1.2 Fracture

Direct comparisons between fracture results from different workers are difficult due to differences in resin chemistry. In a review of the fracture of thermosetting resins, Young [74] showed that for the same resin (Epicote 828), the type and amount of hardener could cause variations in the critical strain energy release rate (G_{Ic}) of between 86 J m^{-2} and 340 J m^{-2}. Phillips *et al.* [75] also showed a great variation in the initiation energy for fracture, G_{Ici}, of between 130 J m^{-2} and 575 J m^{-2}, by varying the type of hardener for Ciba-Geigy MY750. Further work showed that the value of G_{Ici} decreased linearly with increasing log. test speed while the energy for crack arrest, G_{Ica}, was relatively insensitive to the test speed [76].

The fracture behaviour of an epoxy resin, Ciba-Geigy CT200, at various speeds was examined by Young and Beaumont [77]. It was found that high testing speeds favoured continuous crack propagation whilst lower speeds favoured stick-slip crack propagation. The stress intensity factor, K_I, increased linearly with increasing log. test speed, this being consistent with the observations of Scott *et al.* [76]. In the stick-slip region, the value of K_I used was that calculated for a smoothly decelerating crack according to the method of Phillips and Scott [78].

Fracture of epoxy resins above their T_g as a function of the test temperature and crack speed was examined by King and Andrews [79]. It was concluded that the fracture energy obeyed the WLF time-temperature superposition principle[1].

Temperature and test speed effects on the fracture energies for Ciba-Geigy MY750 were studied by Phillips *et al.* [75]. Crack propagation in this resin was found to be stick-slip under all the test conditions investigated, with the crack arrest energy, G_a, being independent of the test variables. The crack initiation energy, G_i, increased with increasing temperature in the range 0 °C to 70 °C. At each individual temperature investigated, G_i was found to decrease logarithmically with increasing speed. The observed changes in G_i were correlated to changes in the size of a hackle zone that was observed as the crack grew slowly, indicating a correlation between G_i and deformation at the crack tip. It was concluded that the variations in G_i were largely due to variations in the critical crack opening displacement δ_c.

Further work by Yamini and Young [65,67] examined the propagation of cracks in epoxy resins. Measurements of the critical stress intensity factor for crack initiation, K_{Ici}, as a function of the cross-head speed over two orders of magnitude using a double torsion technique, showed a decrease with increasing speed whilst the critical stress intensity factor for crack arrest, K_{Ica}, was found to increase slightly. The levels of change in K_{Ici} and K_{Ica} were dependent on the chemical nature of the cured resin and the testing temperature {figure 2.47}. It was found that crack propagation was continuous at low temperatures and stick-slip at high temperatures [67]. The actual temperature of transition from continuous to stick-slip was dependent on the chemical

[1]That features in the temperature response curve can be related to the T_g of the material by a strain rate dependent shift factor.

composition of the resin. It was found that K_{Ic} for continuous crack propagation decreased with increasing temperature in the region of -50 °C to the transition temperature[1]. Above the transition temperature the value of K_{Ici}, increased with increasing temperature whilst K_{Ica} decreased {figure 2.48}. This decrease in K_{Ica} can be compared to the findings of Phillips *et al.* where G_a was found to be independent of the test temperature. The values of K_a and G_a are related by:

$$K_a^2 = E\, G_a \qquad (2.6)$$

for plane stress conditions or:

$$K_a^2 = \frac{E\, G_a}{(1 - \nu^2)} \qquad (2.7)$$

for plane strain conditions. As Young's modulus, E, of the resin decreases with increasing temperature [66,75], the observations of Yamini and Young are not inconsistent with those of Phillips *et al.*.

The effects of strain rate and temperature on the fracture toughness of epoxy resins were studied by Low and Mai [80]. At low strain rates, the value of G_{Ic} decreased with increasing strain rate, but higher strain rates gave values of G_{Ic} that were comparable to those obtained at very low strain rates. Different tests were used in the determination of the values so caution must be exercised in dealing with these results. The temperature work in this paper showed that there was a distinct change in the behaviour of G_{Ic} between impact rate tests and slow speed tests. The impact tests gave an increase in G_{Ic} with increasing temperature up to a peak at about 25 °C, above which G_{Ic} decreased.

---

[1] From continuous to stick-slip.

Work on fracture of epoxy resins by Ochi *et al.* [81] showed that the fracture toughness of some resins could be largely independent of the test temperature in the range -60 °C to 140 °C. The results quoted in this paper showed little temperature sensitivity of K_c below room temperature for either of the resins tested. A different type of resin showed a sharp increase in K_c with increasing temperature from 20 °C to 130 °C.

The temperature dependence of the fracture toughness of some epoxy resins was examined by Mizutani and Yoshii [82]. The actual forms of the K_{Ic} versus temperature plots varied according to the type of resin, but they all displayed a slight increase from -35 °C to room temperature, followed by a rapid increase to a peak value, and a subsequent drop with a further increase in the temperature. The temperature of the peak was taken by the authors to be the T_g. Three types of crack propagation were observed depending on the temperature. These were: continuous stable propagation at low temperatures, stick-slip at temperatures from about 0 °C to the T_g and tearing with shear bands at temperatures above the T_g. For all the resins tested the Young's modulus decreased linearly with increasing temperature up to the T_g followed by a rapid drop above the T_g.

2.2.1.1.3 Conclusion of Epoxy Resins

Although there were a large number of detail differences in the response of the different epoxy resins, some general trends could be identified. Generally, the yield strength and Young's modulus decreased with increasing temperature, the percentage decrease in the strength being greater than for the modulus for the same increase in temperature. Most workers have shown these decreases to be linear except when the T_g was approached. Increases in both properties with increasing strain rate have been

observed, all workers showing a linear relationship with log. strain rate. The coefficient of proportionality has been shown to be dependent on the temperature and the resin condition.

Fracture behaviour showed a distinct change of mode when the temperature increased, being one of continuous crack growth at low temperatures and stick-slip at high temperatures. The fracture toughness of the resins increased with increasing temperature. The response to increasing temperature was shown to be simulated by a decrease in speed. Low strain rates favoured stick-slip crack propagation while high strain rates favoured continuous crack propagation.

2.2.1.2 Polyester Resins

Very little work appears to have been published on the variation in mechanical properties with speed and temperature for polyester resins. Generally, polyester resins are more brittle than epoxy resins [74] yet fracture in polyester resins has been found to be normally of the stick-slip type.

In a review [83], Harding reported that the dynamic flow stress in compression for some polyester resins was more than double that for quasi-static testing.

Various workers have investigated the fracture behaviour of polyesters and have found that it is dependent on the synthesis procedure, molar ratio of unsaturated to saturated acid, the post cure condition and the degree of moisture uptake [84-89].

Some work on speed effects on the properties of polyester resins was presented in section 2.1.4.1.1.1. This work showed that the fracture toughness of a polyester resin increased with increasing test speed.

2.2.2 Composite Properties

Having examined how the mechanical properties of resins and glass fibres vary with strain rate and temperature, it is now appropriate to consider how the variations affect the properties of a composite utilizing the resins as matrix materials. In this review mainly glass reinforcement will be considered, although other types of reinforcement have been studied. Carbon fibre reinforcement has been studied but these composites have been shown to be less rate and temperature sensitive than glass reinforced composites [88].

Pink and Campbell [90,91] showed that the deformation of composites is largely controlled by the matrix, hence the variations in fibre properties with the test variables have been disregarded in this work. This means that the trends that were observed in section 2.2.1 can be applied to the behaviour of composites. The tests that were performed in this work were tensile tests so that the observations may not apply to other types of loading. Also this work was carried out using woven glass cloth as the reinforcement, so the observations may not apply to other reinforcement types or arrangements.

2.2.2.1 Epoxy Resin Reinforcement

Deformation characteristics of glass reinforced epoxy resin composites were studied by Pink and Campbell [90,91]. It was found that at low strain rates there was a slight increase in the strength with increasing strain rate, but that at strain rates in excess of about 0.1 s^{-1}, the increase in strength was more marked. For samples that were tested with the warp direction parallel to the tensile direction, a linear decrease with increasing temperature was recorded. Similar behaviour was observed for the fracture stress, although linearity was not exactly followed. This work showed that the stress

in this material was independent of the strain rate at very low strains, below about 0.5%.

In the second part of this work [91] the temperature dependence of the strain rate sensitivity, λ, was measured. The three regions of deformation that were observed for the pure epoxy resin [64] were also found for the reinforced material and the transition temperatures between the regions were the same for the reinforced material as for the pure epoxy, substantiating the claim that the deformation characteristics of woven glass cloth composites are determined by the behaviour of the matrix. In this work it was noted that the strain rate sensitivity of the reinforced material was greater than for the unreinforced epoxy. It was concluded that there was a stress concentration effect due to the presence of the fibres that accounted for this observation.

The effect of strain rate on the longitudinal and transverse properties of S glass-epoxy composites was examined by Daniel [92]. This work showed very little variability in the elastic and strength properties, but there was an indication that the ultimate strain might have increased at the highest strain rates used for both the longitudinal and transverse directions. Interlaminar shear tests showed little change in the shear modulus or strength with strain rate, but the ultimate strain was found to increase from 7×10^{-3} to 13×10^{-3} for a strain rate increase from $2.8 \times 10^{-4}\ s^{-1}$ to $14\ s^{-1}$.

Some work has been carried out on the effects of temperature on the mechanical properties of sheet moulding compounds by Springer [93]. This work was mainly concerned with polyester resin SMCs but also considered an example using an epoxy resin. The compression strength and modulus of all the SMCs decreased approximately linearly with increasing temperature, although there was a suggestion that the decrease was less at lower temperatures {figure 2.49}. The slope of the

strength versus temperature response was strongly dependent on the material type and testing direction but the slope of the compression modulus versus temperature response was relatively independent of the material type. The flexural strength and modulus showed similar trends to the compression tests.

Impact tests on SMCs by Johnson and Lynskey using a falling weight test, showed a linear decrease in the failure energy with increasing temperature over the range -196 °C to 120 °C [94]. The failure energy at 120 °C was about half of that for -196 °C {figure 2.50}. Charpy tests showed that the decrease in impact energy with temperature was dependent on the fibre volume fraction, with material having a fibre volume fraction of 57% being less temperature sensitive than for 32%.

Work on carbon-epoxy specimens showed that the mode I interlaminar fracture toughness decreased from 180 J m^{-2} to 40 J m^{-2} for an increase in loading rate of four orders of magnitude [95].

It has been reported that the rate dependency of composite toughness is similar to that of the matrix toughness [96]. This work was concerned with the interlaminar fracture toughness of unidirectional carbon-epoxy material tested in mode I and mode II loading. It was found that the fracture toughness in both modes was independent of the loading rate at slow speeds, but that high speeds the fracture toughness decreased rapidly. Similar behaviour was observed for the crack tip plastic zone size, even though the zone size was considerably greater than the inter-fibre distance.

Woven glass cloth-epoxy specimens as tested in compression at quasi-static and impact rates, have been reported by Harding [83]. The compressive modulus of this material was independent of the strain rate but the stress and strain to failure

approximately doubled on increasing the strain rate from the quasi-static 7.4×10^{-5} s^{-1} to the impact rate of 564 s^{-1}.

2.2.2.2 Polyester Resin Matrix

Glass cloth-polyester specimens were tested in tension by Harding and Welsh over seven orders of magnitude of strain rate, using the split Hopkinson pressure bar (SHPB) [97,98]. The failure strength at impact rates was approximately twice as high as at low strain rates. This trend was found for both the warp orientations investigated, at 0° and at 45° to the tensile direction. The mode of failure was found to be different with only a limited amount of fibre pull-out at low strain rate, but a large degree of pull-out at impact speed.

The speed sensitivity of glass cloth-polyester composites is dependent on the type of reinforcement [83]. Plain weave glass cloth-polyester material has been shown to be more strain rate sensitive than the same resin containing a satin weave glass cloth. Both types of material showed a nonlinear log. strain rate response of the elastic modulus, as the increase in modulus for a strain rate increase from 10^{-4} to 10 s^{-1} was about 40%, while that from 10 s^{-1} to 1000 s^{-1} was about 60% {figure 2.51}. Similar behaviour was reported for carbon and Kevlar reinforced polyesters, implying that the strain rate sensitivity of the matrix was more important than that of the reinforcement.

2.2.3 Conclusions of Composite Properties

Some general trends have been identified for both the monolithic resins and composites incorporating these resins. The trends in the properties of the monolithic resins have been summarised in section 2.2.1.1.3 for epoxy resins, but many of the

trends are reflected in trends of the behaviour of the composite materials. These trends can be summarised as follows:

1. Strength and stiffness both increase with increasing strain rate, the increases being approximately linear with increasing log. strain rate.
2. Strength and stiffness decrease with increasing temperature, the decreases being nonlinear and dependent on the strain rate.
3. The sensitivity of the properties to strain rate and temperature is dependent on the fibre type and arrangement.
4. The strain rate sensitivity of the fracture toughness is dependent on the fracture behaviour of the fibres as well as the matrix.

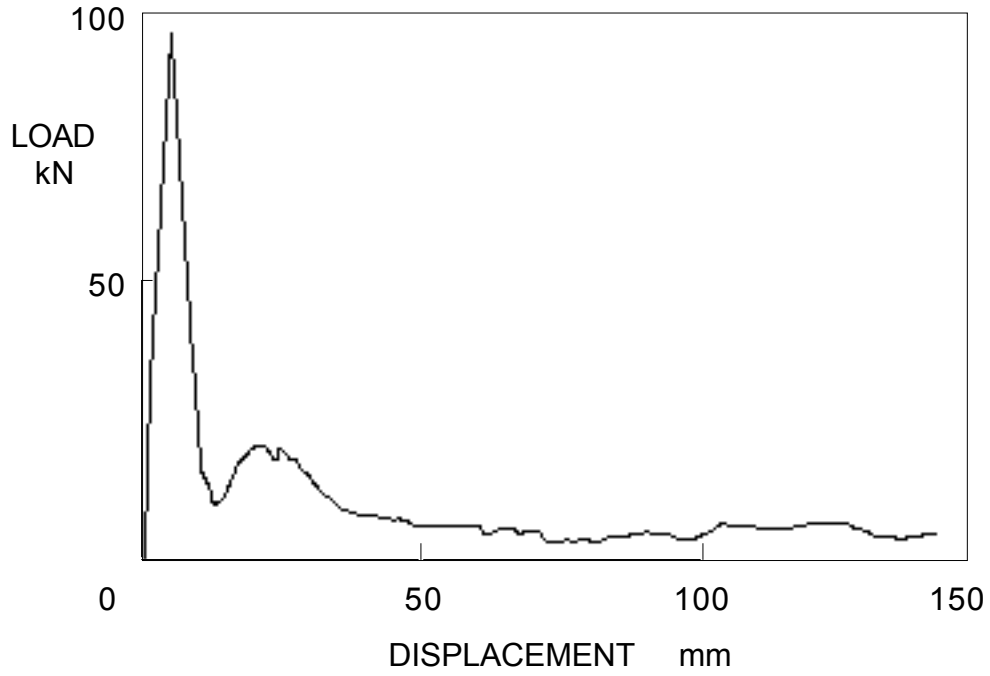

Figure 2.1 Force-Displacement trace from an axially compressed composite tube that underwent central catastrophic failure [19].

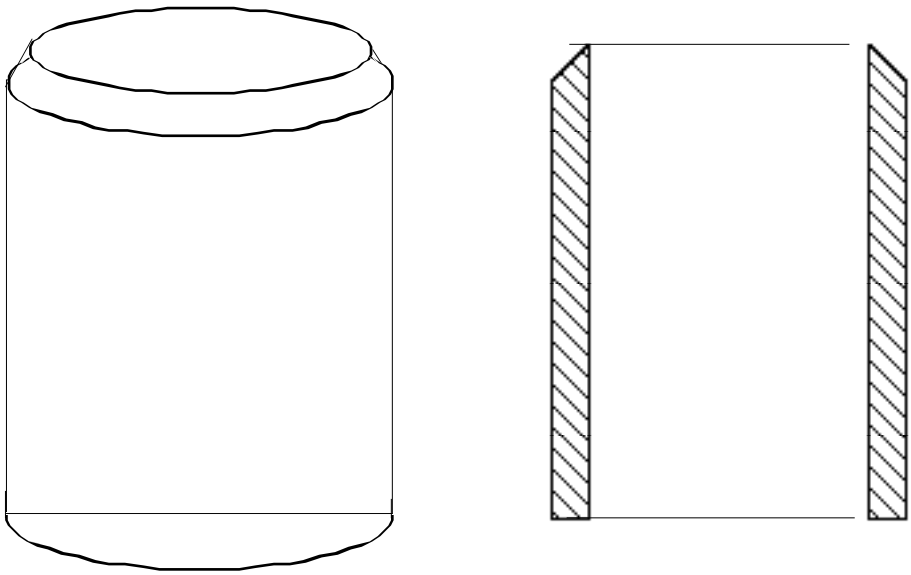

Figure 2.2 Chamfered tube shown in whole and in section (not to scale).

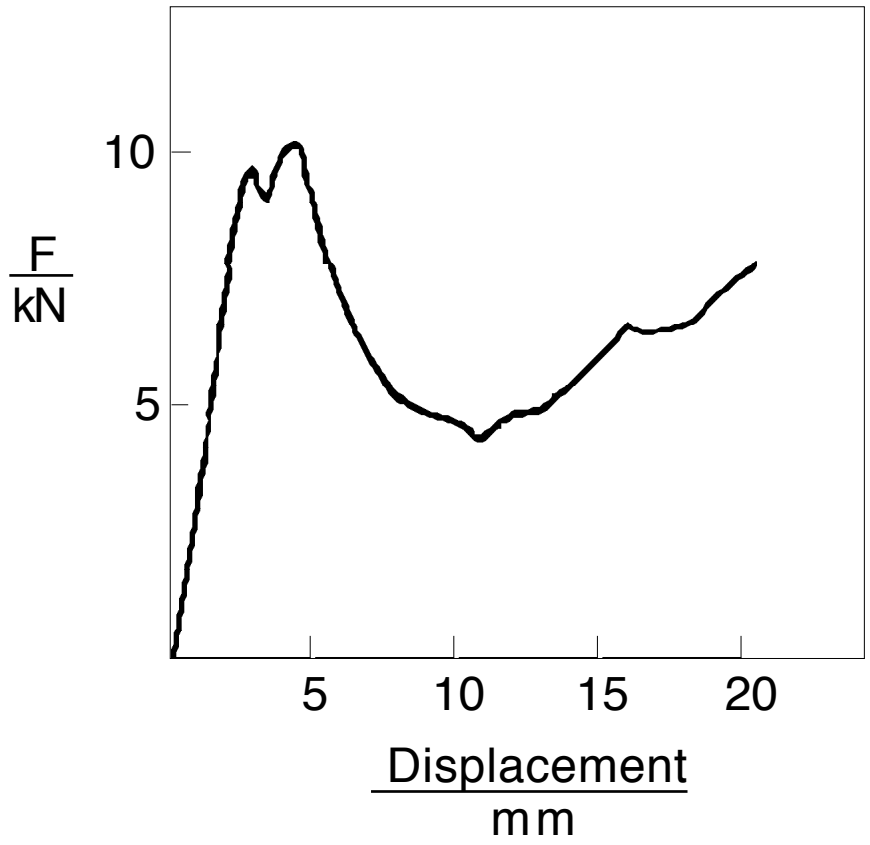

Figure 2.3 Typical force-displacement trace from a Kevlar-epoxy tube [17].

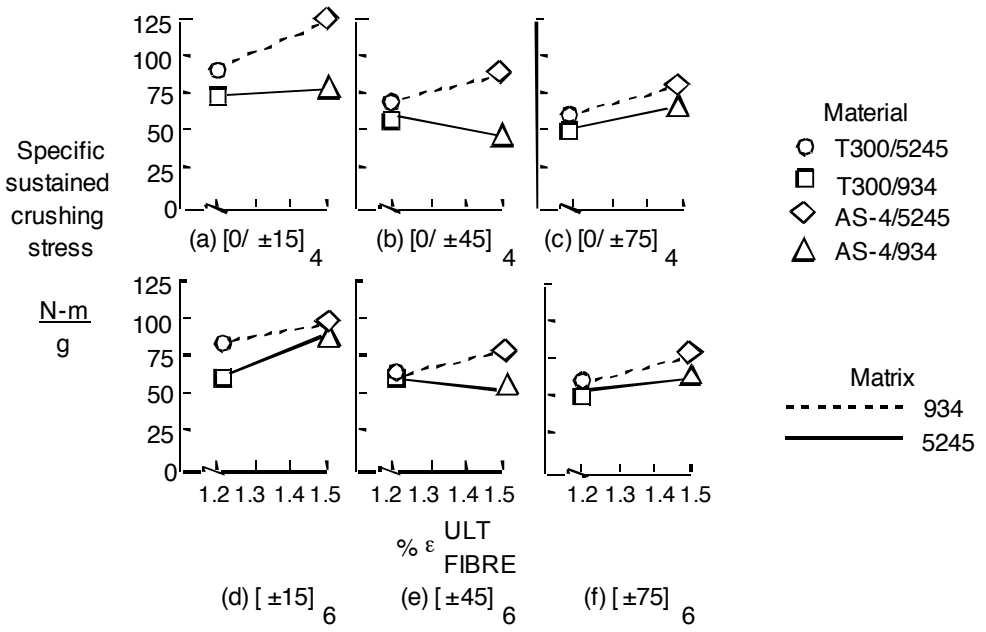

Figure 2.4 Specific energy absorption as a function of the fibre strain to failure for tubes manufactured using two types of carbon fibres with different strains to failure in two different epoxy resins and varying fibre arrangements [27].

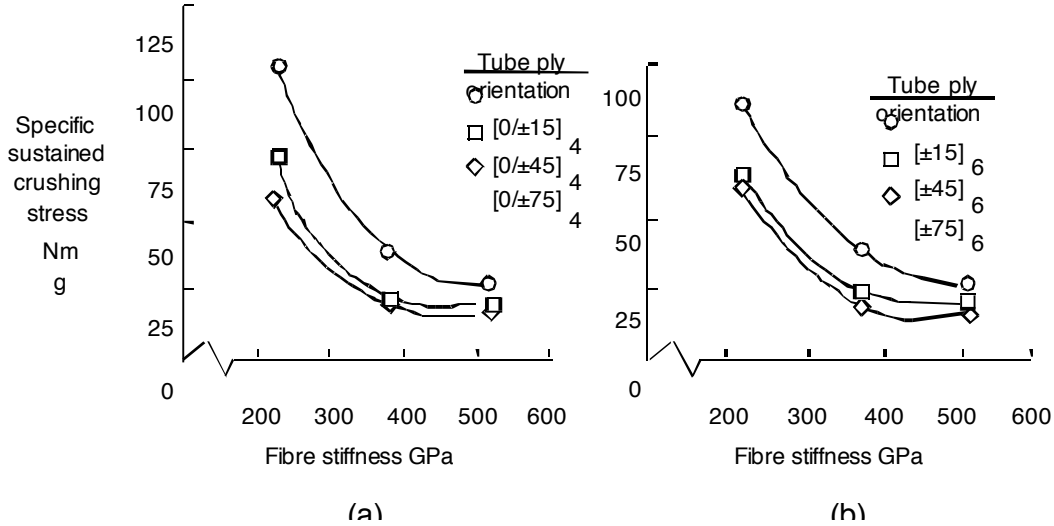

Figure 2.5 Plot of specific energy absorption as a function of the fibre stiffness for carbon-epoxy tubes with different fibre orientations [27].

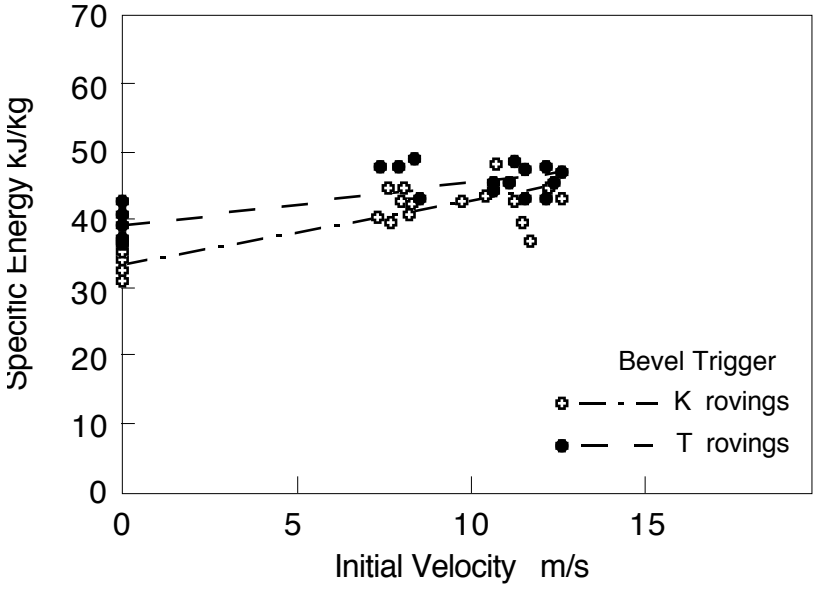

Figure 2.6 (a) Plot of specific energy absorption as a function of the crush speed for circular pultruded tubes with a polyester resin matrix [31].

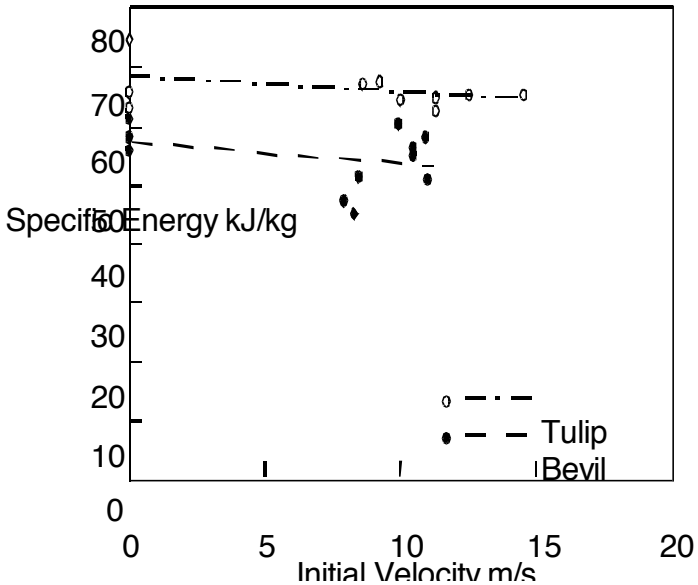

Figure 2.6 (b) Plot of specific energy absorption as a function of the crush speed for circular pultruded tubes with a vinylester resin matrix [31].

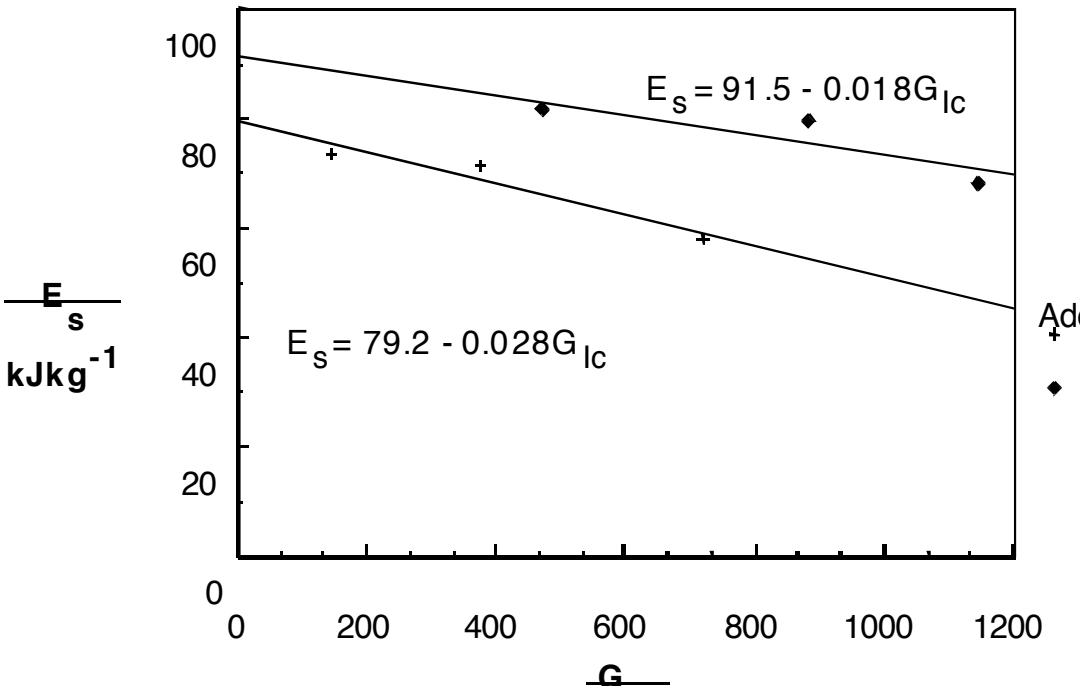

Figure 2.7 Plot of specific energy absorption as a function of the fracture toughness of the bulk resin for filament wound tubes with additives in the basic polyester resin, Crystic 272 [30].

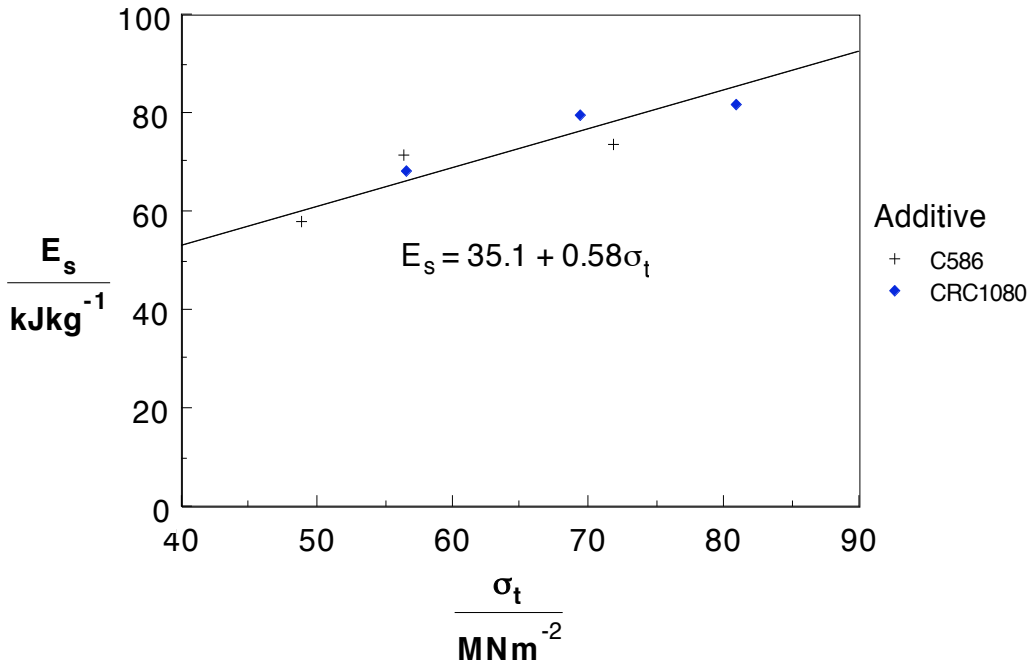

Figure 2.8 Plot of specific energy absorption as a function of the tensile strength of the bulk resin for filament wound tubes with additives in the basic polyester resin, Crystic 272 [30].

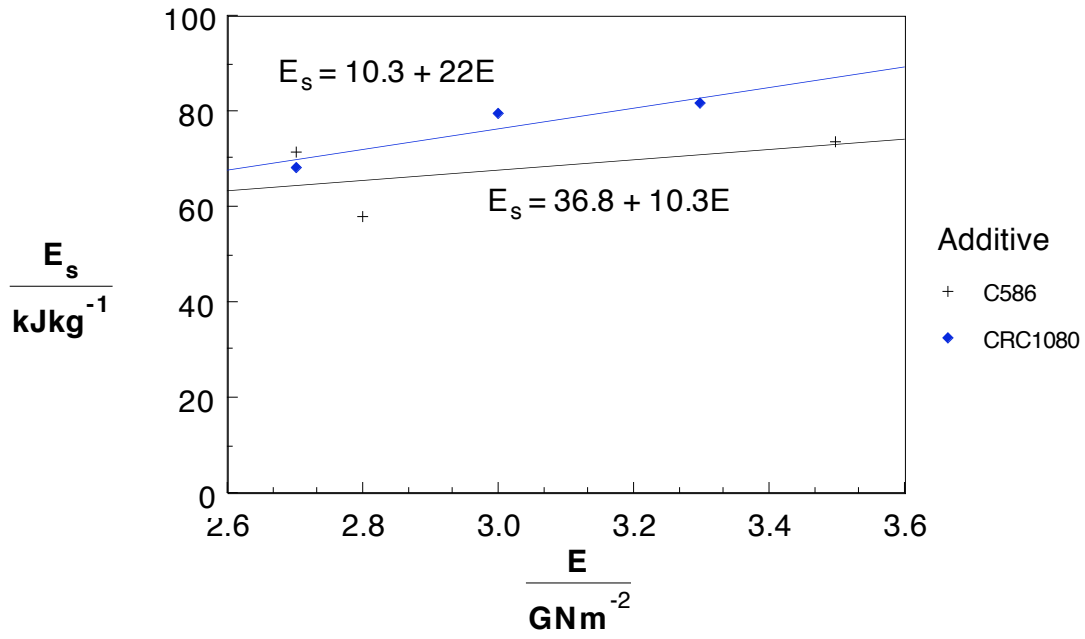

Figure 2.9 Plot of specific energy absorption as a function of the Young's modulus of the bulk resin for filament wound tubes with additives in the basic polyester resin, Crystic 272 [30].

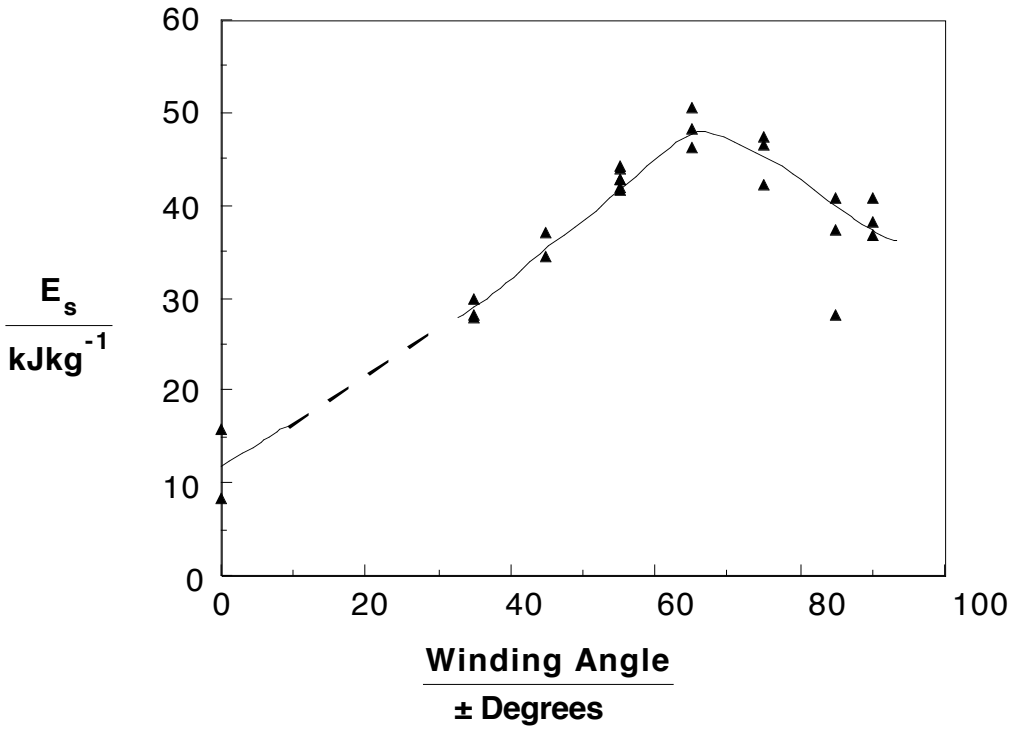

Figure 2.10 Plot of specific energy absorption as a function of the winding angle for filament wound glass-polyester tubes [34,39].

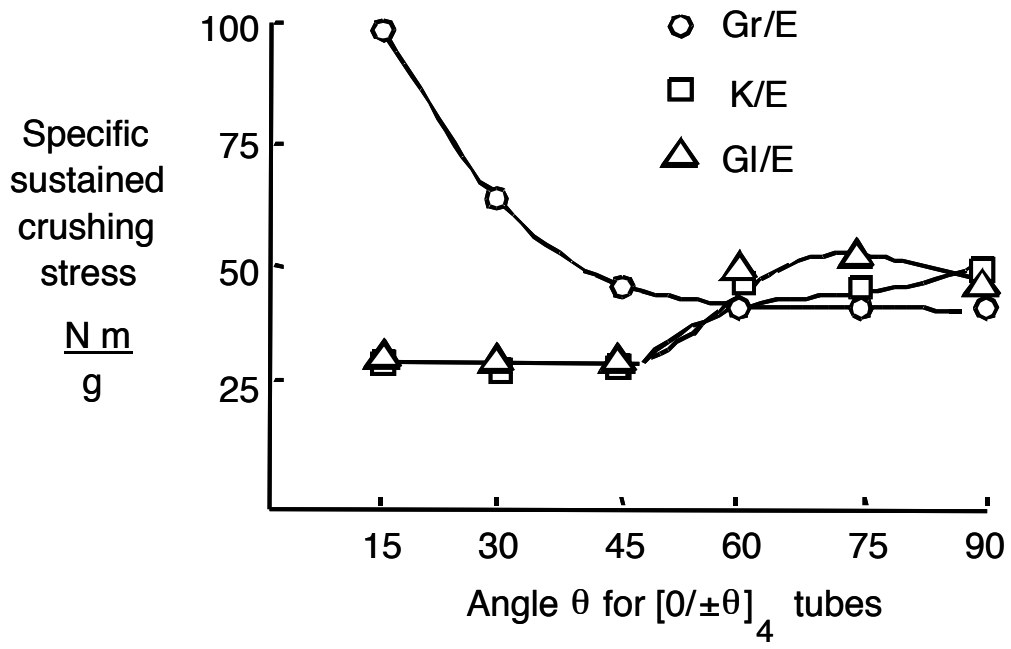

Figure 2.11 Plot of specific energy absorption as a function of the winding angle for carbon, Kevlar and glass fibre reinforced tubes using an epoxy resin matrix [36].

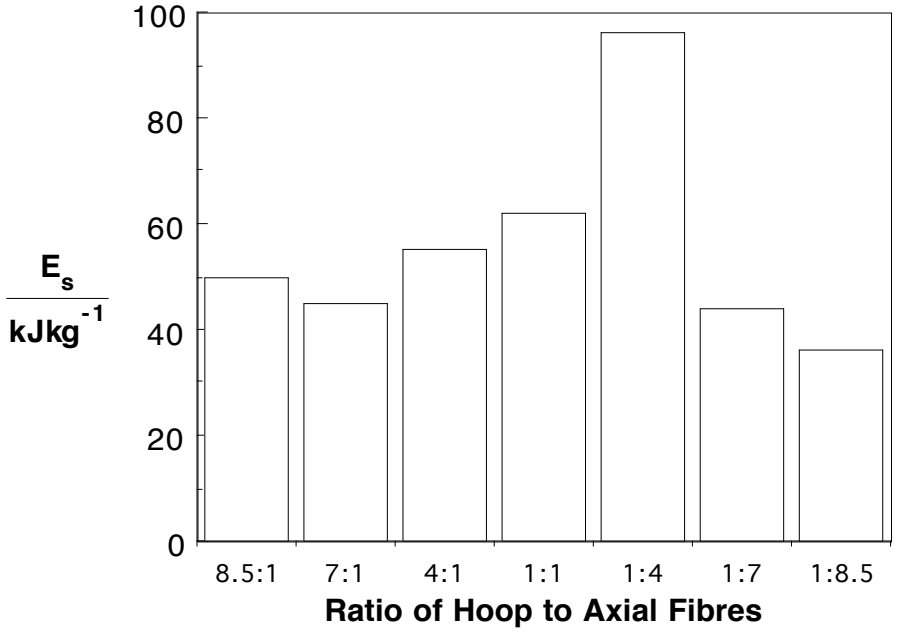

Figure 2.12 Specific energy absorption varying with proportion of hoop to axial fibres for woven glass cloth-polyester tubes [34,39].

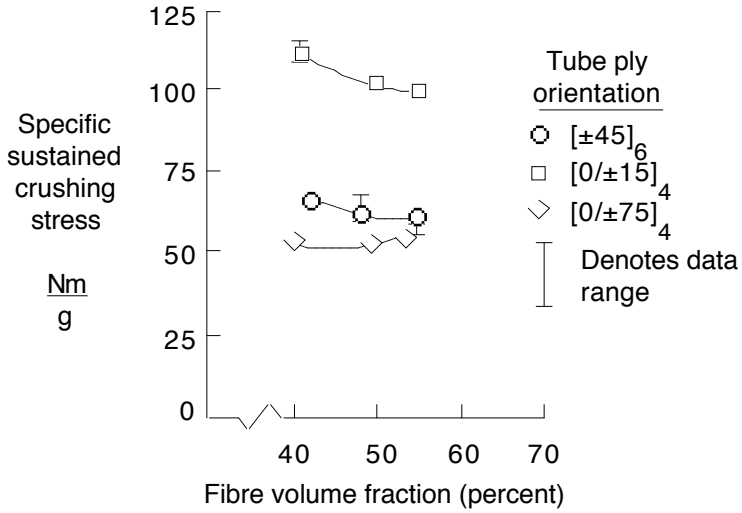

Figure 2.13 Plot of specific energy absorption as a function of the fibre volume fraction for carbon-epoxy tubes with varying lay-ups [36].

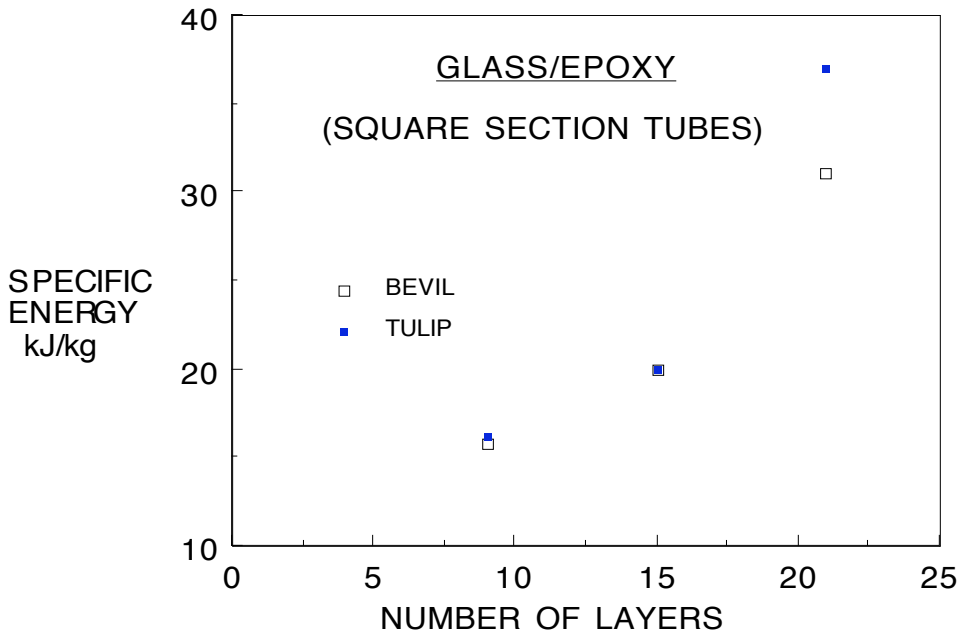

Figure 2.14 Plot of specific energy absorption as a function of the number of layers in the tube wall, hence the wall thickness [41].

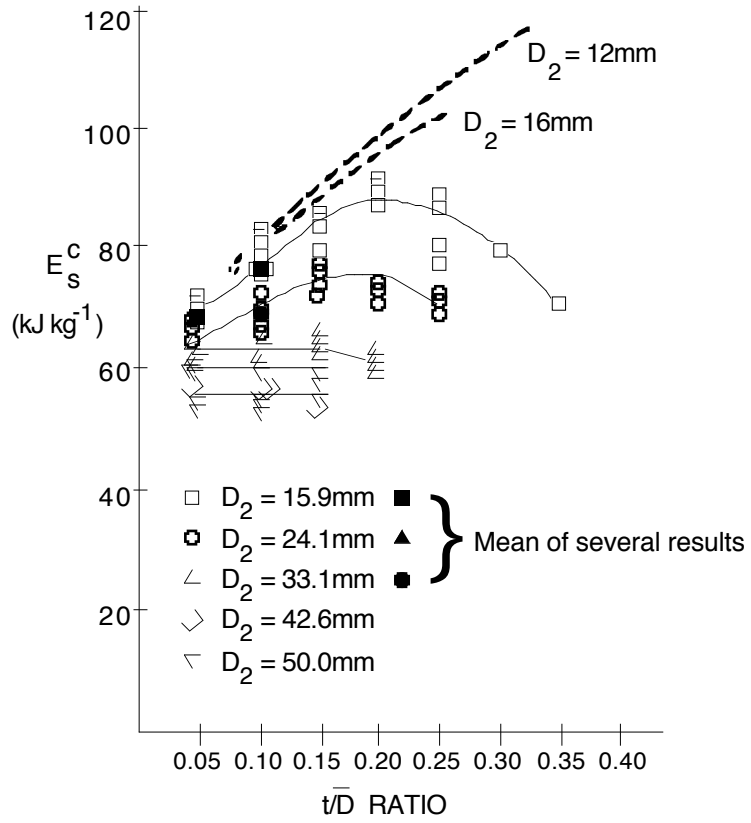

Figure 2.15 Plot of specific energy absorption as a function of the t/D ratio for glass cloth-epoxy tubes [44,46].

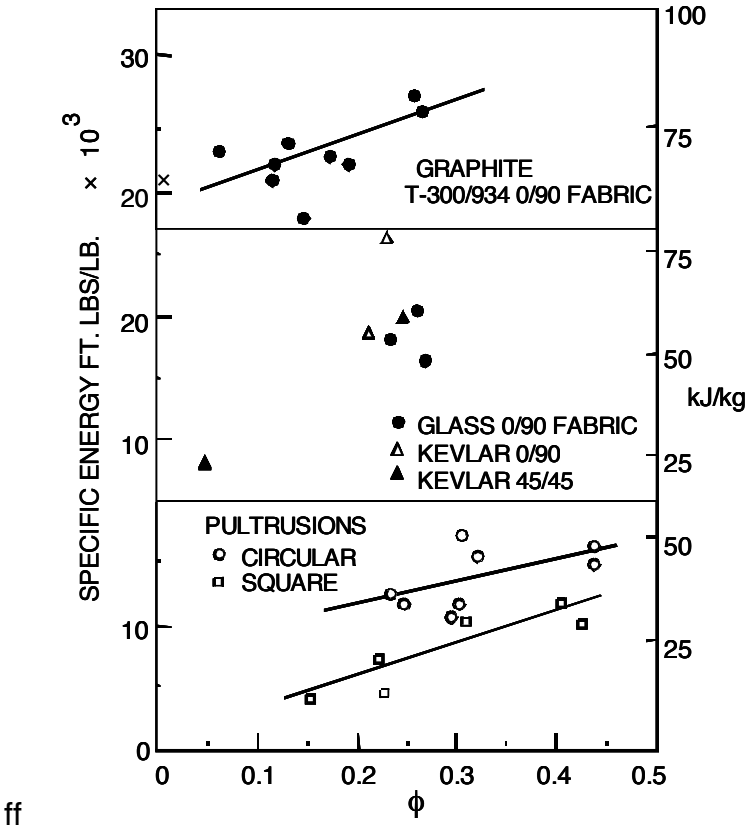

ff

Figure 2.16 Plot of specific energy absorption as a function of the specific density for various types of tube [17].

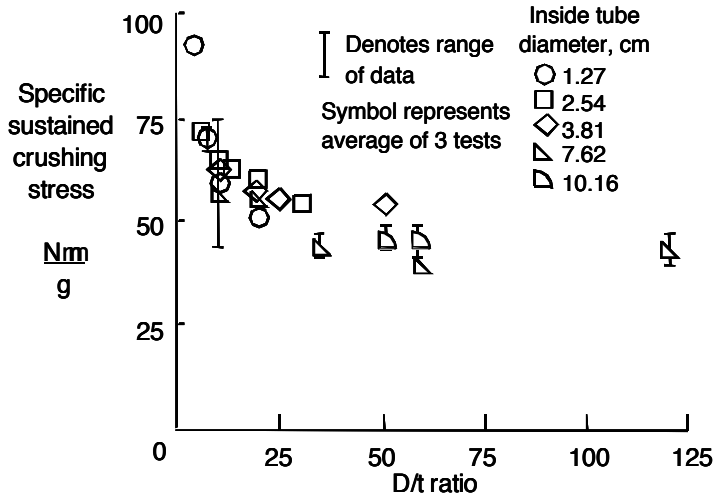

Figure 2.17 (a) Plot of specific energy absorption as a function of the D/t ratio for carbon-epoxy tubes [45].

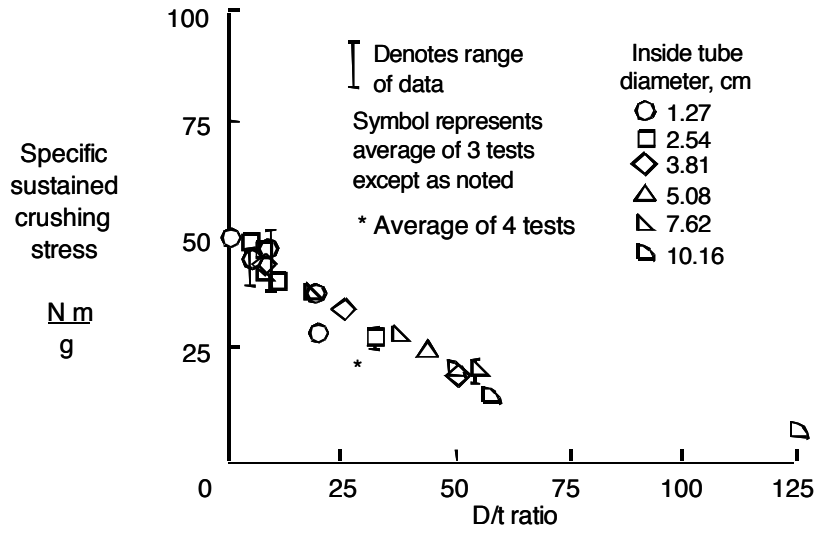

Figure 2.17 (b) Plot of specific energy absorption as a function of the t/D ratio for Kevlar-epoxy tubes [45].

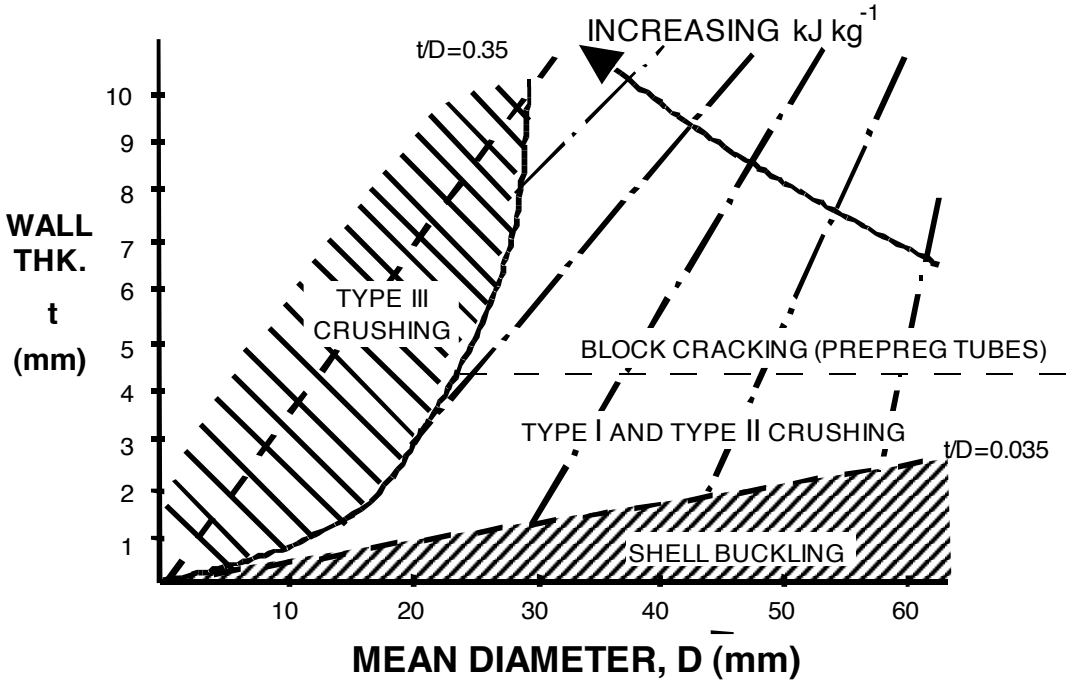

Figure 2.18 Map of the different modes of crushing for glass cloth-epoxy tubes with varying t and D as identified by Fairfull [44,46,51].

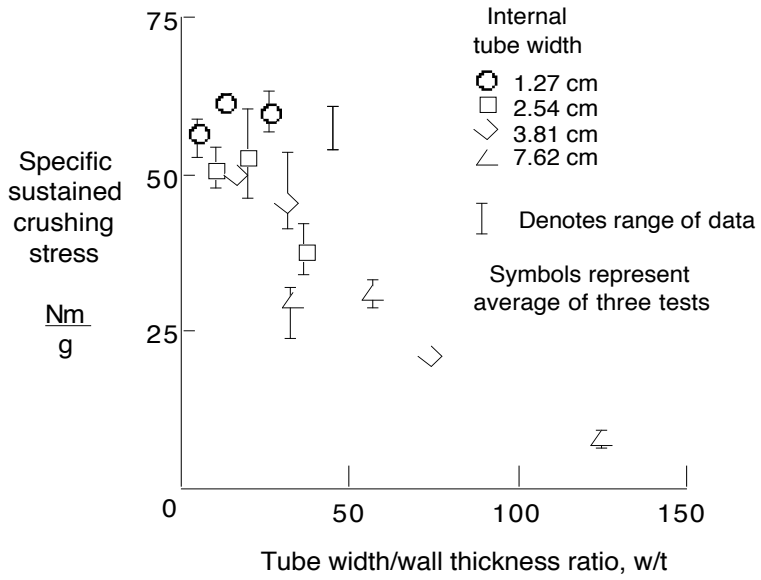

Figure 2.19 (a) Plot of specific energy absorption as a function of the W/t ratio for square section carbon-epoxy tubes [36].

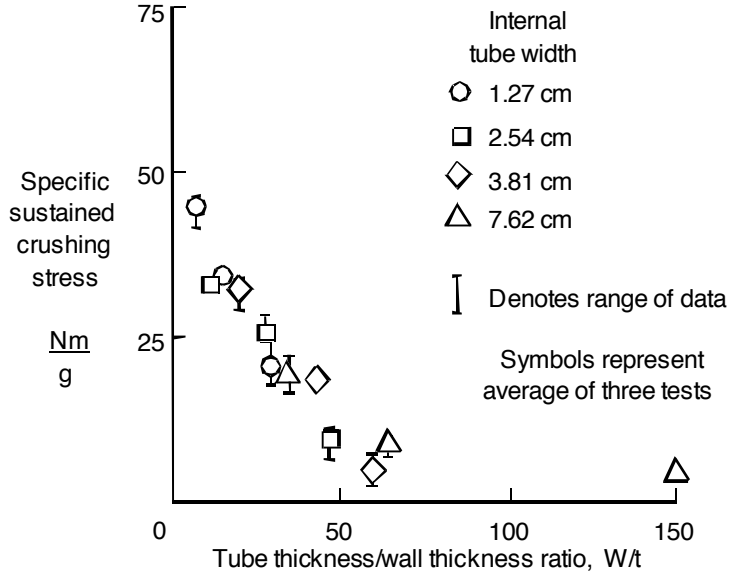

Figure 2.19 (b) Plot of specific energy absorption as a function of the W/t ratio for square section Kevlar-epoxy tubes [36].

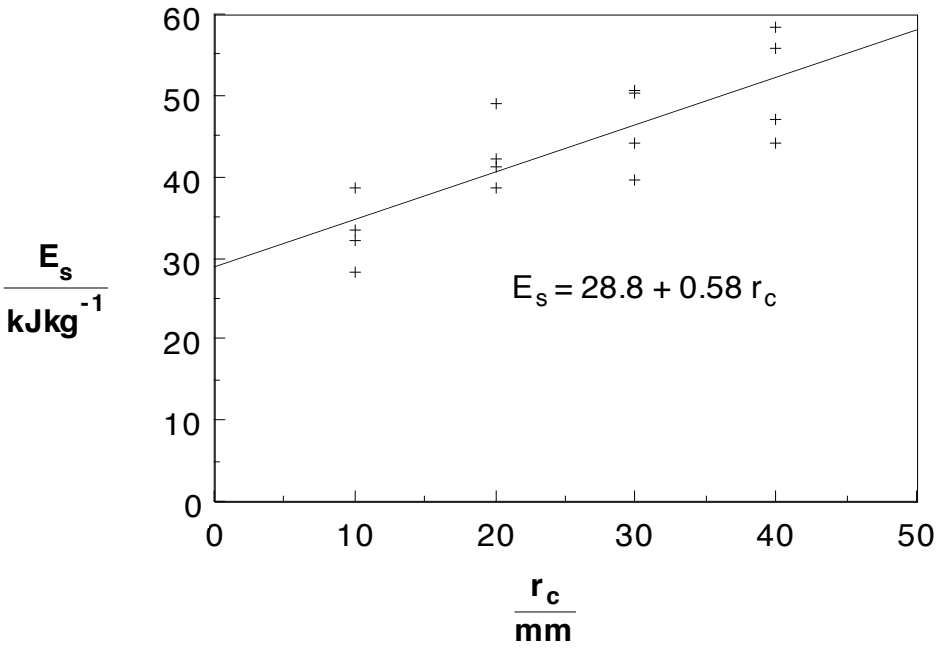

Figure 2.20 Plot of specific energy absorption as a function of the tube corner radius for square section tubes [43].

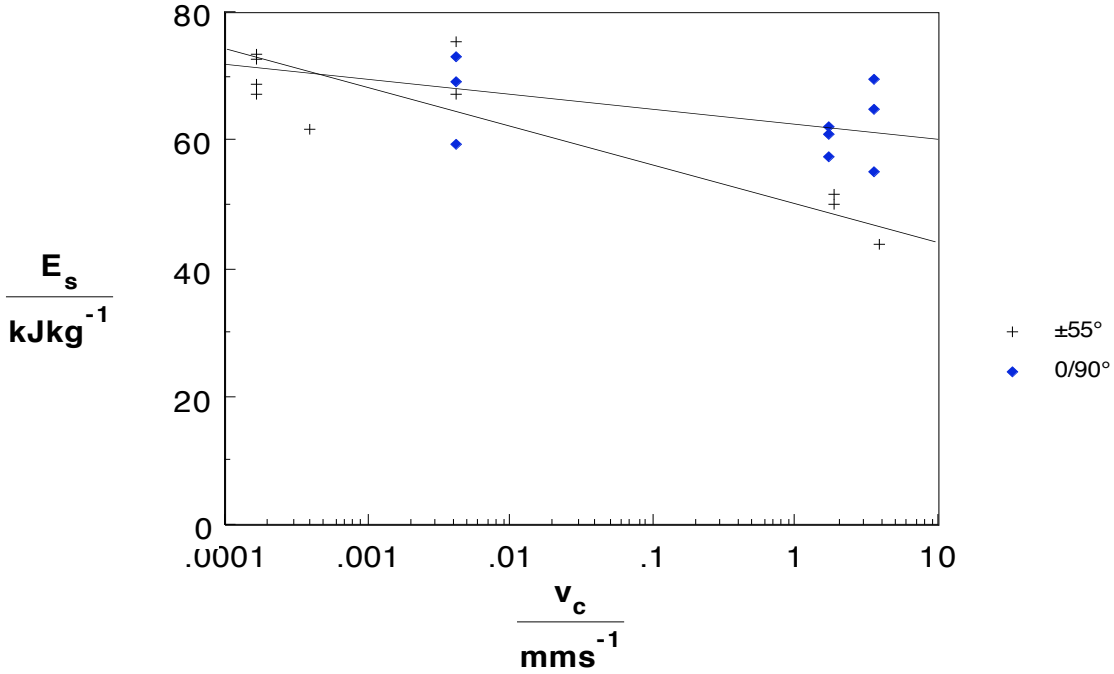

Figure 2.21 Plot of specific energy absorption as a function of the crush speed for filament wound glass-polyester tubes with two different fibre lay-ups [25].

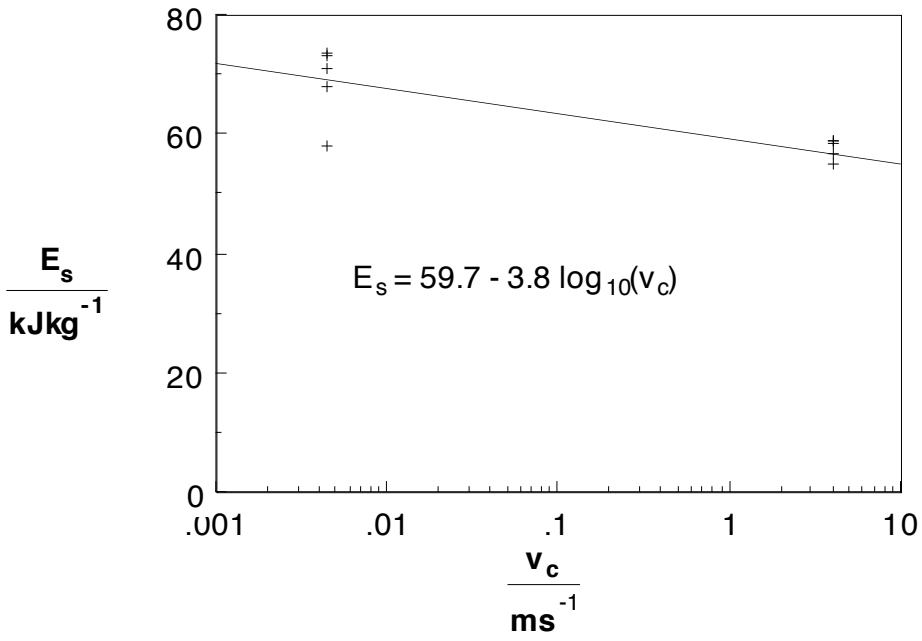

Figure 2.22 Plot of specific energy absorption as a function of the crush speed for filament wound glass-polyester tubes with a winding angle of 90°/0°/0°/90°, incorporating various amounts of C586 additives to the resin [30].

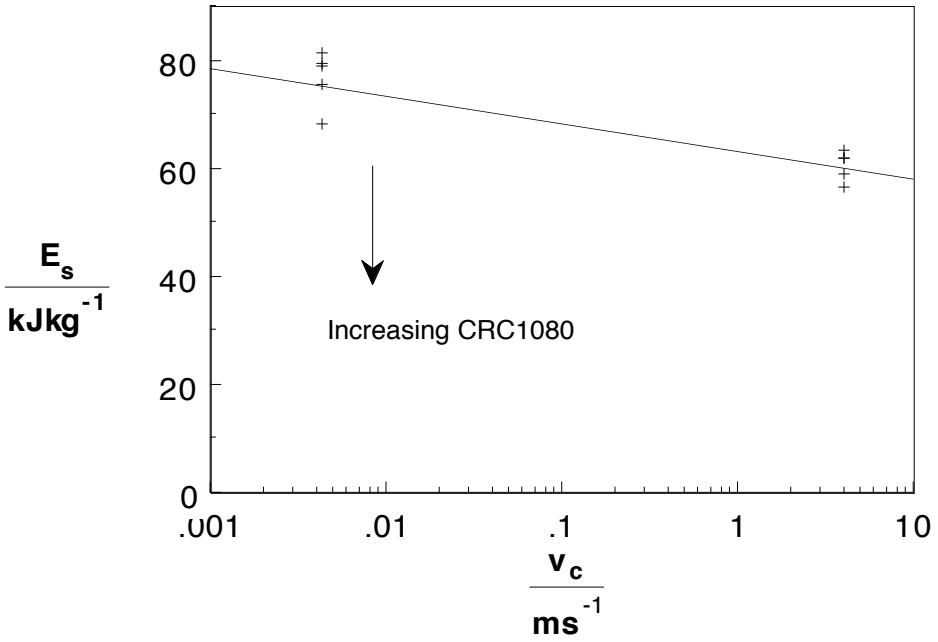

Figure 2.23 Plot of specific energy absorption as a function of the crush speed for filament wound glass-polyester tubes with additions of CRC 1080 to the base resin [30].

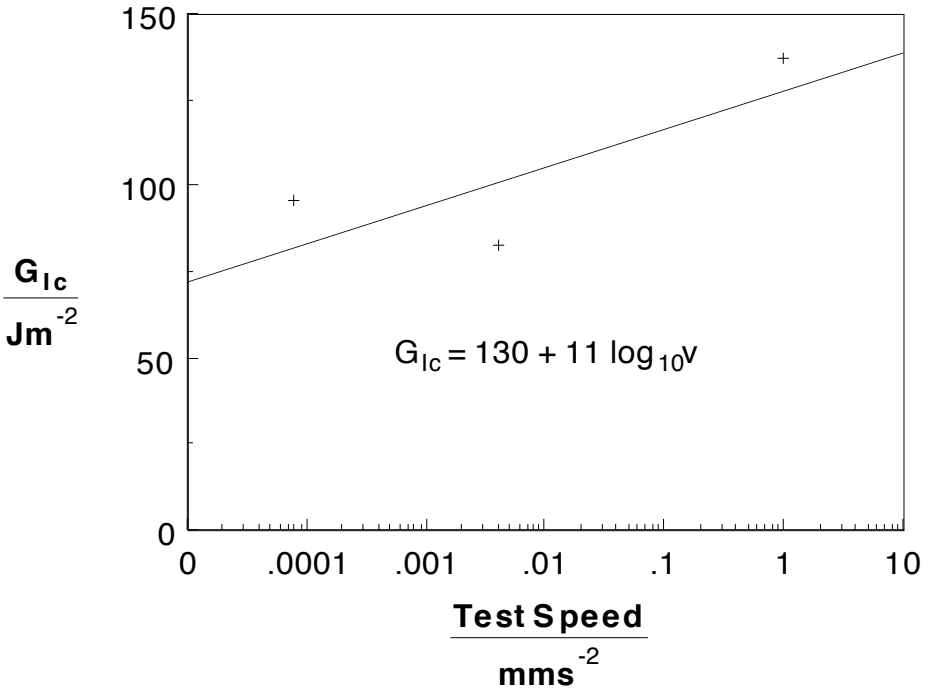

Figure 2.24 Plot of matrix fracture toughness as a function of the testing speed for Scott Bader Crystic 272 [33].

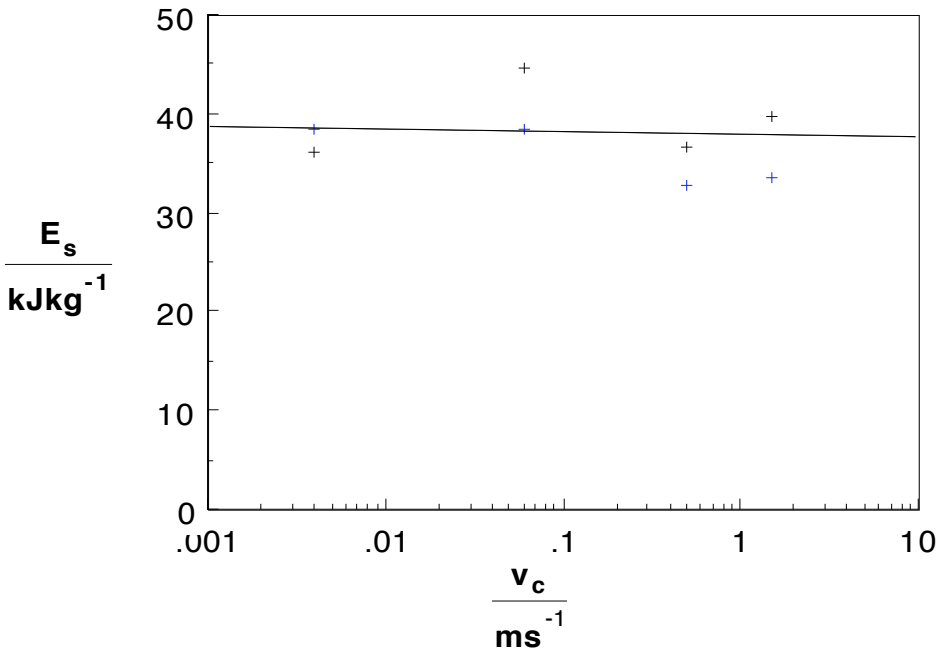

Figure 2.25 Plot of specific energy absorption as a function of the test speed for chopped-strand-mat-polyester tubes [21].

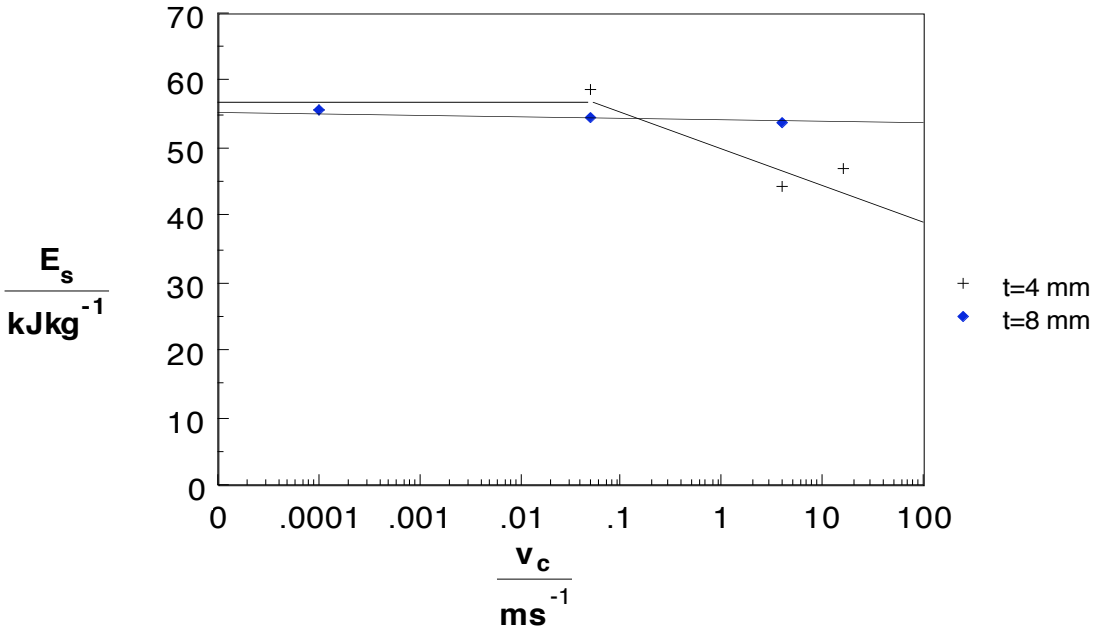

Figure 2.26 Plot of specific energy absorption as a function of the crush speed for glass-polyester tubes produced by resinjection with differing wall thicknesses [43].

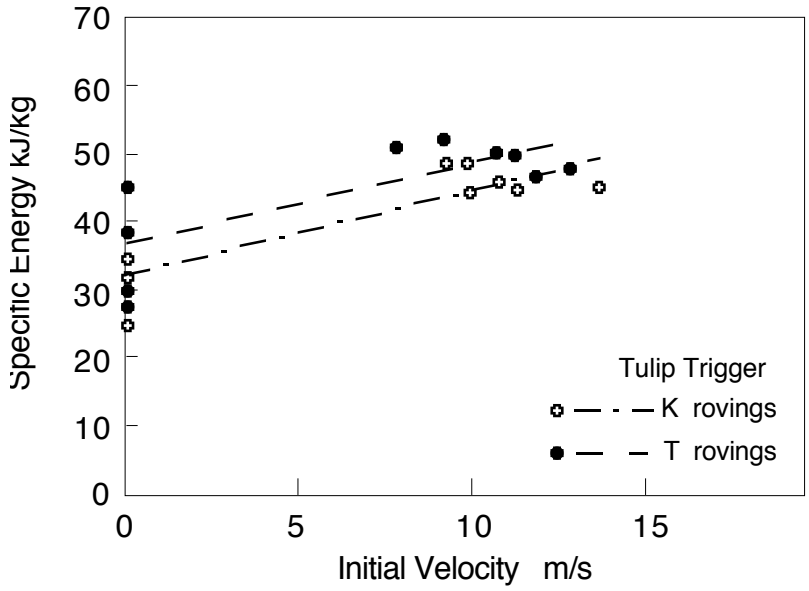

Figure 2.27 Plot of specific energy absorption as a function of the crush speed for glass-polyester pultrusions [31].

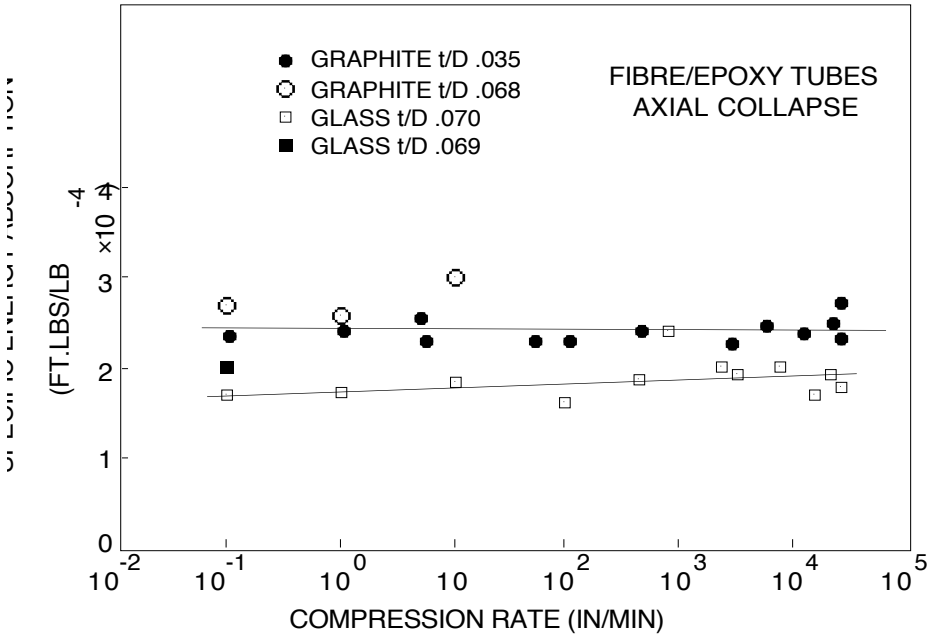

Figure 2.28 Plot of specific energy absorption as a function of the crush speed for glass cloth-epoxy tubes [17].

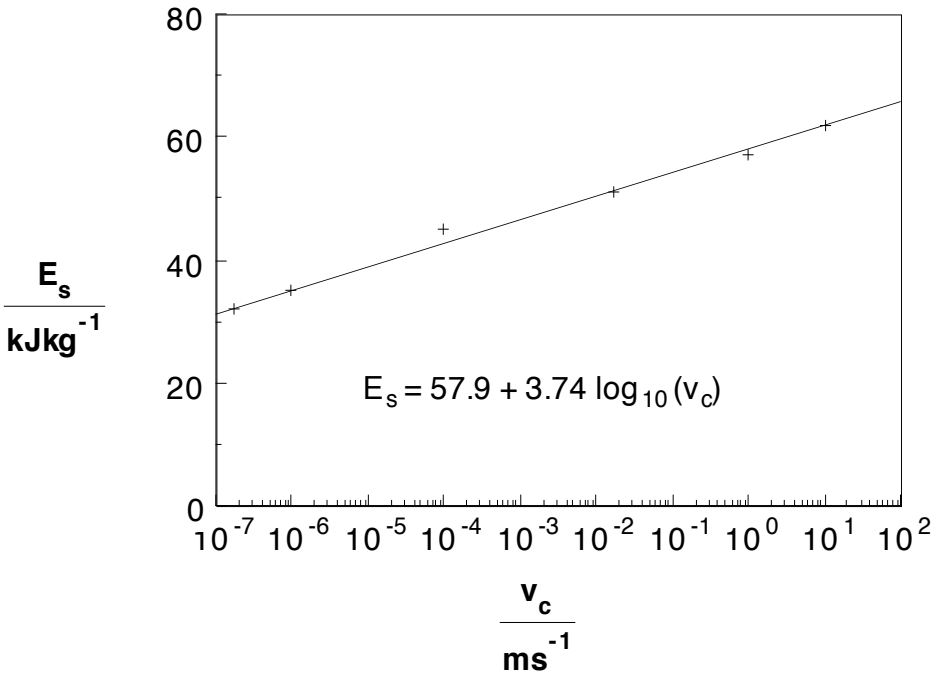

Figure 2.29 Plot of specific energy absorption as a function of the crush speed for glass cloth-epoxy tubes [60].

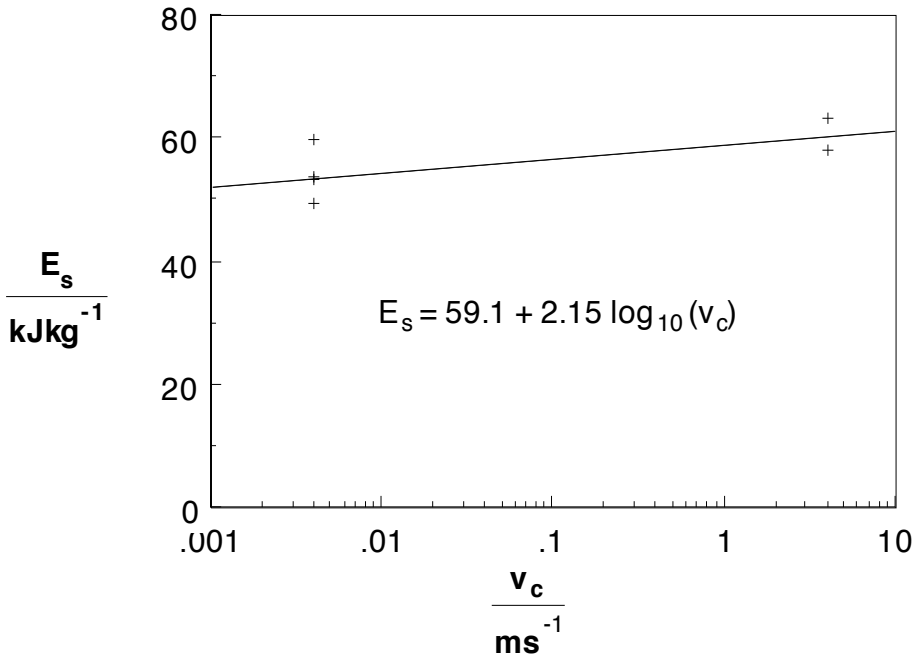

Figure 2.30 Plot of specific energy absorption as a function of the crush speed for filament wound glass-epoxy tubes with a lay up of 0-90° [33].

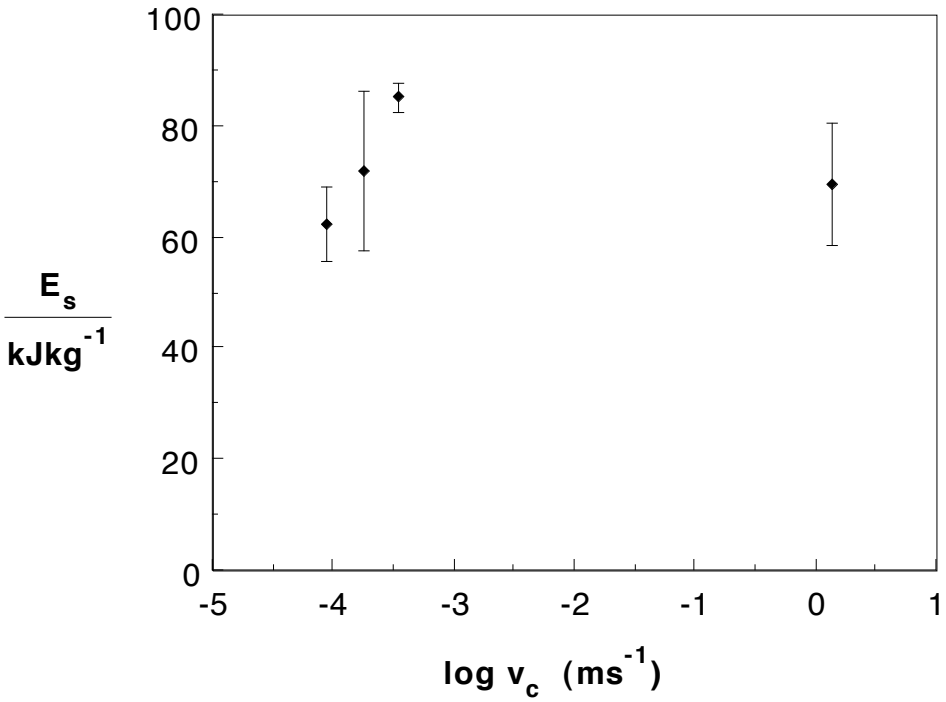

Figure 2.31 Specific energy absorption as a function of the log. crush speed for a cellular structure made from glass cloth-epoxy [50].

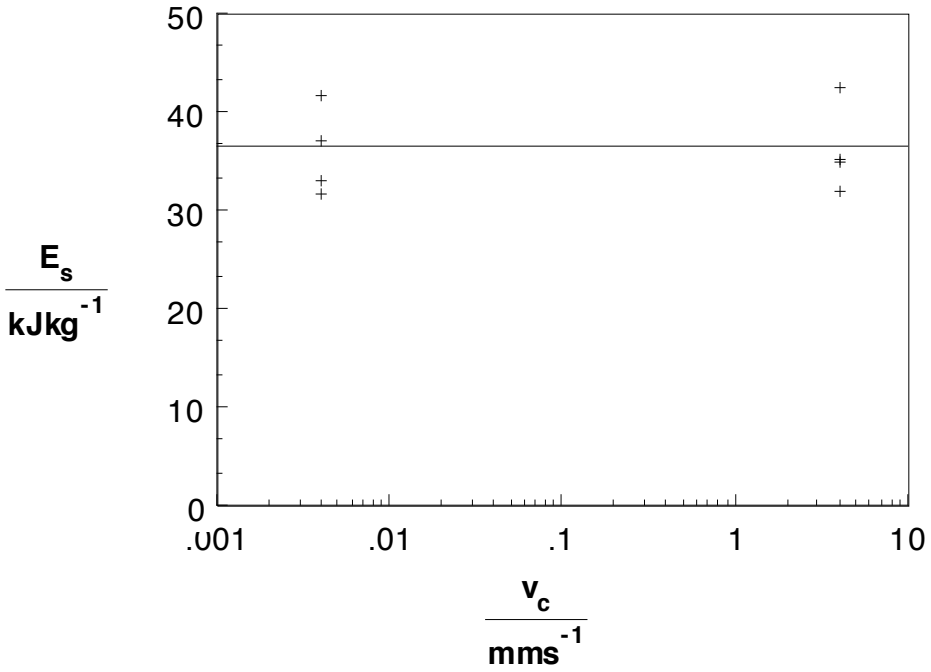

Figure 2.32 Plot of specific energy absorption as a function of the crush speed for filament wound glass:phenolic tubes [33].

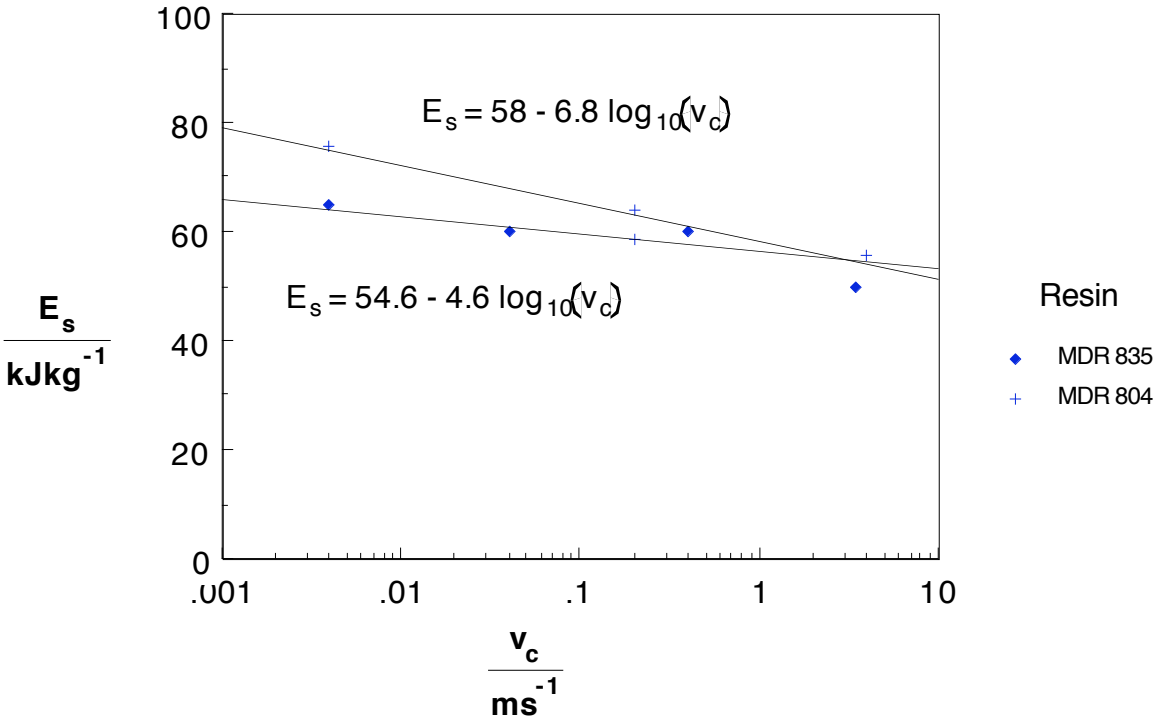

Figure 2.33 Specific energy absorption as a function of the testing speed for glass mat:acrylic tubes with two different matrix resins [35].

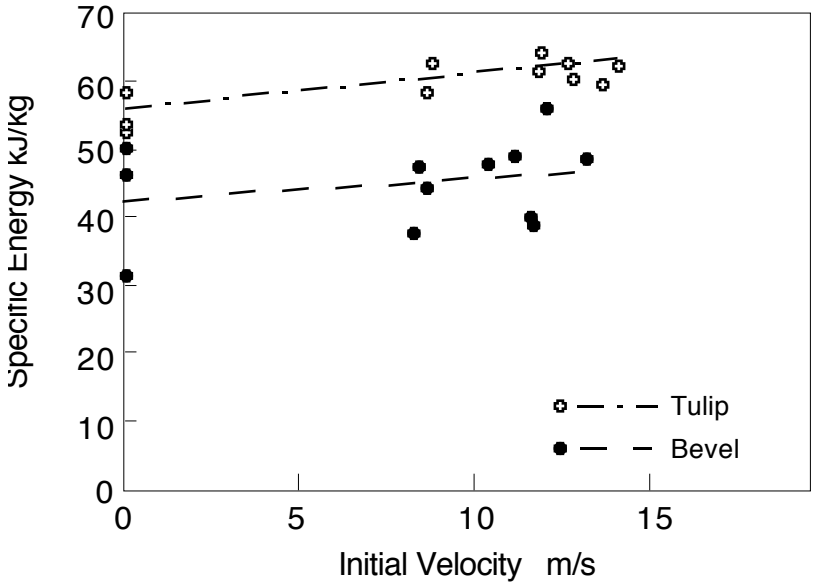

Figure 2.34 Plot of specific energy absorption as a function of the crush speed for pultruded glass-vinylester tubes [31]. See also figure 2.6 (b).

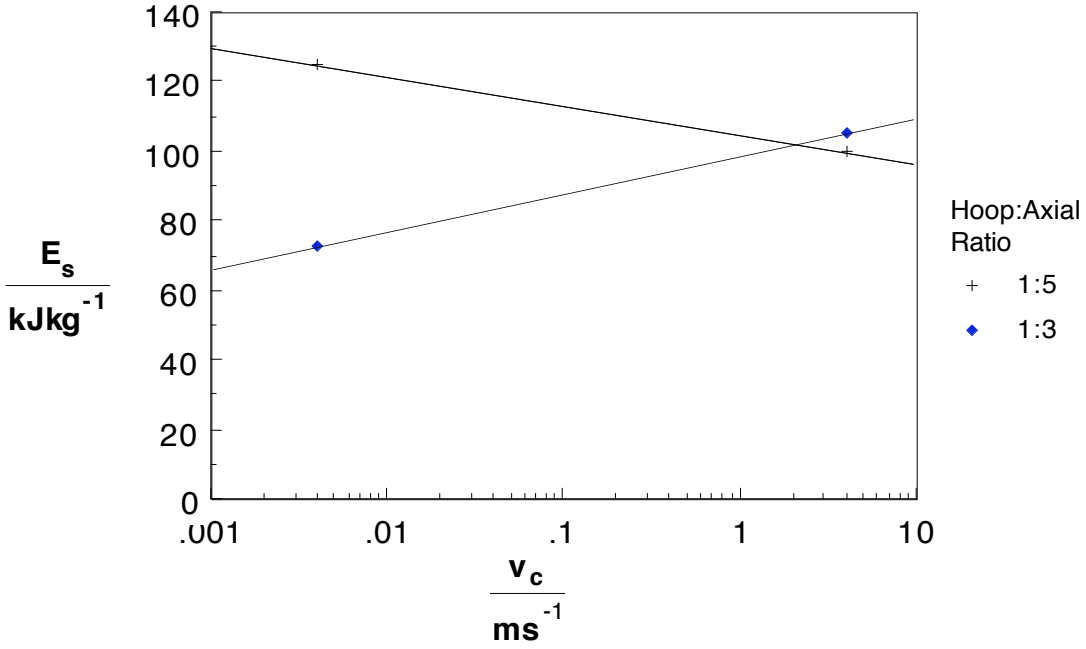

Figure 2.35 Specific energy absorption as a function of the crush speed for carbon-epoxy tubes with differing ratios of hoop to axial fibres [25].

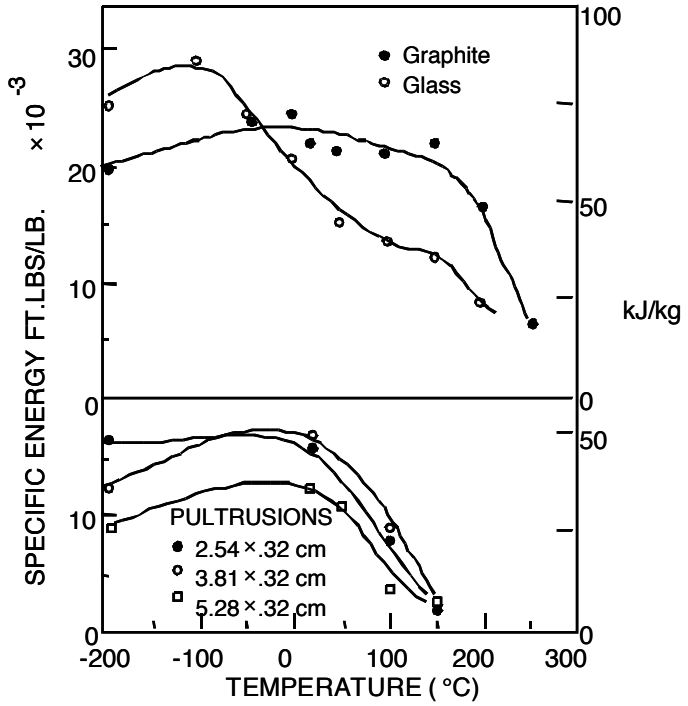

Figure 2.36 Plot of specific energy absorption as a function of the test temperature for glass and carbon fibre reinforced epoxy tubes [17].

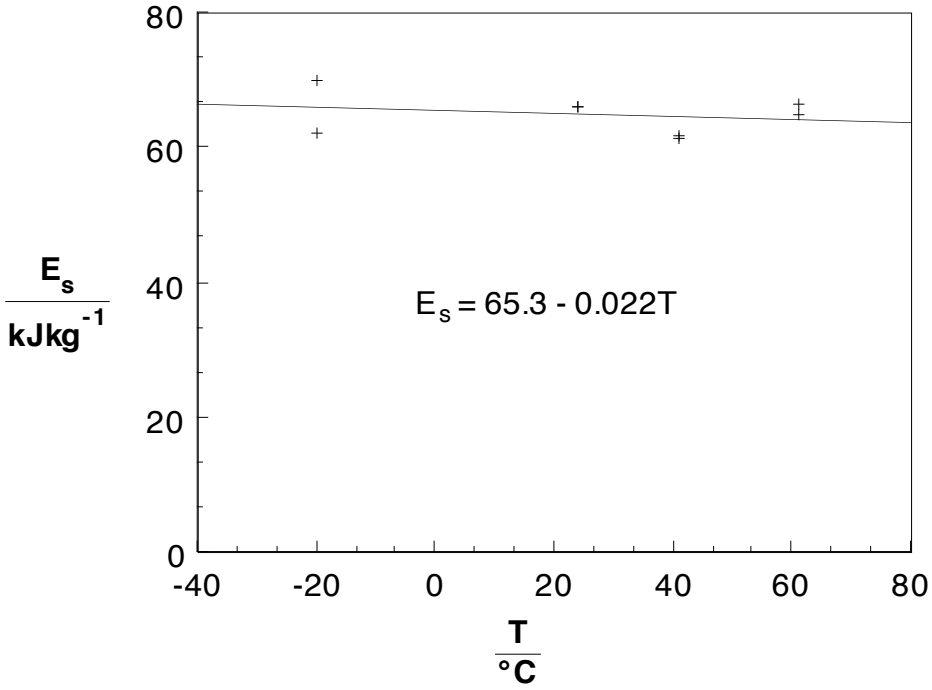

Figure 2.37 Plot of specific energy absorption as a function of the test temperature for filament wound glass-polyester tubes with a fibre lay up of 0-90° [25].

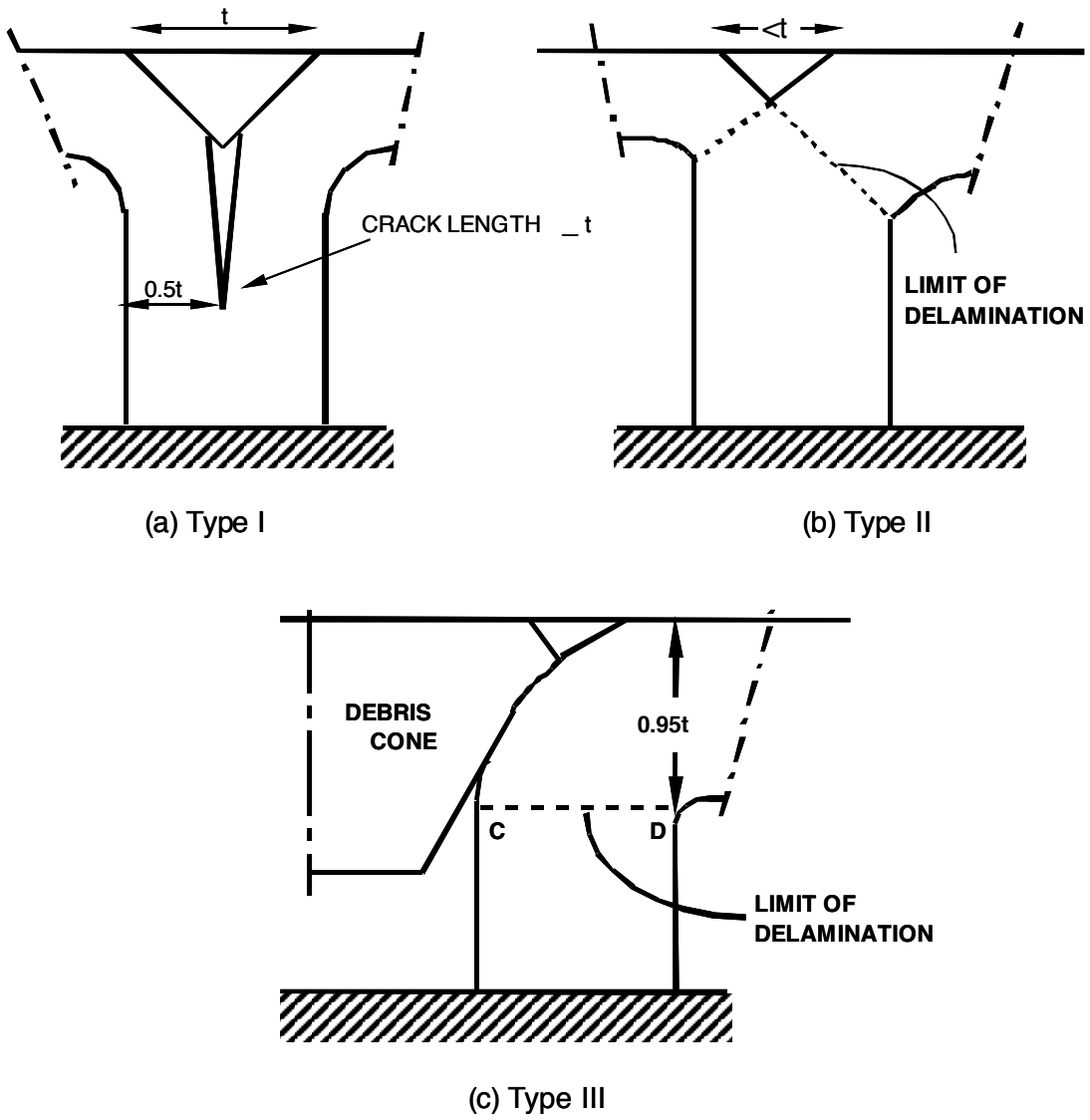

Figure 2.38 Crush modes as defined for glass cloth-epoxy tubes with varying t/D by Fairfull [44,51]. Crush platens are shown at the top.

Figure 2.39 Fragmentation crush mode by Berry and Hull [60]. Crush platen is shown at the bottom.

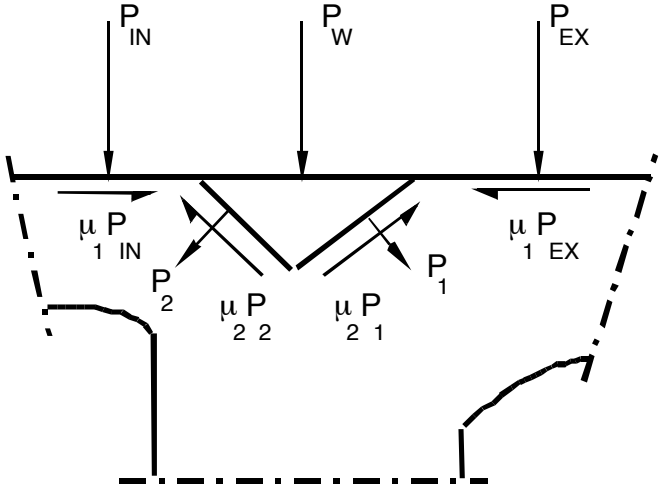

Figure 2.40 Force distribution in the crush zone (shown for a type II crush zone) [51].

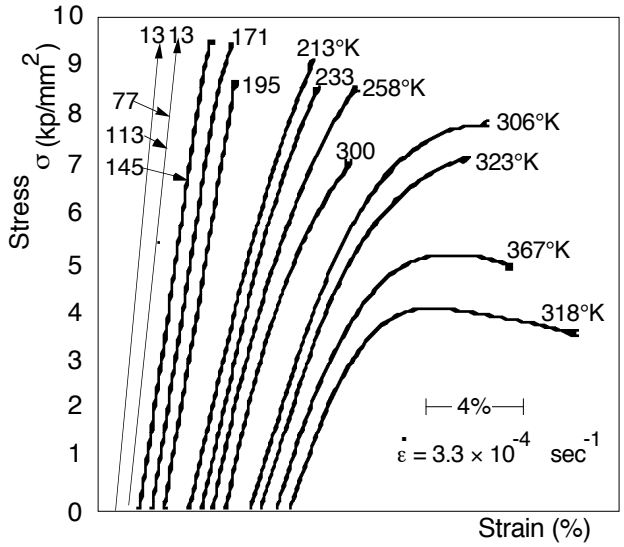

Figure 2.41 Stress-strain curves at different temperatures for an epoxy resin with a Tg of about 423 K (150 °C) [64].

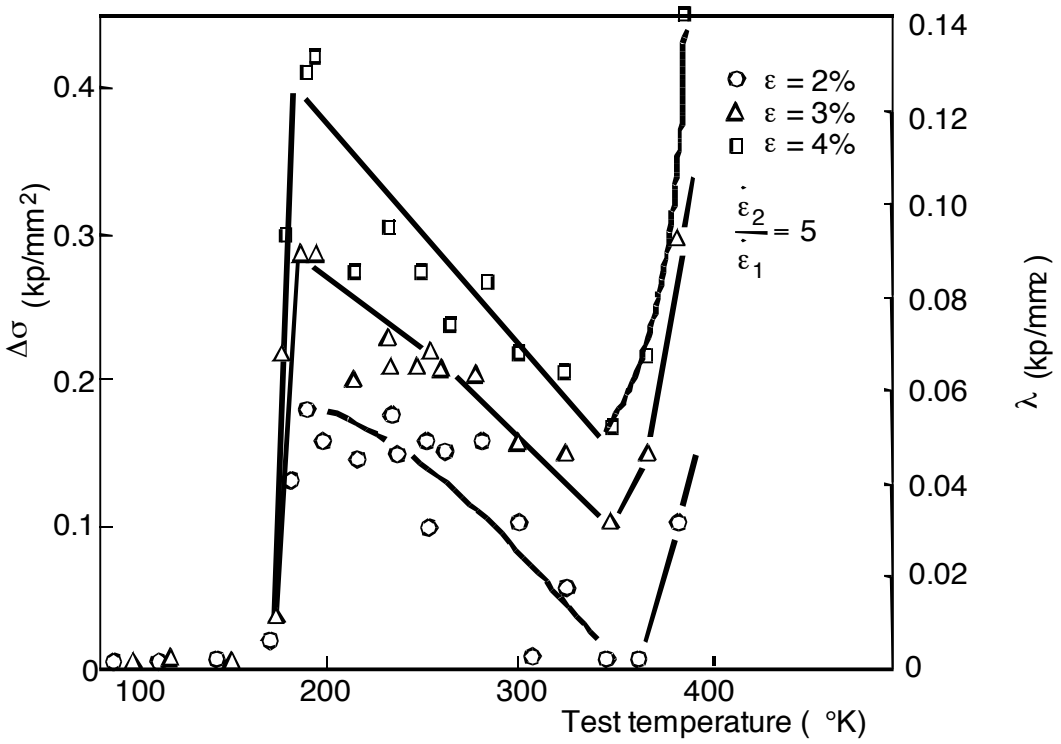

Figure 2.42 Plot of the speed sensitivity of the tensile stress of an epoxy resin as a function of the testing temperature [64].

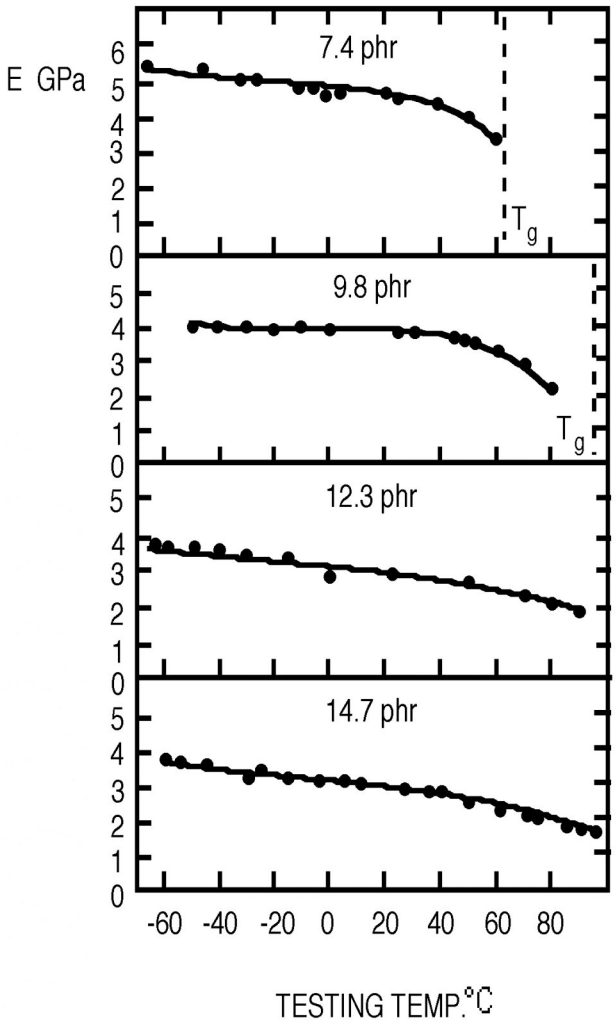

Figure 2.43 Plot of the Young's modulus as a function of the testing temperature for an epoxy resin with varying amounts of hardener [65-67].

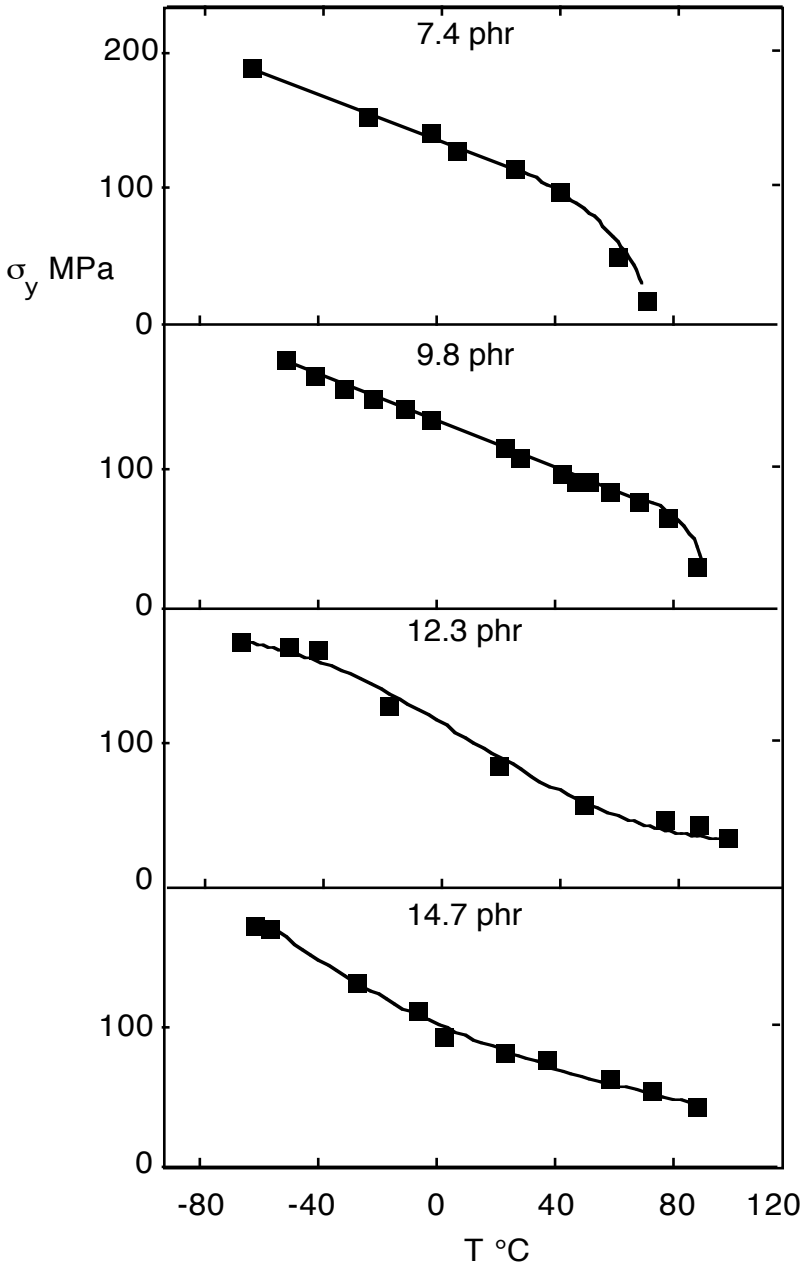

Figure 2.44 Plot of the tensile yield strength as a function of the testing temperature for an epoxy resin with varying amounts of hardener [65-67].

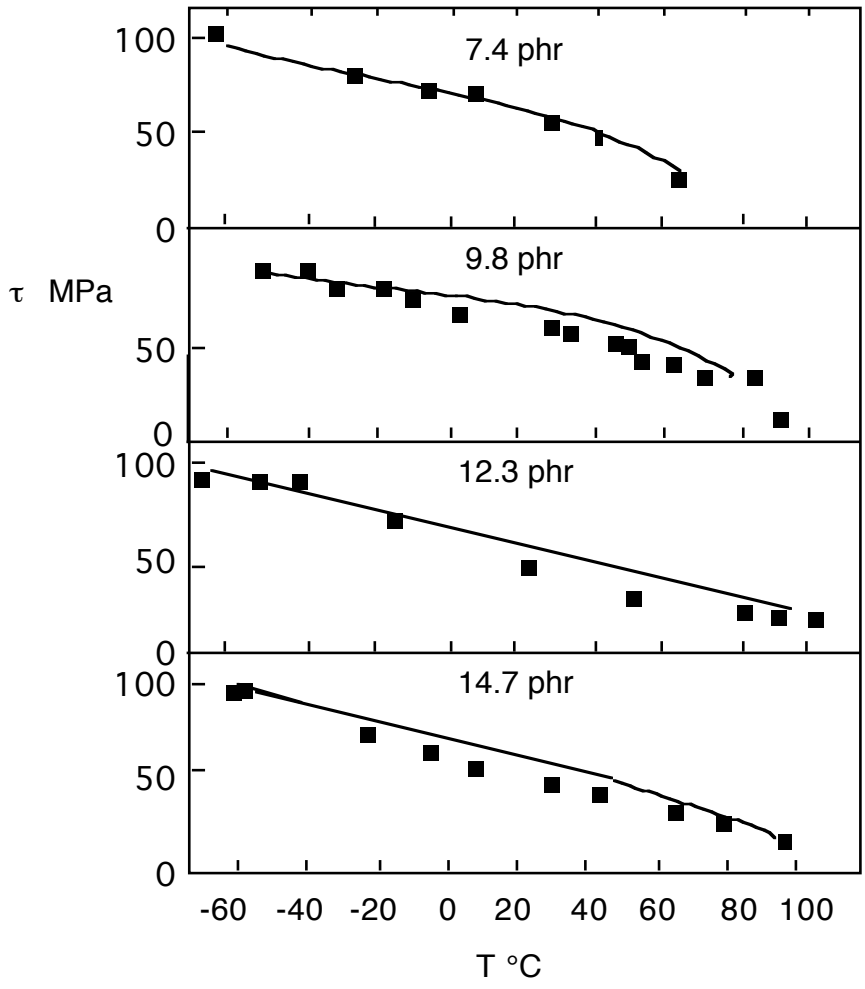

Figure 2.45 Plot of the shear yield strength as a function of the testing temperature for epoxy resin with varying amounts of hardener [65-67].

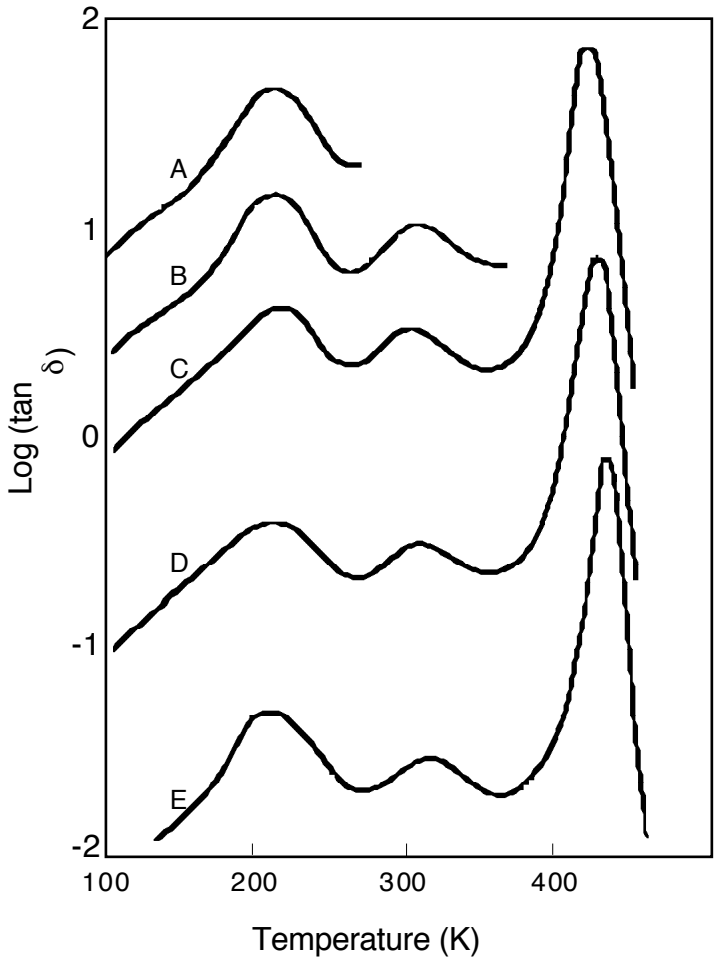

Figure 2.46 Plot of the loss tangent tan(δ) as a function of the testing temperature for epoxy resins [72].

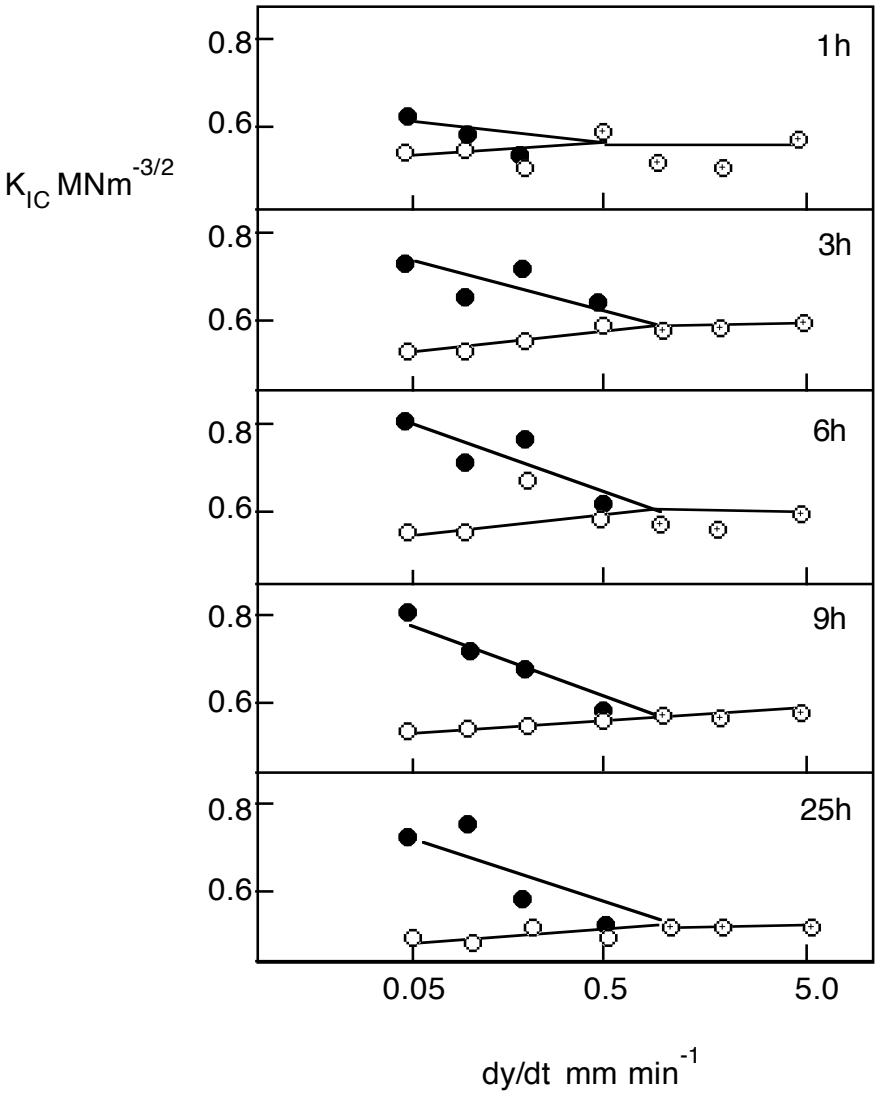

Figure 2.47 Plot of K_{ICi} and K_{ICa} as functions of the testing speed for an epoxy resin cured for different times [65].

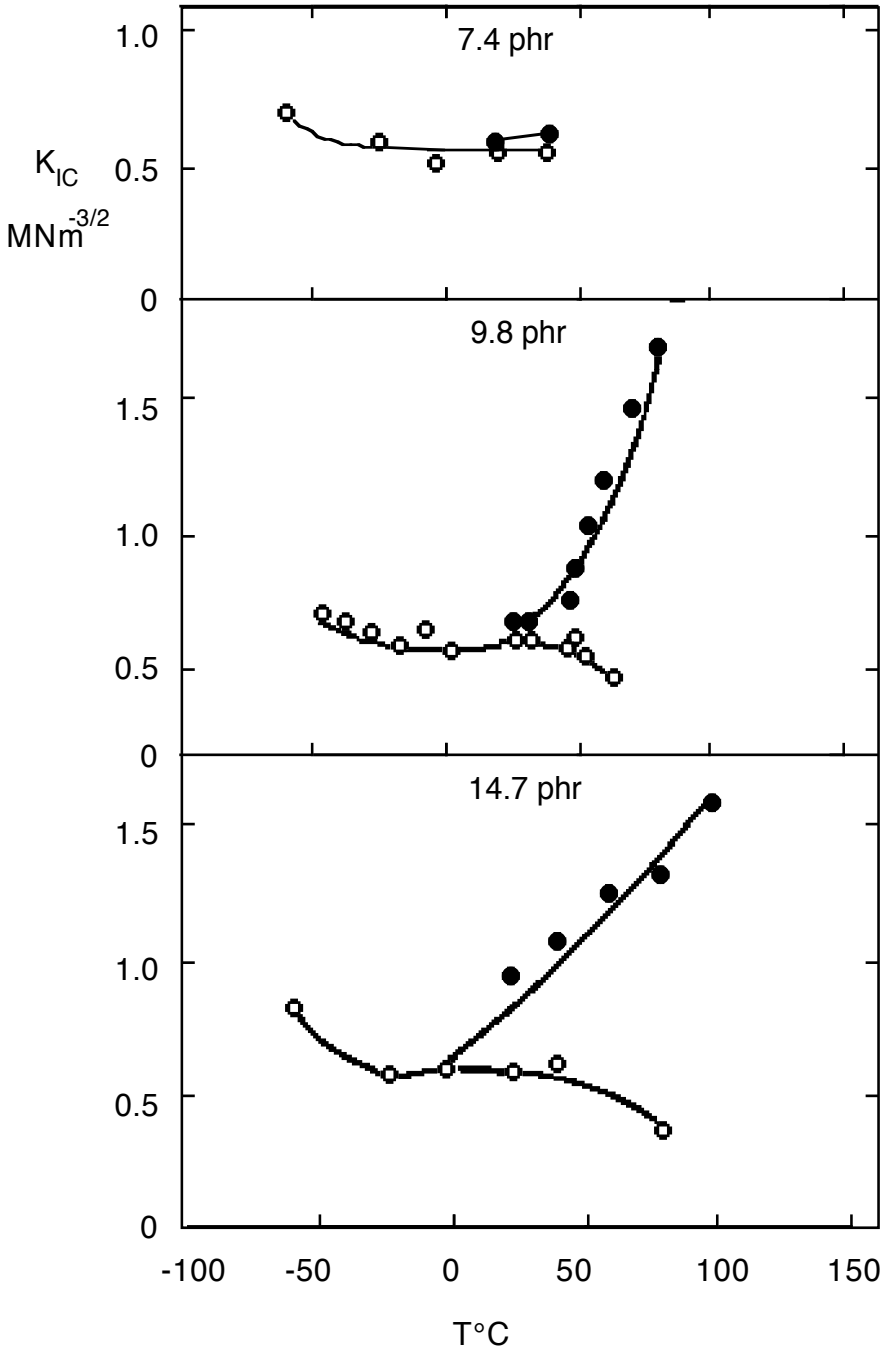

Figure 2.48 Plot of K_{ICi} and K_{ICa} as functions of the testing temperature for an epoxy resin cured with varying amounts of hardener [67].

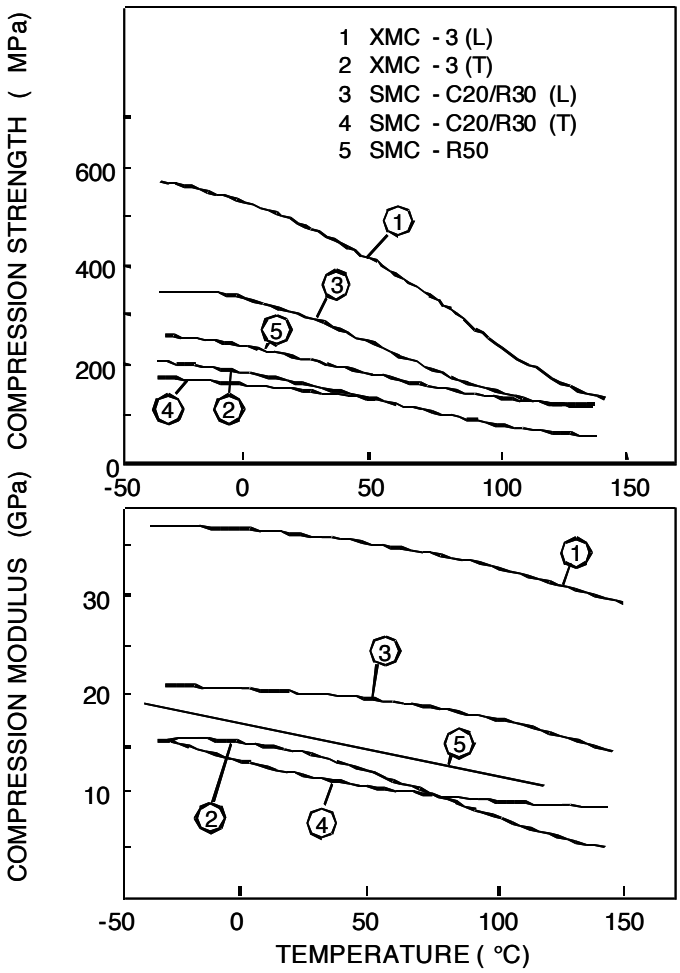

Figure 2.49 Strength and modulus of polyester resin matrix SMCs as functions of the test temperature for both the longitudinal (L) and transverse directions of incorporated aligned fibres (1 to 4 only) [93].

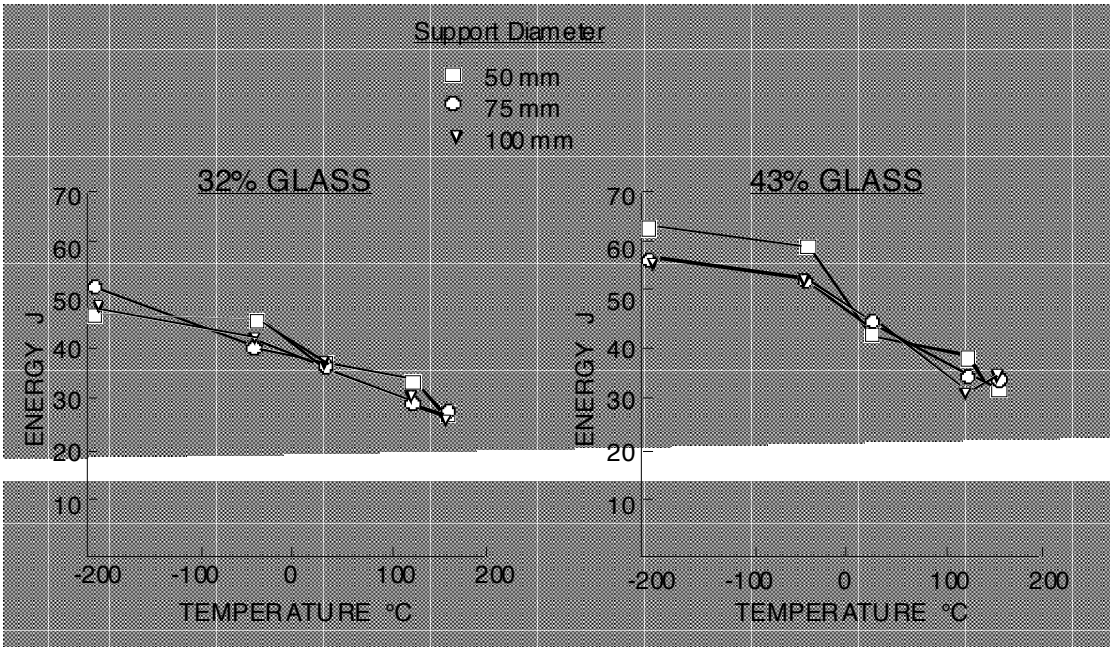

Figure 2.50 Fracture energy as a function of the temperature for SMCs as measured by a falling weight test [94].

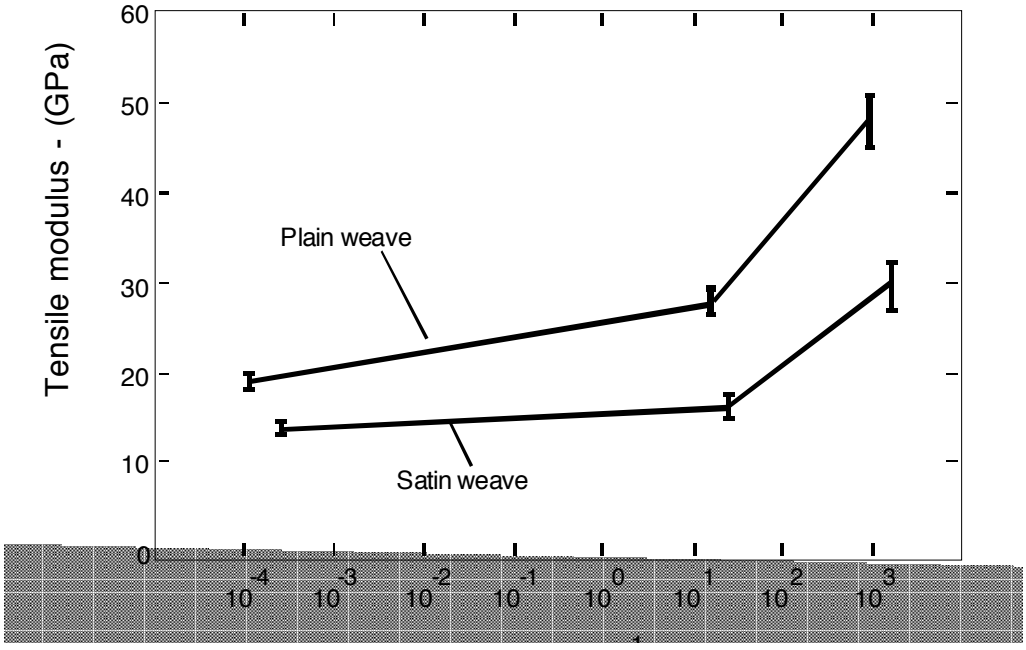

Figure 2.51 Tensile modulus as a function of the strain rate for glass cloth-polyester specimens [83].

3 Experimental Details

3.1 Preparation of Materials

Various types of tube were examined in this investigation; these were: commercial glass cloth-epoxy, glass mat-polyester, resinject random filament glass mat-epoxy and polyester, resinject glass cloth-epoxy and polyester, and pultruded glass-polyester containing an inorganic filler. Some glass cloth-epoxy material was tested as flat plate.

3.1.1 Tufnol Tubes

Commercially available glass cloth-epoxy tubes were examined in this project. These tubes were supplied by Tufnol Ltd. under their product code RLG/1. The manufacturers described the tubes as being made of 80 weave glass cloth in an epoxy matrix. Technical information on the material used in the manufacture of these tubes gave a maximum continuous working temperature of 130 °C with an intermittent working temperature of 150 °C [99].

These tubes were produced by pressure rolling pre-preg onto a hot steel mandrel, and curing for two and a half hours at 135 °C before being removed from the mandrel with a hydraulic press. The tubes were then ground to external dimensional tolerance in a centre-less grinder. The nominal tube dimensions were 50 mm internal diameter and 55 mm external diameter, giving a wall thickness of 2.5 mm and a t/D ratio of 0.048. The tubes were manufactured to comply with BS 6128 Part 8 for external and internal dimensions, and eccentricity [100]. The dimensional tolerance of the tubes was determined using vernier callipers and was found to be very good, within ±0.01 mm of the nominal values. The small number of tubes that were outside this tolerance were discarded for the bulk testing of this project. Small variations within the dimensional tolerance were not important as the calculation of specific crush

stress from the crush loads allowed a degree of normalisation of dimensions that was well within experimental scatter. Unless otherwise stated, "Tufnol tubes" refers to tubes of this type with these dimensions.

The resin used was supplied by Ciba-Geigy under their product code 7065N75 but with some modifications to the final chemistry for processing reasons. These modifications were kept a closely guarded secret by the manufacturers. The resin was described by Ciba-Geigy as an electrical laminating resin [101].

The dimensions of the glass cloth were measured by burning off the resin in an electric furnace at 650 °C for about four hours. The thickness of the cloth normal to the plane of the weave, t, was measured using vernier callipers and was found to be 0.16 mm. The repeat distances of the weave, w, in both the axial and hoop directions were measured by counting the number of strands in a known length of cloth using a low powered microscope. The strand frequency was 12 strands per cm, giving a repeat distance, w, of 0.85 mm {figure 3.1}. In the wall thickness of 2.5 mm there were 15 layers of glass cloth.

The material density varied between tubes from 1.81 g cm^{-3} to 1.91 g cm^{-3}, giving a mass per unit length of between 0.745 g mm^{-1} and 0.790 g mm^{-1}. Assuming a glass density of 2.56 g mm^{-3} [40], a resin density of 1.2 g mm^{-3} [101] and a void volume fraction of 1%[1], the fibre volume fraction was about 53% to 55%.

[1] 1% was the approximate void volume fraction as determined by Fairfull for these tubes [51].

3.1.2 Glass mat-polyester Tubes

Glass mat-polyester tubes were prepared by hand lay-up on polished, hardened steel mandrels of 50 mm diameter and 1 m length, using a brush and roller technique {figure 3.2}. The glass mat used was supplied by Fibreglas Ltd. under their product name Supremat PB, being a powder bound chopped-strand-mat of "density" 450 g m^{-2} and a strand length of 25.4 mm (1 inch) [102]. The resin used in these tubes was a high performance isophthalic polyester resin in a styrene monomer and was supplied by Scott Bader Ltd. under the product name Crystic 272[1] [103]. The resin was cured with 1 vol.% Catalyst M, a methyl ethyl ketone peroxide, and 0.8 vol.% Accelerator E, a Cobalt naphthenate accelerator in a styrene monomer. These proportions of catalyst and accelerator were recommended for cold curing. The tubes were cured at room temperature for about 24 hours, during which they were continuously rotated to avoid sagging, before being post cured at 80 °C for three hours in a forced convection oven, and then oven cooled to room temperature.

At this stage dimensional control was very poor with an irregular wall thickness and surface finish. The tubes were turned on a lathe (while still on the mandrel), to a nominal external diameter of 54 mm, hence producing a wall thickness of 2 mm and a t/D ratio of 0.038. Because of technical problems with the only available suitable lathe, dimensional control was difficult and the external diameter of the tubes varied from the nominal by typically 0.1 mm. Once a tube had been machined it was pressed off the mandrel using a pneumatic press.

[1]This resin was used in some of the work discussed in section 2.1.

Burn off tests showed that these tubes had a fibre volume fraction of about 18% and a void volume fraction of about 3%. These values were subject to a great deal of scatter, typically ±2%[1] for each value.

The dimensional difficulties and the variation of fibre volume fraction meant that a large number of tubes had to be tested to be statistically confident of trends.

3.1.3 Resinject Tubes

The other main types of tubes used in this project were produced by resinjection. They were produced by Moore Plastics of Dartford[2] and were financed by Ford Motor Company Ltd.

These tubes were produced with two types of glass reinforcement, being woven cloth and random filament mat, in two thermosetting resin matrices, an epoxy resin and a polyester resin, giving four possible combinations. These tubes were denoted by four letter abbreviations which described them. The code consisted of RJ, to denote resinjection, P or E to denote a Polyester or Epoxy resin matrix and W or R to denote Woven glass cloth or Random glass mat. For instance, a polyester resin tube reinforced with woven glass cloth and produced by resinjection would be denoted RJPW. This notation has been used throughout this thesis.

The woven glass cloth was Fothergil YO709, having 7-8 strands per cm and a "density" of 200 g m^{-2}. The random filament reinforcement was E-glass mat with a "density" of 450 g m^{-2}. This was supplied by Vetrotex (UK) Ltd. and was designated Unifilo U750 [104]. The epoxy resin was supplied by Ciba-Geigy under their product

[1] Percentage of the total volume.
[2] Who have subsequently closed down.

code CY219 [105]. The polyester resin was the same as that used for the tubes as described in section 3.1.2, i.e. Scott Bader Crystic 272 [103]. The polyester matrix tubes were post cured at 80°C for three hours in a forced draught oven and then oven cooled to room temperature. Ciba-Geigy did not recommend a post cure for CY219.

The dimensions of the tubes were: 50 mm internal diameter and 54 mm external diameter, giving a wall thickness of 2 mm and a t/D ratio of 0.038. Dimensional accuracy was very good, better than ±0.01 mm. Average mass per unit length values and approximate fibre volume fractions for these tubes are given in table 3.1.

Reinforcement	Matrix resin	$\underline{m/l}$ G mm^{-1}	$\underline{v_f}$ %
cloth	polyester	0.57	42
mat	polyester	0.48	24
cloth	epoxy	0.56	40
mat	epoxy	0.49	26

Table 3.1 Average properties of resinject tubes.

3.1.4 Flat Plate Specimens

Flat plate specimens, for testing in three-point-bend, were prepared from material supplied by Tufnol Ltd. under their product code 10G/40. This material was identical to the RLG/1 of the Tufnol tubes [99]. These specimens enabled the speed response of the energy absorbing tubes to be compared to some basic mechanical properties of the material.

Specimens were cut to size using a diamond cutting wheel. Nominal dimensions of the test-pieces were: length 80 mm, width 10 mm and thickness 3 mm according to the

CRAG 2.2 standard [106] {figure 3.3}. The dimensions were measured using vernier callipers measuring to an accuracy of ±0.01 mm.

3.1.5 Tubular Test Piece Preparation

Tubes were prepared for crush testing by cutting into suitable lengths, typically 75 mm to 120 mm, depending on the intended test, coded, measured for external diameter and length, and weighed. The mass per unit length was then calculated for each tube. 45° external chamfers were then machined using a lathe on one end of each tube to act as triggers to initiate progressive crushing {figure 3.4} (section 2.1.3.6).

3.2 Crush Testing

Tests were performed on the tubes by subjecting them to either constant speed crushing or impact testing on a 3 kJ crash rig. In all cases the tubes were crushed against hardened steel platens with a ground finish.

3.2.1 Constant Speed Crushing

Constant speed crushing was carried out over a wide range of speeds from 0.0017 mm s^{-1} to 5 m s^{-1}.

3.2.1.1 Low Speed

Constant, slow speed crushing of the different types of tube, was carried out on a servo-hydraulic Instron model 8032 and on a screw driven Schenk-Trebel RM50. The Instron was capable of a maximum load of 100 kN and a practical speed range of 0.002 mm s^{-1} to 10 mm s^{-1}. This testing machine was fitted with an environmental chamber to enable testing over a temperature range of -150 °C to 350 °C {figure 3.5}. The Schenk had a maximum load capacity of 50 kN, meaning that it could only be

used for low crush load tubes. The speed range for this machine was 0.1 mm min^{-1} to 500 mm min^{-1} (0.0017 mm s^{-1} to 8.3 mm s^{-1}).

3.2.1.1.1 Instantaneous Speed Change Tests

To determine the speed dependence of tubes without encountering problems of specimen variability, tests were performed by crushing tubes at one speed and then changing the speed instantaneously by several orders of magnitude. These tests were performed with the speed change being in both directions. The speeds that were used were 0.002 mm s^{-1} and 10 mm s^{-1}. Typical crush traces for these tests are shown in chapter 4, figures 4.58 to 4.64. These tests were carried out over a range of temperatures in the environmental chamber to determine the speed sensitivity of specific crush stress at different temperatures. The tubes were left for twenty minutes to reach thermal equilibrium before testing commenced.

3.2.1.2 High Speed

High rate, constant speed crushing was carried out on a servo-hydraulic single shot testing machine designed and built for the project at the Cranfield Institute of Technology {figure 3.6}. This machine was capable initially of crush speeds up to 5 m s^{-1}, but subsequent modifications that were required for safety reasons, restricted this speed to about 3.5 m s^{-1}. At the high speeds, the signal was fed to a Gould storage oscilloscope, model 4050, before obtaining a hard copy.

3.2.2 Impact Testing

Impact tests were performed on a 3 kJ crash rig that was designed and built for the project {figures 3.7}. The rig consisted of a sled, of effective mass[1] 11.7 kg, that was mounted on polished steel rails which acted as bearing surfaces, the sled being supported by PTFE bearings. The sled was free to run on the rails and was connected to four bungee cords which were attached to the main frame of the rig at their other end. The sled was winched back against the tension of the bungee cords, using an electric winch, to a preset position. It was held at this position by a pneumatic catch and the winch cable disconnected. The test-piece was then mounted onto the front of the sled as a press-fit on a brass spigot, such that the axis of the tube was parallel to the direction of travel of the sled. The entire rig was then rolled back on wheels, to isolate it from external forces, and the safety screens closed. The sled was then released from the preset position by the pneumatic catch, it was accelerated by the bungee cords along the rails, and the test-piece impacted with a steel crush platen connected to the frame of the rig. The crush platen was mounted on four load washers (Kistler type 9021) and a signal was sent from these to a digital storage oscilloscope where it was captured as a force-time trace {figure 3.8 (a)}[2]. A displacement transducer was used to give a displacement-time trace on the oscilloscope, the gradient of which gave the impact velocity {figure 3.8 (b)}.

It would have been desirable to use the signals from the load washers and displacement transducer to obtain a force-displacement trace, the area under which

---

[1]The mass has been quoted as the effective mass rather then the actual mass of the sled as the test piece will have "seen" a contribution to the mass of the bungee cords. The effective mass was determined from momentum balances on a number of crush traces.

[2]The distance x_{bb} represents a bounce-back of the sled after the test. This is discussed in section 8.1.2.5.

would have given the energy absorbed. However, there was an offset between the signals of about 1 ms which made trying to obtain such a trace impractical. It would be possible to overcome this problem using a pulsed laser device but the improvement was felt too small to justify the extra cost.

For all except the highest speed tests, it was possible to obtain more than one test on each tube. This was due to the amount of material being used up in each impact test being proportional to the square of the impact velocity. The first tests were on tubes with a chamfer trigger while subsequent tests started with the crush zone already established from the previous tests.

Temperature dependence of energy absorption at high speed was investigated by impact testing on the crash rig from 10 m s^{-1}. These tests were performed by pre-heating each tube in a furnace before removing the tube and fitting to the sled for impact testing. Temperature control was not very precise, but this method provided a guide to temperature dependence before the environmental chamber was commissioned. There was typically a delay of about ten seconds between removing the tube from the furnace and the test being carried out, during which time the tube could cool. No measurement was made of the actual tube temperature at the moment of testing, thus the temperatures quoted for these tests are upper bound temperatures. Low temperature tests were carried out by immersing the tubes in liquid nitrogen before testing. For these tests, the quoted values of temperature must be lower bound figures. The tubes used in this investigation were Tufnol and glass mat-polyester. The glass mat-polyester tubes gave problems of mounting onto the spigot for the low temperature testing resulting from thermal contraction.

3.3 Experimental Microscopy

After crush testing, sections through the crush zones of tubes were examined by microscopy in order to determine the mechanisms involved during crushing.

3.3.1 Sample Preparation

The sectioning procedure consisted of mounting the crush zone in resin, sectioning and polishing before microscopic examination.

Mounting of the crush zone was done under load, to try to eliminate the effects of elastic relaxation on removal of the crush load after the crush test. The load was applied using a screw operated mounting press {figure 3.9}. The mounting resin used was Strand Resin C, a low viscosity, unsaturated polyester mounting resin in a styrene monomer, catalysed with 1 vol.% catalyst M. Curing was achieved at room temperature for about 24 hours before the mounted specimen could be removed from the mould. The specimen was then sectioned on a diamond cutting wheel and mounted for easier handling in Scandiplast 9101 mounting resin. Polishing then followed normal metallographic procedures of grinding on silicon carbide papers of grit size 180 to 1200, and polishing using diamond paste. After much experimentation, it was found that the best results could be achieved by about 20 minutes of polishing with 6 μm diamond paste followed by about 5 minutes with 1 μm diamond paste. This combination, although not removing all the scratches from the grinding, was found to give the best contrast between the fibres and the matrix.

3.3.2 Microscopy

After polishing, the sections were examined and photographed on a microscope. The size of the sections caused problems with photography since they were too small to photograph satisfactorily using a camera but were too large to be photographed in a

single frame on a microscope. This problem was overcome by producing photomontage's of the sections, from typically 30 frames. The microscopes used in this examination were a Carl Zeiss and an Olympus BHM, both using a ∞ 4 objective. The film used was Ilford FP4 in 135 size. This film is designed for daylight usage, so a daylight filter was used on the microscope.

The films were printed by contact printing. This method was used for reasons of speed and economy, as well as producing a uniform magnification, if the same microscope set up was used. It also eliminated any problems associated with focussing an enlarger.

For some specimens, it was found that a single photomicrograph could be taken on a Wild MPS 45 microscope. The results obtained were however, of a low quality, hence the move to the photomontage technique.

3.4 Other Experiments

Various experiments were performed to understand better the crushing process.

3.4.1 Bend Tests

Three point bend tests were performed on a screw driven Instron testing machine model TT-CM-L. They were tested over a speed range of 0.5 mm min^{-1} to 50 mm min^{-1}. They were performed in accordance with CRAG 2.2 [106] {figure 3.3}. All the bend tests were carried out at room temperature (22 °C). Although it would have been desirable to extend this series of tests to cover speed-temperature interaction, machine availability prevented this being done.

3.4.2 Length

The effect of the specimen length on the degree of serration of the crush trace, was investigated. Three different types of tube were tested which were selected as they

were known to display very different crush modes, ranging from little fibre fracture and mainly fibre splaying, to large debris pieces breaking off with no fibre splaying. Some tubes were supplied by Pultrex Ltd., being pultruded glass-polyester tubes with an inorganic filler in the matrix which was thought to be calcium carbonate. The fibres in these tubes were largely axially aligned with an outer covering of random fibres to provide some hoop restraint. These tubes had an internal diameter of 38.7 mm and a wall thickness of 2.65 mm. They were tested over the length range of 58 mm to 720 mm. The other tubes were supplied by Tufnol Ltd. and were as described in section 3.1.1, except one set of tubes had an internal diameter of 16 mm and a wall thickness of 5.9 mm. This set of tubes were tested over the range of lengths of 36.5 mm to 762 mm. The latter length was too long for stable crushing and the tube failed by bending and catastrophic centre failure. The 2.5 mm wall thickness Tufnol tubes were tested over the length range of 25.7 mm to 723 mm. These tests were performed on the Instron 8032 at 0.5 mm s^{-1}. Due to the crush reducing the tube length during the test, the crush distance was kept to the minimum that enabled a representative crush trace to be obtained. This was about 10 mm.

3.4.3 Residual Stresses

Residual stresses, resulting from differential thermal contraction of the fibres and matrix were found in some of the tubes used in this project. To avoid any variability of the elastic properties of the material, they were treated as strains rather than stresses.

3.4.3.1 Hoop Strains

Residual strains were present in the hoop direction of some of the tubes investigated. These strains were detected resulting from the closing up of axial slits when they were cut into rings cut from tubes of the material {figure 3.10}.

The residual strain distribution was investigated by machining off layers of the material and measuring the residual strain for that ring using the Crampton method [107]. This method involved the slitting of the tube in the axial direction and measuring the difference in external diameter before and after slitting. All the tubes investigated were slit using a diamond saw and the dimensions measured using vernier callipers measuring to an accuracy of ±0.01 mm. The residual hoop strain ε_h was given by:

$$\varepsilon_h = t\left(\frac{1}{D_i} - \frac{1}{D_a}\right) \qquad (3.1)$$

where t was the wall thickness, D_i and D_a were the tube diameters initially and after the tube was slit. This procedure was carried out for Tufnol tubes and the four different types of resinject tubes.

3.4.3.2 Longitudinal Stresses

A glass cloth-polyester tube made by resinjection was examined to see whether the residual hoop strains were accompanied by residual longitudinal strains. This type of tube was chosen because they had been found to have the highest level of residual hoop strain (section 4.7.1). The method used was that devised by Anderson and Fahlman [107] of cutting a longitudinal tongue in the tube wall and measuring the deflection of the end of the tongue from the outside of the tube wall {figure 3.11}. The residual strain ε_l was given by:

$$\varepsilon_l = \frac{t\,f}{l^2} \qquad (3.2)$$

where t was the tube wall thickness, f the deflection of the end of the tongue from the tube wall and l the length of the tongue.

3.4.3.3 Effect of Residual Stresses

To try to gain some insight into the effects of residual hoop stresses two polyester matrix resinject tubes, one with each type of reinforcement, were cut into four sections each, having been numbered along the tube. The even numbered tubes were then post cured for one hour at 120 °C and then removed from the furnace and quickly cooled to room temperature. The tubes were then chamfered at one end, the ends being selected such that crushing would start from what had been the join between the 80 °C and 120 °C post cure sections {figure 3.12} thereby reducing the amount of error resulting from specimen variations except for the post cure conditions. All the tubes were then crushed at room temperature at a speed of 0.1 mm s^{-1}.

3.4.4 Differential Scanning Calorimetry

A differential scanning calorimeter (DSC) was used to try to measure the T_g of the various matrix materials and the specific heat capacity of the material. The machine was a Perkin-Elmer DSC 7 and was used with a heating rate of 20 °C min^{-1}. Typical traces for the resin from the Tufnol tubes are shown in figures 3.13 and 3.14. Although the resin for each test was from the same piece of material, they showed different behaviours. Any explanation for this anomaly is outside the scope of this work.

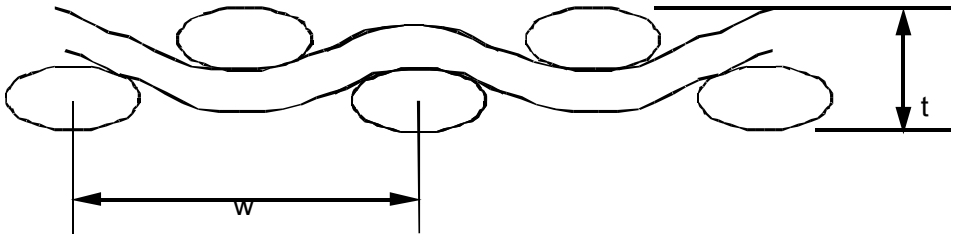

Figure 3.1 Glass cloth notation.

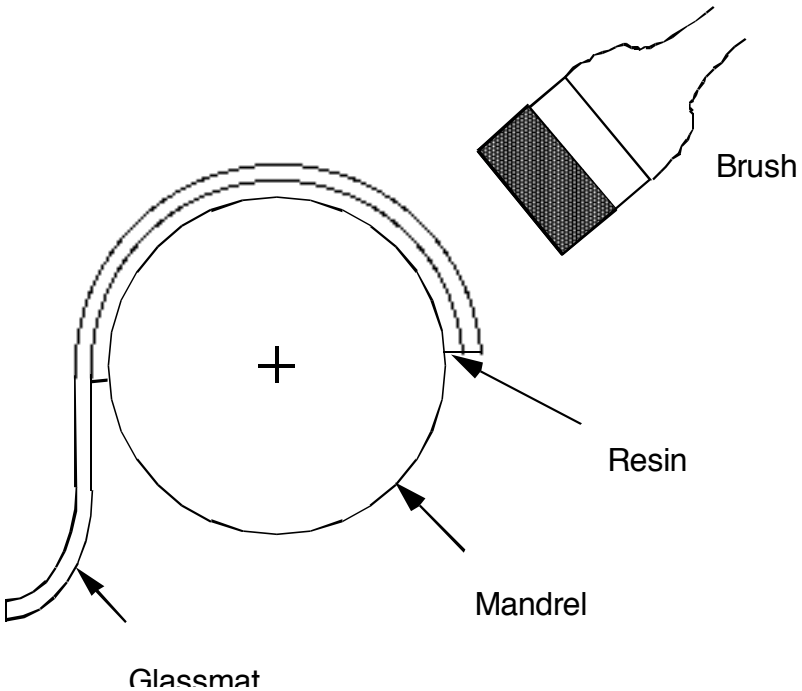

Figure 3.2 Hand lay up onto mandrel.

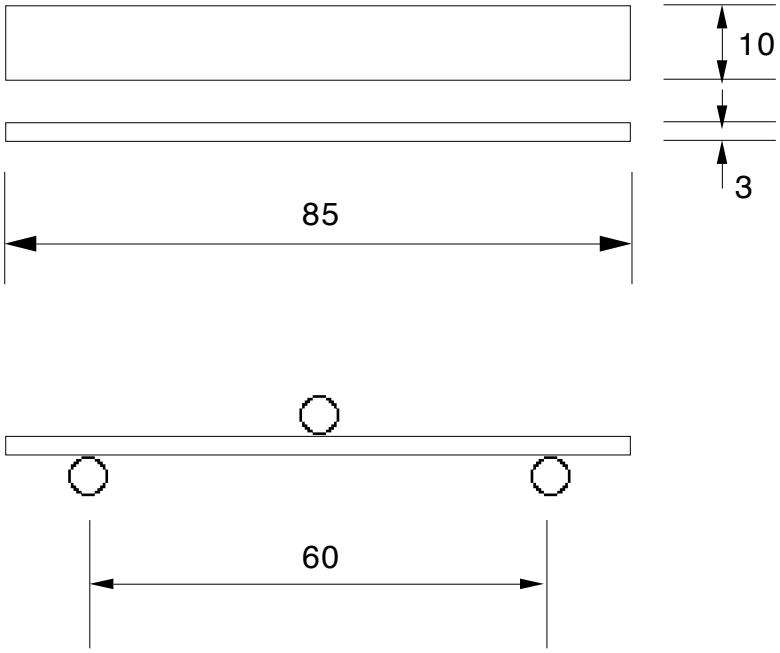

Figure 3.3 Bend test specimen dimensions.

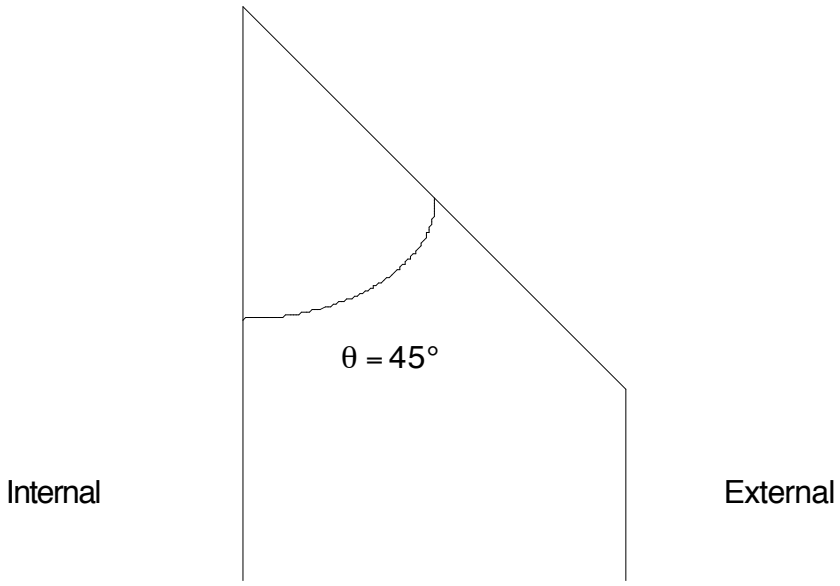

Figure 3.4 Chamfer angle on the end of the tubes, shown in cross-section.

Figure 3.5 Instron testing machine fitted with the environmental chamber.

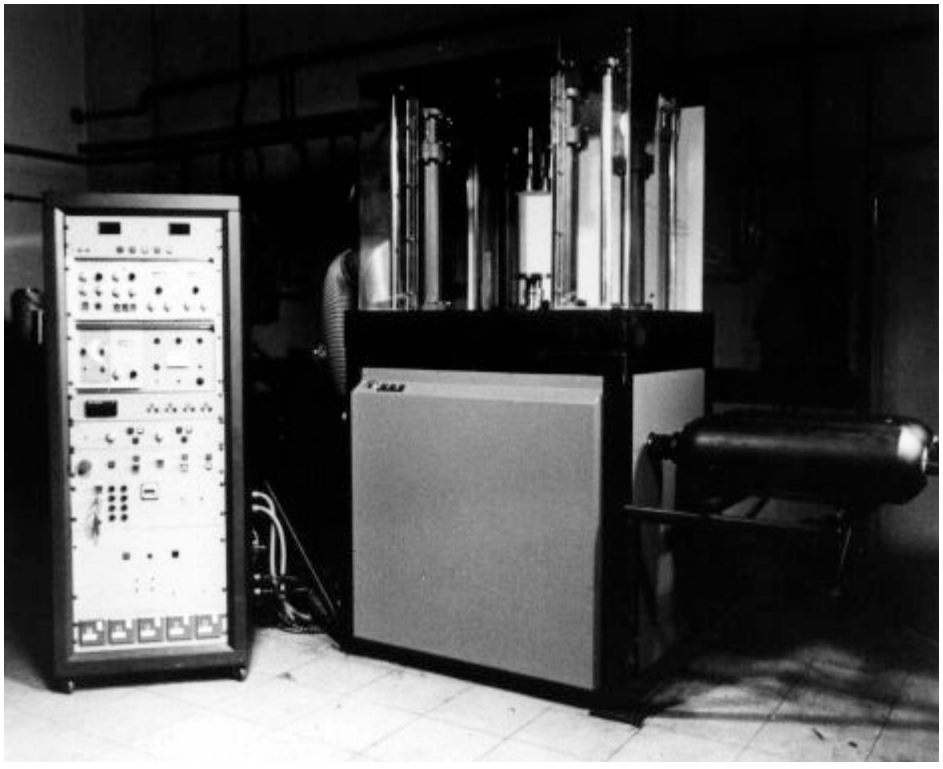

Figure 3.6 Cranfield high speed testing machine.

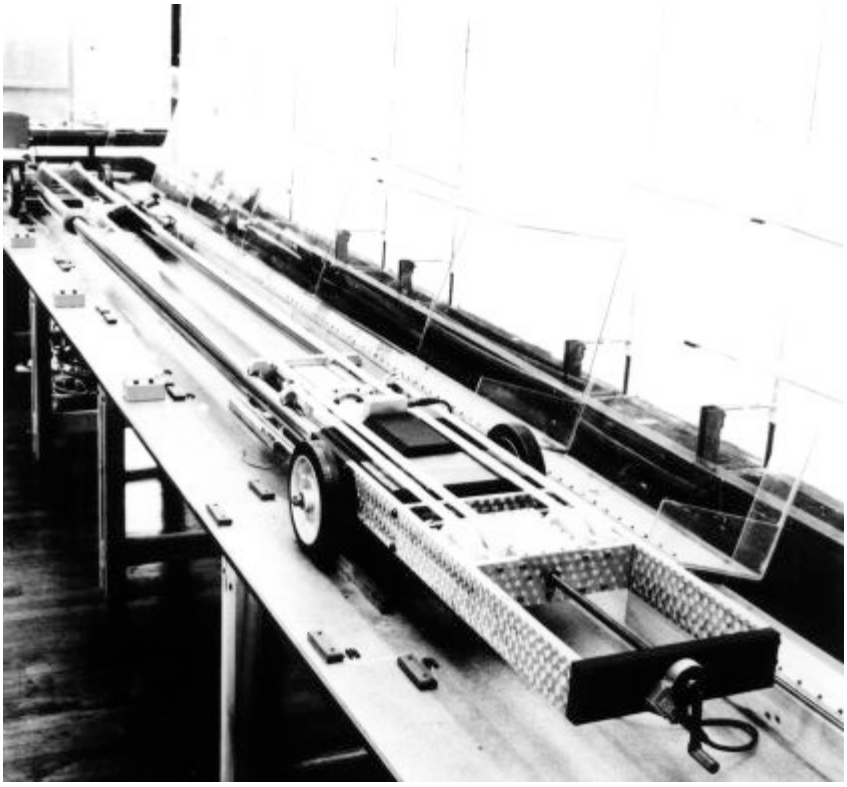

Figure 3.7 (a) 3 kJ crash rig, from the instrumented head end.

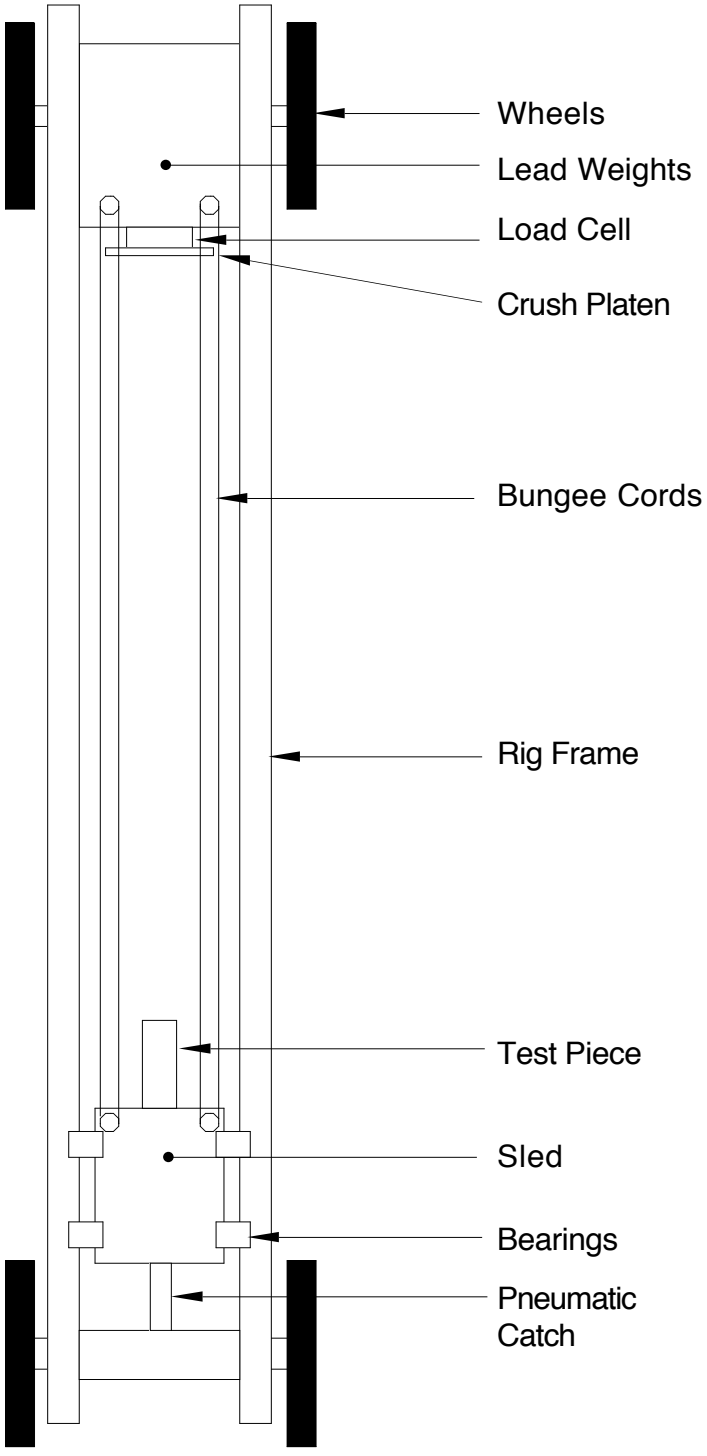

Figure 3.7 (b) Schematic plan view of the 3 kJ crash rig.

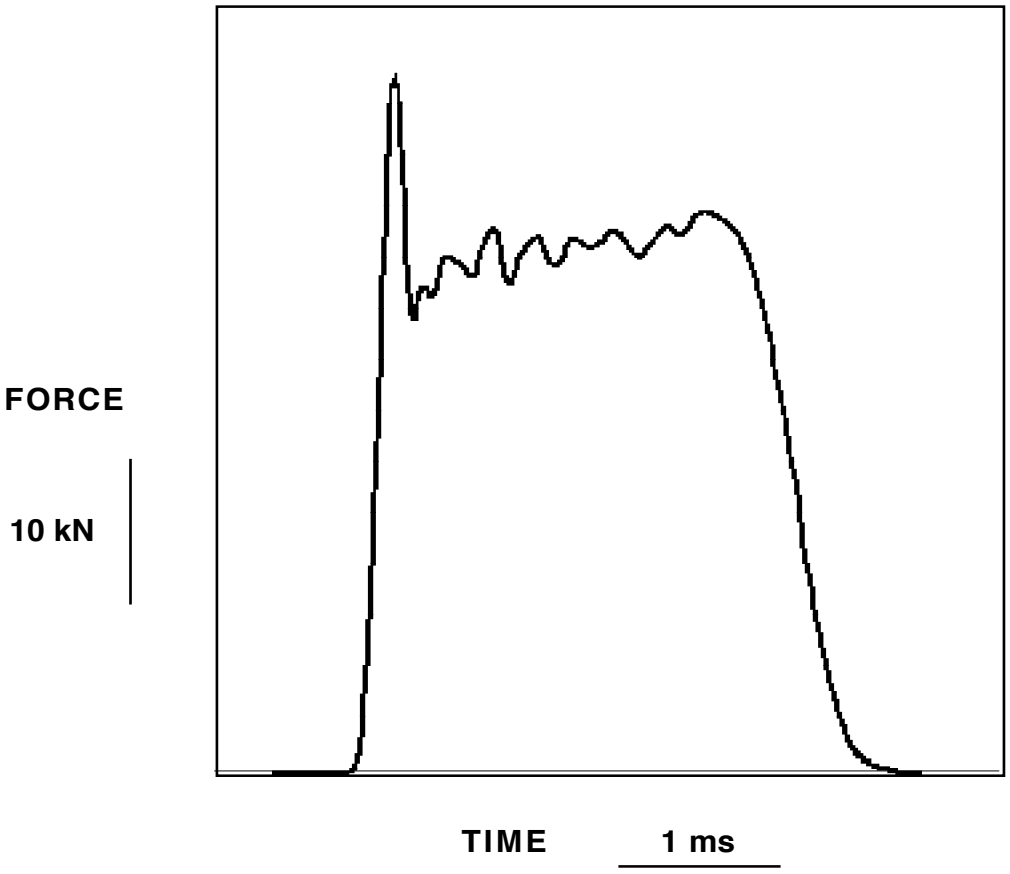

Figure 3.8 (a) Force-time trace from the crash rig for a glass mat-polyester tube impact tested from 10 m s^{-1}.

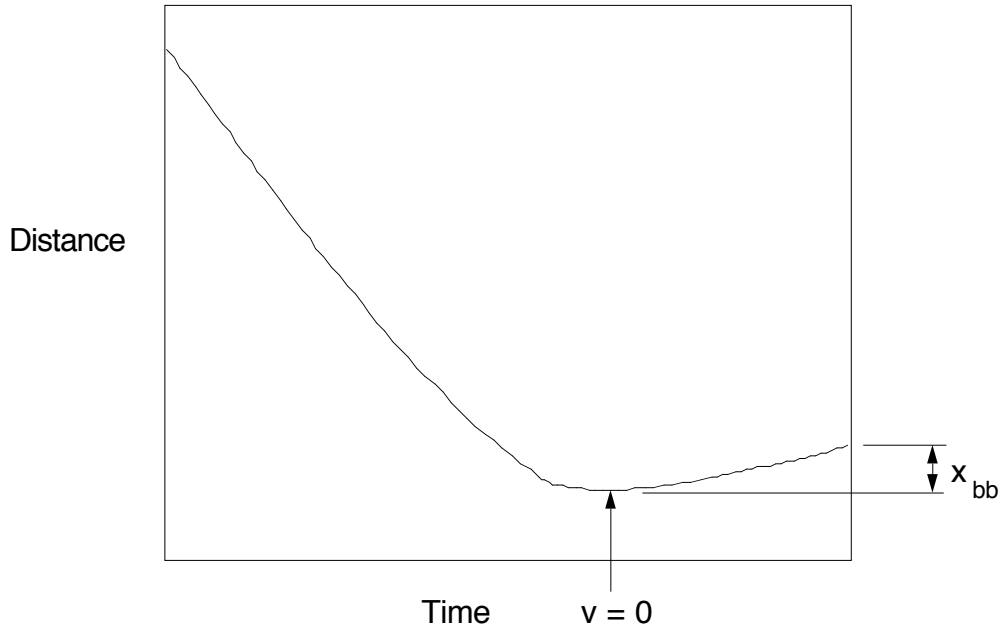

Figure 3.8 (b) Displacement-time trace from the crash rig for a tube impact tested from 10 m s^{-1}.

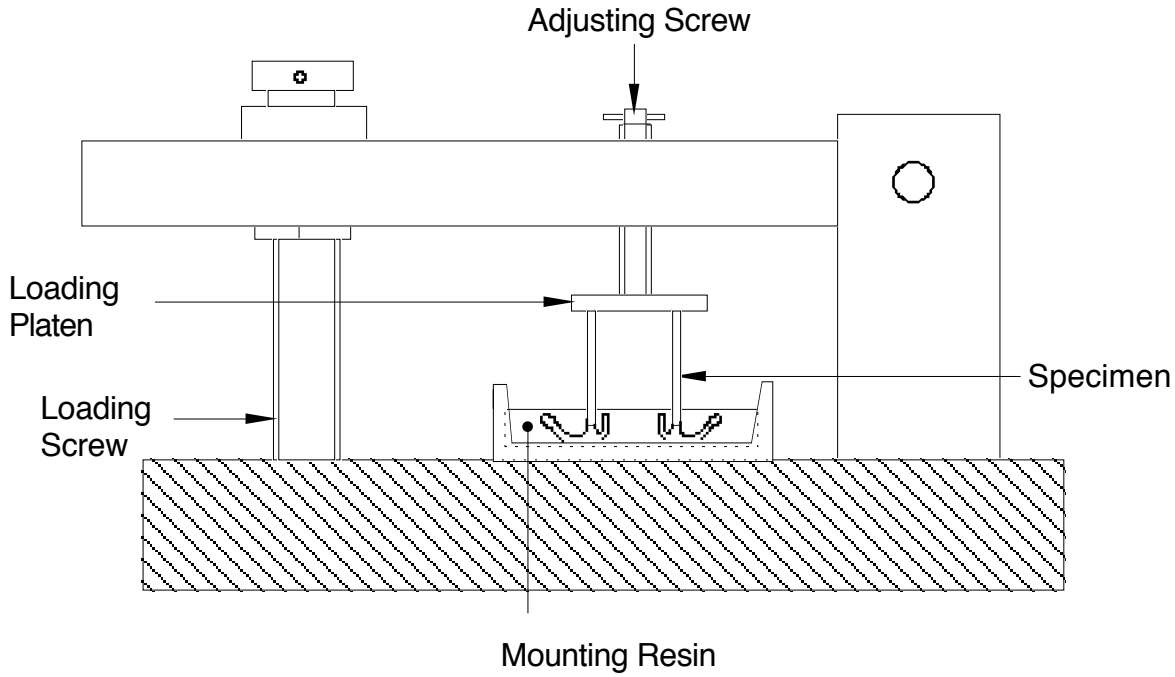

Figure 3.9 Specimen mounting press.

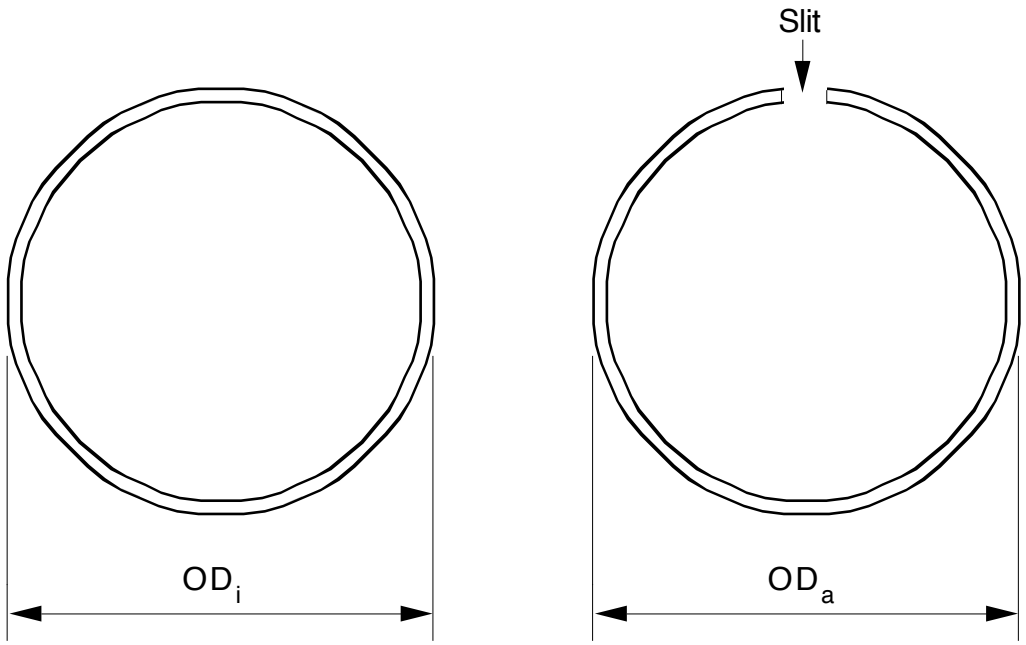

Figure 3.10 Residual stress ring notation.

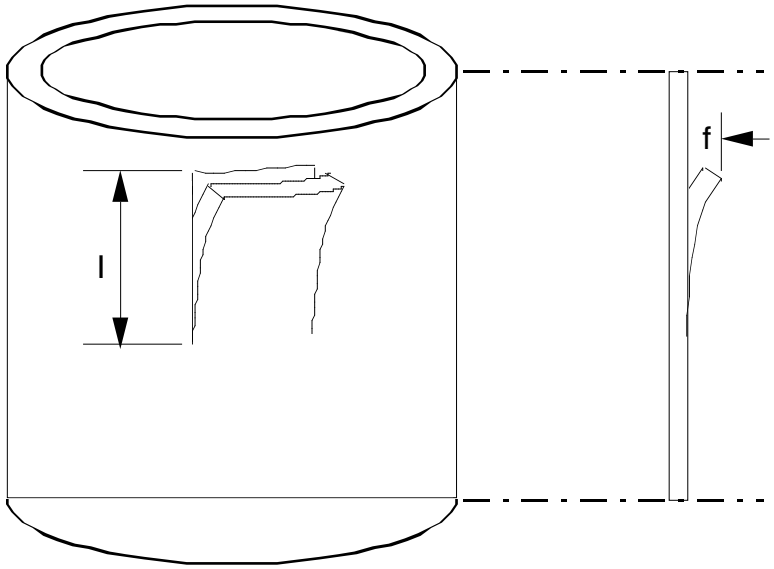

Figure 3.11 Longitudinal residual stress tongue.

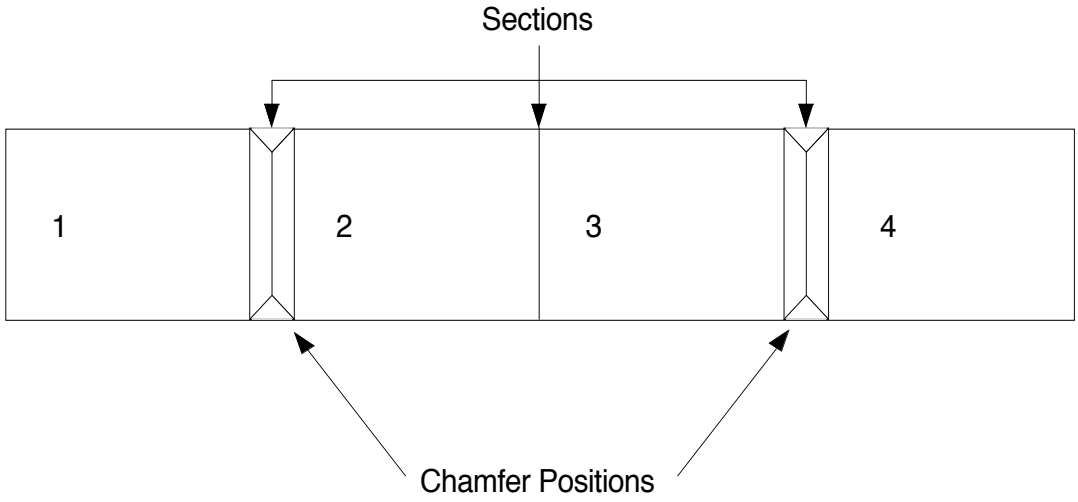

Figure 3.12 Orientation of the sections cut from polyester resinject tubes for investigation of the effect of residual stresses.

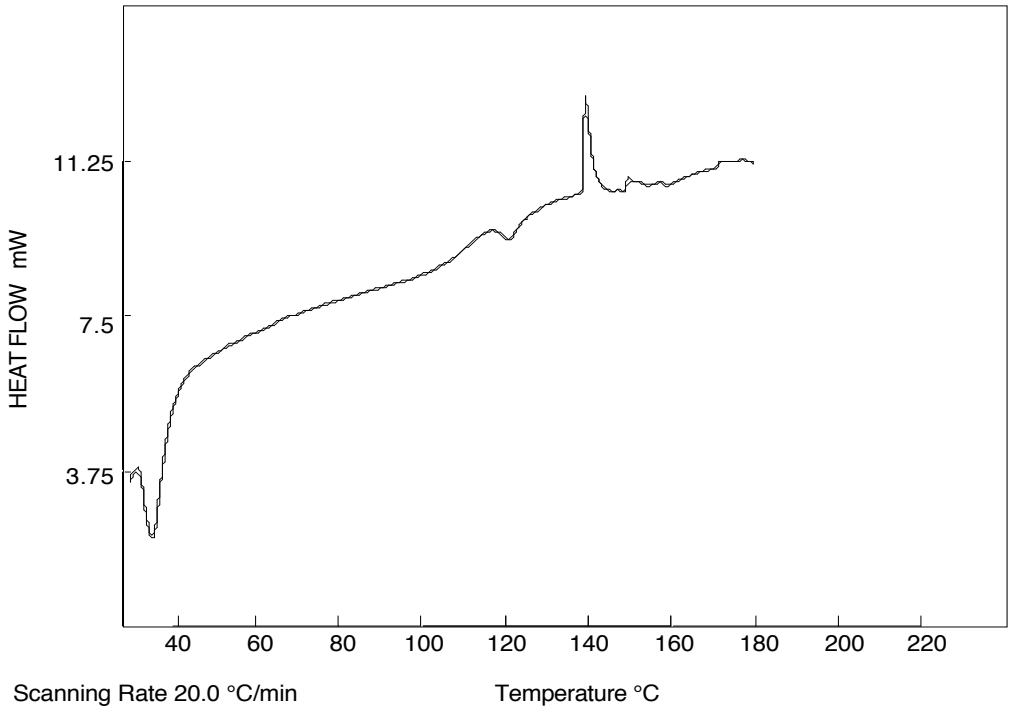

Figure 3.13 (a) DSC trace from the epoxy resin used in the Tufnol tubes.

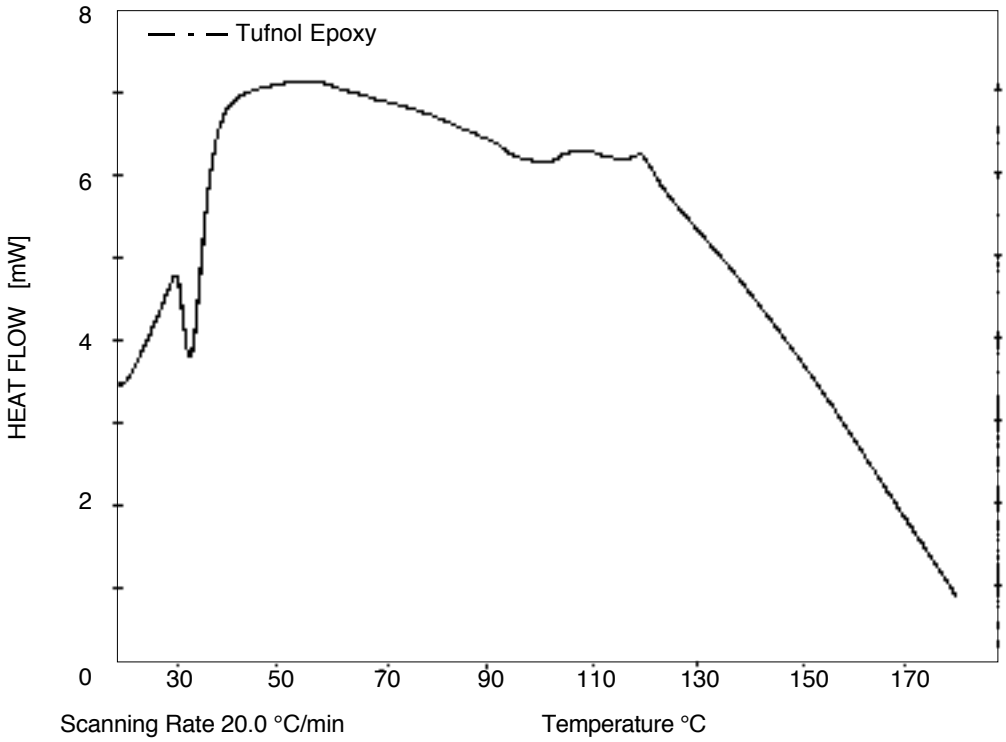

Figure 3.13 (b) DSC Trace from the epoxy resin used in the Tufnol tubes.

4 Results

The main part of this section is concerned with the crush tests that constituted the basis of this project. This is followed by the results from the other experiments, particularly the bend tests and the measurement of residual strains.

4.1 Presentation of Crush Test Results

For most of the work that has been carried out, the crush ratio, as defined in section 1.4, could be taken as unity and the specific energy absorption used. However, some work has been performed where the crush ratio was greater than unity, particularly at high temperatures where the failure mode was one of shell buckling. For this work, determining the crush ratio was difficult, so the concept of specific crush stress was introduced. This quantity was calculated in the same way as the specific energy absorption but the crush ratio was not required; specific crush stress being simply the crush stress in the uncrushed tube wall divided by the material density. The physical meaning was somewhat different to the specific energy absorption, because the stress distribution in the crush zone was not considered, but trends were still relevant. The specific crush stress was denoted by upper case sigma, Σ, sigma to indicate stress, and upper case to designate a specific quantity. All the results from this investigation have been quoted in terms of the specific crush stress for reasons of uniformity. This work may be directly compared to the results presented in the literature review in section 2.1, where the results were quoted as specific energy absorption.

The units that were used formerly for specific energy absorption were kJ kg^{-1}. These units were reasonably in keeping with S.I. unit nomenclature (although $\times 10^3$ J kg^{-1} would be more in keeping), and could be seen to be relevant to the quantity that was being measured, being an energy term. Although the specific crush stress was often

the same quantity as the specific energy absorption, and had the same units, quoting the specific crush stress in terms of an energy per unit mass did not appear to be immediately relevant. However, using S.I. nomenclature for a stress per unit density would have given: $N\ m^{-2}/kg\ m^{-3}$, which was somewhat cumbersome and reduced immediately to $N\ m\ kg^{-1}$, or $J\ kg^{-1}$. Reducing the units to fundamental units would have given $m^2\ s^{-2}$ which did not appear to have any immediate physical relevance, and implied that the quantity being measured was simply velocity squared, clearly a misleading situation, especially when considering speed sensitivity. One way round this difficulty was to use the specific density of the material instead of the actual density, as specific density is a dimensionless quantity and enabled the specific crush stress to be quoted in terms of $N\ m^{-2}$. Under these circumstances, $1\ MN\ m^{-2} = 1\ kJ\ kg^{-1}$, for a crush ratio of unity.

In this section, the presentation of the specific crush stress as a function of the crush speed for constant speed crushing, has been made with the speed axis on a direct reading logarithmic scale, calculated for crush speeds in $mm\ s^{-1}$. However, the equations that have been presented associated with these plots, have been based on crush speeds calculated in $m\ s^{-1}$ and presented as a linear relationship of the specific crush stress with the natural logarithm of the crush speed. The reasons for this were that the graph presentation enabled reading of the speed directly while keeping the axis labelling neat, and the equation presentation gave the value of speed sensitivity, λ, as defined in section 2.2.1.1.1, from the gradient while keeping to S.I. units. The line equations presented associated with each plot were calculated from the data, after suitable adjustment for units and axes; using an interpolation method incorporated in the graph drawing package Cricket Graph 1.2, as used on the Apple Macintosh.

4.2 Room Temperature Speed Results

This section has been divided according to the type of tube from which the results were obtained. Results from constant speed crushing have been separated from those from impact tests, unless a direct comparison was deemed appropriate. Constant speed crush results have been presented with a logarithmic speed scale while those from impact tests have been presented on a linear scale. The reason for the difference was that the speed range for constant speed crushing was over, typically, five orders of magnitude of speed while the impact tests were performed over less than one.

4.2.1 Tufnol Tubes

A plot of specific crush stress as a function of the crush speed on a logarithmic scale for Tufnol tubes, is shown in figure 4.1. There was a clear trend to higher values of specific crush stress at higher crush speeds and a logarithmic line fit was reasonable.

Figure 4.2 shows the specific crush stress as a function of the impact speed on a linear scale, for tests performed on the crash rig. A trend to higher values of specific crush stress with increasing impact speed was apparent from these data. These results were from test pieces cut from the same tube, thus reducing the potential degree of scatter resulting from variations between tubes. These results were divided into three sections, according to the impact speed, for the purposes of performing a statistical analysis using Student's t statistic. These sections were below 7 m s^{-1}, 10 m s^{-1} to 13 m s^{-1} and 18 m s^{-1} to 20 m s^{-1}. There were no results in the intervening sections. The results from each section were compared with the results from the other two sections and in all cases there was no significant similarity. This finding showed there was a definite increase in the measured value of specific crush stress with increasing impact speed. Although figure 4.2 was drawn with a straight line plot on a linear speed scale, if a

logarithmic plot was used, then the value of R that was obtained, being a measure of the fit of the line to the data, was the same as for the linear plot, indicating that the fit of a logarithmic plot was as good as a linear plot.

A regularly observed feature of the impact tests on the Tufnol tubes was that the initial impact, the tube having a chamfered end, gave a higher value of the crush load than for the subsequent impacts. A statistical analysis was carried out and it was found that there was no statistical similarity between the data obtained from the first impact and from those obtained from subsequent impacts, indicating a real effect. This observation is discussed in section 8.1.2.1.

All the impact tests that were performed on Tufnol tubes with the crush zone already established, displayed an initial peak load before crushing commenced, similar to that shown in figure 3.9 (a). It was observed that the higher impact speed tests tended to give higher levels of the initial peak load, F_i. Figure 4.3 shows the normalised peak load, F_i/F, as a function of the impact speed showing a trend to higher values of F_i/F at higher speeds. The two main groups of data, 3 m s^{-1} to 5 m s^{-1} and 10 m s^{-1}, were compared using the t-test and a significance of 0.016 found, meaning there was almost certainly a trend to higher values of the normalised peak load at higher impact speeds. This peak load is discussed in section 8.1.2.3.

4.2.2 Glass mat-polyester Tubes

Specific crush stress values obtained from constant speed crush tests on glass mat-polyester tubes, are shown as a function of the crush speed on a logarithmic scale in figure 4.4. Within the large amount of scatter in these results, there was no significant speed sensitivity of the specific crush stress.

Values obtained from similar tubes from impact tests on the crash rig are shown as a function of the impact speed on a linear scale in figure 4.5. These results showed no significant speed sensitivity of the specific crush stress.

A combination of the results in figures 4.4 and 4.5, is shown in figure 4.6 on a logarithmic speed scale. This shows clearly that the values of specific crush stress obtained from the impact tests were lower than those obtained from the constant speed crush tests. The two sets of results were compared using Student's t statistic and a significance of 0.000 was found, meaning there was no significant similarity between the sets of results. Although the level of scatter in the results was great, there were sufficient data available to enable a confident conclusion that high speed impact tests gave lower levels of specific crush stress than slow speed crush tests for these tubes. Mean values of specific crush stress can be given as being 59.7 MN m^{-2} for the slow speed crushing and 48.4 MN m^{-2} for impact tests.

Comparisons between the results obtained from the initial impact and subsequent impacts indicated that there might be a slight difference between the results (see section 4.2.1). However, performing the same statistical analysis on these tubes showed there to be no significant difference between the results obtained from the first test and subsequent tests.

4.2.3 Resinjection Tubes

The results obtained from the tubes produced by resinjection have been divided; initially according to the matrix used and then by the form of glass reinforcement.

4.2.3.1 Polyester Matrix Tubes

Figure 4.7 shows a plot of specific crush stress as a function of the crush speed, on a logarithmic scale, for RJPW tubes. It may be seen that there appeared to be a trend to higher crush stress at higher crush speeds. The number of tests performed was small, so the results from 0.001 mm s^{-1} were compared with those from the higher speeds using Student's t statistic. This showed that there was a significance of 0.016 which meant that, at a 5% confidence level, there was no significant similarity between the results. It can be concluded that there was a definite trend to higher crush stress at higher speeds within the speed range investigated.

Figure 4.8 shows a plot of specific crush stress as a function of the impact speed, on a linear scale, for RJPR tubes. This plot showed no significant speed variability over this range of speeds. This finding was consistent with the findings for the glass mat-polyester tubes (see section 4.2.2). These tubes were not tested extensively at constant speed but the few tests that were performed on the Instron at 0.5 mm s^{-1} and on the Cranfield at 3 ms^{-1} indicated that the specific crush stress decreased with increasing speed in this speed range. Comparison of the results obtained from the impact tests and those from the Cranfield using Student's t-test, gave a significance of 0.000, meaning there was no significant similarity between the sets of results and that the impact tests gave a lower value of specific crush stress than the Cranfield tests. The mean values found were: 53.8 MN m^{-2} for 3 m s^{-1} and 48.7 MN m^{-2} for the impact tests. This finding was consistent with the behaviour of the glass mat-polyester tubes.

4.2.3.2 Epoxy Matrix Tubes

Figure 4.9 shows a plot of specific crush stress as a function of the crush speed on a logarithmic scale, for RJEW tubes. This plot showed a definite increase in specific crush stress with increasing speed; this being consistent with the behaviour of the Tufnol tubes. Applying Student's t-test to these data, using paired data as the values came from instantaneous speed change tests, gave a significance of 0.056, meaning that the two data sets were probably significantly different, the low number of observations limiting the confidence that can be placed in the data.

Figure 4.10 shows a plot of specific crush stress as a function of the impact speed on a linear scale, for RJEW tubes. This plot showed a slight increase in specific crush stress with increasing speed. Applying Student's t-test to these data, using unpaired samples, gave a significance of 0.002 for the data between 5 m s^{-1} and 10 m s^{-1}, indicating that there was probably a significant increase in specific crush stress with increasing impact speed. However, there was no significant difference between the values obtained at 10 m s^{-1} and those from 20 m s^{-1}, a significance of 0.303 being calculated.

Figure 4.11 shows the specific crush stress as a function of the impact speed on a linear scale, for RJER tubes. This plot indicated a possible slight increase in specific crush stress with increasing velocity. However, applying Student's t-test to these data using unpaired samples, gave a significance of 0.049, showing that there was probably a significant difference between the data from 5 m s^{-1} and those from 13 m s^{-1}. A significance of 0.07 was calculated when comparing the 5 m s^{-1} values with those obtained from 10 m s^{-1}, indicating there might have been an effect. However, the

variability between samples and the low number of tests carried out must lead to the conclusion that no significant variation was observed.

4.3 Speed-Temperature Interaction

The results in this section have been divided into two main types for each type of tube, speed sensitivity of the specific crush stress at different bulk temperatures, and temperature sensitivity at different speeds. Each of these plots can be regarded as being a vertical section through a three-dimensional plot of specific crush stress as a function of the speed and temperature.

4.3.1 Tufnol Tubes

4.3.1.1 Speed Sensitivity at Different Temperatures

Figures 4.12 to 4.20 show the specific crush stress as functions of the crush speed for Tufnol tubes from the series of tests performed with instantaneous speed changes over a range of tube bulk temperature, from -90 °C to 110 °C. Some other results were incorporated into these graphs where appropriate. These plots were made with a logarithmic speed scale, and the lines drawn and best fit equations given, were calculated using a computer graph drawing package as mentioned in section 4.1. All the plots showed an increase in specific crush stress with increasing speed, the magnitude of the increase being dependent on the temperature. This finding is discussed further in sections 5.1 and 8.3.2.

4.3.1.2 Tufnol Temperature at Speed

Figures 4.21 to 4.24 show plots of the specific crush stress of Tufnol tubes as functions of the test temperature over the speed range 0.002 mm s^{-1} to 10 mm s^{-1}, and the impact tests from 10 m s^{-1}. At the higher temperatures tested, the tubes collapsed

by unstable buckling. The transition temperature between the frond splaying type of crushing and buckling was dependent on the crush speed.

Figures 4.21 to 4.24 show a slight decrease in specific crush stress, on increasing the temperature from the low temperatures tested to room temperature, followed by a more rapid decrease as the temperature exceeded about 40 °C.

Figure 4.25 shows a test map of the different modes of collapse, showing a clear transition from the normal frond-wedge-frond mode at low temperatures to a buckling mode at higher temperatures. The transition, as taken from the uncertain mode points, was both speed and temperature sensitive.

Figure 4.26 is a plot of the specific crush stress as a function of the reciprocal of the absolute temperature, for two crush speeds. This plot was made for the purposes of calculating activation energies for crushing.

4.3.2 Glass mat-polyester Tubes

The glass mat-polyester tubes were not tested extensively over a range of temperatures but some tests were carried out on the crash rig after pre-heating as described in section 3.2.2. Results from these tests are presented in figure 4.27. Although the low temperature tests were performed after immersion in liquid nitrogen, hence the results could be presented as having been at -196 °C, the actual temperature was probably somewhat higher resulting from problems of fitting the tubes to the mounting spigot on the sled, caused by thermal contraction. Thus the results have been presented as being at about -150 °C.

The behaviour of these tubes was similar to that of the Tufnol tubes, but the decrease in specific crush stress on increasing the temperature from liquid nitrogen immersion

to room temperature was less, as was the decrease on increasing the temperature to about 80 °C. It must be concluded that these tubes were less sensitive to the testing temperature than the Tufnol tubes.

4.3.3 Resinject Tubes

Only results from the resinject tubes incorporating woven cloth reinforcement are presented here extensively. This is because the random mat tubes collapsed unstably at temperatures that were too low to enable any significant trends to be identified. Typically they collapsed at temperatures above 60 °C, although some tubes collapsed at even lower temperatures.

4.3.3.1 RJPW Speed at Temperature

Figures 4.28 to 4.35 show plots of the specific crush stress of RJPW tubes as functions of the test speed, over the temperature range -20 °C to 90 °C. The specific crush stress increased with increasing crush speed for all except the -20 °C tests. At that temperature, there was no speed sensitivity of the specific crush stress. Two tests were performed at -40 °C, at 0.002 mm s^{-1} and 10 mm s^{-1} but no difference was found in the measured values of specific crush stress.

4.3.3.2 RJPW Temperature at Speed

Figures 4.36 to 4.40 show plots of the specific crush stress for RJPW tubes as functions of the test temperature over the speed range 0.002 mm s^{-1} to 10 mm s^{-1}. Figure 4.41 shows the specific crush stress as a function of the reciprocal of the absolute temperature for the extremes of the speed range as in section 4.3.1.2. All the figures show a rapid decrease in specific crush stress with increasing temperature above room temperature.

4.3.3.3 RJPR Results

The results from the RJPR tubes are presented as a plot of specific crush stress as a function of the test temperature for the two speeds investigated, in figure 4.42. The specific crush stress as a function of the reciprocal of the absolute temperature is shown in figure 4.43.

4.3.3.4 RJEW Speed at Temperature

Figures 4.44 to 4.50 show the specific crush stress as a function of the crush speed for RJEW tubes over the temperature range -40 °C to 85 °C. These plots show an increase in specific crush stress with increasing speed, the magnitude of the increase being dependent on the temperature. This is discussed further in sections 5.1 and 8.3.2.

4.3.3.5 RJEW Temperature at Speed

Figures 4.51 to 4.56 show plots of the specific crush stress for RJEW tubes, as functions of the test temperature, over the speed range 0.002 mm s^{-1} to 10 mm s^{-1}. These plots show similar behaviour to the Tufnol tubes.

Figure 4.57 shows the specific crush stress as a function of the reciprocal of the absolute temperature for the extremes of the speed range as in section 4.3.1.2 above.

4.4 Instantaneous Speed Change Crush Traces

Figures 4.58 to 4.64 show the force-displacement responses of Tufnol tubes tested at temperatures ranging from -90 °C to 80 °C, incorporating a change in the crush speed after the crush had progressed about 20 mm. Speed changes in both directions are shown. These traces show several noteworthy features, both as a result from the change in speed and the differences in temperature between the tests. In all cases, the

lower crush speed (0.002 mm s^{-1}) is distinguishable by the greater thickness of the line. This was because of instability of the chart recorder when used at such a slow speed, this stage of the crush taking about three hours to complete. In all cases, the mean crush load was higher for the faster speed crush (10 mm s^{-1}).

The transition between the speeds is shown clearly in the traces from tests at 22 °C and 60 °C. In each case the load took a short distance to settle down to a constant mean level after the speed change. This distance can be seen to be present in all the traces, independent of the speed change direction. The transition is clearest in the traces for 60 °C. In both tests the crush load took about 3 mm of crush distance to settle down to the equilibrium mean value for that speed and temperature.

One significant difference between the speed change directions was the presence of a load peak immediately after the speed change from slow to fast, after which the crush load settled down to an equilibrium mean value. The traces for the speed change from fast to slow showed a drop in load. However, this load drop was accompanied by a reverse movement of the signal from the displacement transducer which was recovered on further crushing, implying that it was because of a testing machine response instead of a material response.

The other major observation that was made from these traces concerned the degree of serration of the crush trace. The traces obtained from the -90 °C tests had a much higher degree of serration than those tested at higher temperatures. Generally, it was found that the degree of serration decreased with increasing temperature. It was difficult to make any firm conclusions regarding the effect of the speed on the degree of serration as, at low speeds, it was dependent to some extent on the stability of the load cell signal and the chart recorder while the serrations at higher speeds were

dependent on the speed of response of the chart recorder. However, the degree of serration observed in the -90 °C, 10 mm s^{-1} test implied that the latter problem might only have been of significance in those tests.

4.5 Length Test Results

The figures measured for the level of serration of the crush traces were normalised with relation to the mean crush load to enable comparisons between different tubes to be made.

Figures 4.65 to 4.67 show the normalised level of serration of the crush traces as functions of the tube length, for the three types of tube described in section 3.4.2. In each of the plots, the tube length has been presented as the mean tube length. This was due to the length of the tube changing during the crush. The mean length was taken as being the original tube length, minus half the crush distance.

Although best fit lines indicated trends in the level of serration, the degree of scatter indicated that there was no clear dependence on length of the degree of serration of the crush trace for the tubes tested in this study.

4.6 Bend Test Results

Figures 4.68 to 4.70 show the flexural modulus, flexural strength and flexural strain to failure respectively, for Tufnol 10G40 flat plate material, as functions of the cross-head speed on a logarithmic scale. The flexural modulus showed a linear decrease with log. speed over the range tested while both the flexural strength and strain to failure showed linear increases. However, applying Student's t-test to these data showed that there was no significant trend in the modulus results while both the

strength and strain to failure results showed significant increases with increasing speed.

4.7 Residual Strains

Two types of residual strains were investigated in the tubes, being hoop strains and longitudinal strains.

4.7.1 Hoop Strains

Residual strains were found to be present in the hoop direction of the Tufnol tubes and the glass-polyester tubes produced by resinjection. No measurable residual hoop strains were found in either type of resinject glass-epoxy tubes.

The residual strain distribution as a function of the wall thickness was found to be as given in tables 4.1 to 4.3, and shown in figures 4.71 to 4.73. It should be noted that while the figures given for the strains are quoted as being positive, all the measured strains were compressive.

t mm	ε %
0.90	0.032
1.12	0.045
1.24	0.049
1.64	0.058
1.91	0.055
2.15	0.067
2.41	0.076
2.52	0.062

Table 4.1 Residual strain measured as a function of the wall thickness for a Tufnol tube.

t mm	ε %
0.67	0.039
0.95	0.069
1.33	0.115
1.64	0.128
1.99	0.133

Table 4.2 Residual strain measured as a function of the wall thickness for a RJPW tube.

t mm	ε %
0.07	0.033
0.66	0.030
0.93	0.090
1.21	0.089
1.50	0.082
1.77	0.130
1.96	0.111

Table 4.3 Residual strain measured as a function of the wall thickness for a RJPR tube.

It can be seen that, for the tubes investigated, the strain increased with increasing wall thickness. Residual strains are dealt with further in section 5.2.

4.7.2 Longitudinal Strains

The presence of longitudinal residual strains was investigated as described in section 3.4.3.2.

An RJPW tube was the only one tested for longitudinal residual strains, as this type of tube had shown the highest level of residual hoop strain.

No measurable deflection of the tongue was found when measured using vernier callipers. It was deduced that there was no significant residual strain in the longitudinal direction.

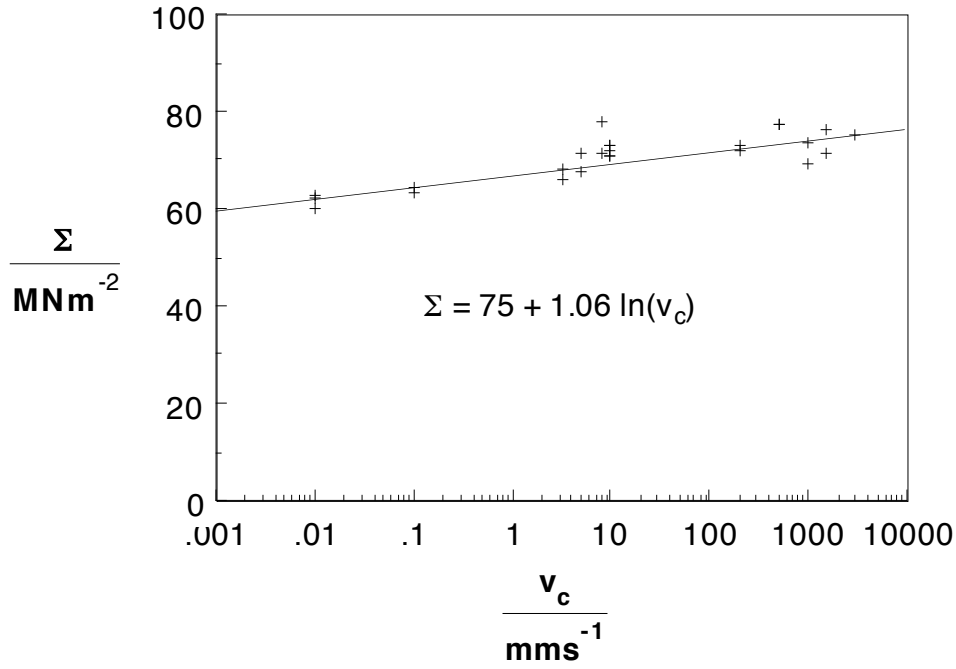

Figure 4.1 Plot of specific crush stress as a function of the crush speed for Tufnol tubes.

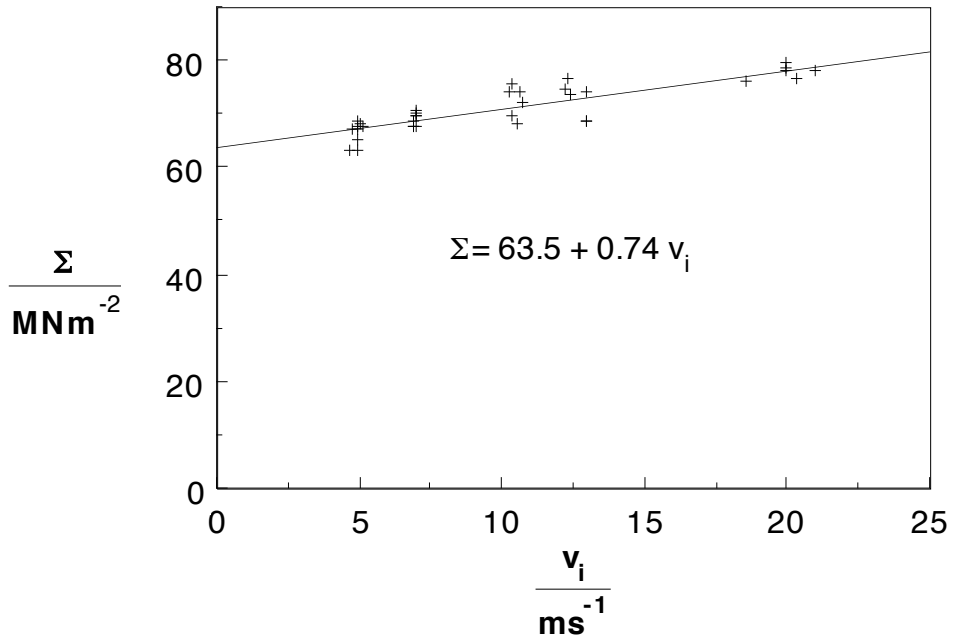

Figure 4.2 Plot of specific crush stress as a function of the impact speed for Tufnol tubes.

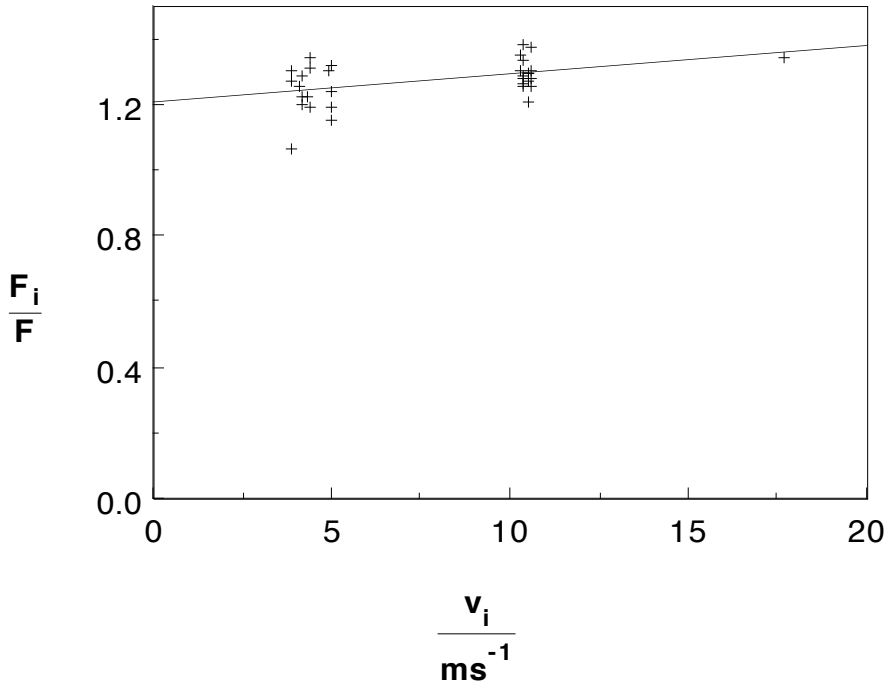

Figure 4.3 Plot of F_i/F as a function of the impact speed for Tufnol tubes.

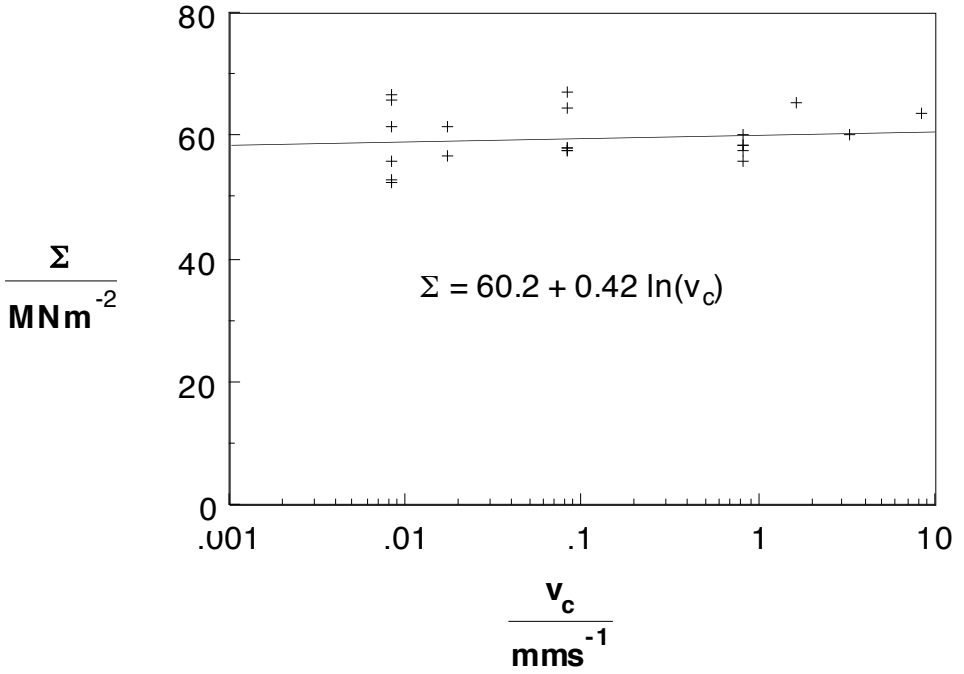

Figure 4.4 Plot of specific crush stress as a function of the crush speed on a logarithmic scale for glass mat-polyester tubes.

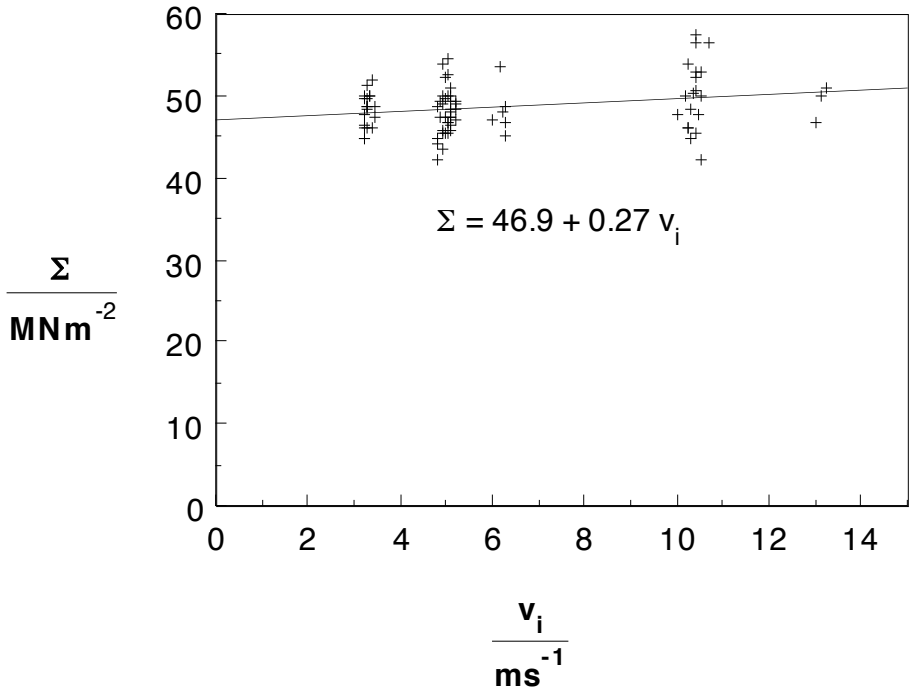

Figure 4.5 Plot of specific crush stress as a function of the impact speed on a linear scale for glass mat-polyester tubes.

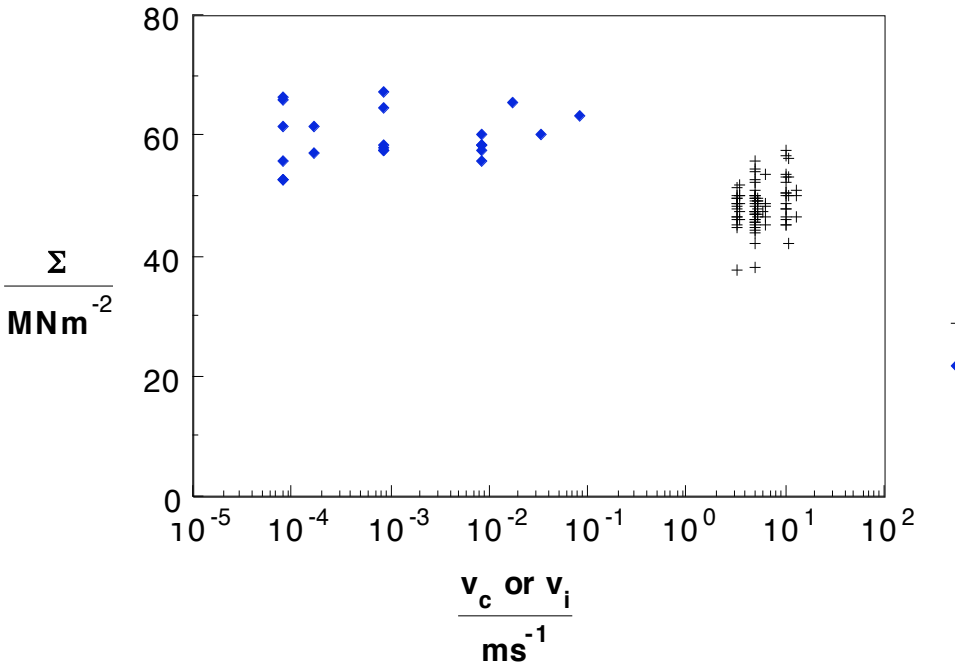

Figure 4.6 Comparison of the specific crush stress of glass mat-polyester tubes tested in constant speed crushing (♦) or impact (+).

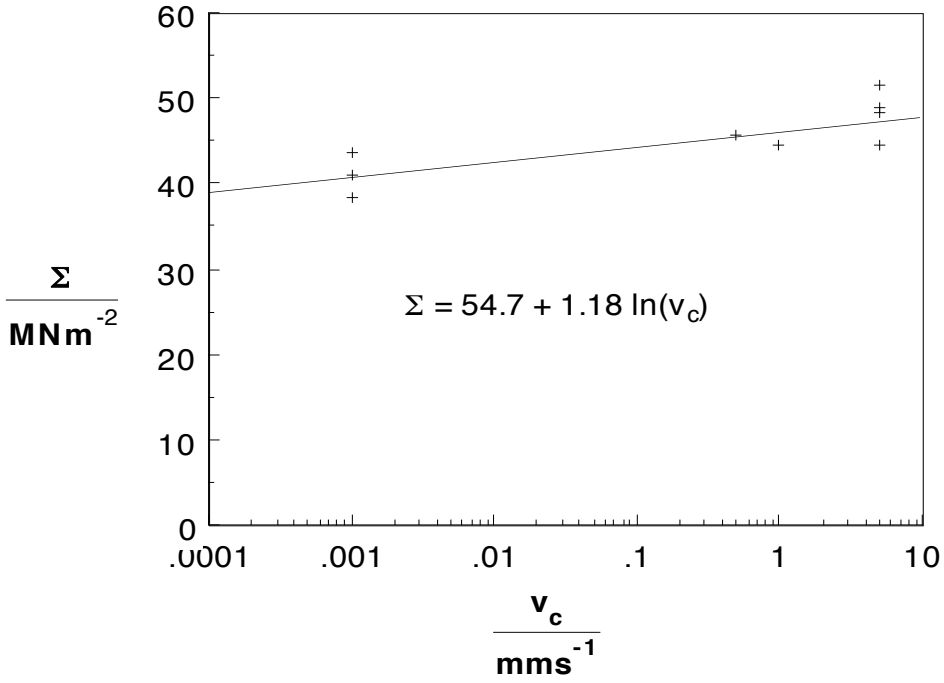

Figure 4.7 Plot of specific crush stress as a function of the crush speed for RJPW tubes.

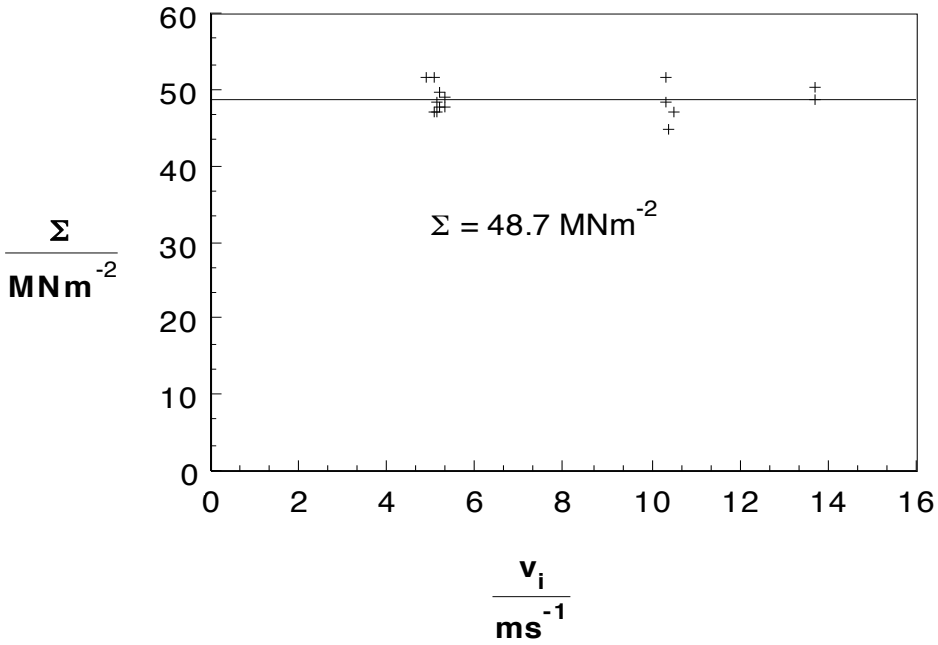

Figure 4.8 Plot of specific crush stress as a function of the impact speed for RJPR tubes.

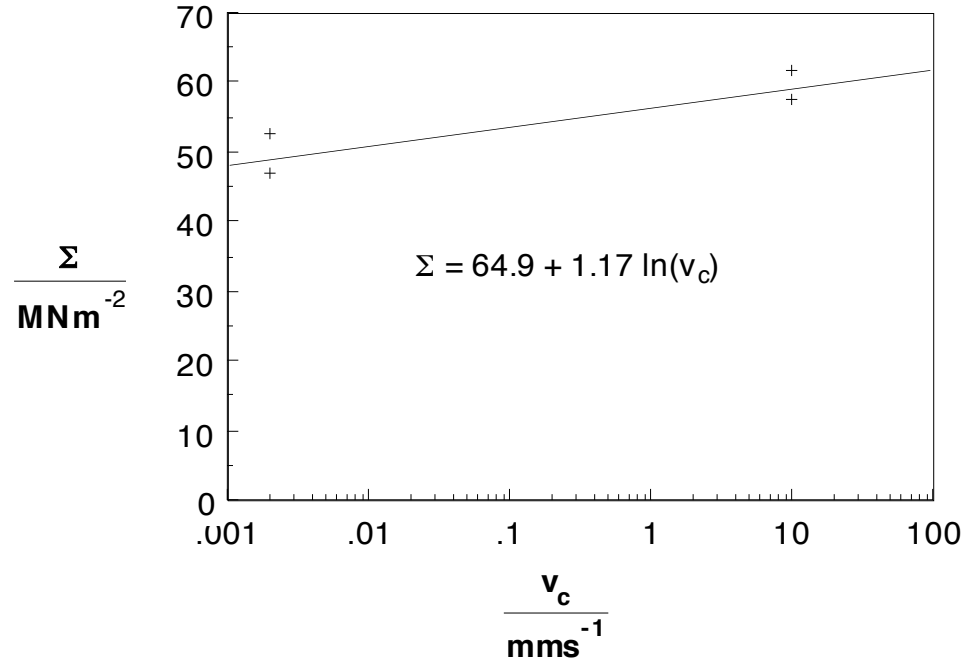

Figure 4.9 Plot of specific crush stress as a function of the crush speed for RJEW tubes.

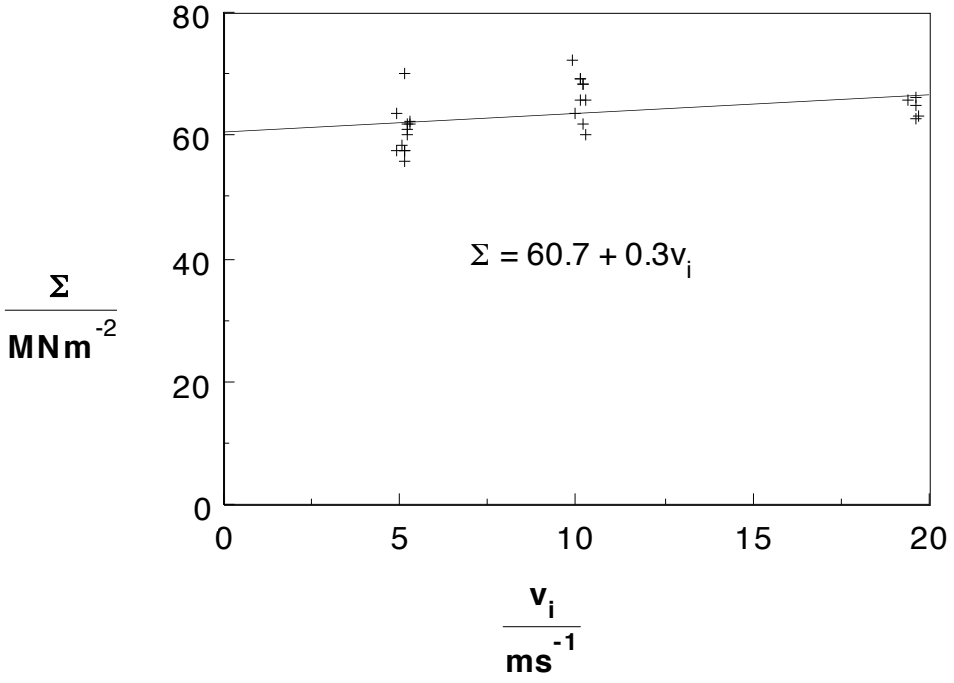

Figure 4.10 Plot of specific crush stress as a function of the impact speed for RJEW tubes.

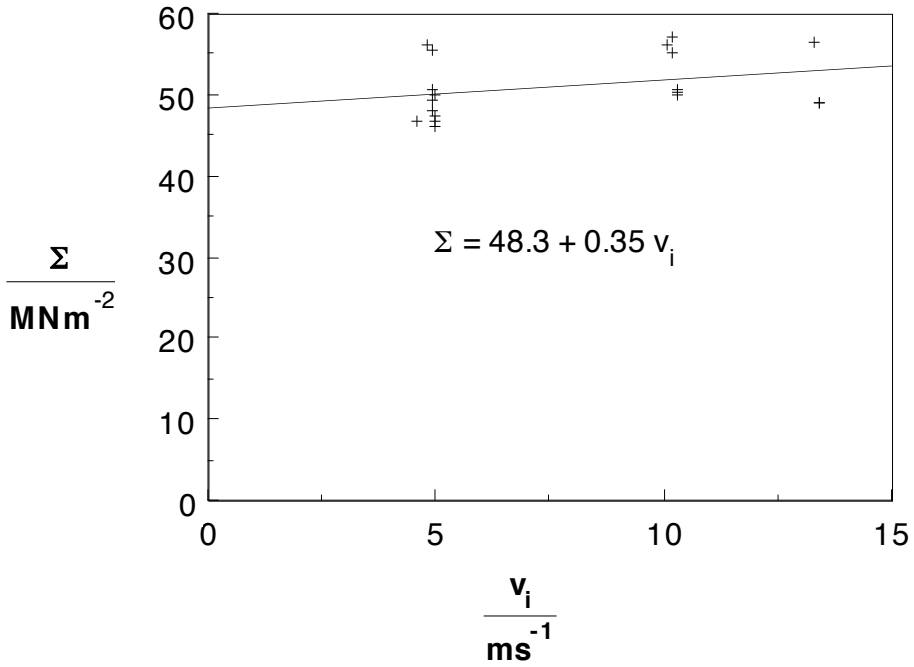

Figure 4.11 Plot of specific crush stress as a function of the impact speed for RJER tubes.

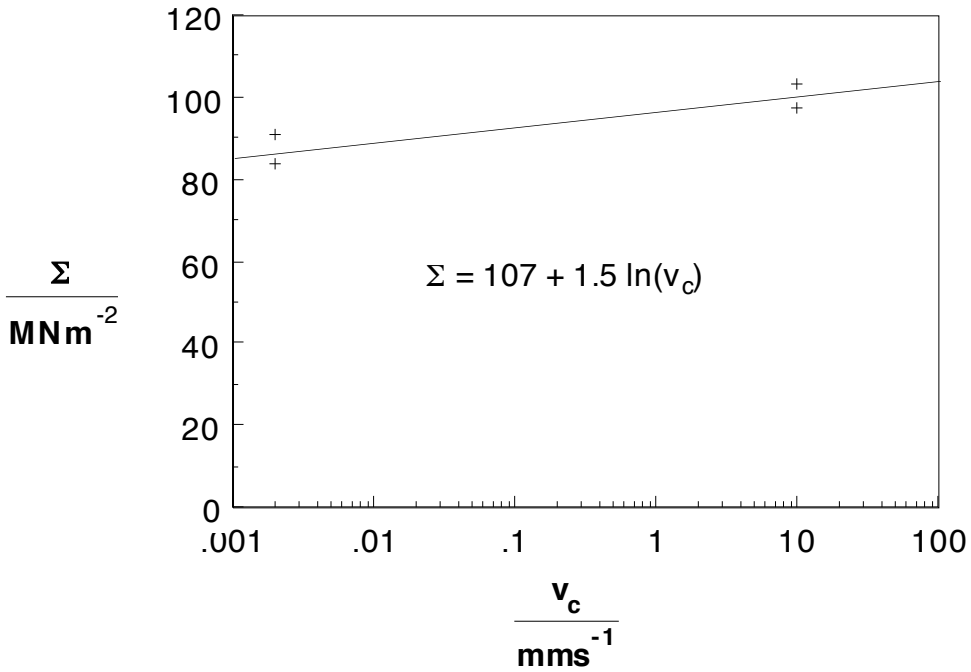

Figure 4.12 Plot of specific crush stress as a function of the crush speed for Tufnol tubes tested at -90 °C.

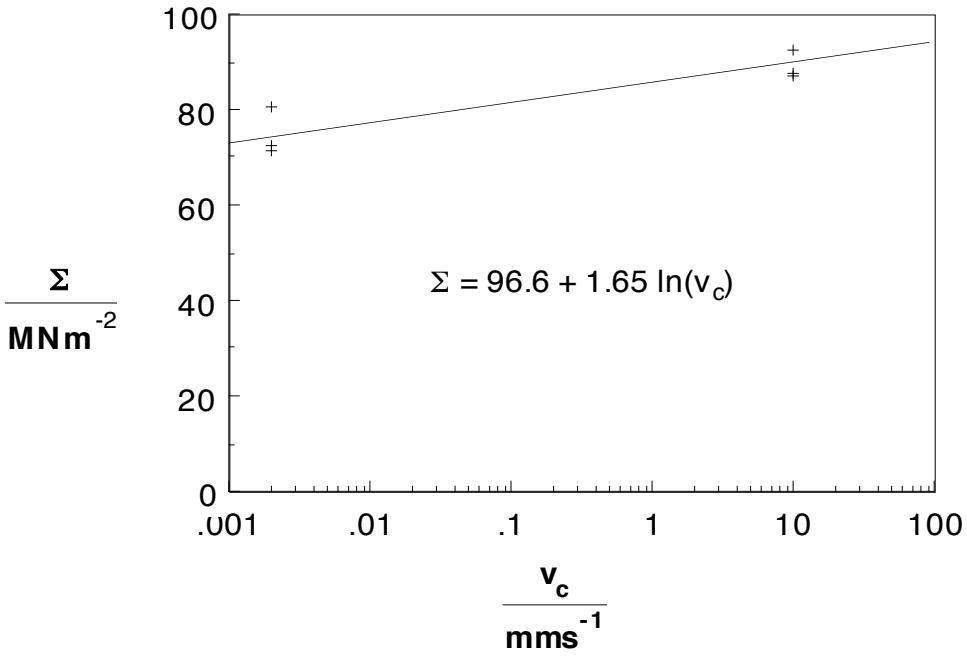

Figure 4.13 Plot of specific crush stress as a function of the crush speed for Tufnol tubes tested at -20 °C.

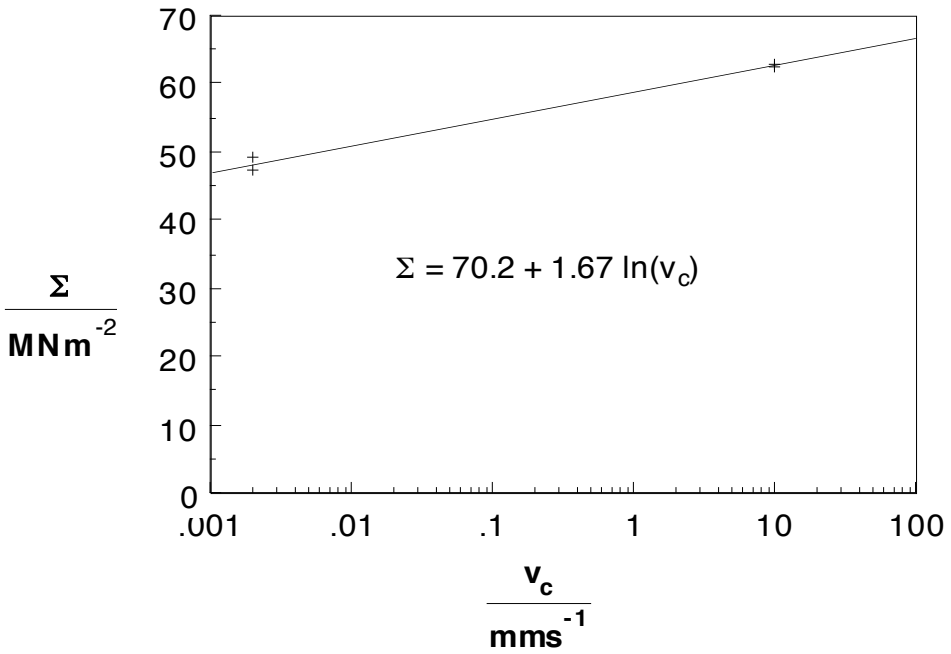

Figure 4.14 Plot of specific crush stress as a function of the crush speed for Tufnol tubes tested at 50 °C.

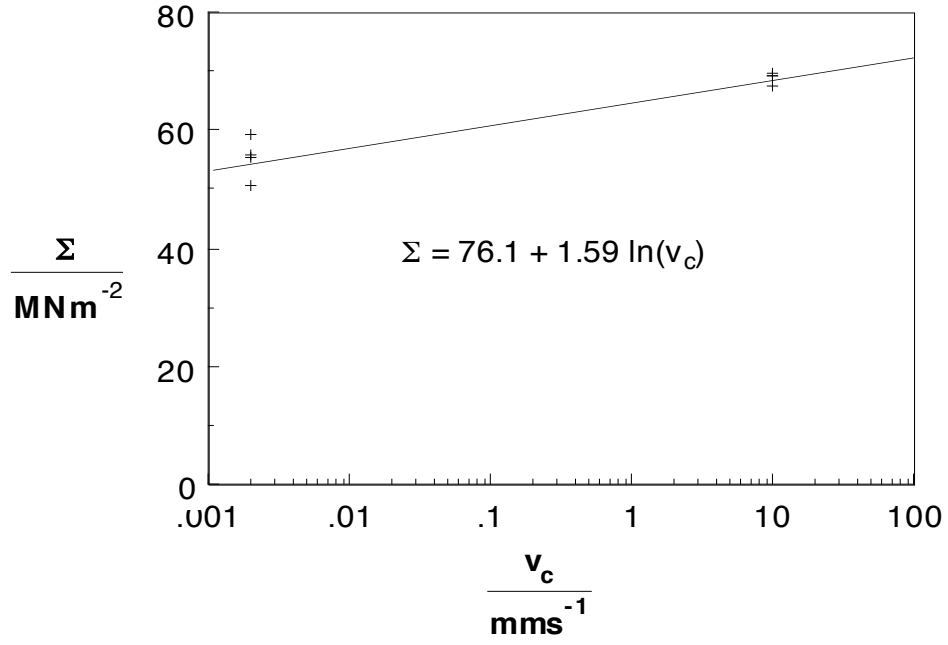

Figure 4.15 Plot of specific crush stress as a function of the crush speed for Tufnol tubes tested at 60 °C.

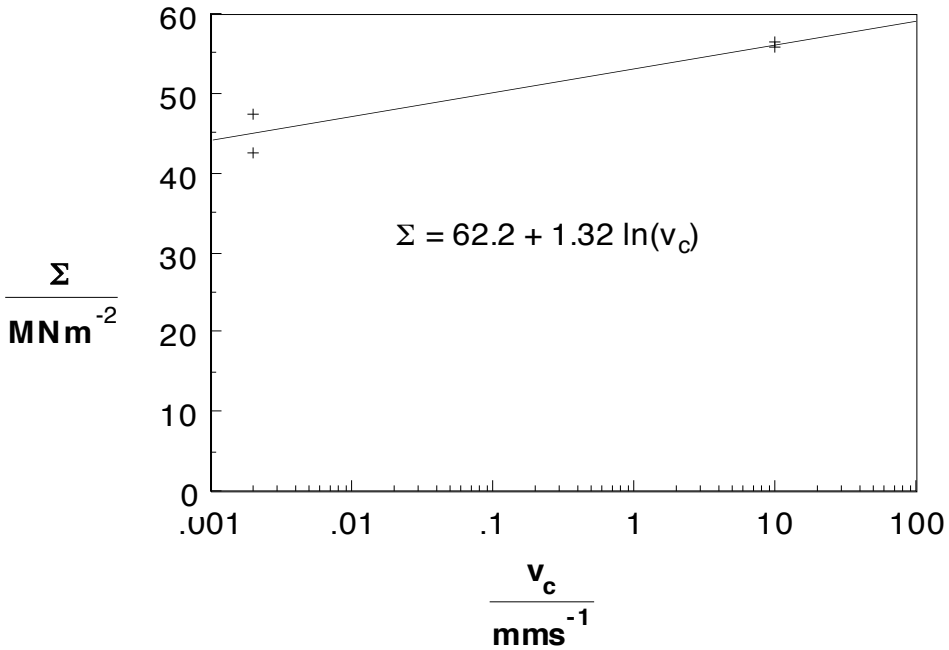

Figure 4.16 Plot of specific crush stress as a function of the crush speed for Tufnol tubes tested at 70 °C.

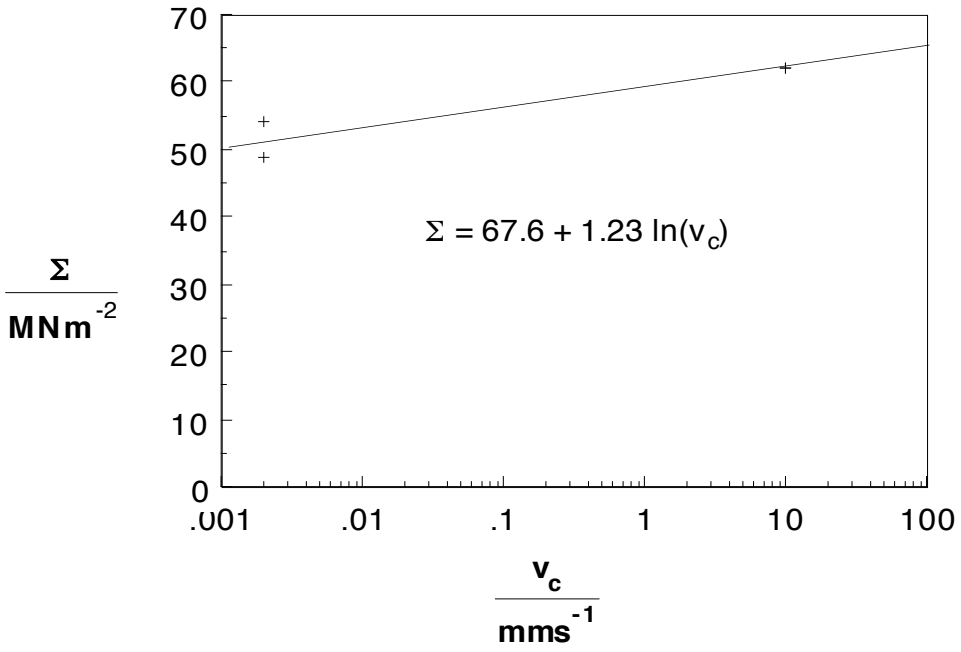

Figure 4.17 Plot of specific crush stress as a function of the crush speed for Tufnol tubes tested at 80 °C.

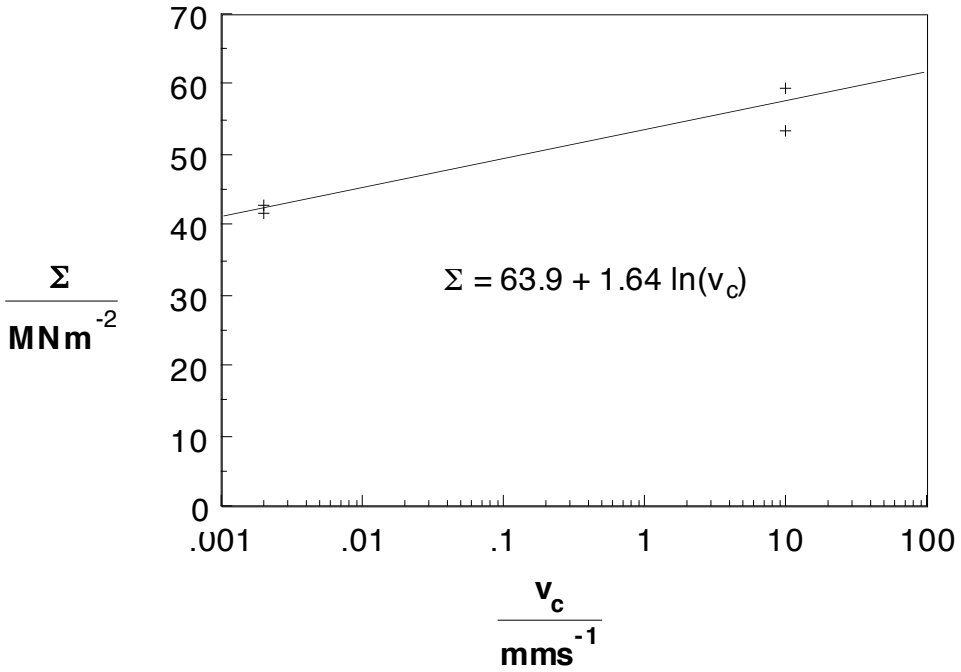

Figure 4.18 Plot of specific crush stress as a function of the crush speed for Tufnol tubes tested at 90 °C.

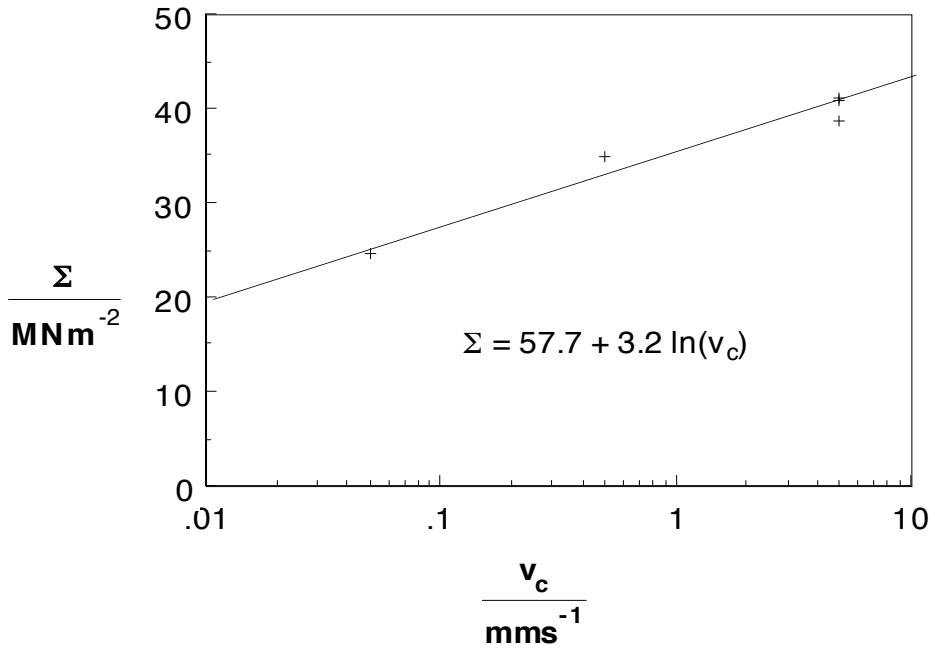

Figure 4.19 Plot of specific crush stress as a function of the crush speed for Tufnol tubes tested at 100 °C, the results from tubes that collapsed by buckling having been excluded.

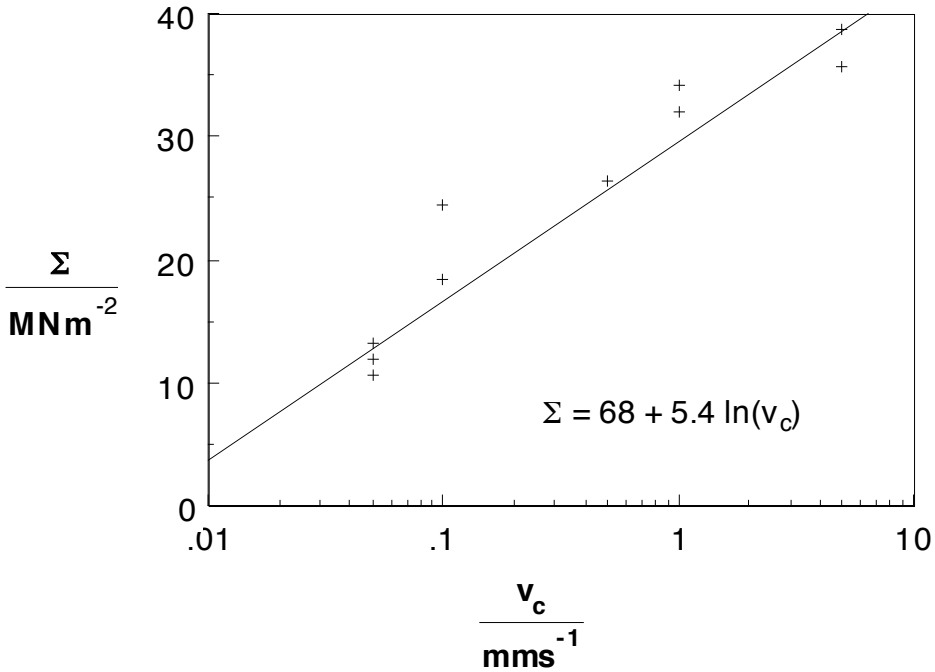

Figure 4.20 Plot of specific crush stress as a function of the crush speed for Tufnol tubes tested at 110 °C, the results from tubes that collapsed by buckling having been excluded.

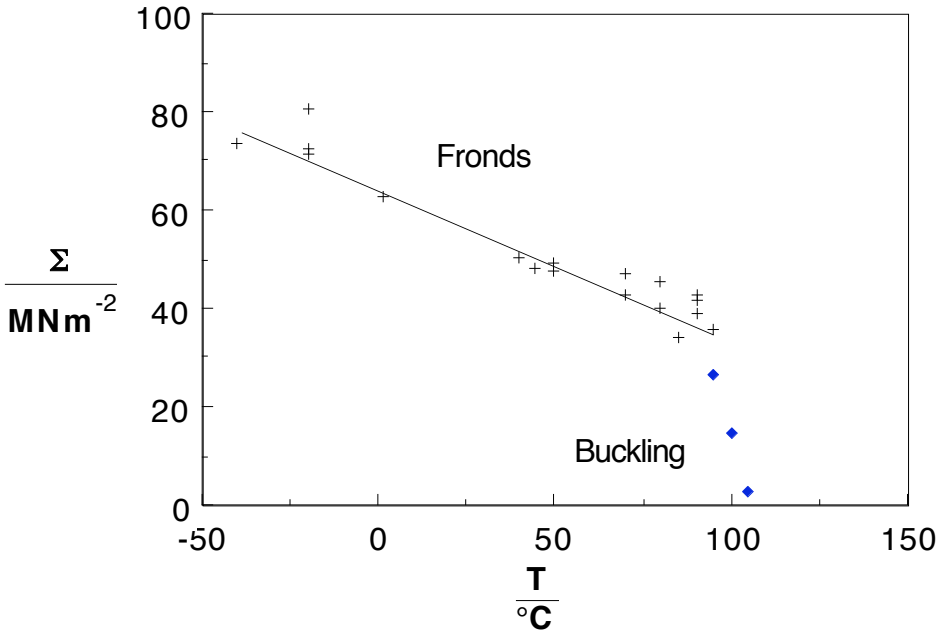

Figure 4.21 Plot of specific crush stress as a function of the test temperature for Tufnol tubes tested at 0.002 mm s^{-1}.

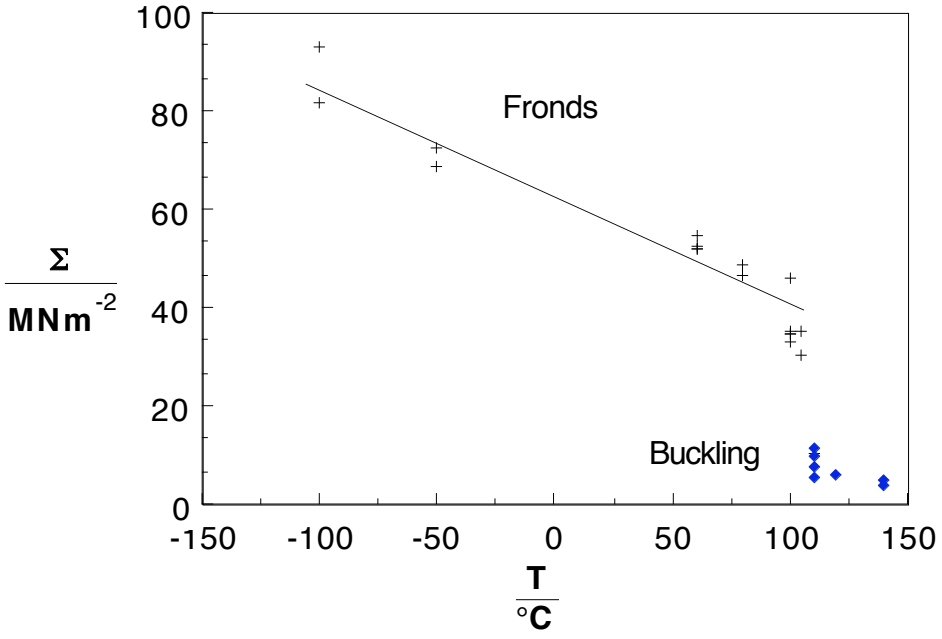

Figure 4.22 Plot of specific crush stress as a function of the test temperature for Tufnol tubes tested at 0.5 mm s^{-1}.

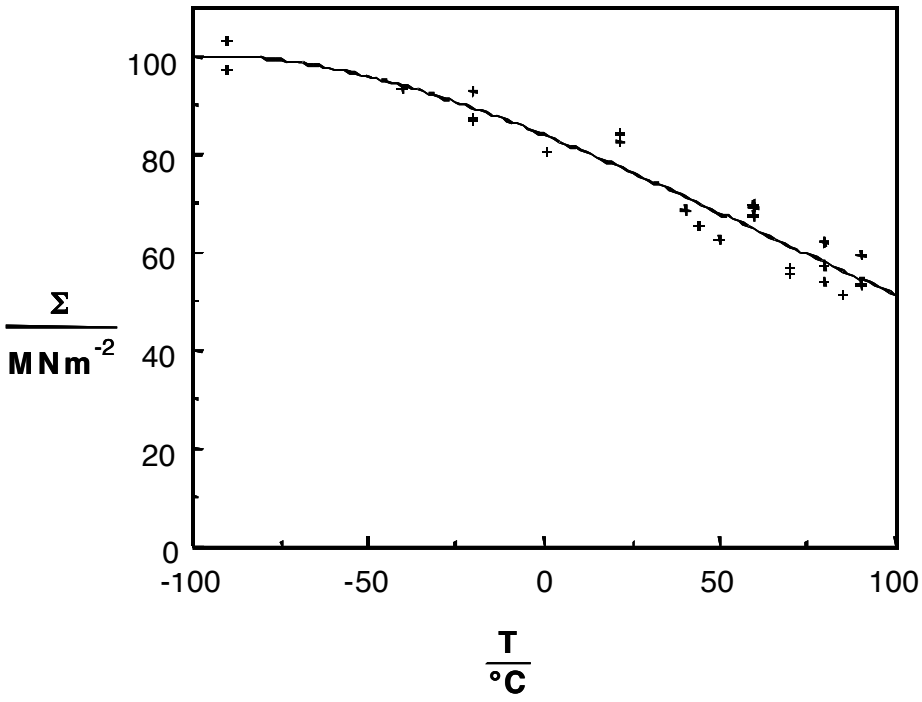

Figure 4.23 Plot of specific crush stress as a function of the test temperature for Tufnol tubes tested at 10 mm s^{-1}.

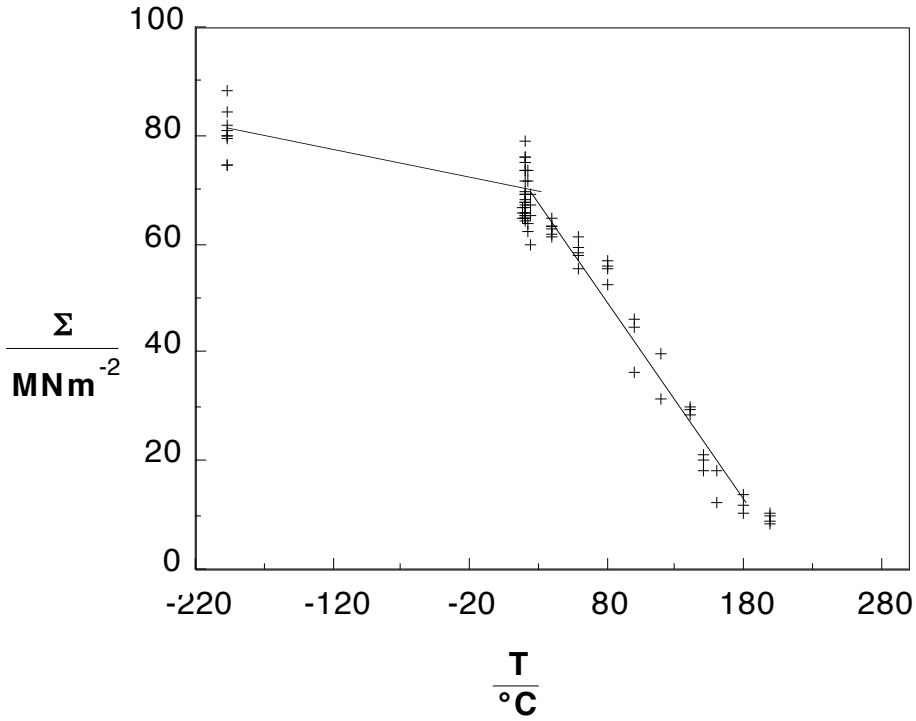

Figure 4.24 Plot of specific crush stress as a function of the test temperature for Tufnol tubes impact tested from 10 m s^{-1}.

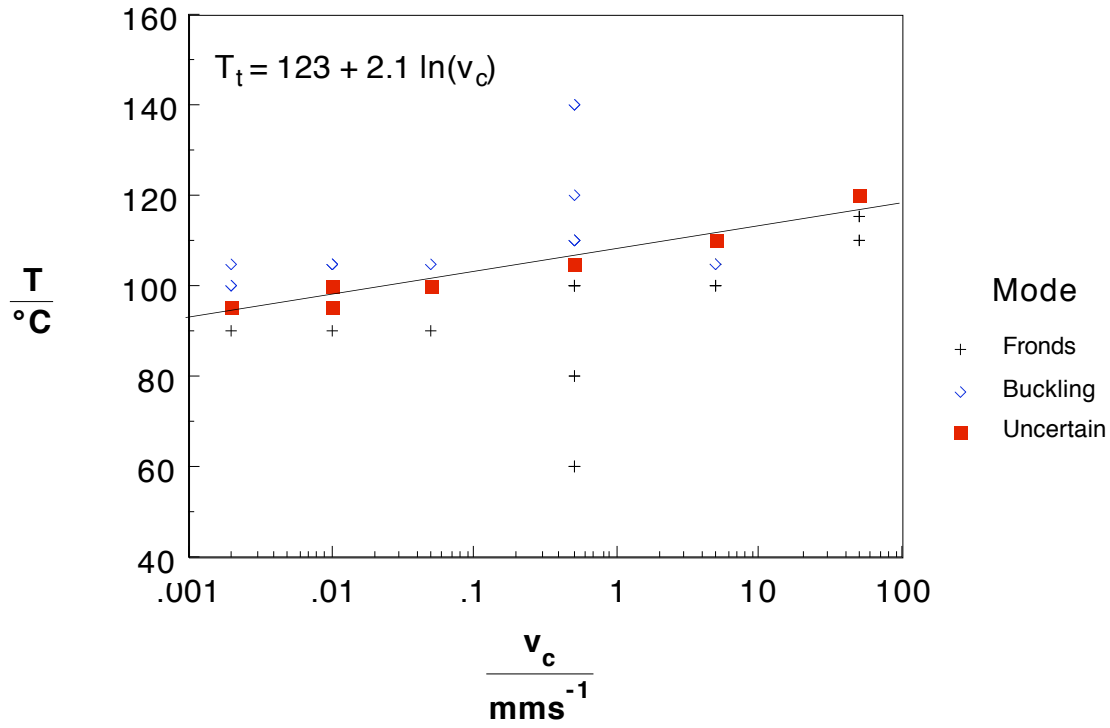

Figure 4.25 Map of the different basic modes of failure for Tufnol tubes as functions of speed and temperature. T_t is the transition temperature.

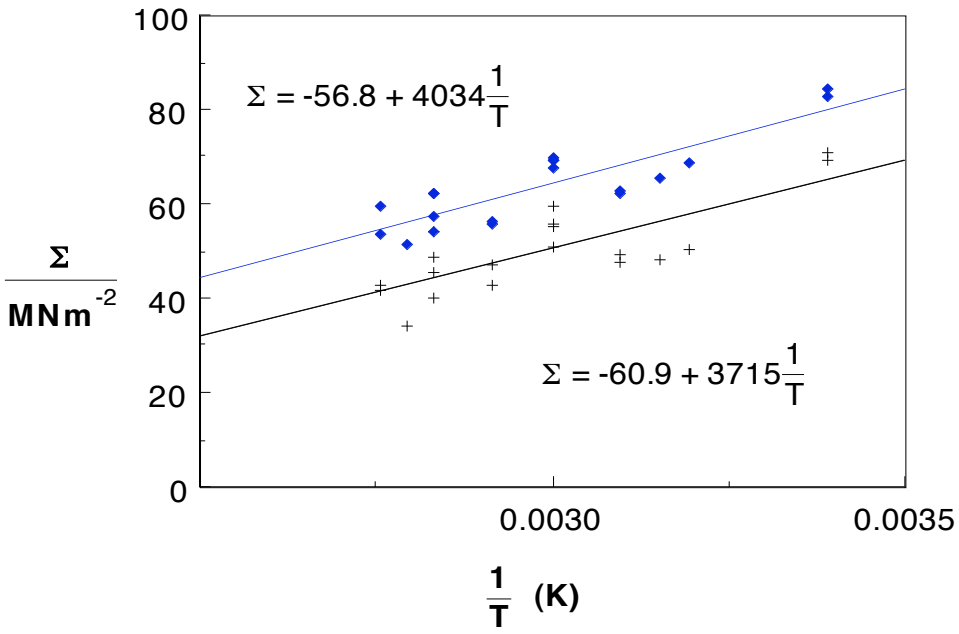

Figure 4.26 Plot of specific crush stress as a function of the reciprocal absolute temperature for Tufnol tubes. + denotes a speed of 0.002 mm s^{-1} and ♦ denotes a speed of 10 mm s^{-1}.

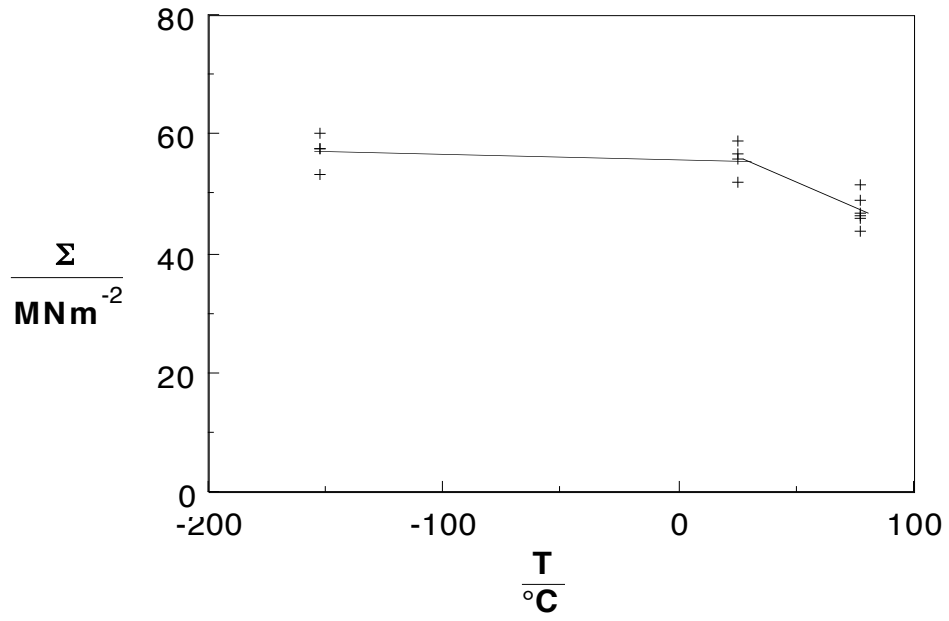

Figure 4.27 Plot of specific crush stress as a function of the test temperature for glass mat-polyester tubes impact tested from 10 m s^{-1}

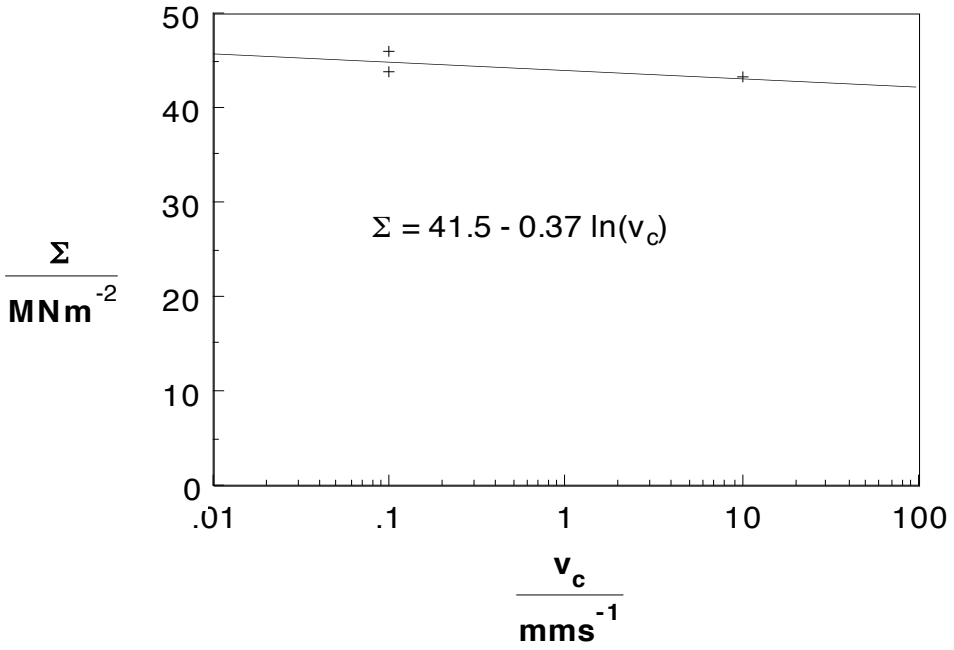

Figure 4.28 Plot of specific crush stress as a function of the crush speed for RJPW tubes tested at -20 °C.

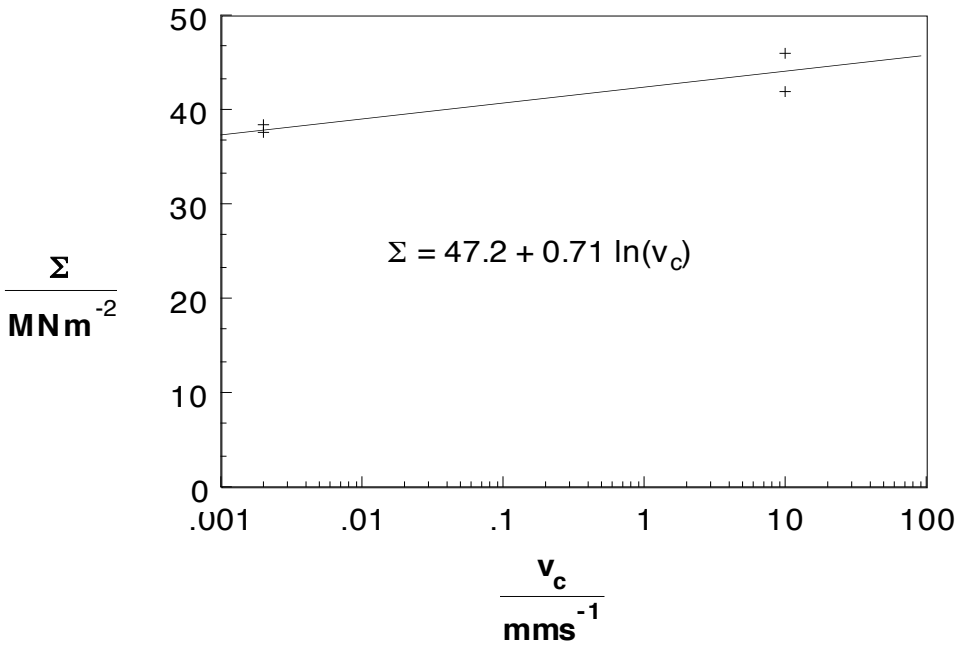

Figure 4.29 Plot of specific crush stress as a function of the crush speed for RJPW tubes tested at 0 °C.

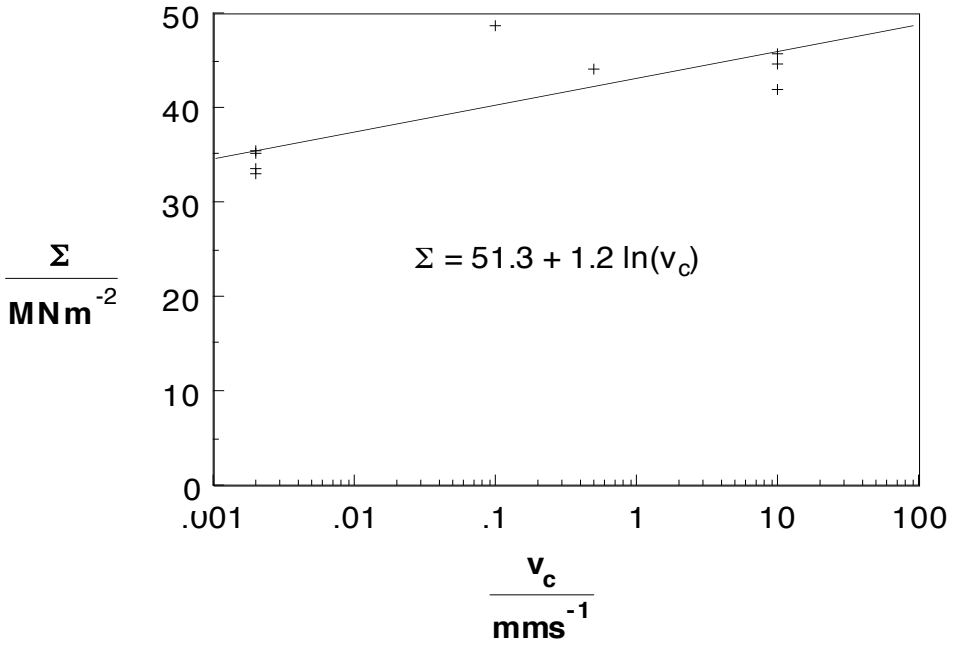

Figure 4.30 Plot of specific crush stress as a function of the crush speed for RJPW tubes tested at 40 °C.

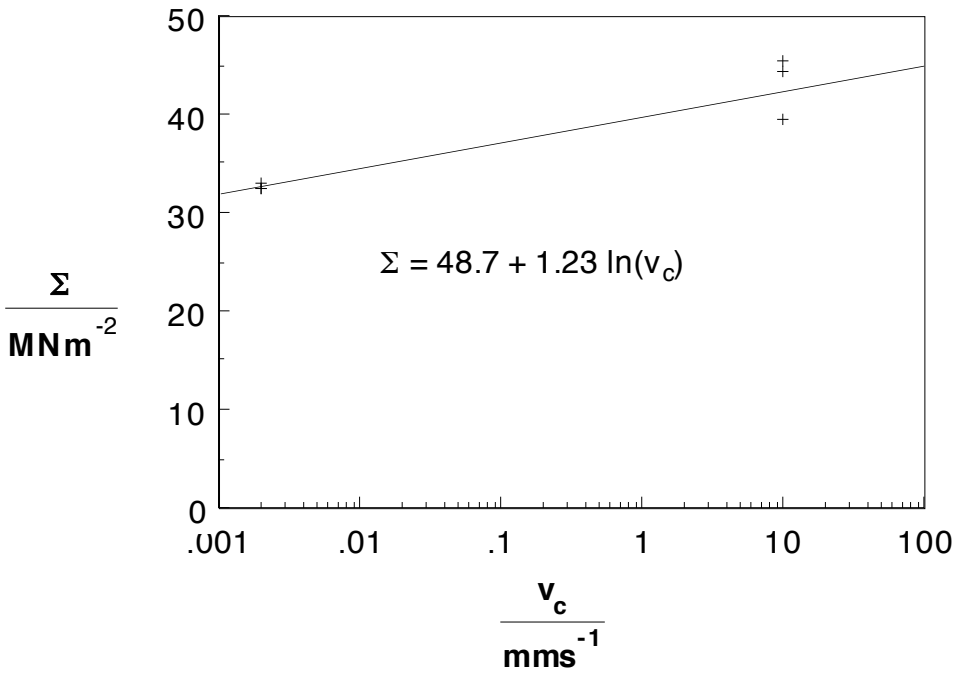

Figure 4.31 Plot of specific crush stress as a function of the crush speed for RJPW tubes tested at 50 °C.

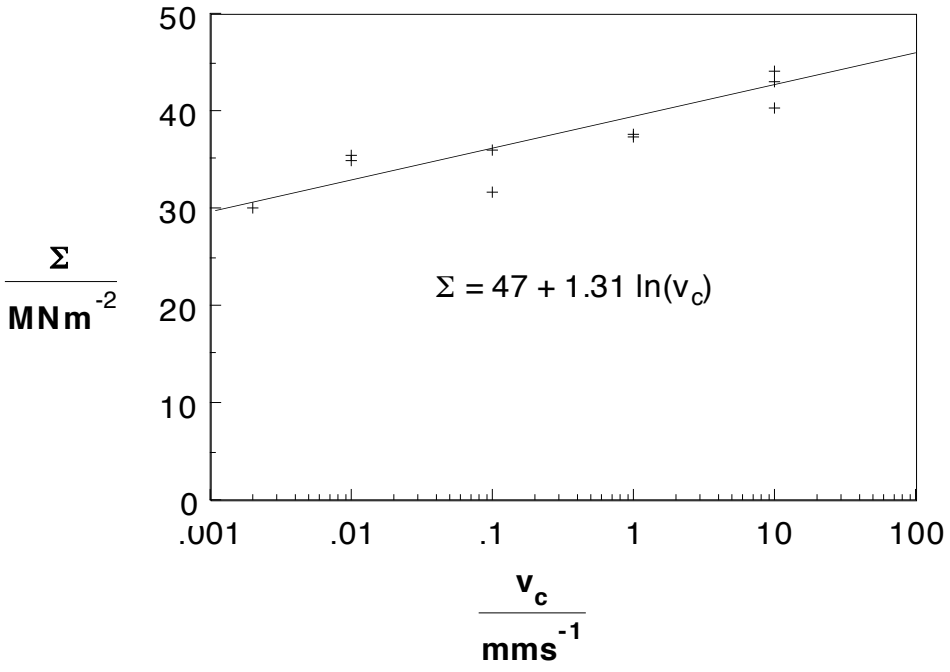

Figure 4.32 Plot of specific crush stress as a function of the crush speed for RJPW tubes tested at 60 °C.

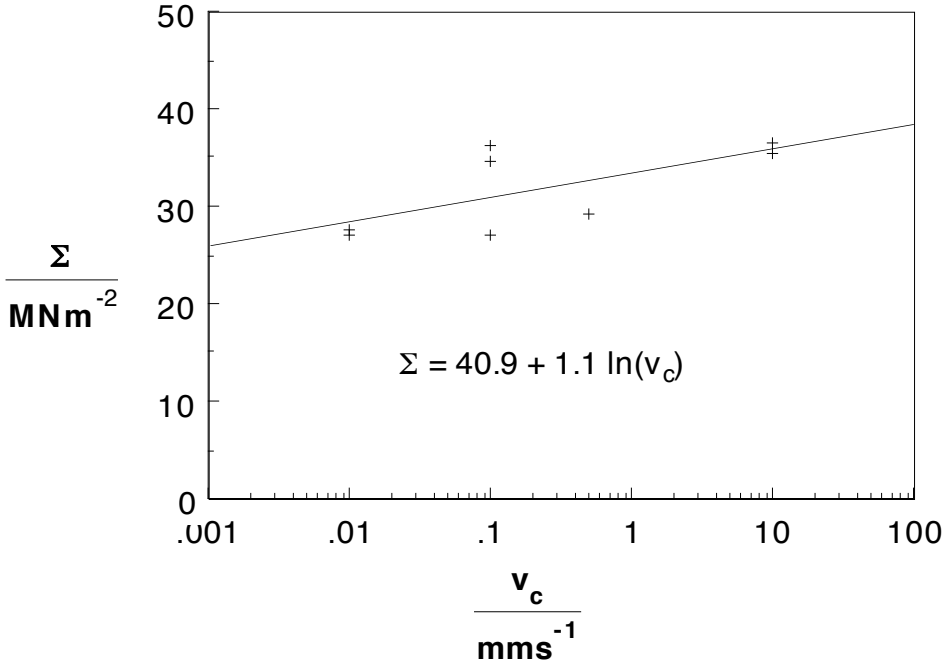

Figure 4.33 Plot of specific crush stress as a function of the crush speed for RJPW tubes tested at 70 °C.

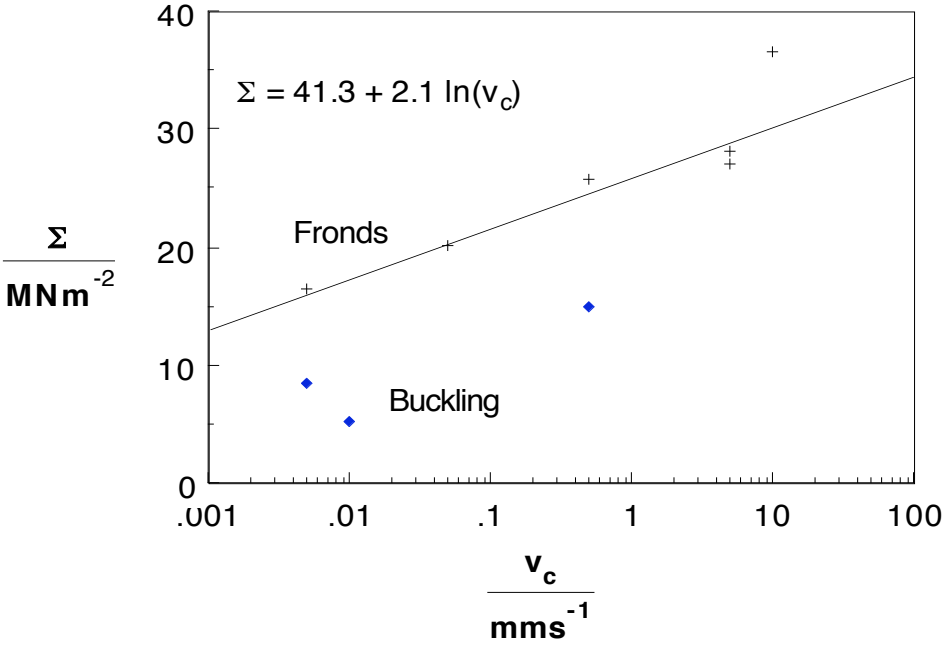

Figure 4.34 Plot of specific crush stress as a function of the crush speed for RJPW tubes tested at 80 °C.

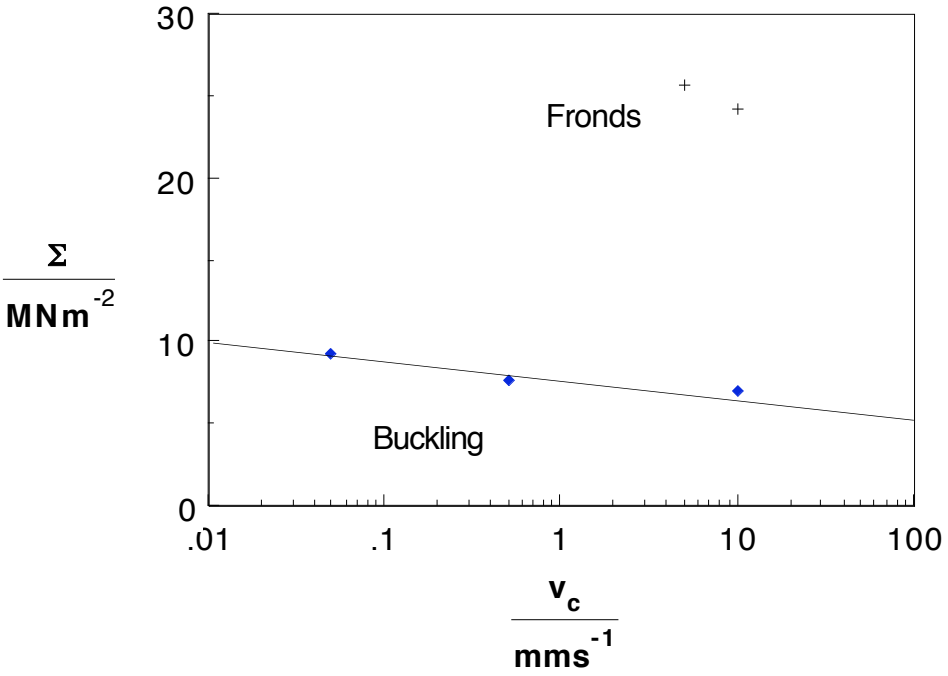

Figure 4.35 Plot of specific crush stress as a function of the crush speed for RJPW tubes tested at 90 °C.

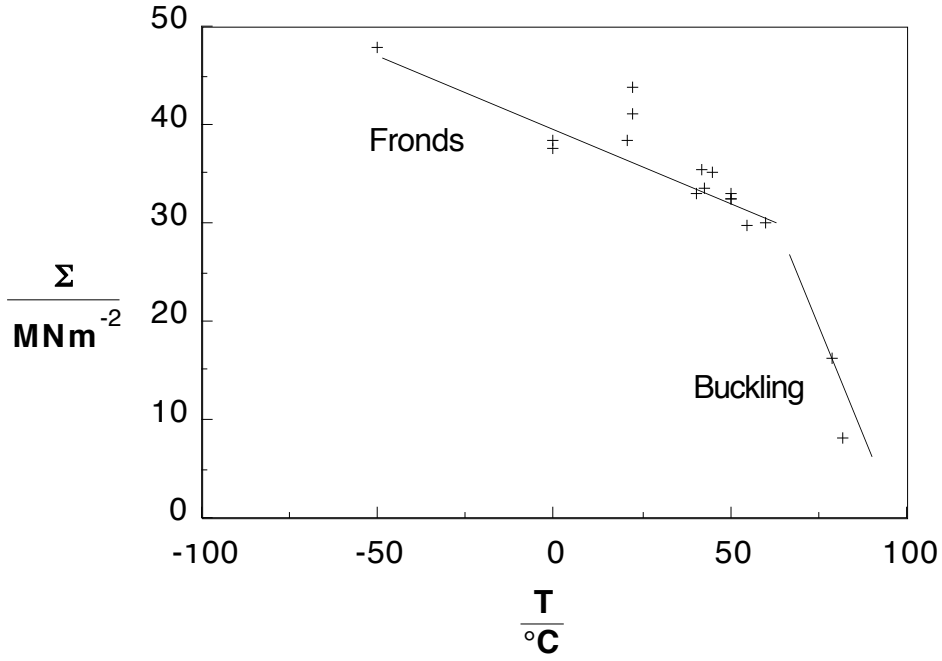

Figure 4.36 Plot of specific crush stress as a function of the test temperature for RJPW tubes tested at 0.002 mm s^{-1}.

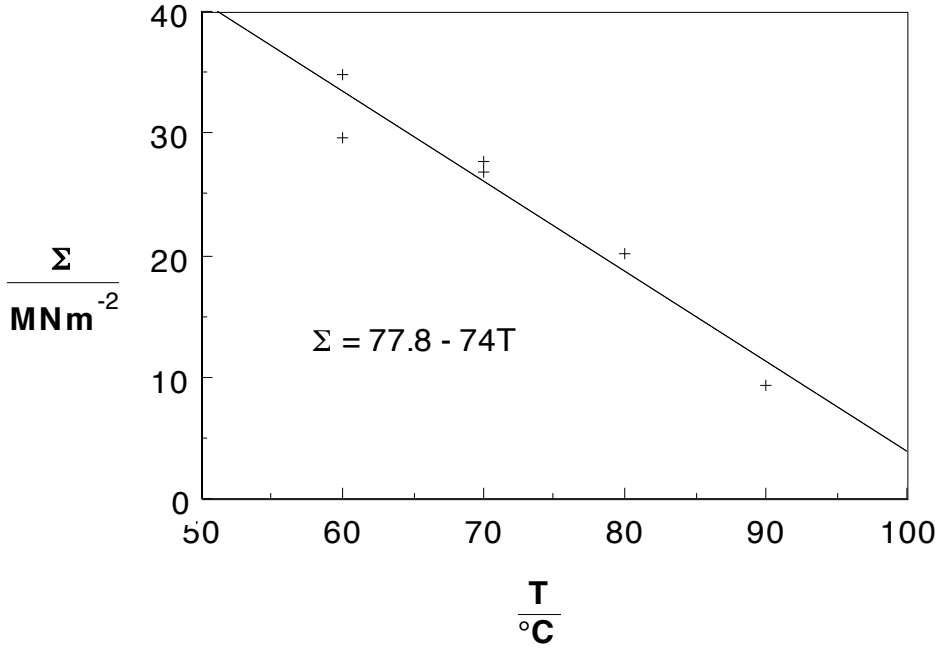

Figure 4.37 Plot of specific crush stress as a function of the test temperature for RJPW tubes tested at 0.01 mm s^{-1}.

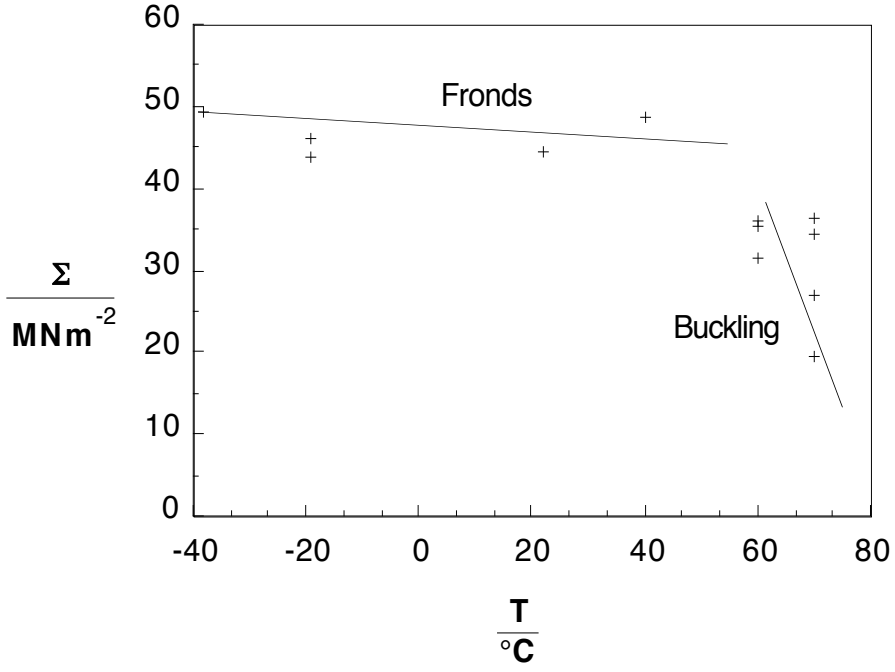

Figure 4.38 Plot of specific crush stress as a function of the test temperature for RJPW tubes tested at 0.1 mm s^{-1}.

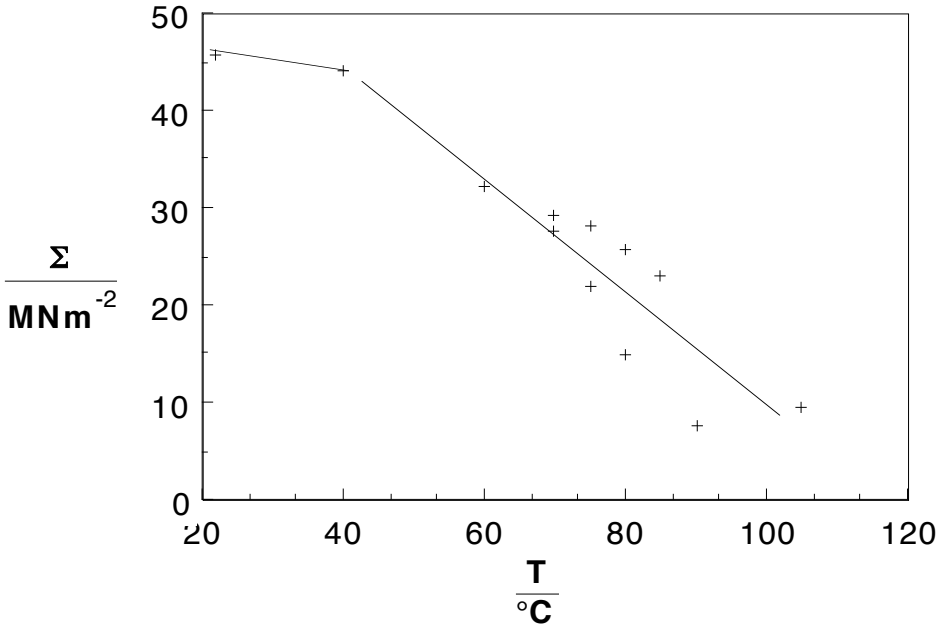

Figure 4.39 Plot of specific crush stress as a function of the test temperature for RJPW tubes tested at 0.5 mm s^{-1}.

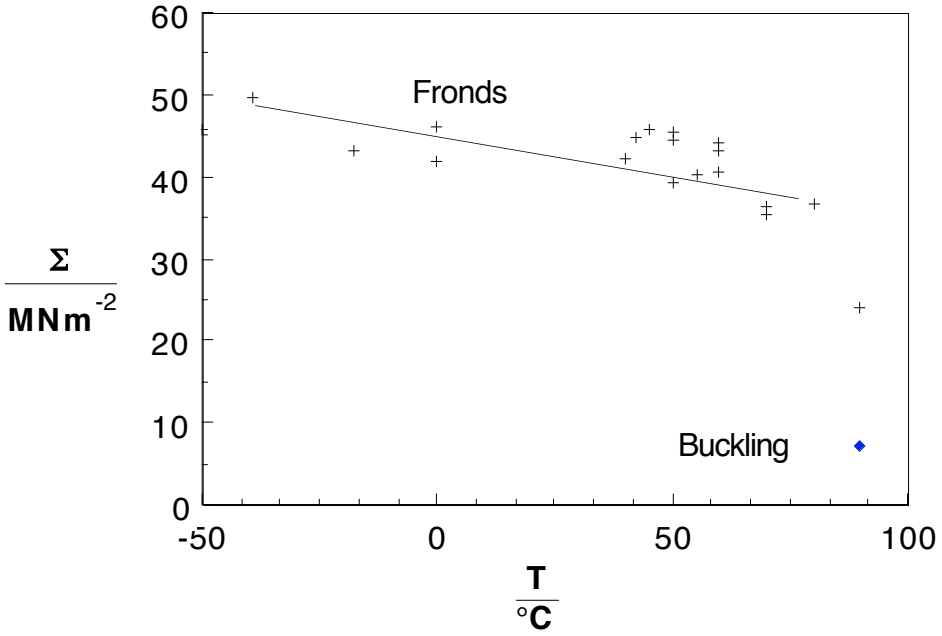

Figure 4.40 Plot of specific crush stress as a function of the test temperature for RJPW tubes tested at 10 mm s^{-1}.

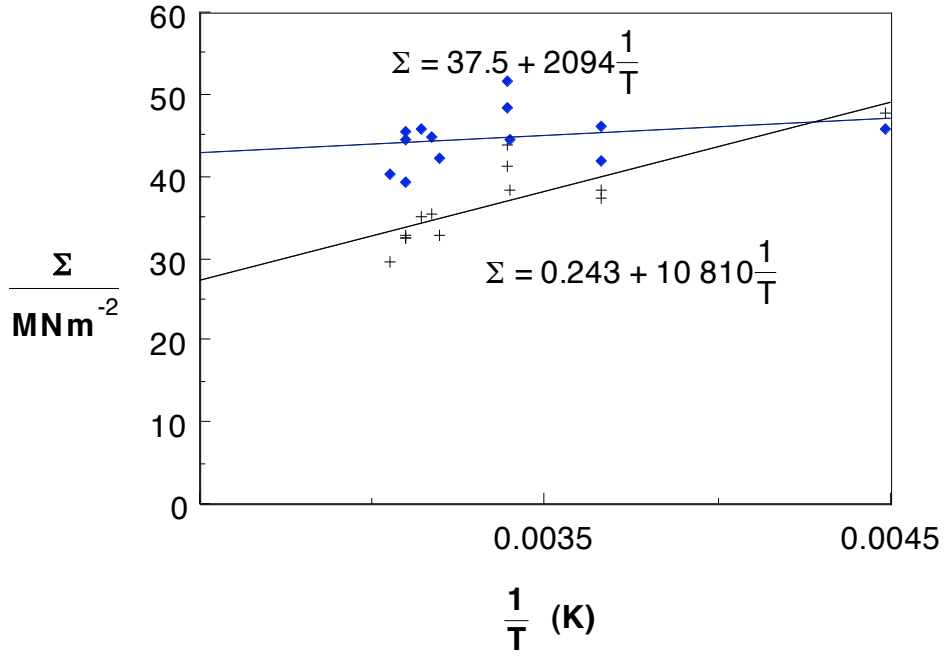

Figure 4.41 Plot of specific crush stress as a function of the reciprocal absolute temperature for RJPW tubes. + denotes a speed of 0.002 mm s^{-1} and ♦ denotes a speed of 10 mm s^{-1}.

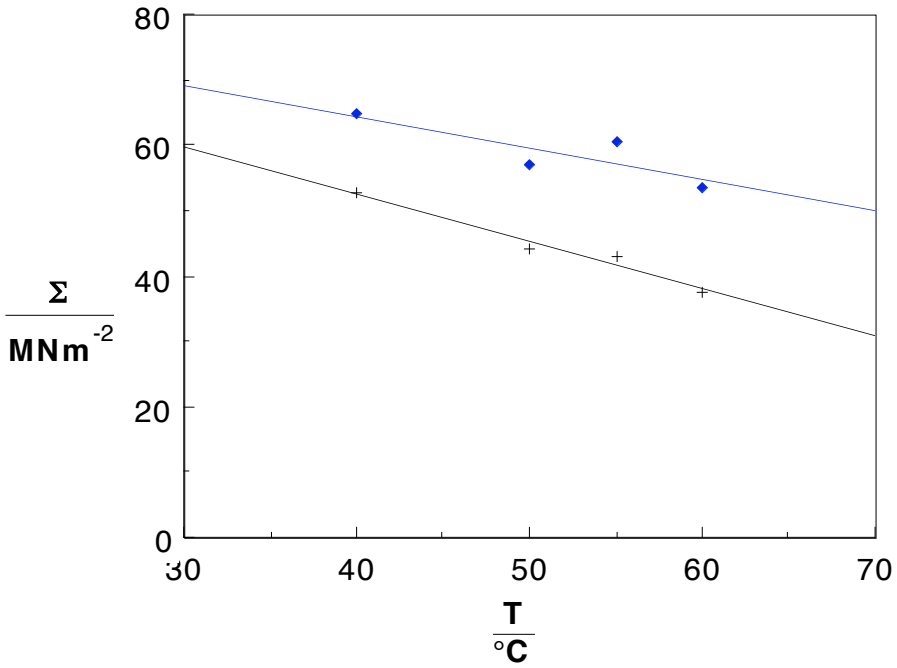

Figure 4.42 Plot of specific crush stress as a function of the test temperature for RJPR tubes. + denotes a speed of 0.002 mm s^{-1} and ♦ denotes a speed of 10 mm s^{-1}.

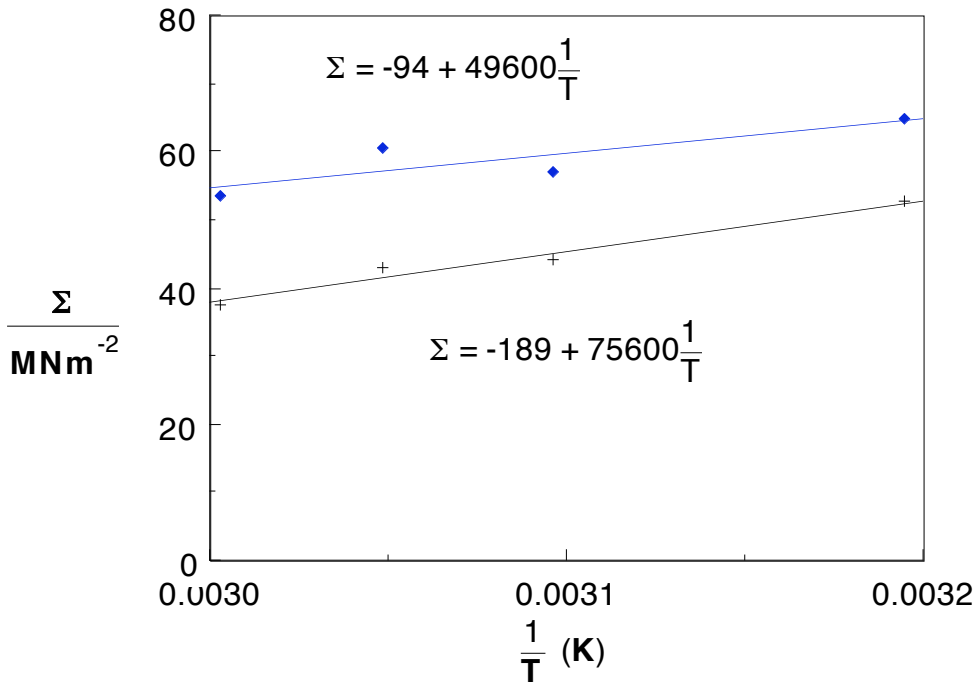

Figure 4.43 Plot of specific crush stress as a function of the reciprocal absolute temperature for RJPR tubes. + denotes a speed of 0.002 mm s^{-1} and ♦ denotes a speed of 10 mm s^{-1}.

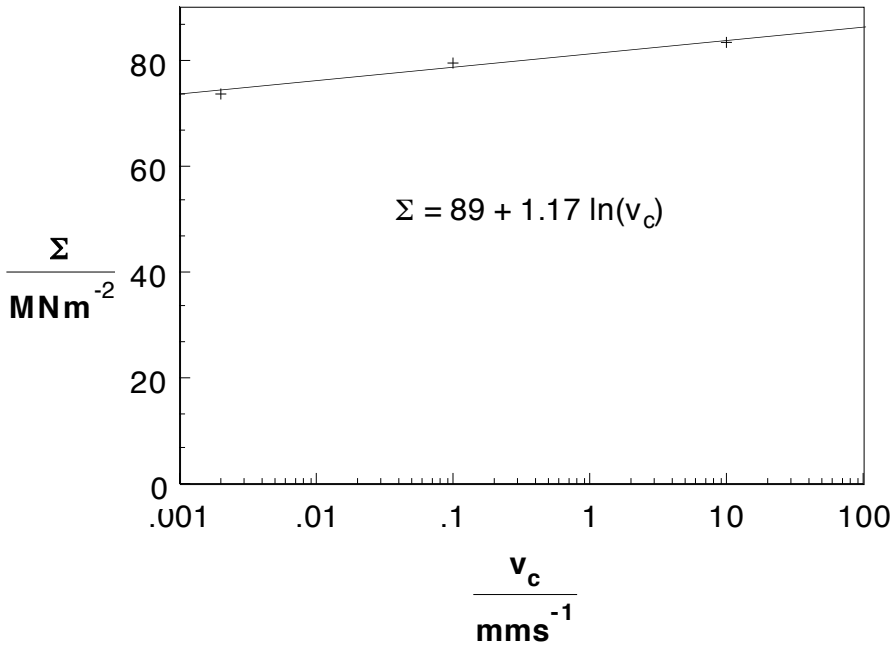

Figure 4.44 Plot of specific crush stress as a function of the crush speed for RJEW tubes crushed at -40 °C.

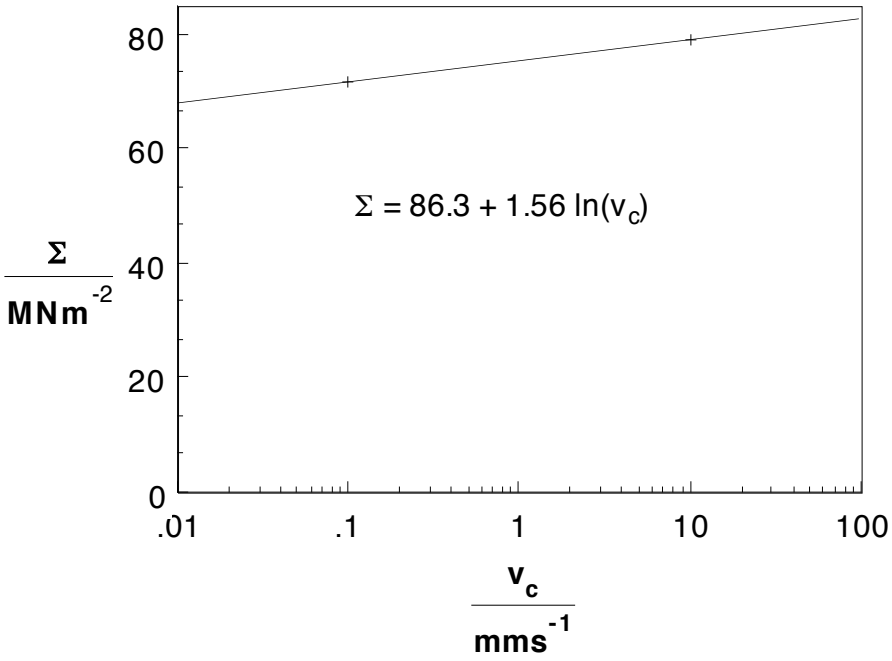

Figure 4.45 Plot of specific crush stress as a function of the crush speed for RJEW tubes crushed at -20 °C.

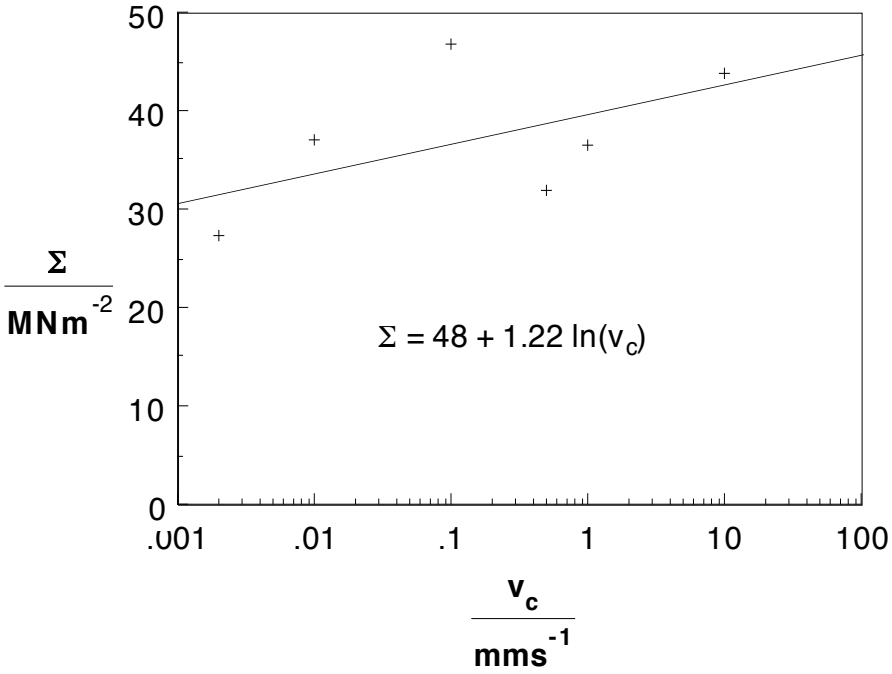

Figure 4.46 Plot of specific crush stress as a function of the crush speed for RJEW tubes crushed at 60 °C.

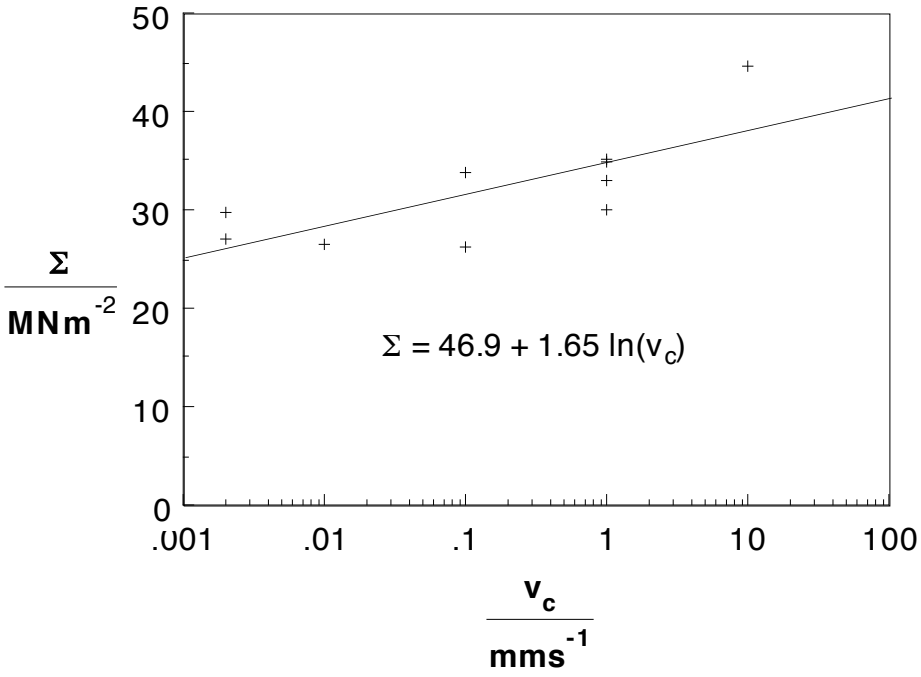

Figure 4.47 Plot of specific crush stress as a function of the crush speed for RJEW tubes crushed at 70 °C.

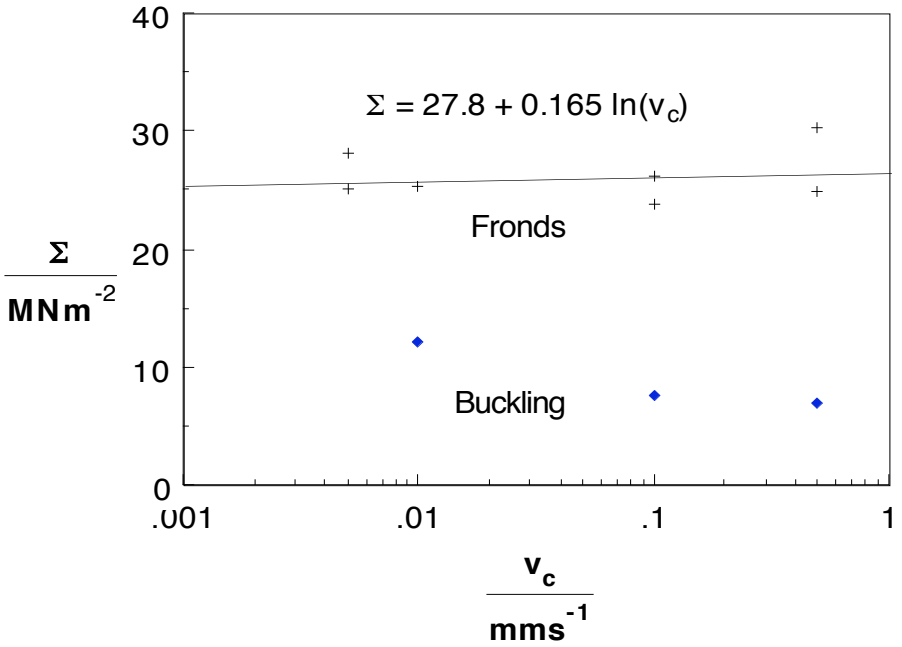

Figure 4.48 Plot of specific crush stress as a function of the crush speed for RJEW tubes crushed at 75 °C.

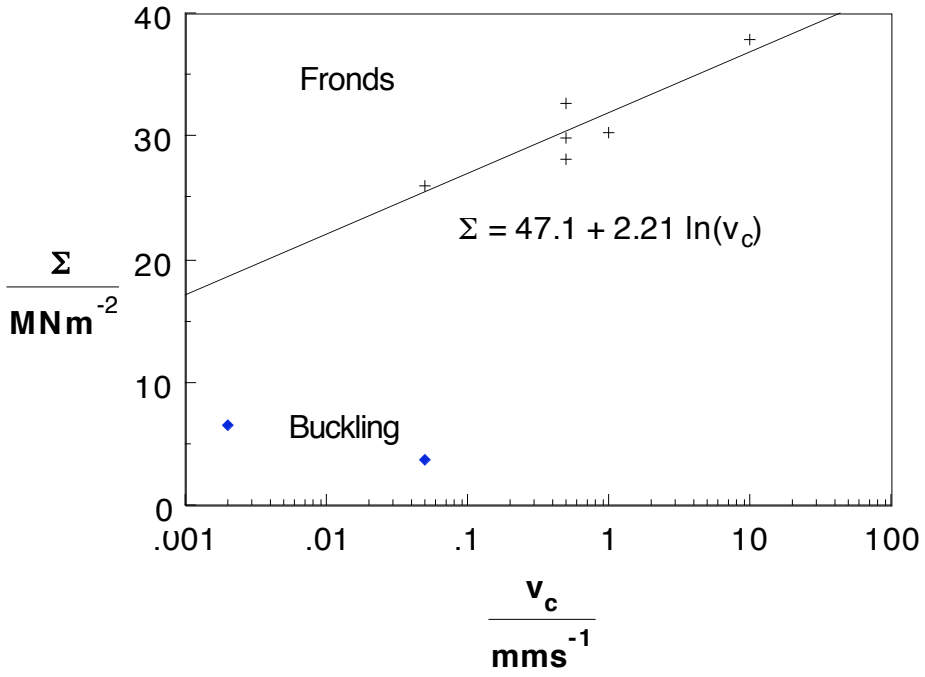

Figure 4.49 Plot of specific crush stress as a function of the crush speed for RJEW tubes crushed at 80 °C.

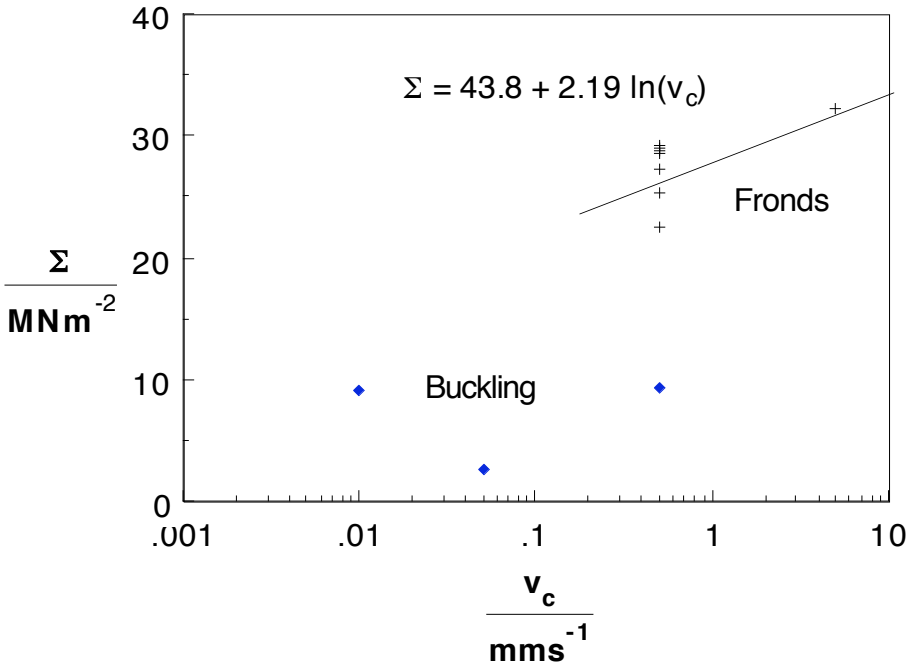

Figure 4.50 Plot of specific crush stress as a function of the crush speed for RJEW tubes crushed at 85 °C.

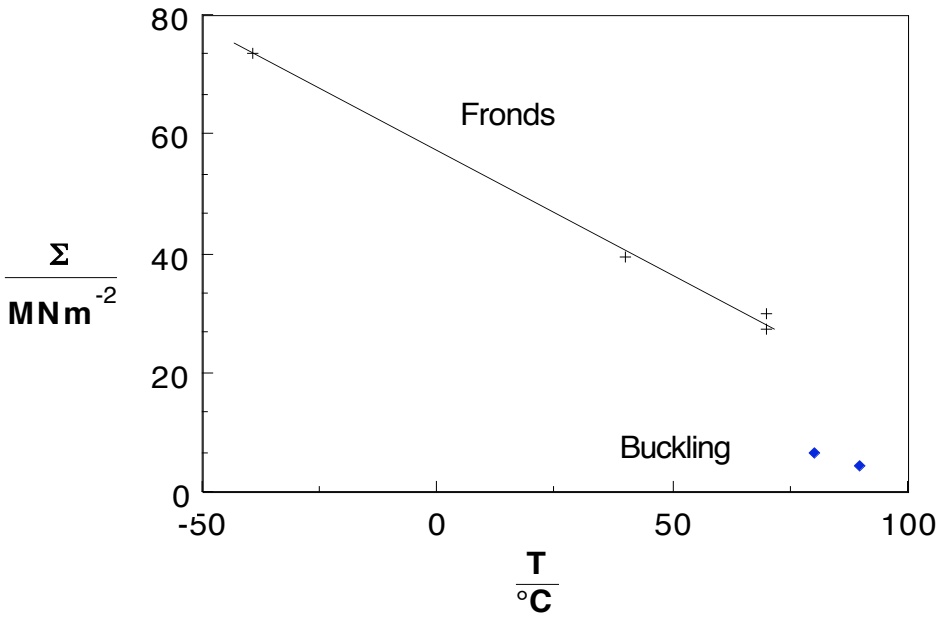

Figure 4.51 Plot of specific crush stress as a function of the test temperature for RJEW tubes tested at 0.002 mm s^{-1}.

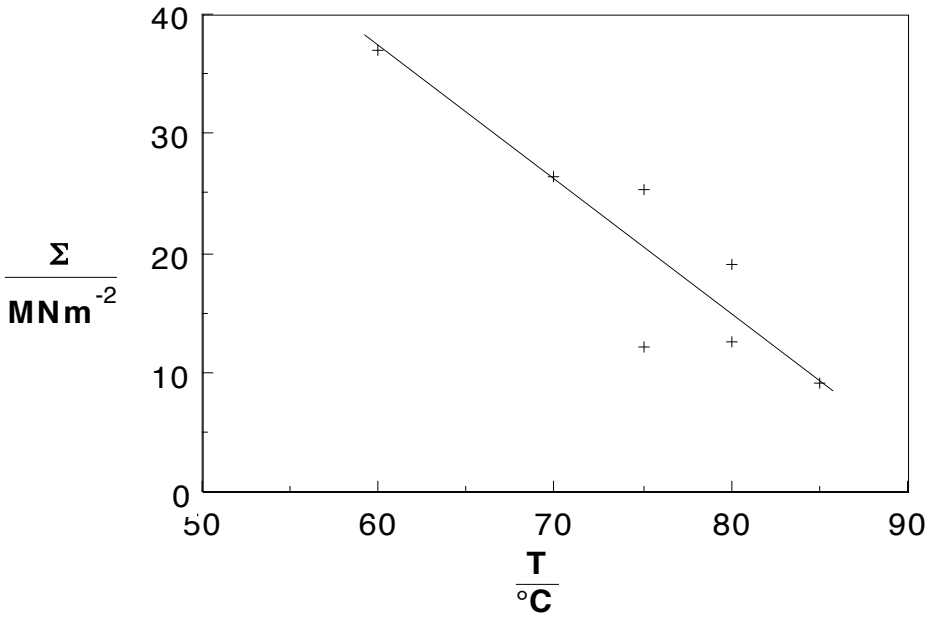

Figure 4.52 Plot of specific crush stress as a function of the test temperature for RJEW tubes tested at 0.01 mm s^{-1}.

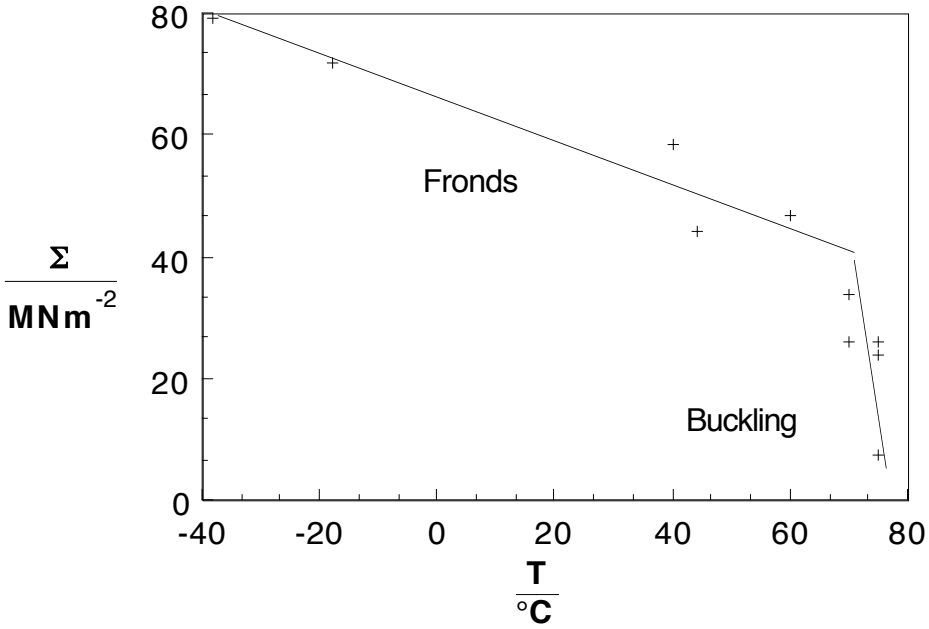

Figure 4.53 Plot of specific crush stress as a function of the test temperature for RJEW tubes tested at 0.1 mm s^{-1}.

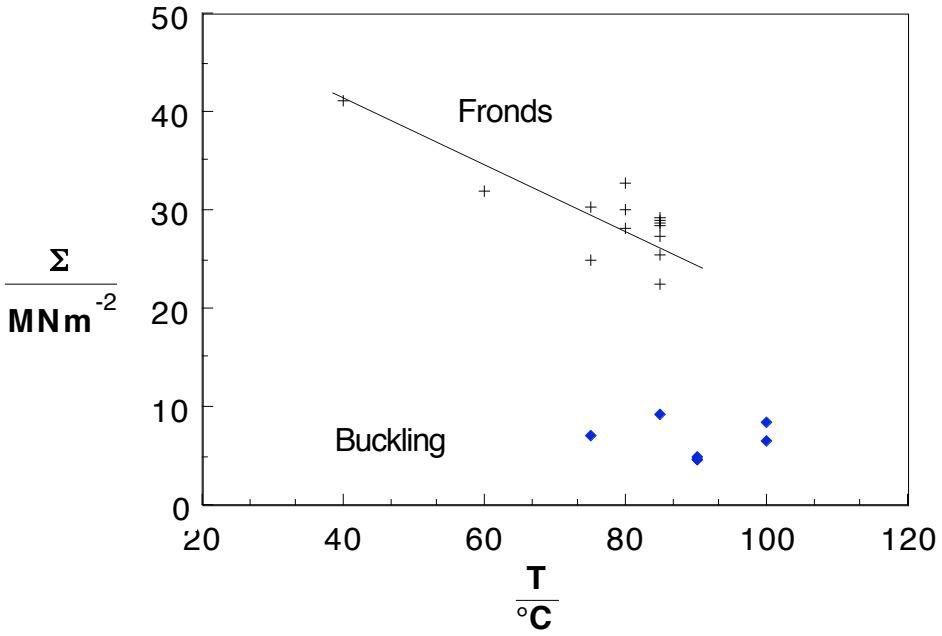

Figure 4.54 Plot of specific crush stress as a function of the test temperature for RJEW tubes tested at 0.5 mm s^{-1}.

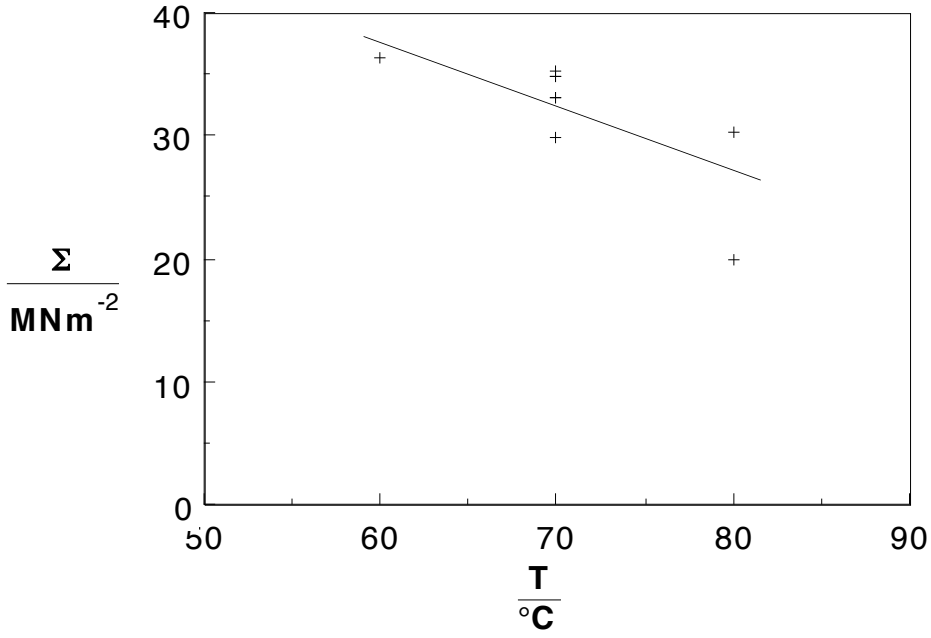

Figure 4.55 Plot of specific crush stress as a function of the test temperature for RJEW tubes tested at 1 mm s^{-1}.

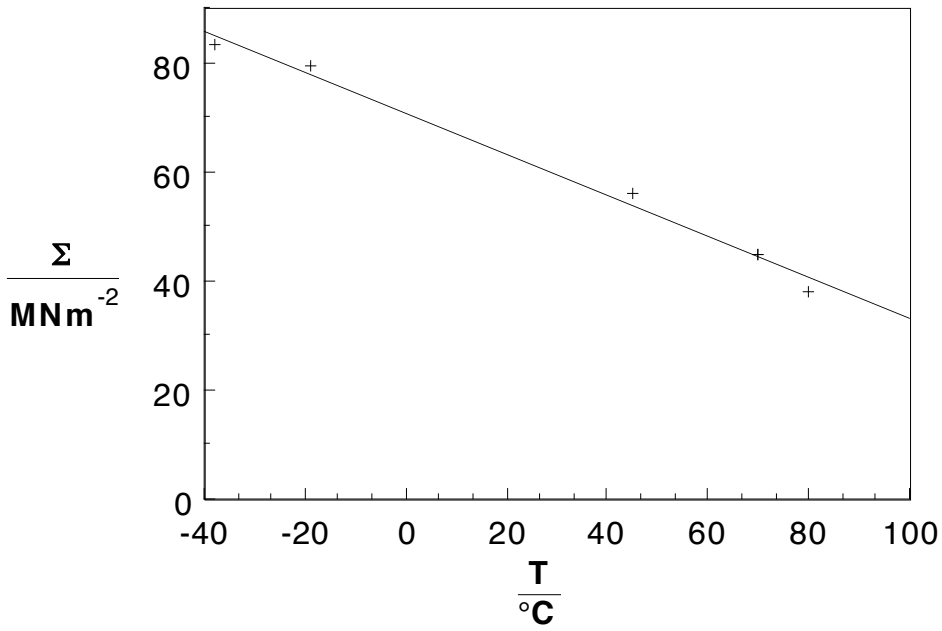

Figure 4.56 Plot of specific crush stress as a function of the test temperature for RJEW tubes tested at 10 mm s^{-1}.

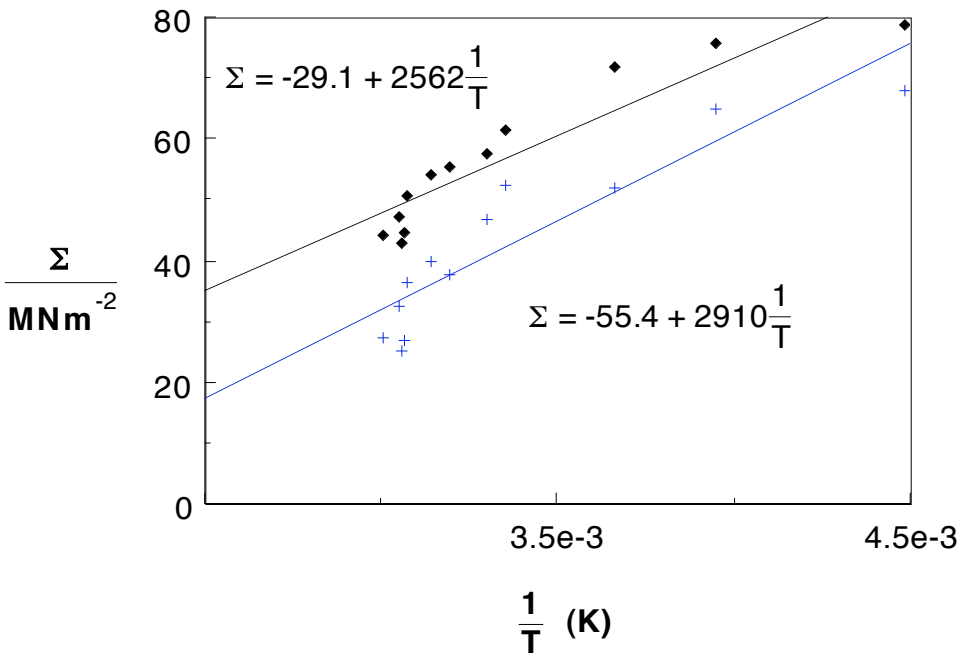

Figure 4.57 Plot of specific crush stress as a function of the reciprocal absolute temperature for RJEW tubes. + denotes a speed of 0.002 mm s^{-1} and ♦ denotes a speed of 10 mm s^{-1}.

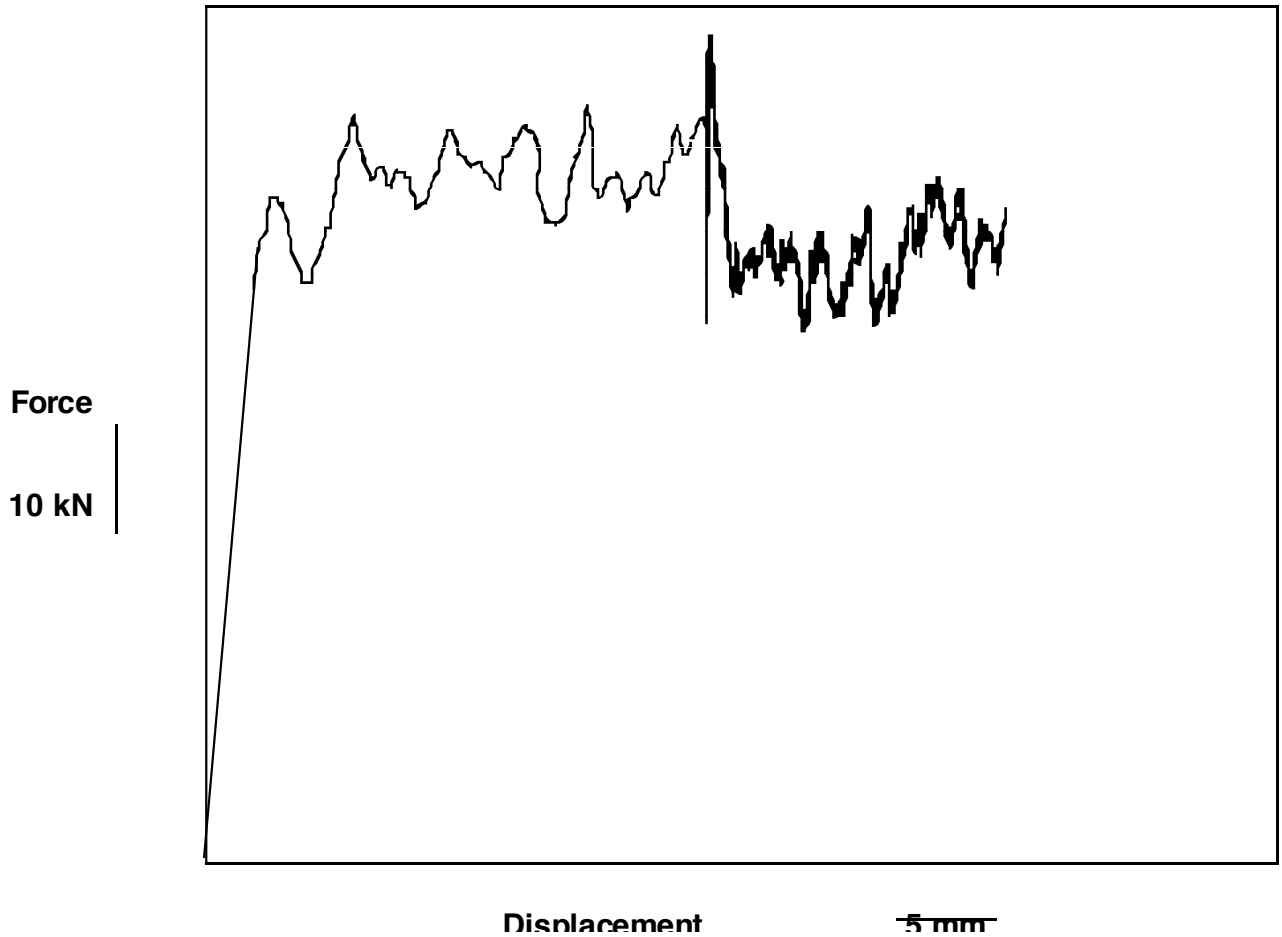

Figure 4.58 Force-displacement trace from a Tufnol tube instantaneous speed change test at -90 °C, speeds were 10 mm s^{-1} then 0.002 mm s^{-1}.

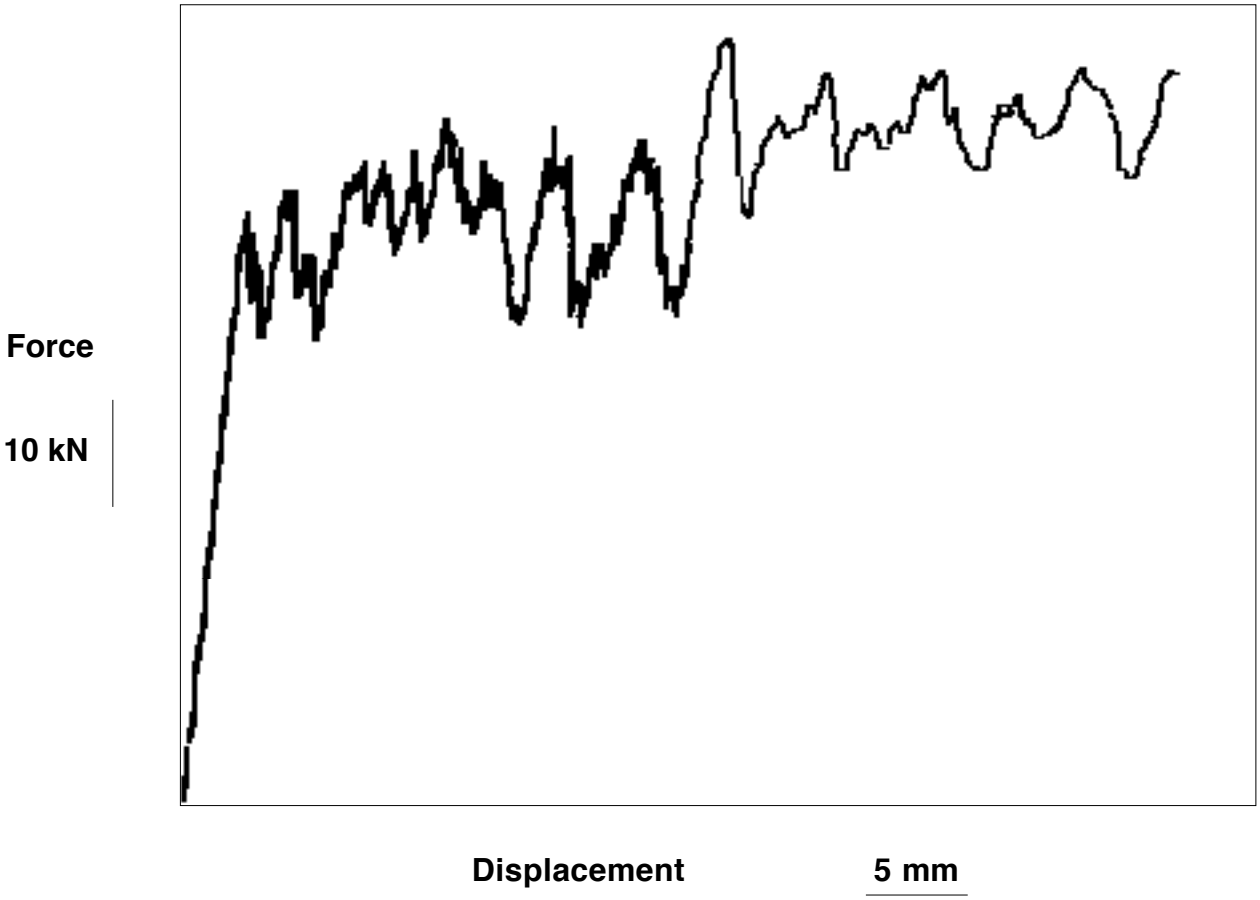

Figure 4.59 Force-displacement trace from a Tufnol tube instantaneous speed change test at -90 °C, speeds were 0.002 mm s^{-1} then 10 mm s^{-1}.

Figure 4.60 Force-displacement trace from a Tufnol tube instantaneous speed change test at 22 °C, speeds were 10 mm s^{-1} then 0.002 mm s^{-1}.

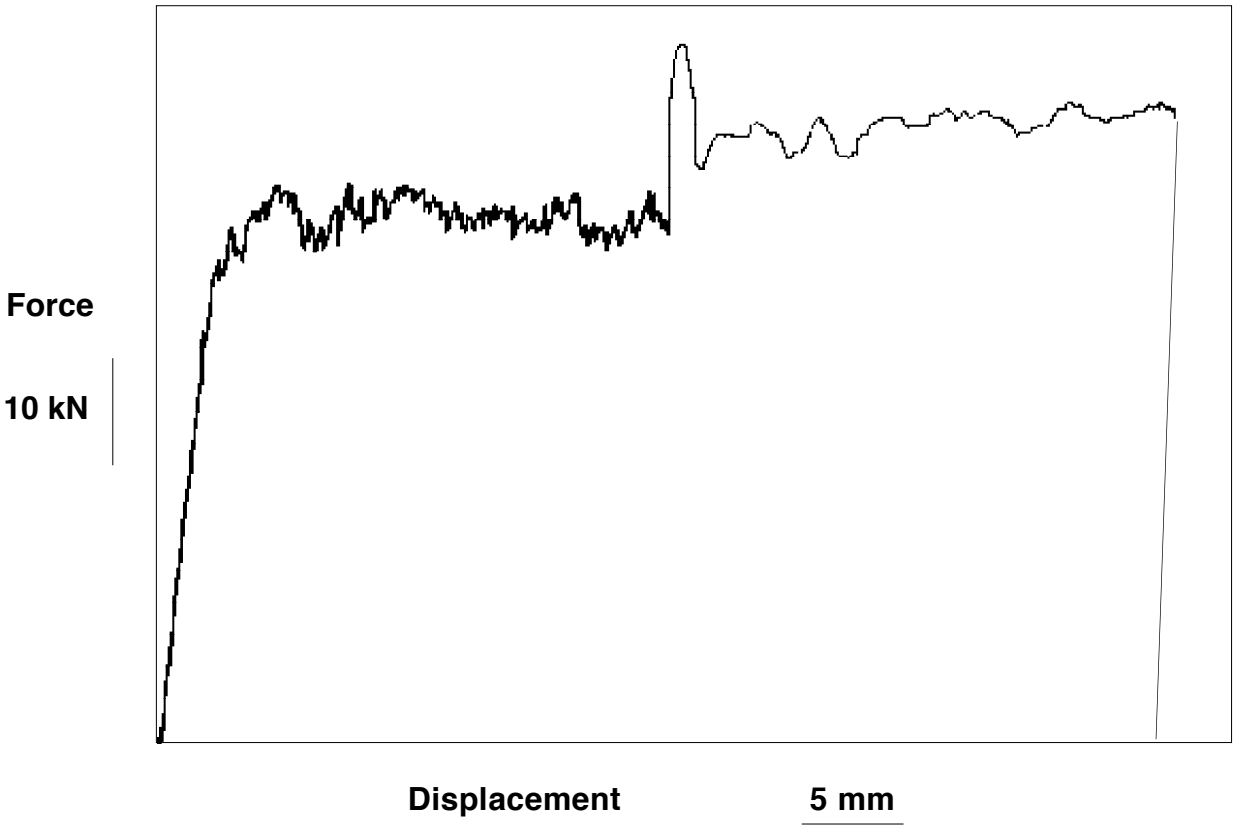

Figure 4.61 Force-displacement trace from a Tufnol tube instantaneous speed change test at 22 °C, speeds were 0.002 mm s^{-1} then 10 mm s^{-1}.

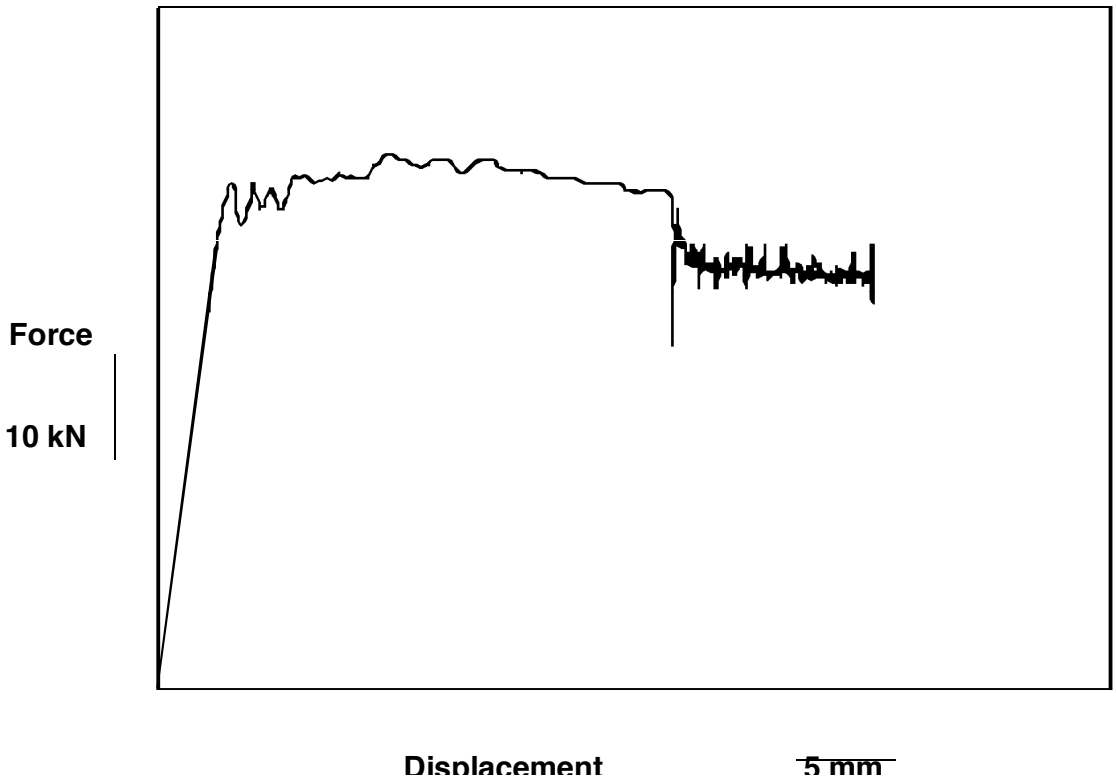

Figure 4.62 Force-displacement trace from a Tufnol tube instantaneous speed change test at 60 °C, speeds were 10 mm s^{-1} then 0.002 mm s^{-1}.

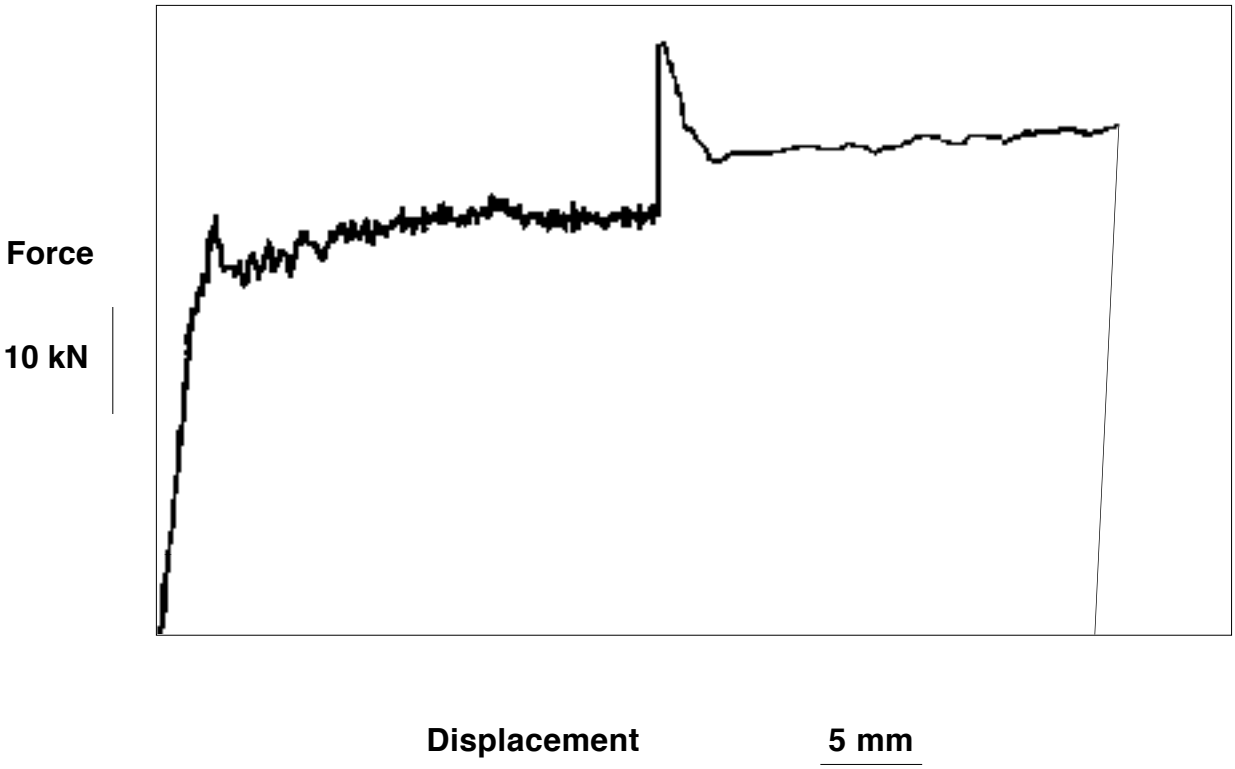

Figure 4.63 Force-displacement trace from a Tufnol tube instantaneous speed change test at 60 °C, speeds were 0.002 mm s^{-1} then 10 mm s^{-1}.

Figure 4.64 Force-displacement trace from a Tufnol tube instantaneous speed change test at 80 °C, speeds were 10 mm s^{-1} then 0.002 mm s^{-1}.

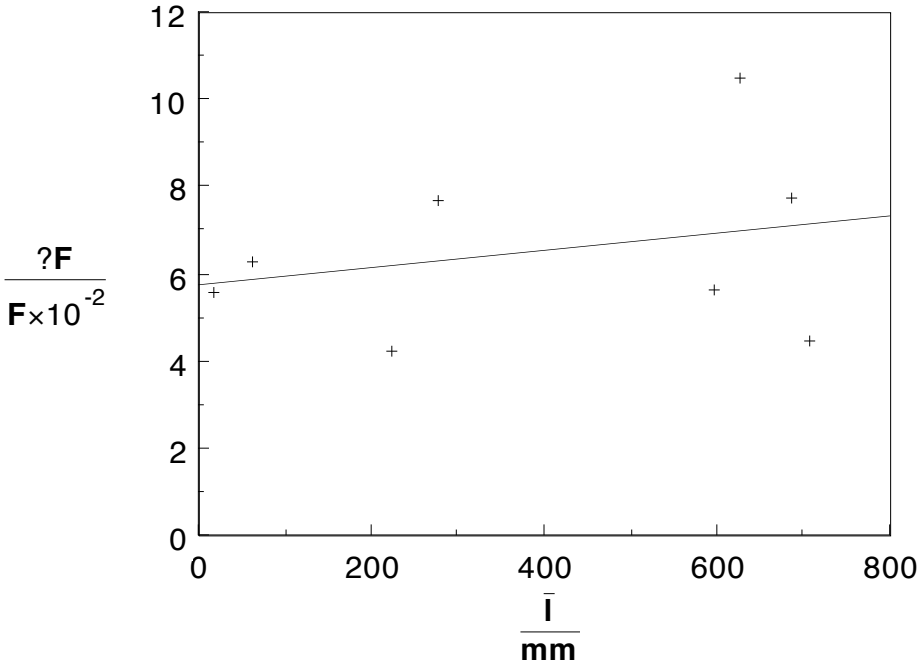

Figure 4.65 Plot of the normalised magnitude of serration as a function of the tube length for Tufnol tubes.

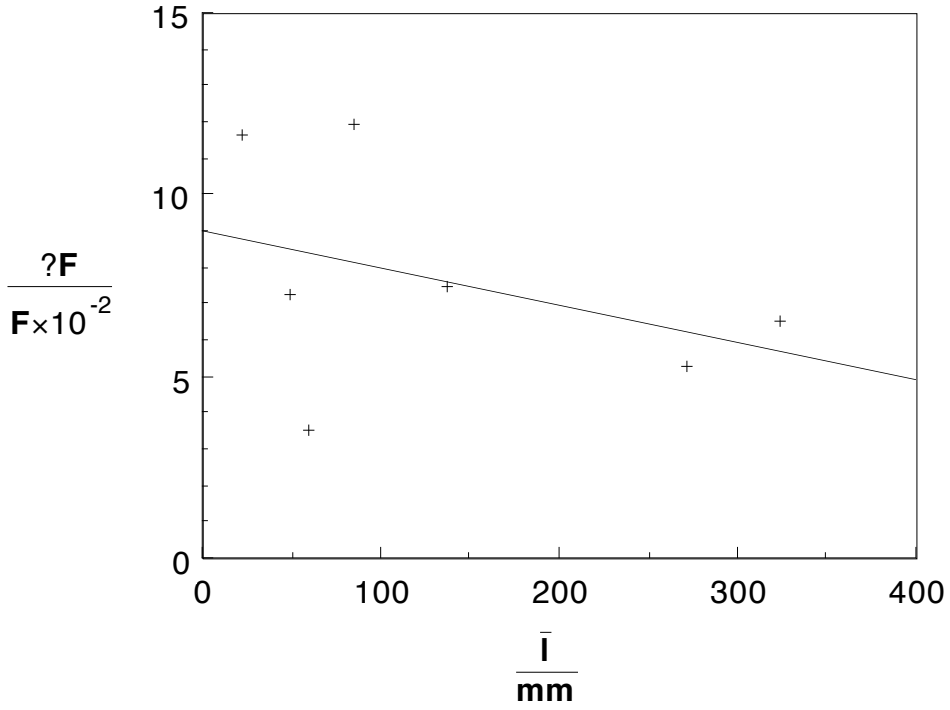

Figure 4.66 Plot of the normalised magnitude of serration as a function of the tube length for Tufnol tubes with a t/D of 0.27.

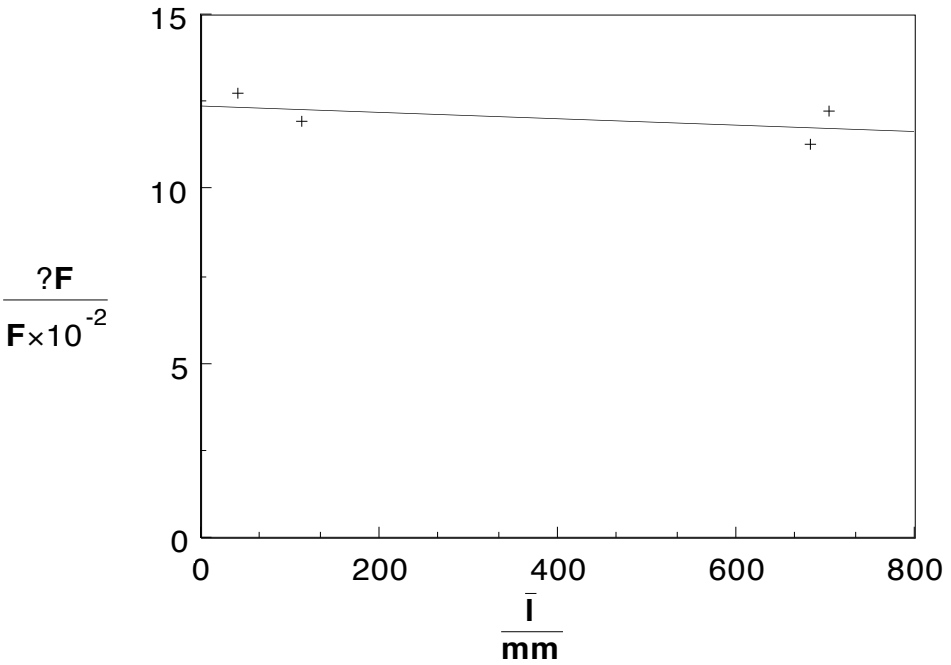

Figure 4.67 Plot of the normalised magnitude of serration as a function of the tube length for Pultrex tubes with a t/D of 0.064.

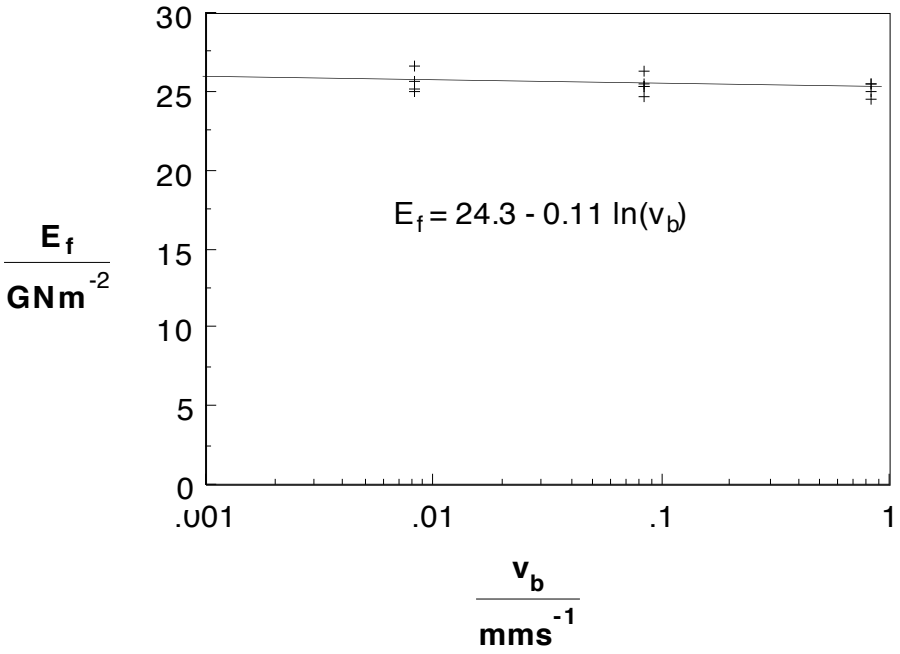

Figure 4.68 Plot of flexural modulus as a function of the cross-head speed on a logarithmic scale for Tufnol 10G40.

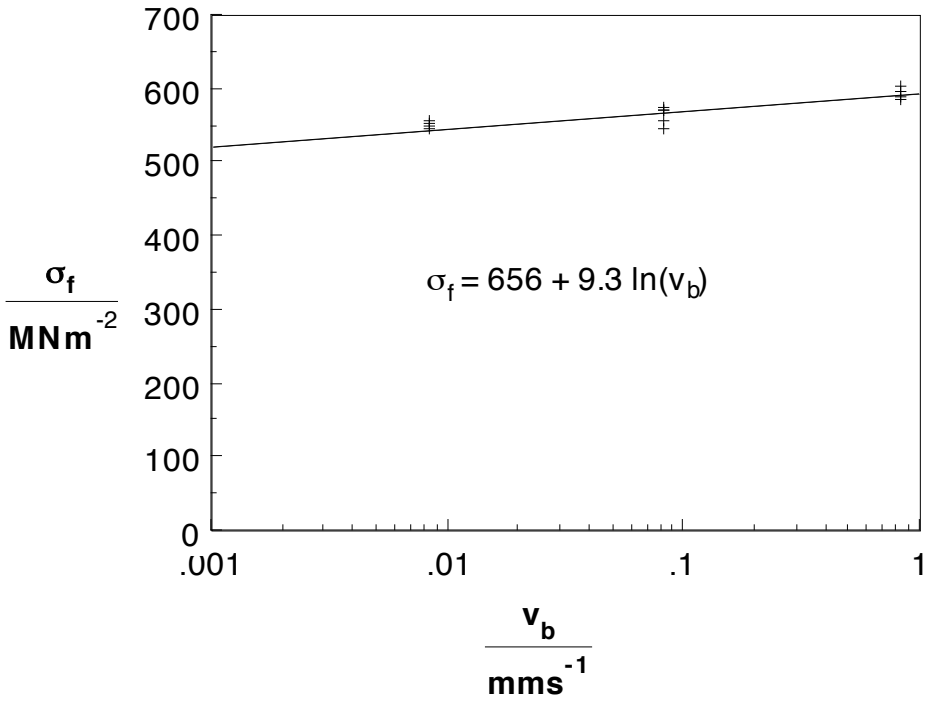

Figure 4.69 Plot of flexural strength as a function of the cross-head speed on a logarithmic scale for Tufnol 10G40.

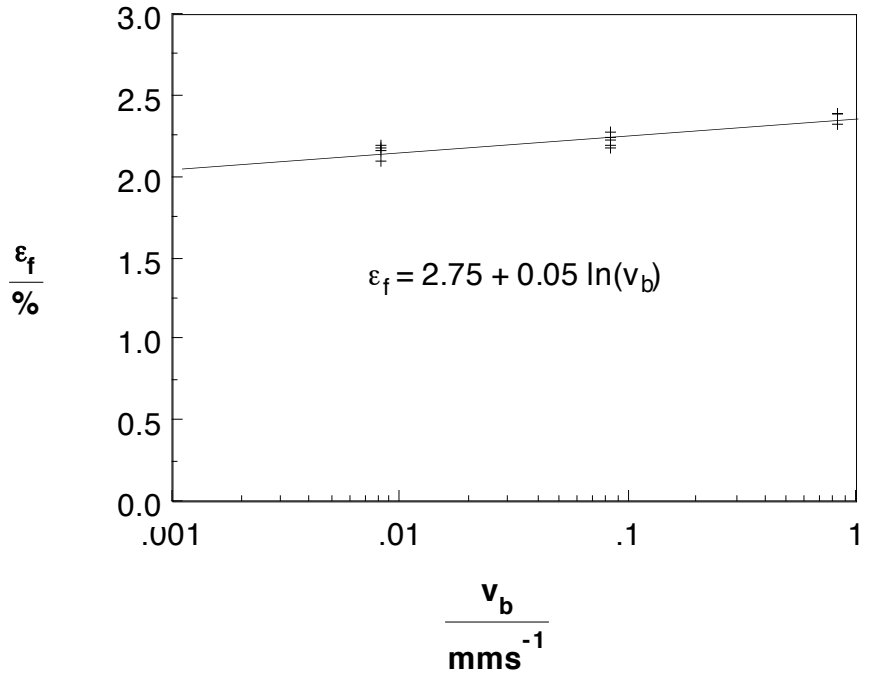

Figure 4.70 Plot of the flexural strain to failure as a function of the cross-head speed on a logarithmic scale for Tufnol 10G40.

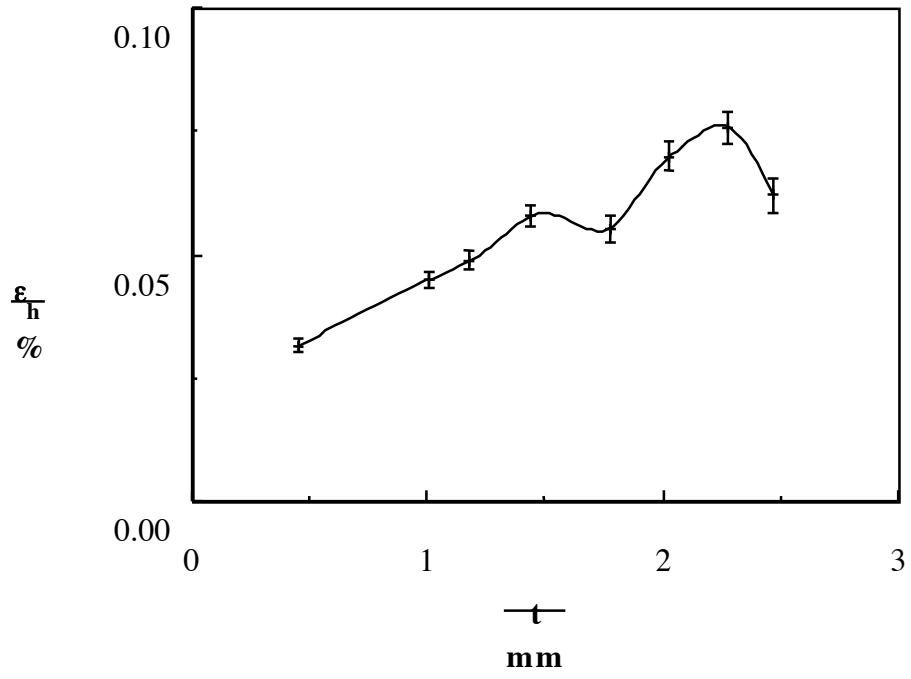

Figure 4.71 Plot of the residual hoop strain as a function of the tube wall thickness for a Tufnol tube.

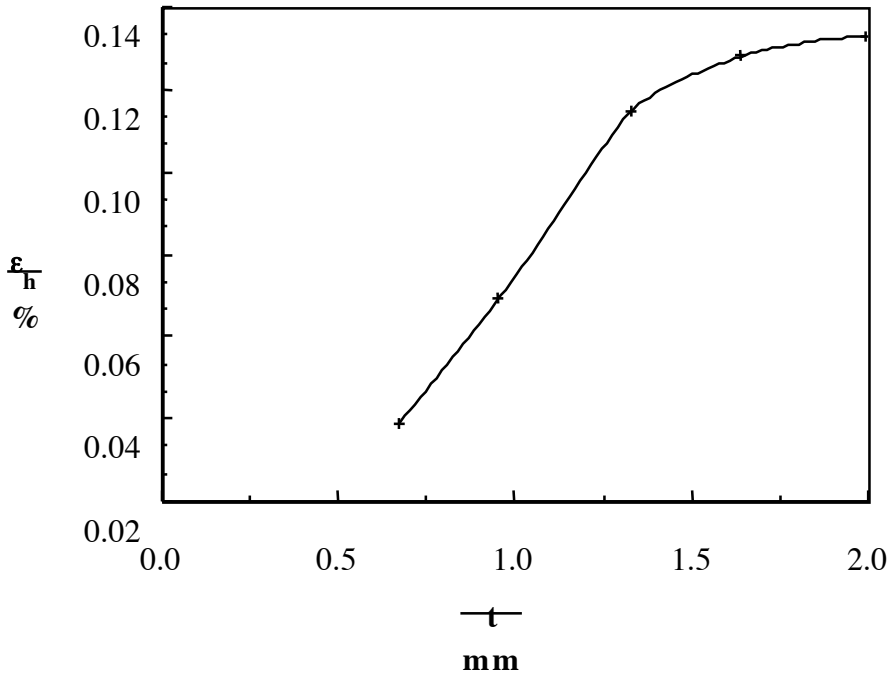

Figure 4.72 Plot of residual hoop strain as a function of the wall thickness for an RJPW tube.

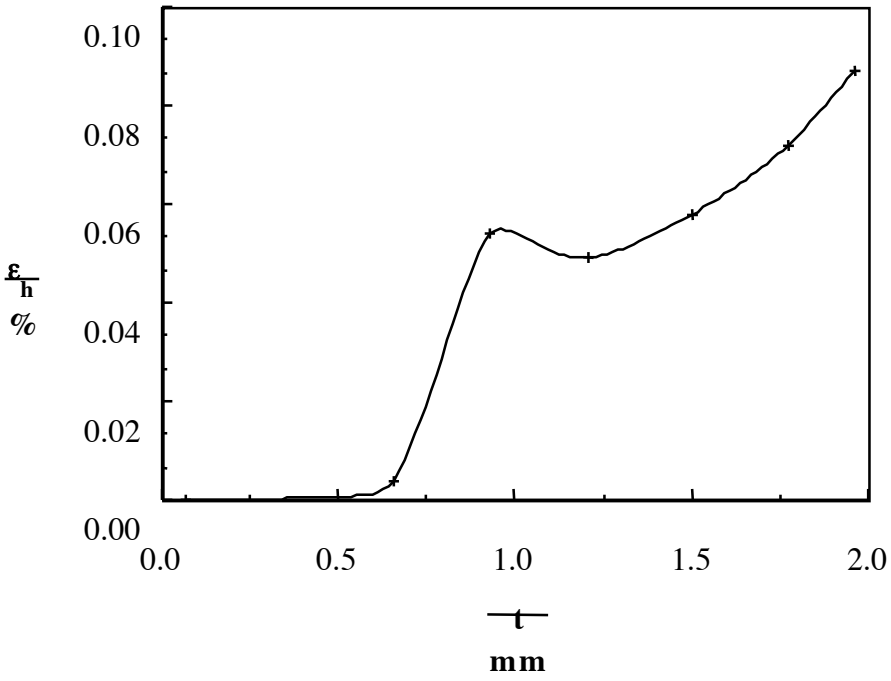

Figure 4.73 Plot of the residual hoop strain as a function of the wall thickness for an RJPR tube.

5 Data Analysis

Two main types of data analysis were performed, these were: the calculation of the speed sensitivity of the specific crush stress for the various different tubes tested, and the residual strain distributions in the individual layers of the tubes after machining off the outer layers.

5.1 Speed Sensitivities

From the data obtained from the crush tests performed in the environmental chamber, incorporating instantaneous speed changes, it was possible to obtain a numerical basis to indicate speed sensitivity. Two different ways of calculating the speed sensitivity have been used, although they are closely related.

From the literature (section 2.2.1.1.1, equation 2.4 [64]) a speed sensitivity, λ, was defined as being:

$$\lambda = \frac{\Delta\sigma}{\ln\left(\frac{\dot{\varepsilon}_2}{\dot{\varepsilon}_1}\right)} \qquad (5.1)$$

where $\Delta\sigma$ was the change in tensile stress for a strain rate change of $\dot{\varepsilon}_1$ to $\dot{\varepsilon}_2$. This was the slope of the s versus $\ln(\dot{\varepsilon})$ trace, assuming a straight line fit. Equation 5.1 was adapted for the case of progressive crushing by replacing the tensile strength by the specific crush stress and the strain rate by the crush speed v_c. This gave:

$$\lambda = \frac{\Delta\Sigma}{\ln\left(\frac{v_{c2}}{v_{c1}}\right)} \qquad (5.2)$$

In this case the value of λ had units of MN m^{-2}. As the values of λ were only for a comparison, their absolute values were not important. Each value of λ was taken from the gradient of the plots of specific crush stress versus the natural logarithm of the

crush speed. The plots in chapter 4 all show the plots as a function of the actual speed on a logarithmic scale. This assumed that the straight line fits to each of these data sets was valid, this is discussed in section 8.1.1.1.

The calculation of λ enabled the calculation of an activation energy for the process, ΔH. This was done by considering the temperature sensitivity of the specific crush stress at the speed in question and equating it with the calculated value of λ. If the slope, m, of the plot of specific crush stress versus the reciprocal of the absolute temperature was determined, then ΔH was given by:

$$\Delta H = \frac{m\,k}{\lambda} \qquad (5.3)$$

where k was Boltzmann's constant.

Plots of λ and ΔH as functions of the test temperature are given in figures 5.1 to 5.8 for Tufnol, RJPW, RJPR and RJEW tubes.

5.2 Residual Strain Distributions

The residual strain distributions for Tufnol and resinject polyester resin matrix tubes have been shown in figures 4.71 to 4.73. However, as the machining was all done from the outside of the tube, the strains measured were for the total wall remaining. As the strains measured increased towards the outside of the tube wall, the contribution to the total strain from the internal plies was less than for the outer plies. From the figures given in tables 4.1 to 4.3 it was possible to calculate the actual local residual strain distributions in these tubes. To do this the strains were converted to forces. From Crampton [107]:

$$\sigma_h = E' t_l \left(\frac{1}{D_i} - \frac{1}{D_a} \right) \qquad (5.4)$$

where σ_h was the hoop stress and E' was given by:

$$E' = \frac{E}{(1 - \nu^2)} \tag{5.5}$$

where E was the Young's modulus and ν the Poisson's ratio. In this case t_l was the thickness of the layer in question. As stress is defined as being the force per unit area, this could be converted to a force by multiplying by the area of the tube wall normal to the hoop direction a_h which was given by:

$$a_h = t_l \, l \tag{5.6}$$

where l was the length of the tube. Thus the force on the section R was given by:

$$R = \frac{E \, t_l^2 \, l}{(1 - \nu^2)} \left(\frac{1}{D_i} - \frac{1}{D_a} \right) \tag{5.7}$$

When working from the figures given in tables 4.1 to 4.3, the values of E, ν and l could be taken as constants so it was possible to define a constant S as:

$$S = \frac{E \, l}{(1 - \nu^2)} \tag{5.8}$$

Thus:

$$R = t_l^2 \, S \left(\frac{1}{D_i} - \frac{1}{D_a} \right) \tag{5.9}$$

The value of the force R, was the total force over the wall thickness. By subtracting the force on the remainder of the tube, after that layer had been removed, it was possible to determine the force on that layer and thus evaluate the strain on that layer. This strain, to a reasonable approximation, may be said to have been acting at the centre of that layer, so that a strain distribution could be given as in tables 5.1 to 5.3 and drawn as in figures 5.9 to 5.11.

t mm	ε %
0.45	0.032
1.01	0.100
1.18	0.084
1.44	0.086
1.78	0.040
2.03	0.186
2.28	0.126
2.46	-0.23

Table 5.1 Residual strains in individual layers as a function of the distance of the centre of the layer from the inner edge of the tube for a Tufnol tube.

t mm	ε %
0.34	0.040
0.81	0.139
1.14	0.231
1.49	0.186
1.82	0.155

Table 5.2 Residual strains in individual layers as a function of the distance of the centre of the layer from the inner edge of the tube for an RJPW tube.

t mm	ε %
0.035	0.003
0.365	0.033
0.795	0.238
1.070	0.087
1.355	0.051
1.635	0.400
1.865	-0.07

Table 5.3 Residual strains in individual layers as a function of the distance of the centre of the layer from the inner edge of the tube for an RJPR tube.

It should be noted that the residual strains have been found to be greater than 10% of the failure strain in bending, as measured for the Tufnol flat plate material, of about 2% (see section 4.6). While the great majority of the strains were compressive, in some cases the layer residual strains were found to be tensile, particularly at the outside of the tubes. It should be noted that the figures calculated in this analysis were subject to a high degree of error in their measurement. An error analysis was performed based on the precision of the vernier calipers used to make the measurements (±0.01 mm). This error analysis has been illustrated in the plots of layer strain versus the mid layer position as error bars. During measurement of the dimensions after slitting, a great deal of care was taken to ensure that no pressure was exerted on the ring which would have distorted the ring and caused large deviations from the true value. However, it is very possible that some pressure was exerted and that the results might have been severely affected.

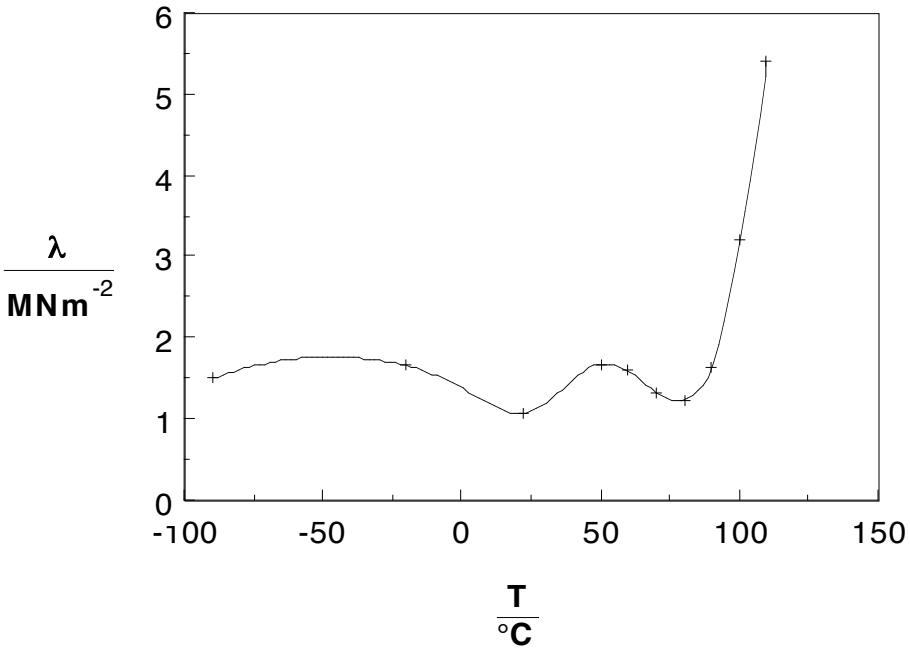

Figure 5.1 Plot of the speed sensitivity λ as a function of the test temperature for Tufnol tubes.

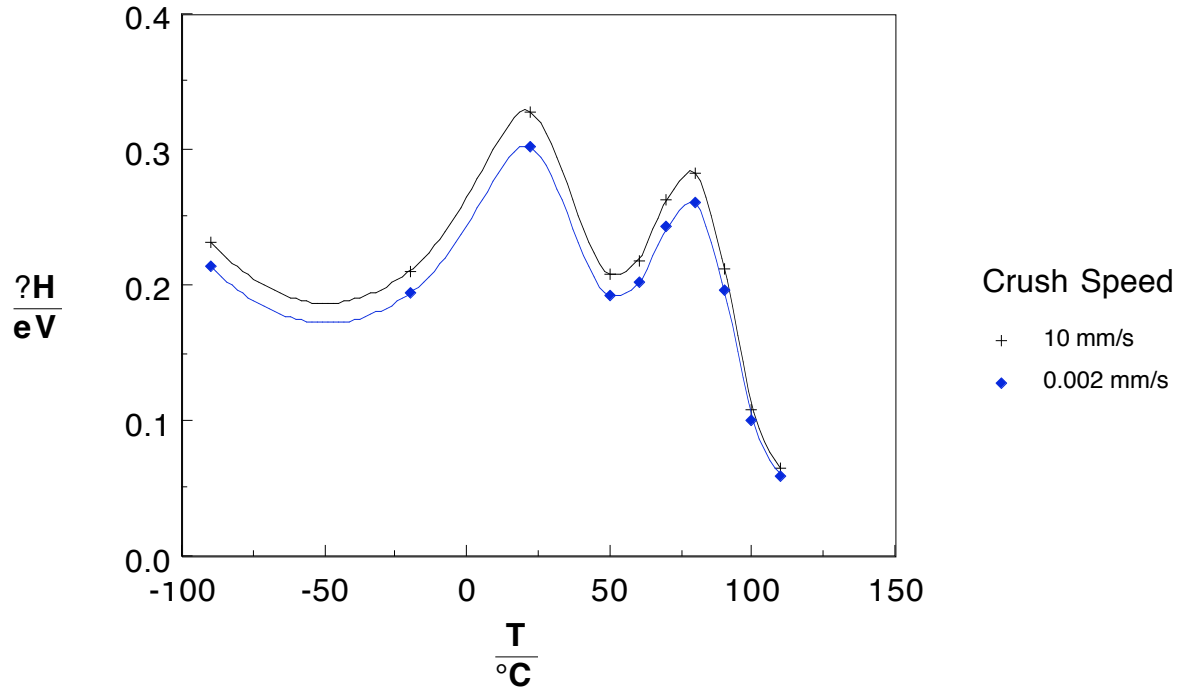

Figure 5.2 Plot of activation energy for crushing as a function of the test temperature for Tufnol tubes tested at 0.002 and 10 mm s^{-1}.

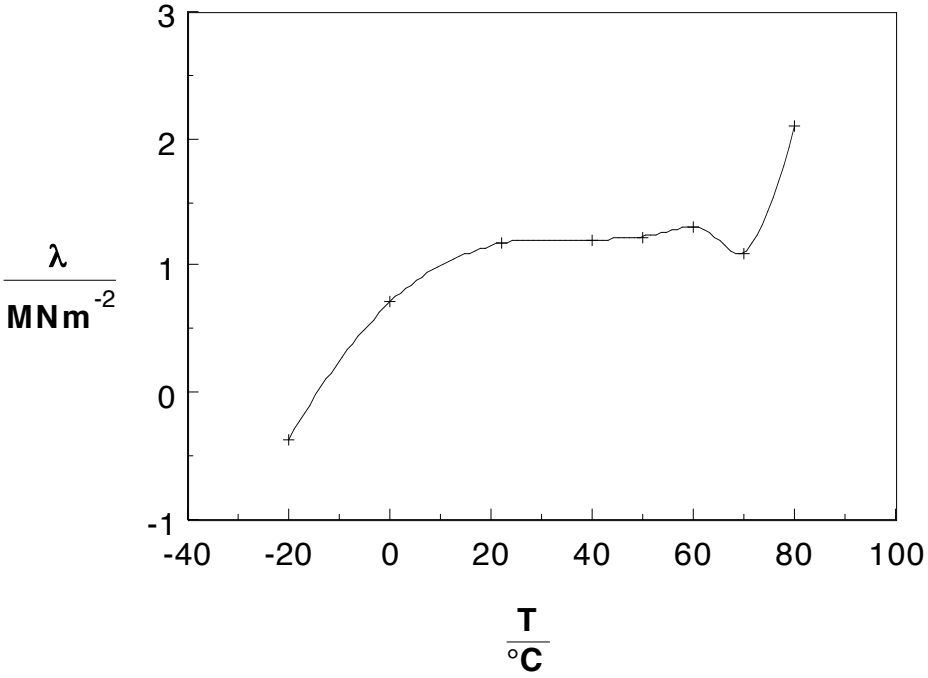

Figure 5.3 Plot of the speed sensitivity λ as a function of the test temperature for RJPW tubes.

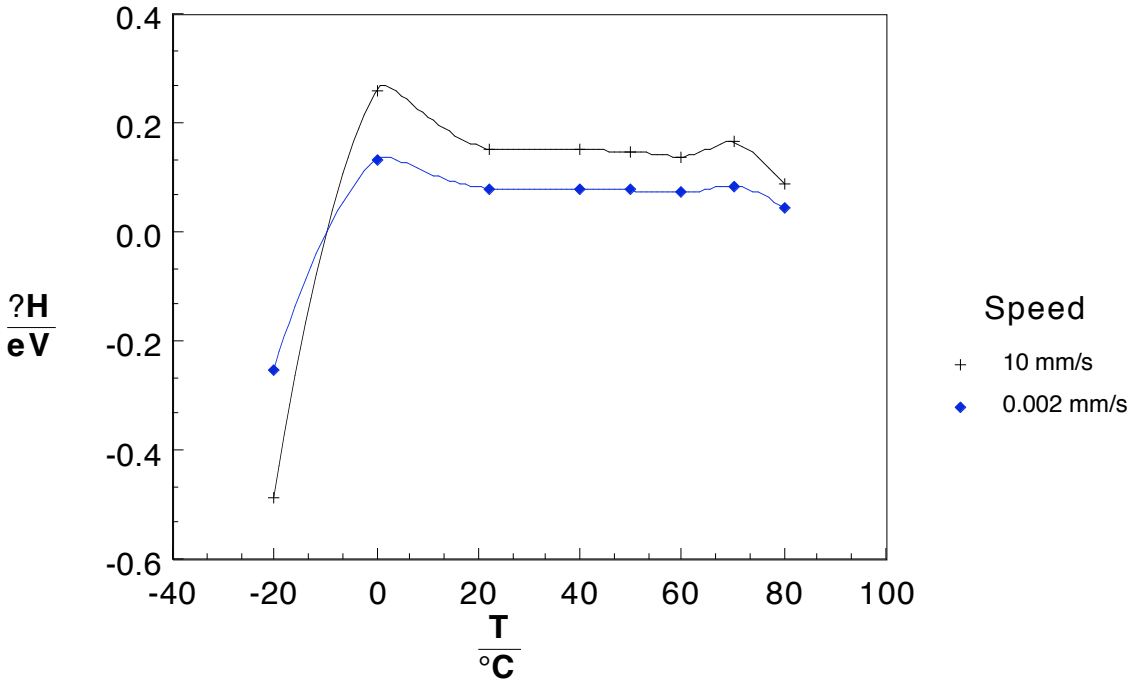

Figure 5.4 Plot of activation energy for crushing as a function of the test temperature for RJPW tubes.

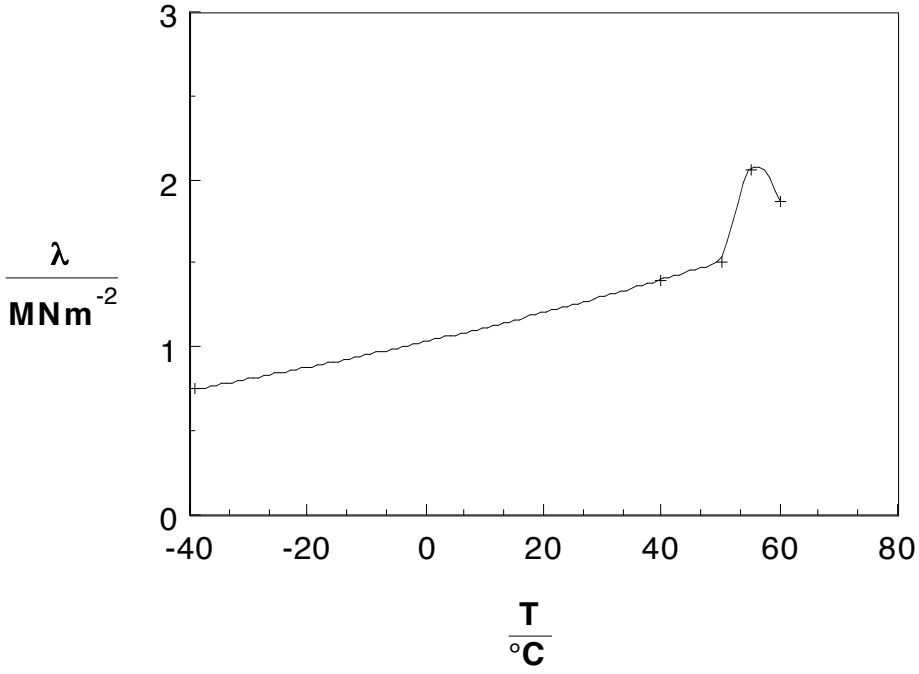

Figure 5.5 Plot of the speed sensitivity λ as a function of the test temperature for RJPR tubes.

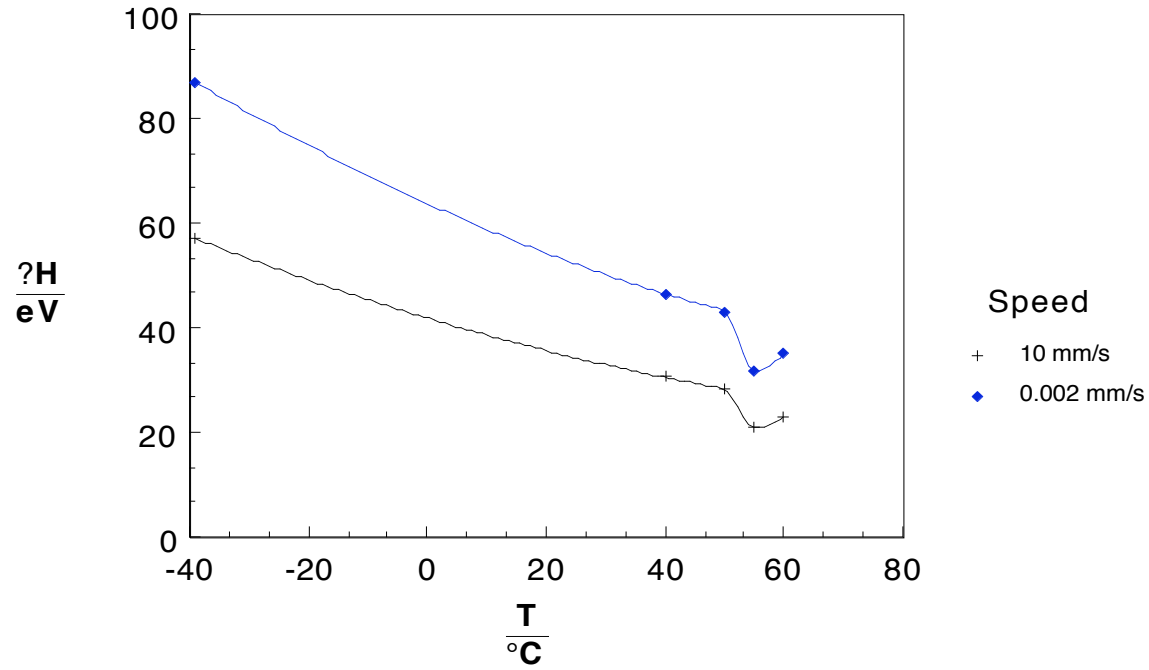

Figure 5.6 Plot of activation energy for crushing as a function of the test temperature for RJPR tubes.

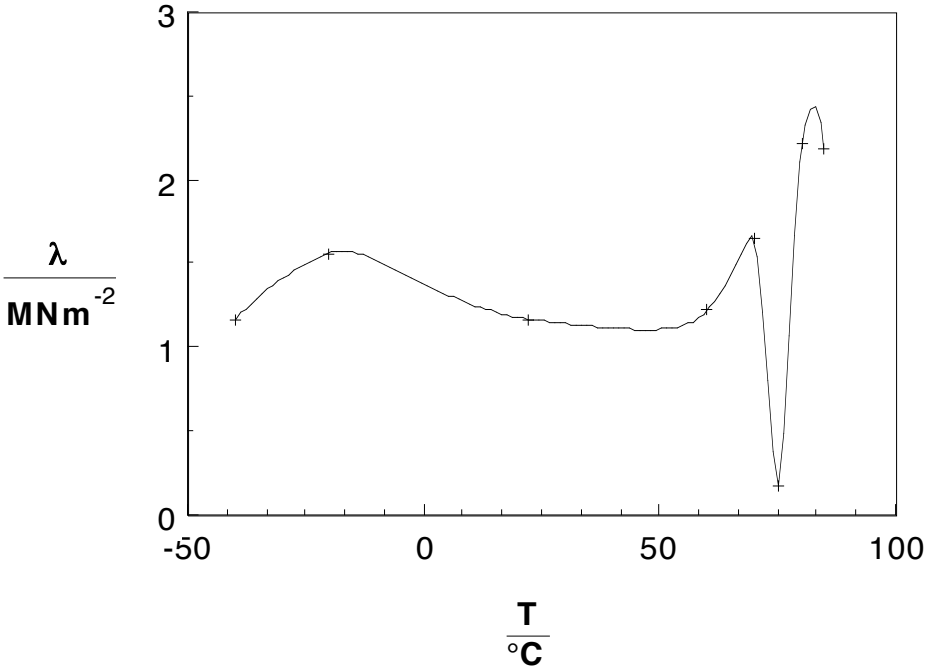

Figure 5.7 Plot of the speed sensitivity λ as a function of the test temperature for RJEW tubes.

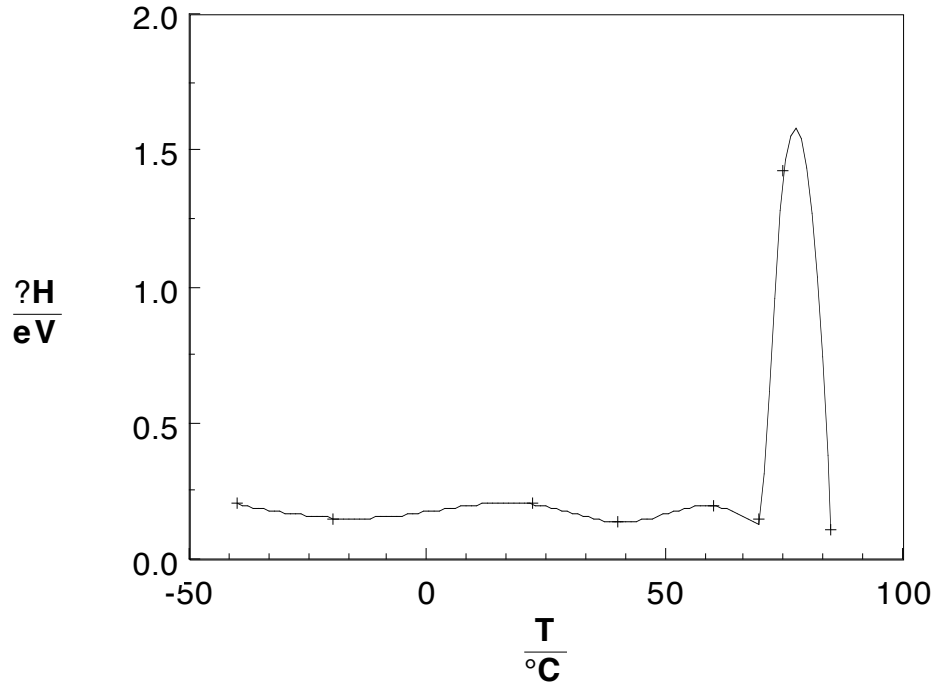

Figure 5.8 Plot of activation energy for crushing as a function of the test temperature for RJEW tubes crushed at 10 mm s^{-1}.

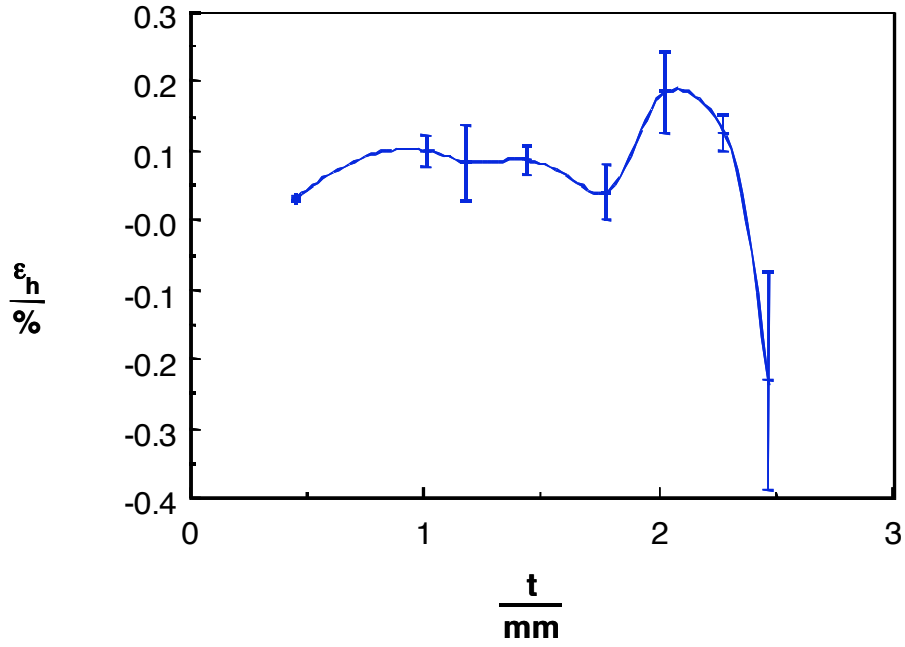

Figure 5.9 Residual hoop strain distribution through the thickness of a Tufnol tube.

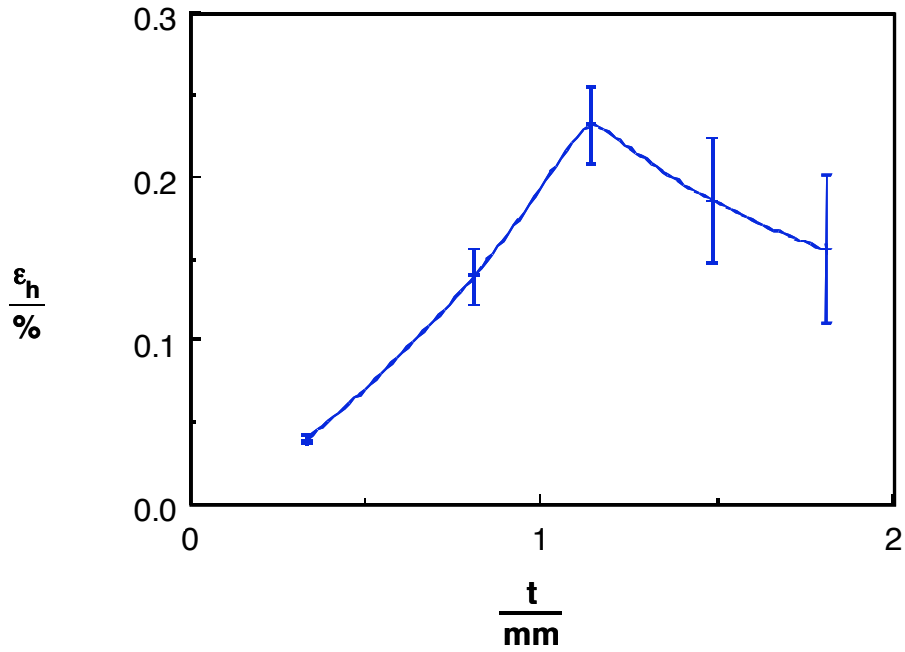

Figure 5.10 Residual hoop strain distribution through the thickness of an RJPW tube.

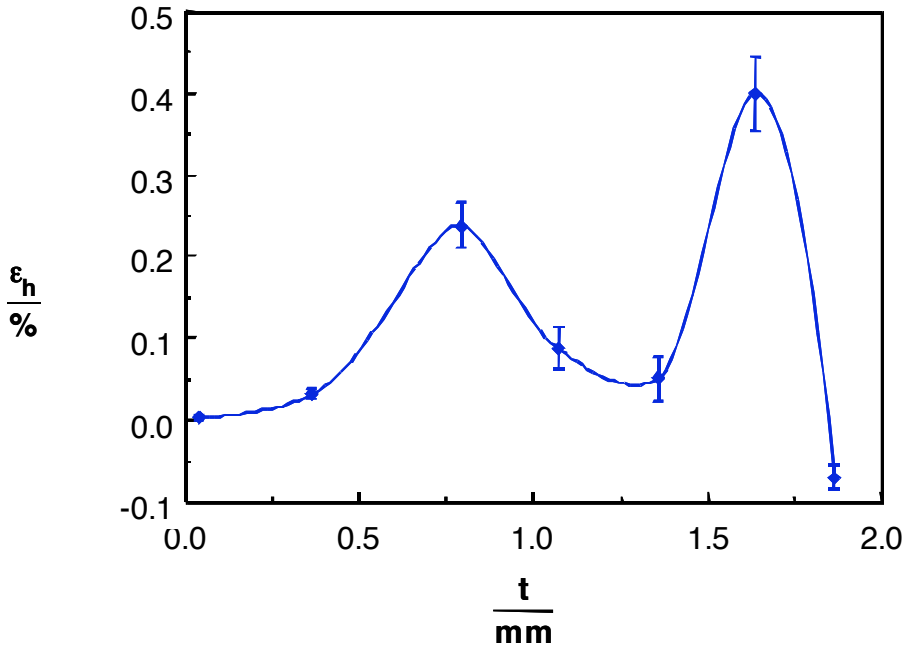

Figure 5.11 Residual hoop strain distribution through the thickness of an RJPR tube.

6 Photography

Two types of photography were used in this project; micrography of sections through the crush zones of various tubes and macro photography of tubes after testing to show more global effects.

6.1 Crush Zone Micrographs

Figures 6.1 to 6.21 show sectional micrographs of the crush zones of various Tufnol tubes after testing and preparation as described in section 3.3.1. These micrographs were taken using the photomontage technique as described in section 3.3.2. Figures 6.22 and 6.23 show schematics of the crush zones for Tufnol tubes tested at room temperature and at about 80 °C, based on the observations made on figures 6.1 to 6.5, 6.18 and 6.19. These schematics show most of the important features which are discussed in section 8.4.1.

Figures 6.24 and 6.25 show sectional micrographs through the crush zones of glass mat-polyester tubes tested at room temperature. These micrographs were each taken as a single frame as described in section 3.3.2, on the Wild microscope.

6.1.1 Tufnol Tubes

These tubes were tested over a range of speeds and temperatures and showed a variety of features in the crush zones. Most of the tubes showed a frond-wedge-frond type of crush zone, although there was a substantial variation in their detail features. Some other forms of crush zone were also displayed, particularly involving a high degree of fragmentation.

This section gives a description of the main features of each cross section. For a discussion of the meaning the features see section 8.4.1.

Each micrograph has been photographically enlarged. As the degree of frond splaying varied, it was not possible to use the same magnification while keeping the micrographs within page size constraints and showing the main features. The scale of the micrographs can be taken from the tube wall thickness which was 2.5 mm for the Tufnol tubes. In each case the external side has been labelled.

6.1.1.1 Room Temperature Constant Speed Tests

Figures 6.1 to 6.7 show sections through the crush zones of tubes crush tested at room temperature and constant speed. These sections cover the speed range of 0.01 mm s^{-1} to 1.5 m s^{-1}.

The sections from 0.01 mm s^{-1} {figures 6.1 and 6.2} showed a large difference between the behaviour of the internal and external debris as the internal debris was subjected to a high degree of delamination while the external debris was less fragmented and showed the presence of hackles. These hackles are discussed in detail in section 8.4.1.1. Both of the sections showed the presence of a debris wedge, in both cases slightly displaced towards the inside of the tube.

Figures 6.3 to 6.5 show sections taken from tubes crushed at 10 mm s^{-1}. The most significant feature of these sections was the presence of hackles in both the internal and external fronds. However, although all the sections exhibited hackles, they did not all feature hackles on both internal and external fronds, only the section shown in figure 6.3 had hackles on both fronds. Figure 6.4 shows hackles on the internal fronds with no hackles on the external fronds. In this section, the external fronds fragmented and showed some degree of matrix deformation as detected by void flattening. All the sections for 10 mm s^{-1} showed a distinct debris wedge. The wedge was approximately

central in the tube wall but figures 6.4 and 6.5 show a slight off-set, externally in figure 6.4 and internally in figure 6.5, in each case away from the frond exhibiting hackles. The radius of curvature of the wedge-frond interface was approximately 3.2 mm.

Figures 6.6 and 6.7 show sections through crush zones of tubes tested at 0.5 ms^{-1} and 1.5 m s^{-1} respectively. Both tubes showed a high degree of fragmentation and delamination in the debris. Figure 6.6 shows a suggestion of the presence of hackles in the external frond but there was no suggestion of hackles at the higher speed. Figure 6.7 shows a high void content which could account for the level of delamination in this section. This feature might have obscured any genuine speed effects.

6.1.1.2 Room Temperature Impacts

Figures 6.8 to 6.13 show sections through the crush zones of tubes that were impact tested from 5 m s^{-1}, 10 m s^{-1} and 20 m s^{-1}.

Figures 6.8 and 6.9 show sections through a tube impact tested from 5 m s^{-1}. Both these sections showed a distinct debris wedge with fronds that contained a degree of delamination. The fronds showed a lesser degree of fragmentation than those from the higher speed tests but they appeared to have had little integrity compared with those from the lower speed tests. In each case a centre wall crack was shown clearly. Shear fractures were observed in the impact tested sections {figures 6.10 to 6.13} but were not as apparent in the lower speed impact sections as in the sections from higher speeds.

The two sections from the tube impact tested from 10 m s^{-1} {figures 6.10 and 6.11} showed a high degree of fragmentation in both the internal and external debris. A debris wedge could be discerned in figure 6.10, shear cracks were also apparent.

The 20 m s^{-1} impact sections showed a large degree of fragmentation with delamination in the fronds and a clear debris wedge {figures 6.12 and 6.13}. One feature that was of note was the apparent shear crack between the wedge and the edge of the tube wall. In figure 6.12 the shear crack ran from the wedge to the inside of the tube while in figure 6.13 the crack ran to the outside of the tube. These two sections were taken from the same tube, being cut such that they were approximately diametrically opposite each other. It is noteworthy that, in each case, the crack ran to the side that was further from the wedge, meaning that it will have had to propagate through the greater amount of material. This observation might have been because of the difference in bend stiffness of the two sets of debris[1]. Similar shear cracks were observed in sections from lower speed tests but they were not as clear {figures 6.6 to 6.11}.

6.1.1.3 Low Temperature Impacts

Figures 6.14 and 6.15 show sections through the crush zone of a tube impact tested from 10 m s^{-1} after immersion in liquid nitrogen, the temperature of the tube at the moment of impact being below -110 °C[2]. This test represented one extreme of the test conditions, high speed and low temperature. Although these sections were from the same tube, the crush zone morphologies of the two sections were very different

[1]This would indicate that the cracks were not formed by simple shearing alone. However they are termed "shear" cracks for reasons of brevity.

[2]This was estimated from consideration of the extrapolated temperature of buckling for impact tests.

although in both cases very little matrix deformation occurred and a high degree of fracture was apparent. The size of the pieces of debris was approximately constant at about 2.5 mm in length, the same as the wall thickness of the tube. This observation could simply have been a coincidence, as this dimension was for the length of the fragment which was originally in the axial direction instead of a through thickness piece. This tube was impact tested several times before mounting and sectioning to produce the micrographs. However, the crush distance for each impact test was about 9 mm, so that the size of the debris pieces was smaller than the crush distance, thus the debris as seen in the micrographs was formed in a single impact. There appeared to be a high degree of interlaminar fracture, as well as through thickness fracture, which was probably due to bending of the debris to remove it from the crush zone. The differences between the two sections appeared to be due to the presence of voids. In the tube shown in figure 6.14, where there was a clear centre wall crack and the void content was much higher than in figure 6.15, where no centre wall crack was apparent. Close examination of the sides of the crack showed that the path of the crack was along the fibre-matrix interface and through voids. Although figure 6.15 showed no centre wall crack, two cracks were present about 0.7 mm from the outside of the tube wall on either side. These were probably due to a localised effect, the need for the material between the two cracks to be moved away from the crush zone meaning that this geometry would not have remained if crushing had progressed further.

6.1.1.4 High Temperature Crushes

Figures 6.16 to 6.21 show sections from tubes crush tested at 0.5 mm s^{-1} at temperatures above room temperature.

6.1.1.5 60 °C Crush

Figures 6.16 and 6.17 show sections through the crush zone of a tube crushed at 60 °C. These sections showed very distinct hackles in both internal and external fronds and a debris wedge, although in the section in figure 6.17 the wedge appeared to have detached from the crush zone when the test was halted. The hackles in the external frond in the section in figure 6.16 appeared to have grown such that fragments detached from the rest of the debris. At the trailing edge of each of these fragments, clear evidence could be seen of the shear fracture that formed the fragments and was involved in the formation of the hackles. Figure 6.17 showed very clear hackles with a regular spacing of 0.8 mm for the external frond and 0.9 mm for the internal frond. The external frond shows a clear curvature with a radius of about 7 mm. The depth of the hackles appeared to be reasonably constant but this was difficult to measure accurately.

6.1.1.6 80 °C Crush

Figures 6.18 and 6.19 show sections from a tube tested at 80 °C. Although in general appearance they resembled the sections from 60 °C, there were some important differences, particularly in the hackles which were much smaller than for 60 °C. The hackle spacing was however, similar at about 0.9 mm, this being similar to the repeat distance for the glass cloth (see section 3.1.1). There also appeared to be a high degree of matrix deformation and delamination in the fronds. The radius of curvature for the external frond in figure 6.18 was about 8 mm.

6.1.1.7 100 °C Crush

Figures 6.20 and 6.21 show sections through the crush zone from a tube crushed at 100 °C. The fronds in these sections were much cleaner and more coherent than those

from the lower temperature tests with little evidence of hackle formation. Features could be discerned on the inside of the frond curvature that resembled hackles, with a repeat distance of about 0.9 mm. The section in figure 6.20 showed considerable evidence of matrix deformation through void flattening, but in that in figure 6.21, the external frond featured voids which appeared to have remained largely undeformed during the traverse of the crush zone.

6.1.1.8 Schematics

Schematic crush zones for Tufnol tubes tested at ambient and high temperatures are given in figures 6.22 and 6.23. These two schematics have various features in common, particularly the presence of the wedge and fronds, a centre wall crack at the tip of the wedge, hackles on what was the outside of the tube wall and elongated voids in the fronds. However, the extent of these features differed between the high and low temperature tests. In general, the size of the hackles was greatly reduced by increasing the temperature while the degree of void flattening increased.

6.1.2 Glass mat-polyester Tubes

Figures 6.24 and 6.25 show sectional micrographs through the crush zones of glass mat-polyester tubes tested at room temperature. Both of these sections showed a frond-wedge-frond type of crush mode and that in figure 6.24 showed a number of cracks in the external tube wall, perpendicular to the centre wall crack. Crush zones for these tubes were very inconsistent in their appearance due to a high level of material variability, but the wedge angle was consistently smaller than for the Tufnol tubes.

6.2 Macro Photographs

Figures 6.26 to 6.29 show axial macro photographs taken from the crushed end of Tufnol tubes tested over the temperature range 22 °C to 100 °C at 0.1 mm s^{-1}. These tubes showed a trend in the number and size of the external fronds, from a large number of small fronds at low temperature to a few large fronds at high temperature. Table 6.1 shows the number of fronds in the crush zone for each test temperature and the average width of the fronds.

Figure No.	Temperature °C	Number of Fronds	Frond Width mm
6.26	22	11	15.7
6.27	40	10	17.3
6.28	80	8	21.6
6.29	100	6	28.8

Table 6.1 Number of fronds and the average frond width as a function of the test temperature for Tufnol tubes.

Increasing the temperature further led to a buckling mode of collapse as illustrated in figure 6.30. This tube was tested at 110 °C at 0.1 mm s^{-1}.

Figure 6.31 shows a resinject tube that collapsed with centre failure and interpenetration. This tube was of the RJPR type, tested at 70 °C at 0.5 mm s^{-1}.

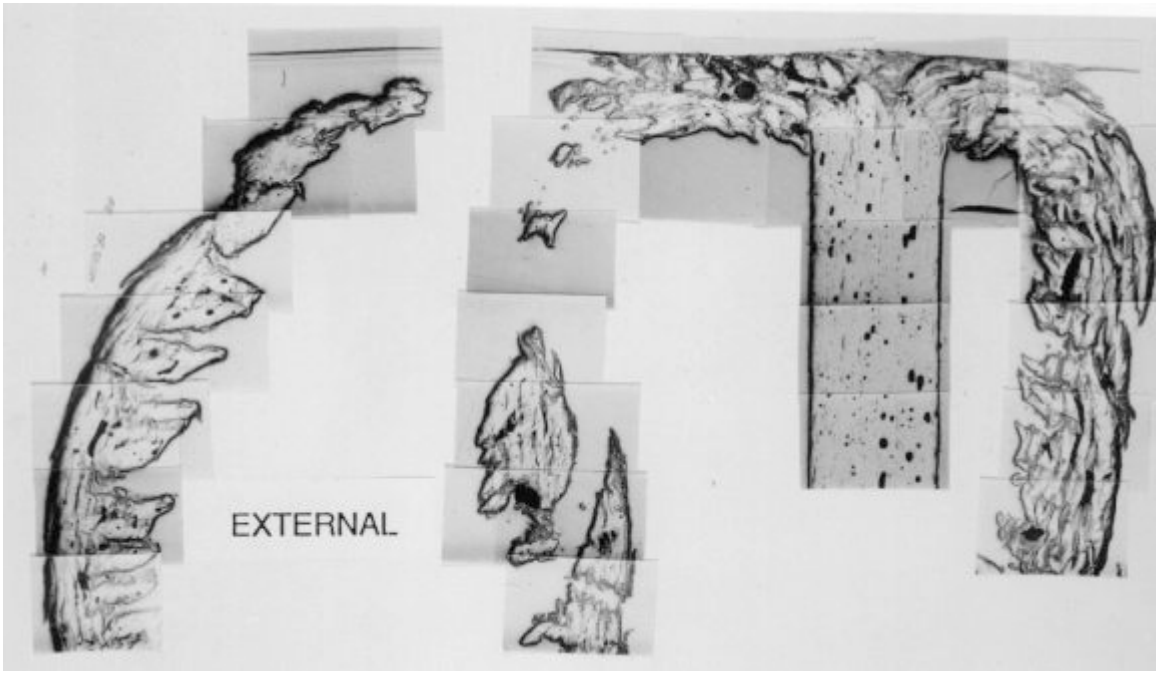

Figure 6.1 Section through the crush zone of a Tufnol tube crushed at 0.01 mm s^{-1} at room temperature.

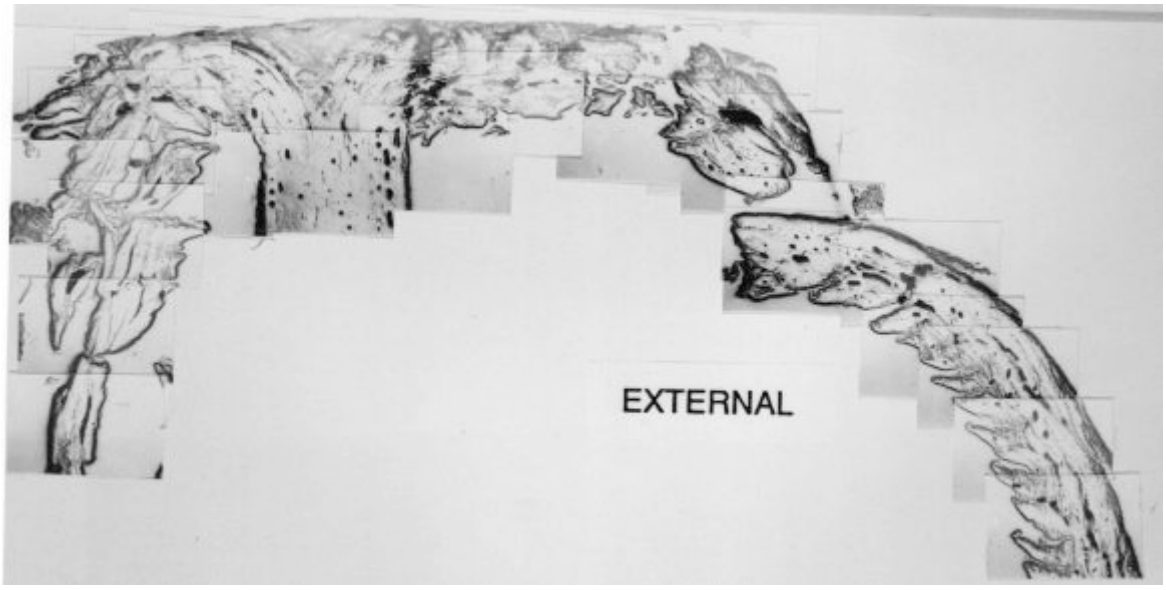

Figure 6.2 Section through the crush zone of a Tufnol tube crushed at 0.01 mm s^{-1} at room temperature.

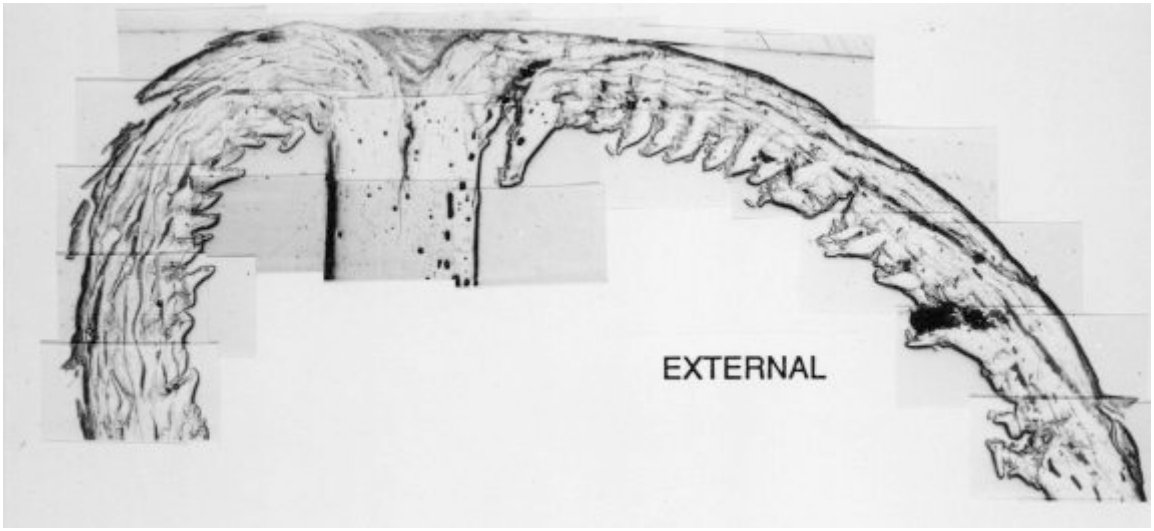

Figure 6.3 Section through the crush zone of a Tufnol tube crushed at 10 mm s^{-1} at room temperature.

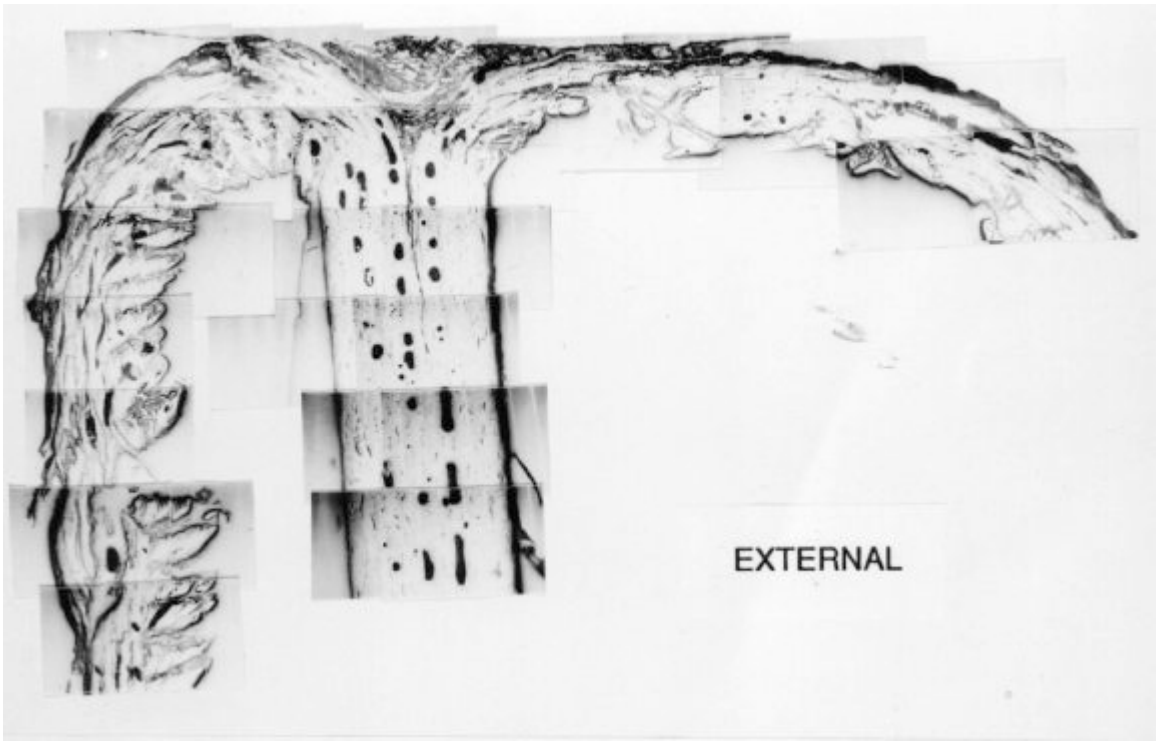

Figure 6.4 Section through the crush zone of a Tufnol tube crushed at 10 mm s^{-1} at room temperature.

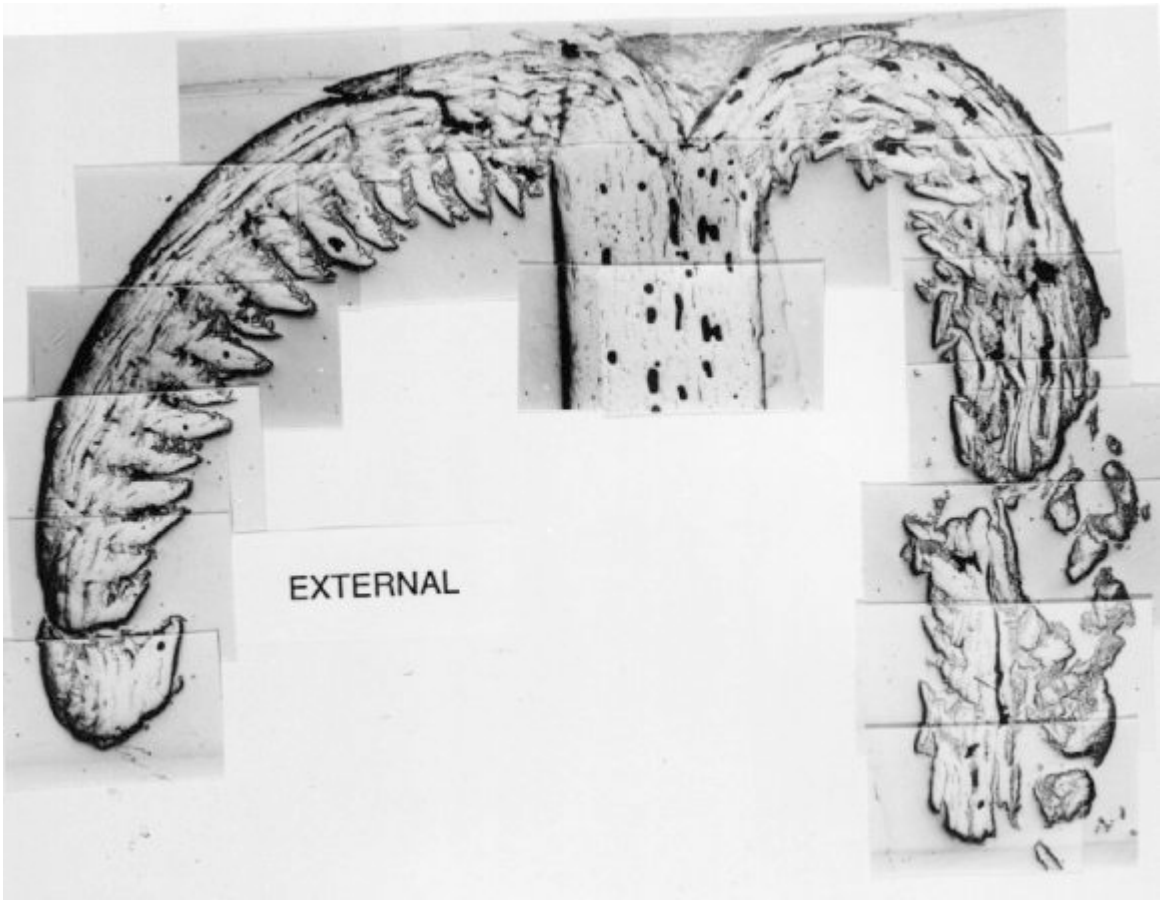

Figure 6.5 Section through the crush zone of a Tufnol tube crushed at 10 mm s^{-1} at room temperature.

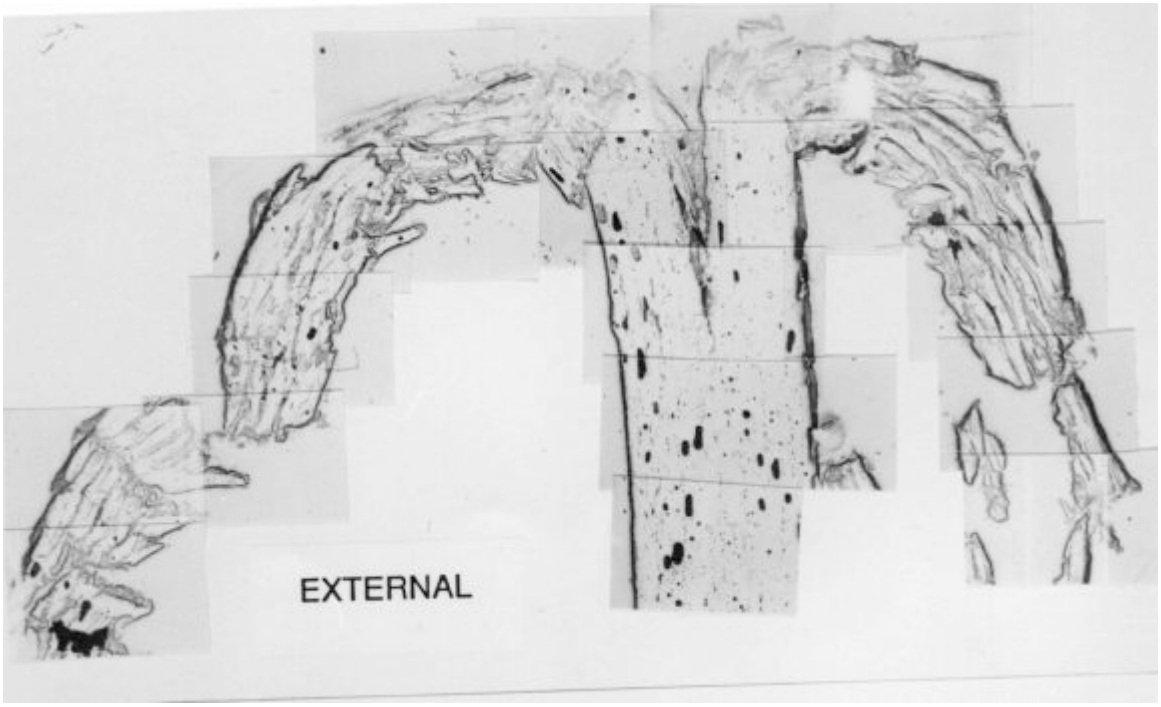

Figure 6.6 Section through the crush zone of a Tufnol tube crushed at 0.5 m s^{-1} at room temperature.

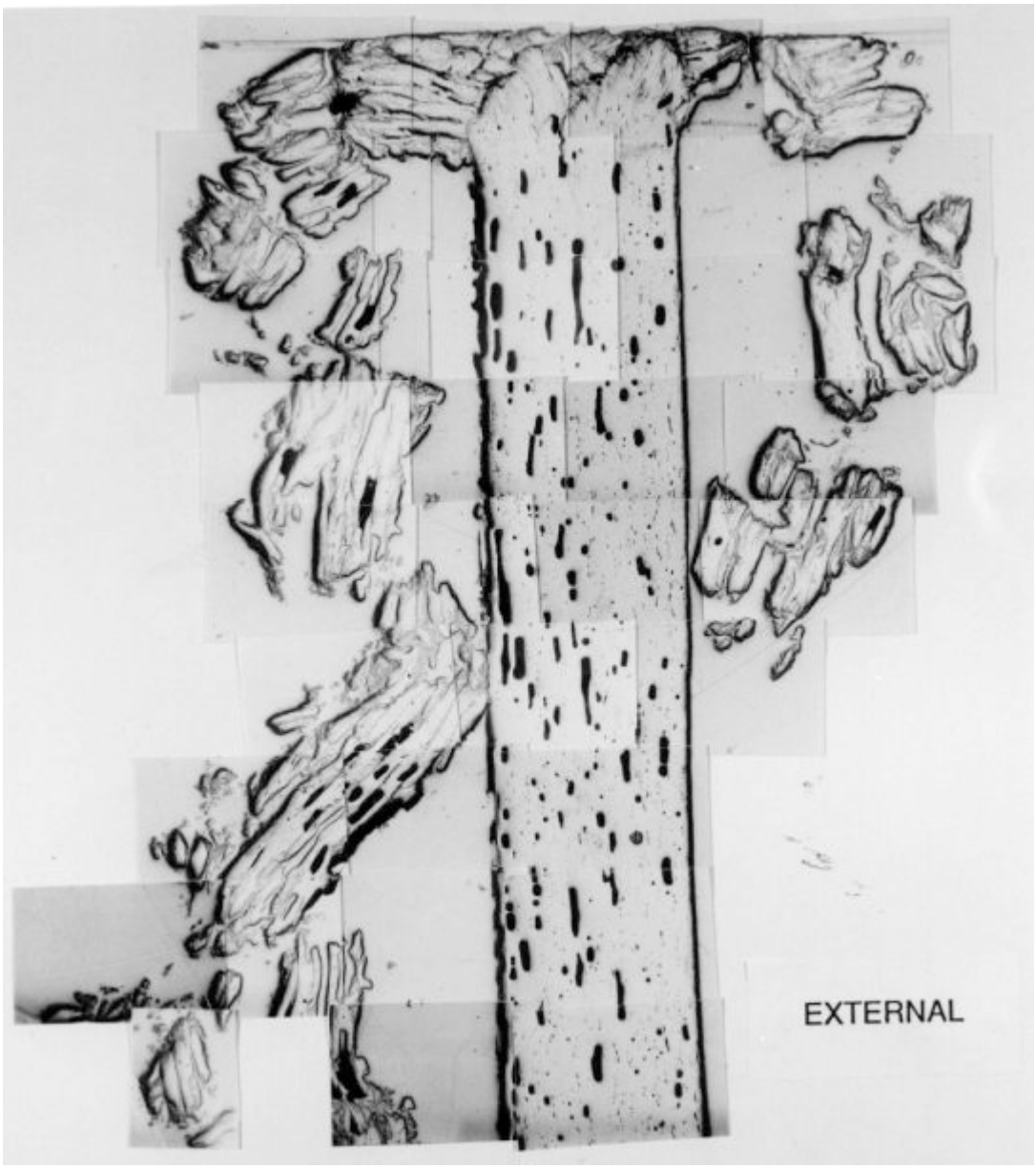

Figure 6.7 Section through the crush zone of a Tufnol tube crushed at 1.5 m s^{-1} at room temperature.

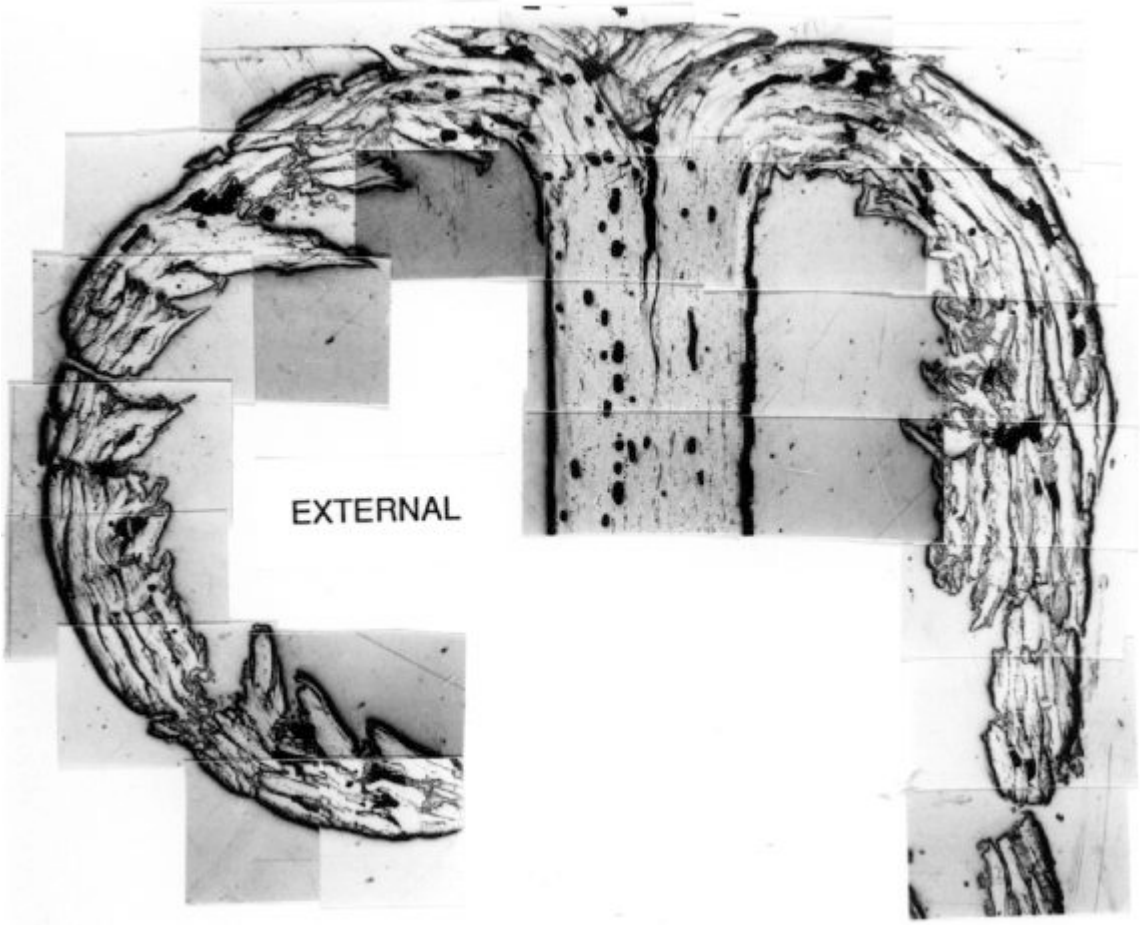

Figure 6.8 Section through the crush zone of a Tufnol tube impacted from 5 m s^{-1} at room temperature.

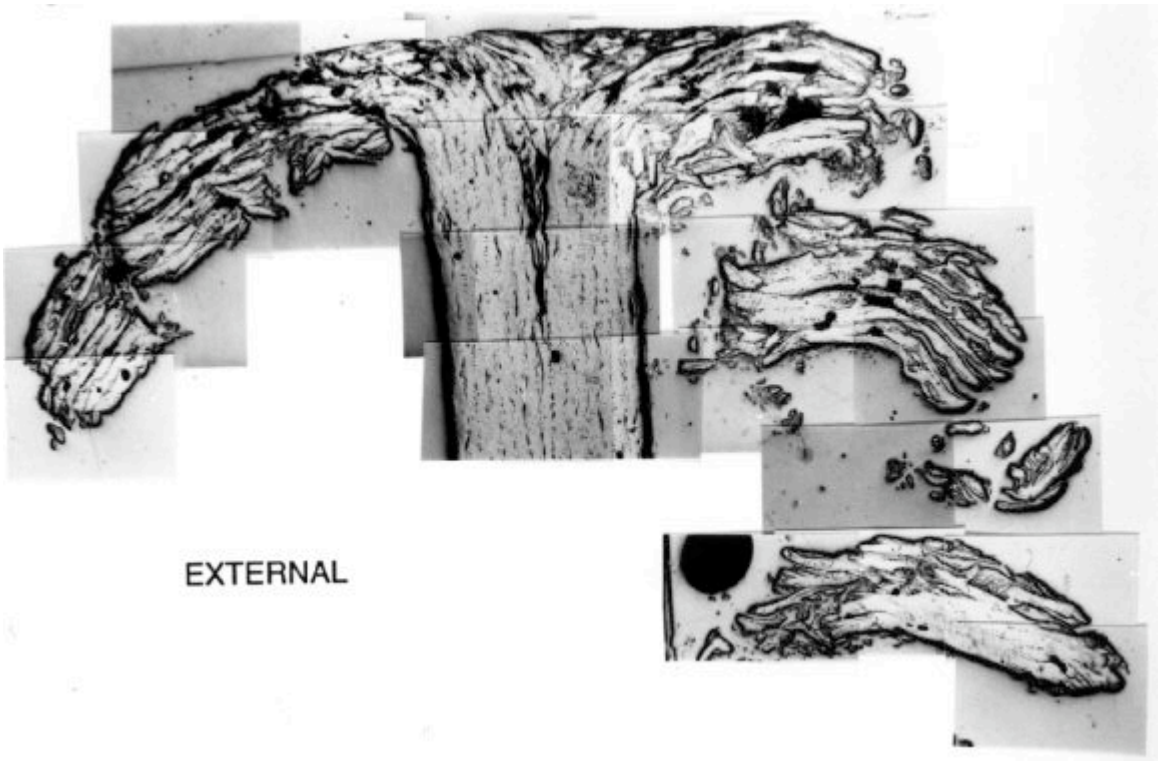

Figure 6.9 Section through the crush zone of a Tufnol tube impacted from 5 m s^{-1} at room temperature.

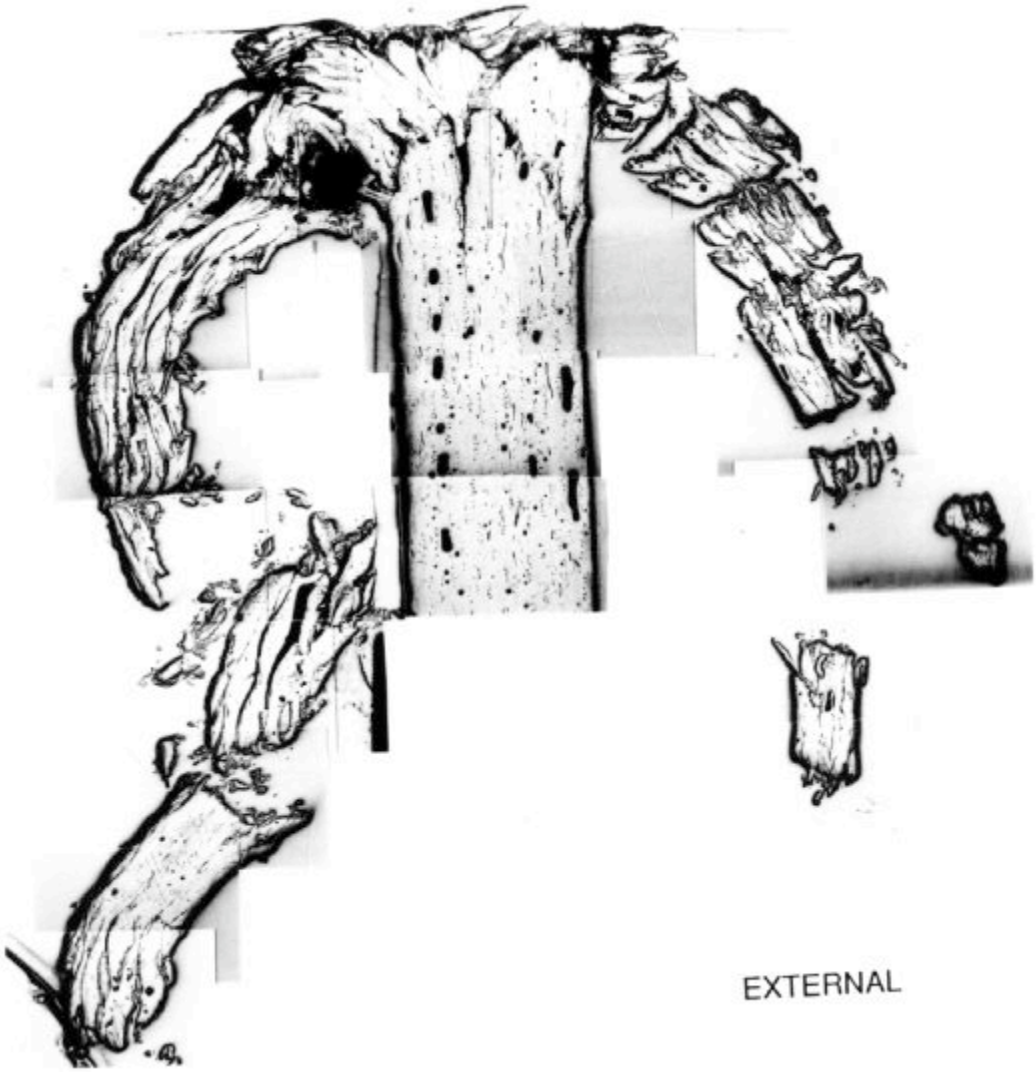

Figure 6.10 Section through the crush zone of a Tufnol tube impacted from 10 m s^{-1} at room temperature.

Figure 6.11 Section through the crush zone of a Tufnol tube impacted from 10 m s^{-1} at room temperature.

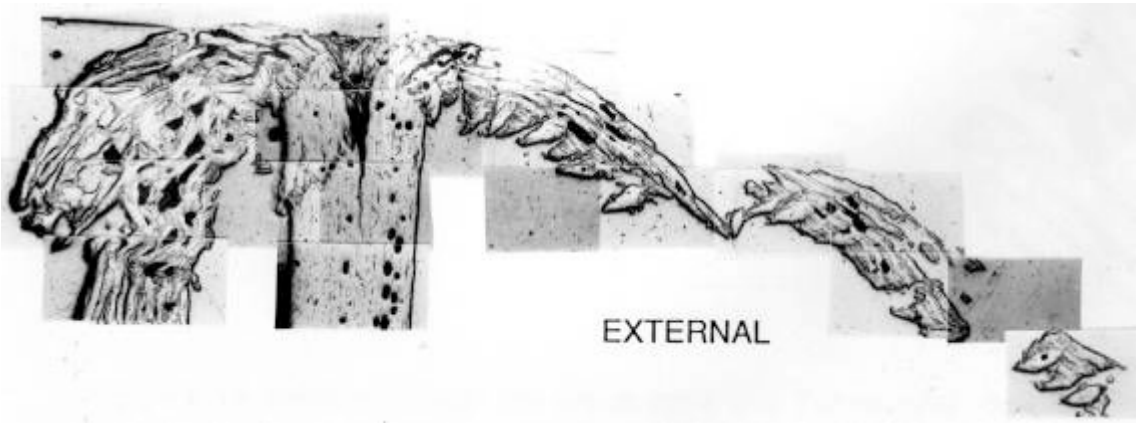

Figure 6.12 Section through the crush zone of a Tufnol tube impacted from 20 m s^{-1} at room temperature.

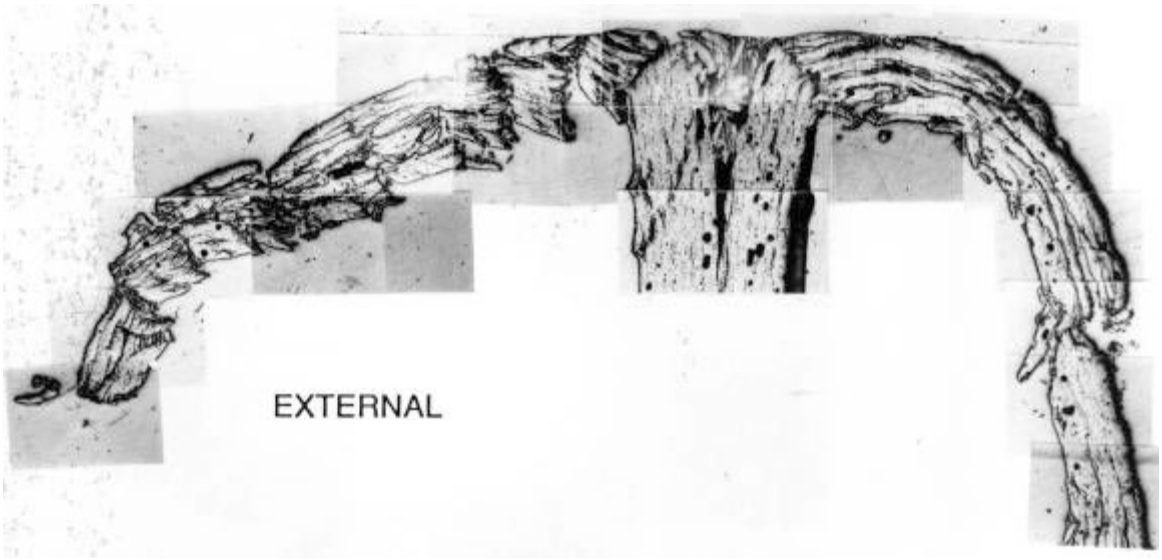

Figure 6.13 Section through the crush zone of a Tufnol tube impacted from 20 m s^{-1} at room temperature.

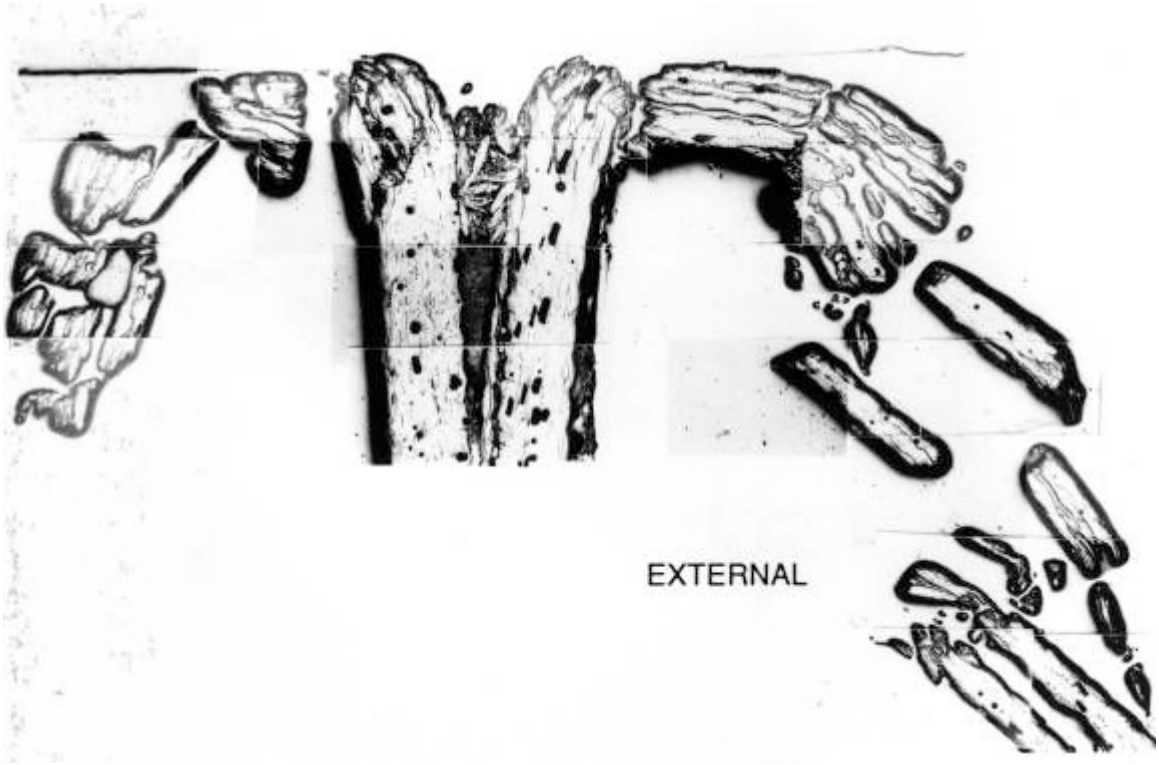

Figure 6.14 Section through the crush zone of a Tufnol tube impacted from 10 m s^{-1} after immersion in liquid nitrogen.

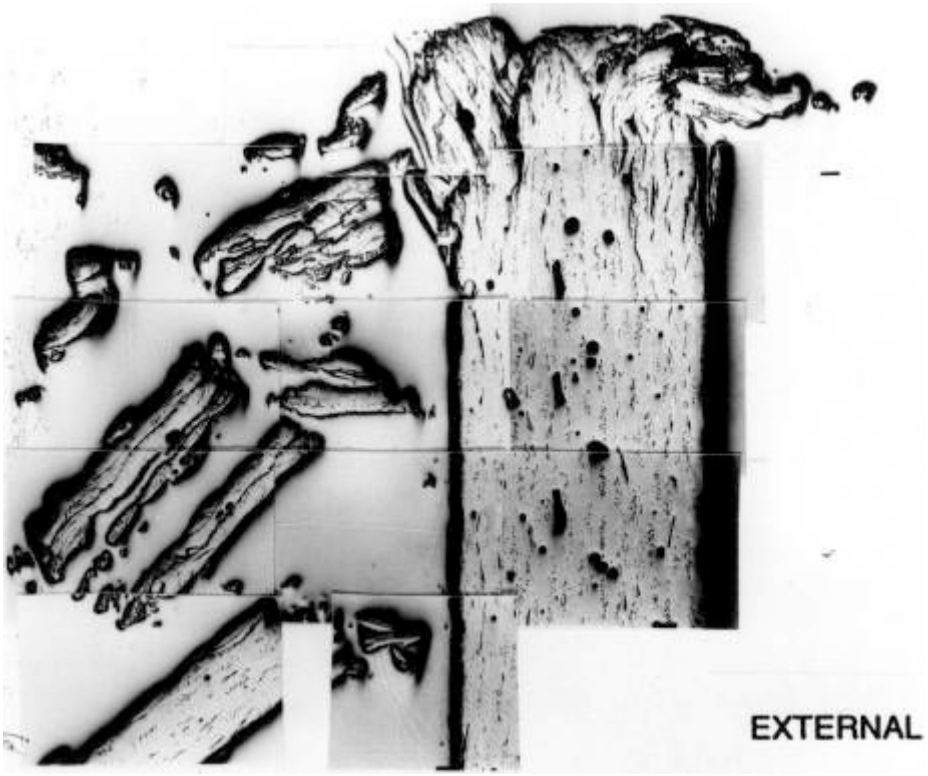

Figure 6.15 Section through the crush zone of a Tufnol tube impacted from 10 m s^{-1} after immersion in liquid nitrogen.

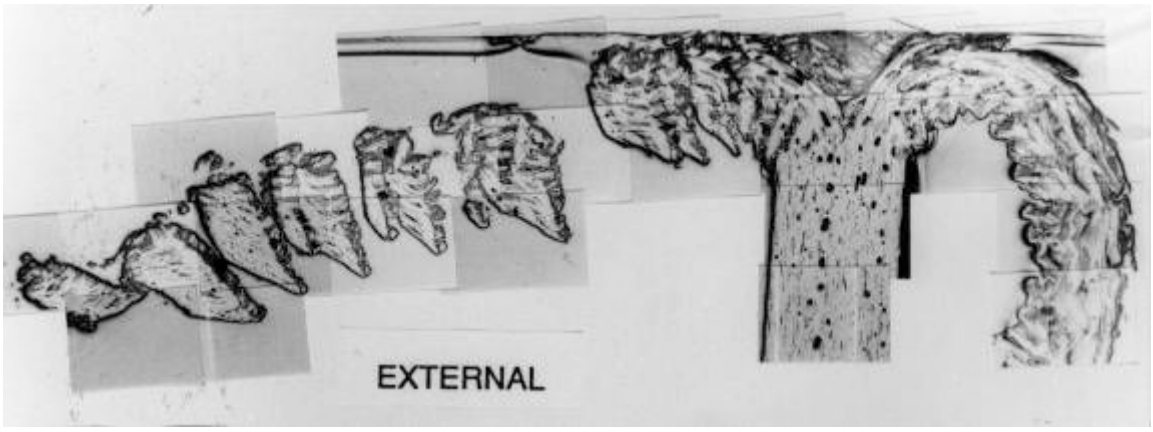

Figure 6.16 Section through the crush zone of a Tufnol tube crushed at 0.5 mm s^{-1} at 60 °C.

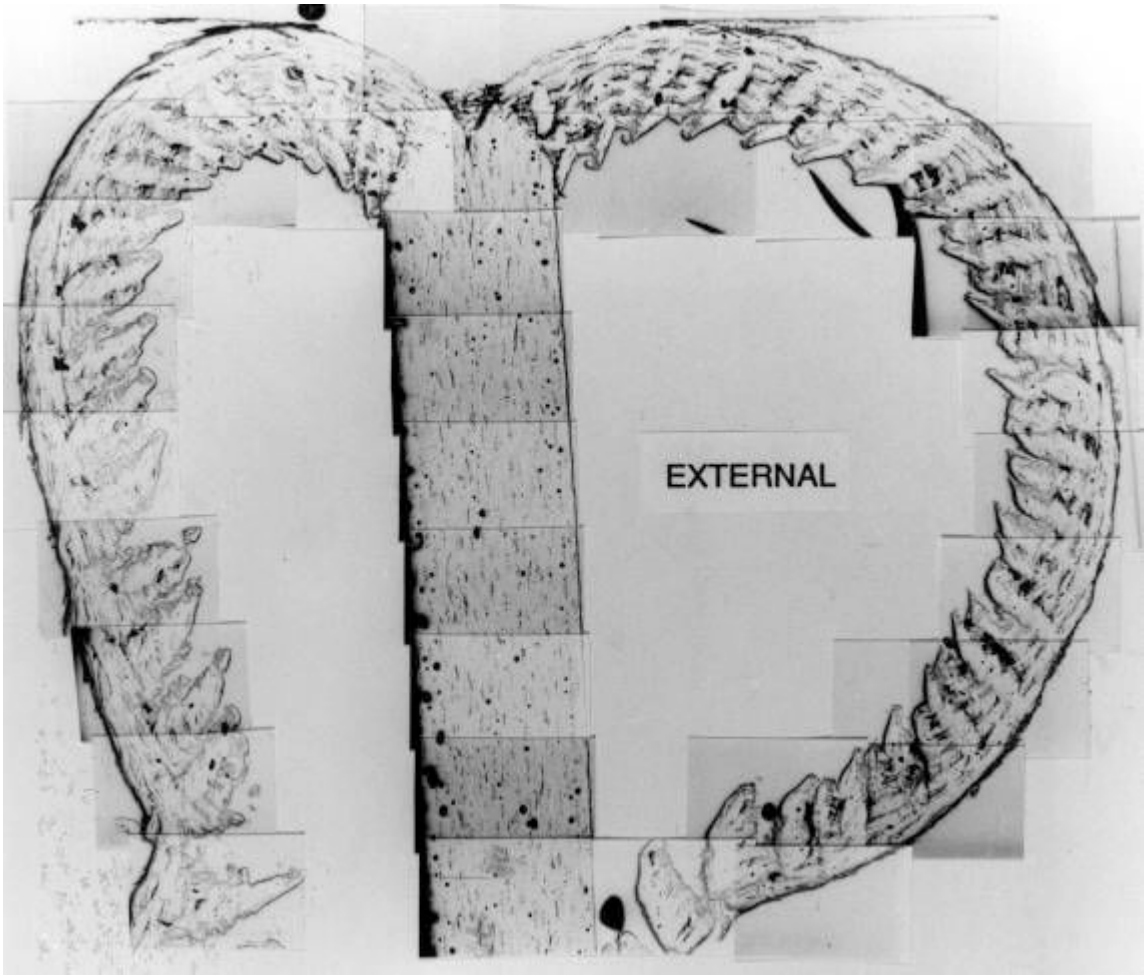

Figure 6.17 Section through the crush zone of a Tufnol tube crushed at 0.5 mm s^{-1} at 60 °C.

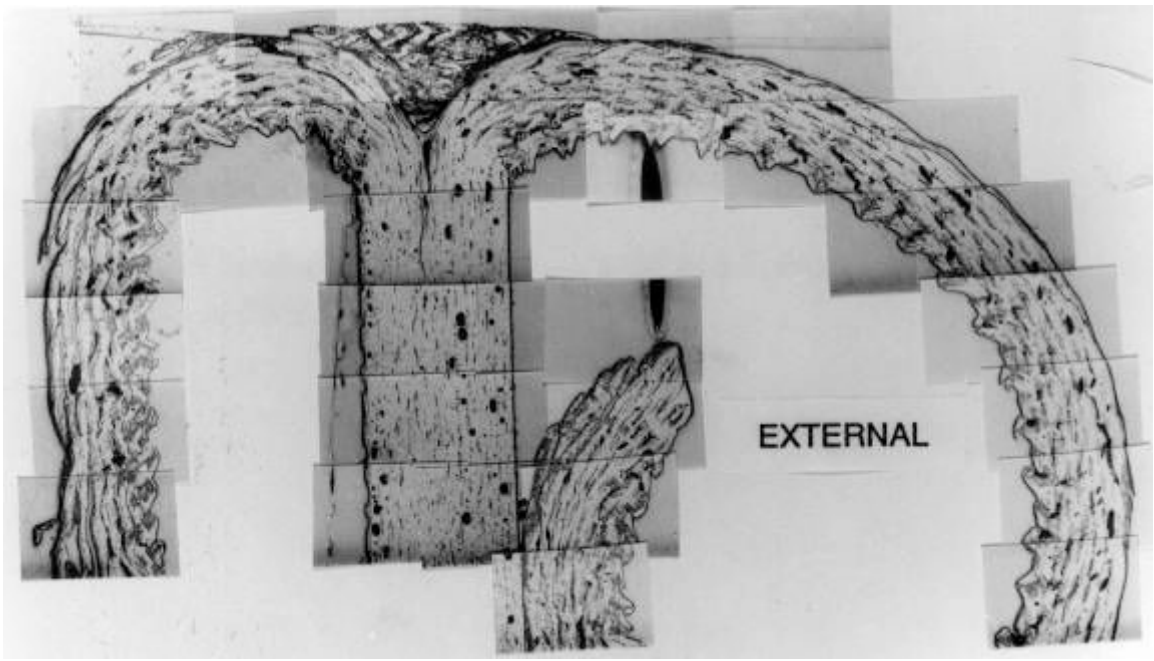

Figure 6.18 Section through the crush zone of a Tufnol tube crushed at 0.5 mm s^{-1} at 80 °C.

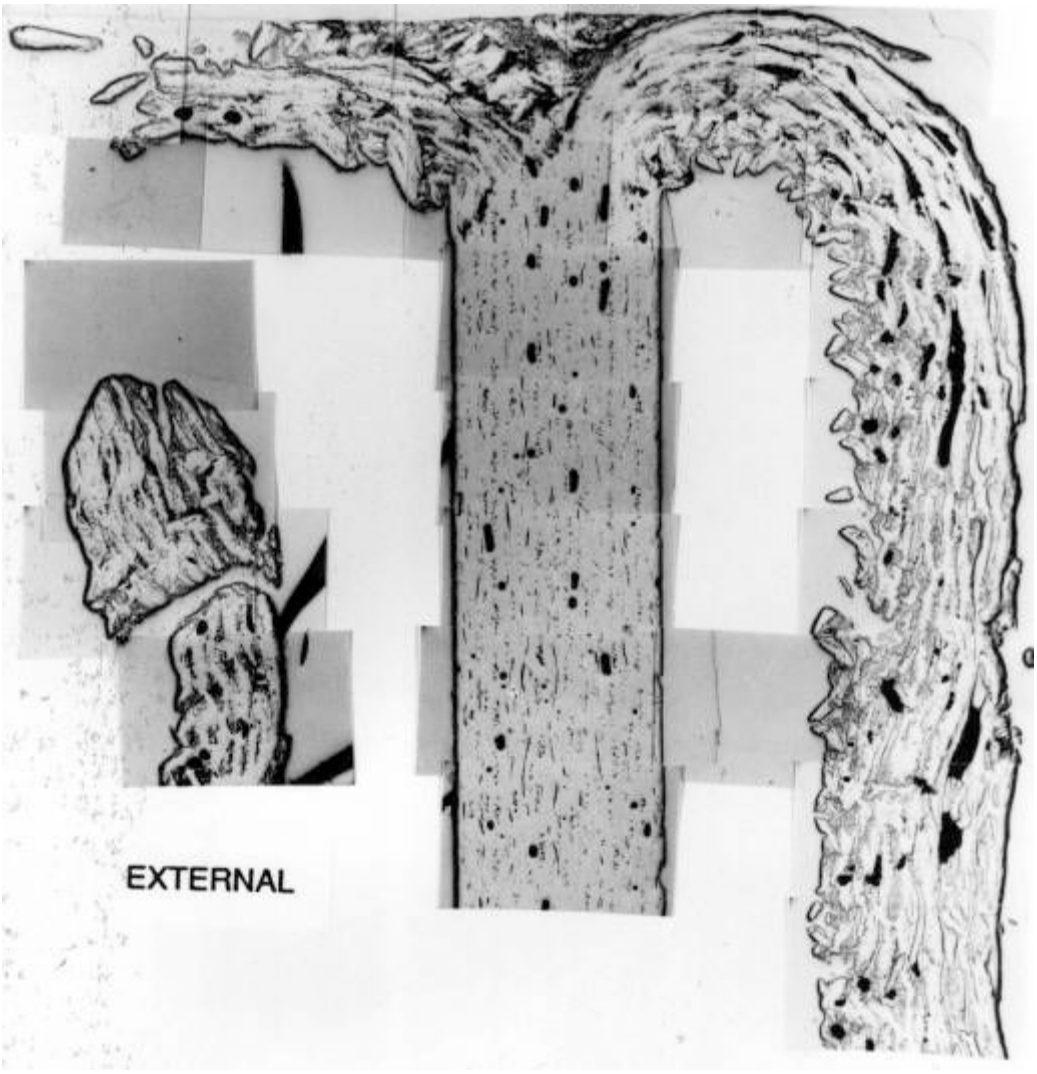

Figure 6.19 Section through the crush zone of a Tufnol tube crushed at 0.5 mm s^{-1} at 80 °C.

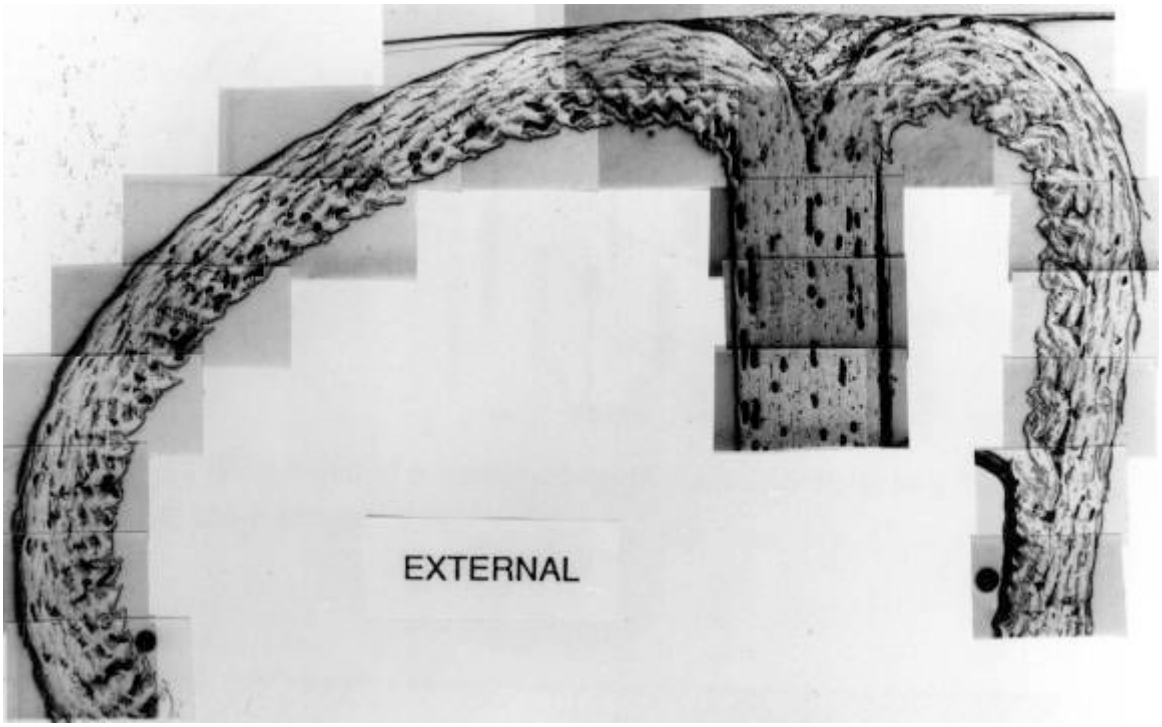

Figure 6.20 Section through the crush zone of a Tufnol tube crushed at 0.5 mm s^{-1} at 100 °C.

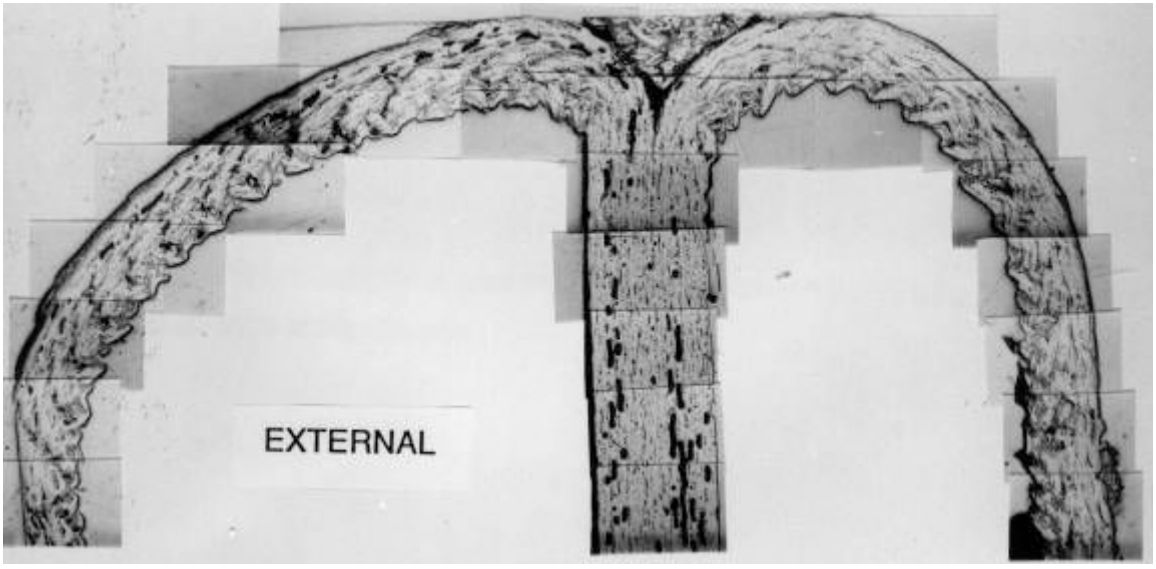

Figure 6.21 Section through the crush zone of a Tufnol tube crushed at 0.5 mm s^{-1} at 100 °C.

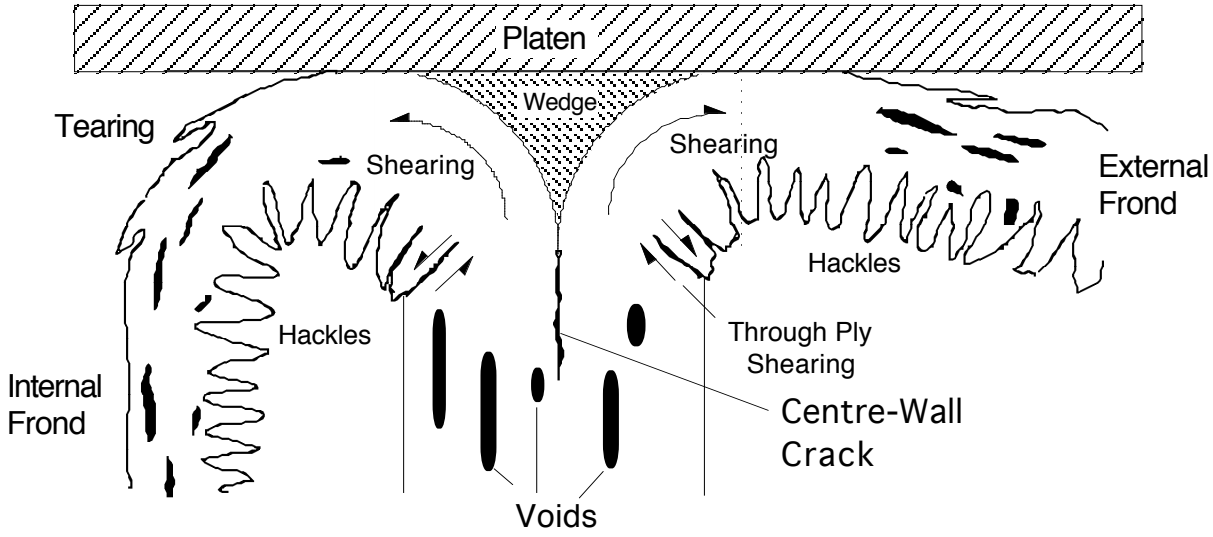

Figure 6.22 Schematic of a section through the crush zone of a Tufnol tube crushed at room temperature.

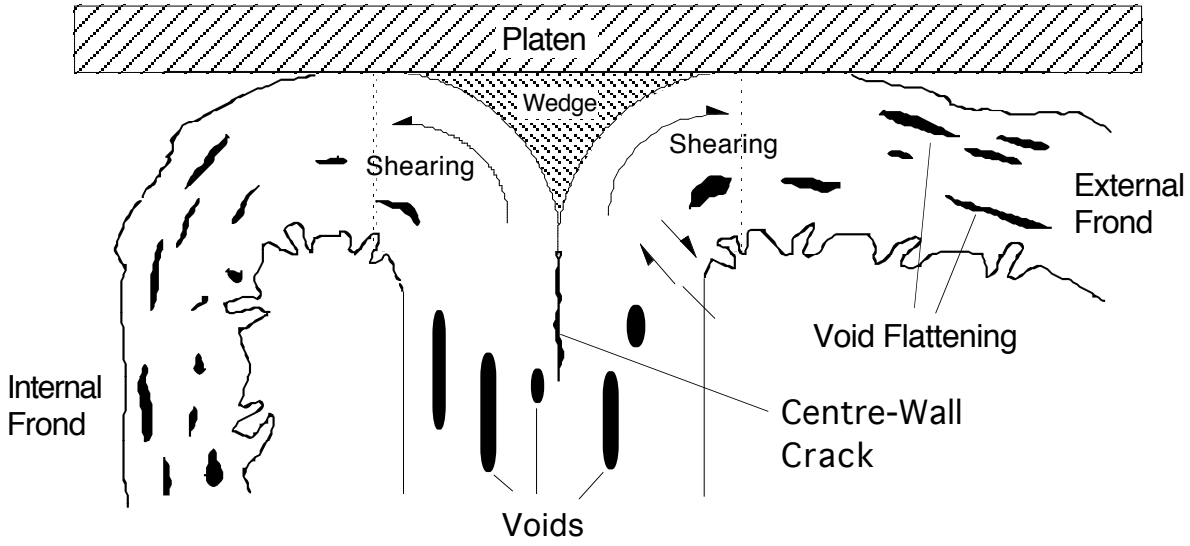

Figure 6.23 Schematic of a section through the crush zone of a Tufnol tube crushed at high temperature.

Figure 6.24 Section through the crush zone of a glass mat-polyester tube crushed at room temperature.

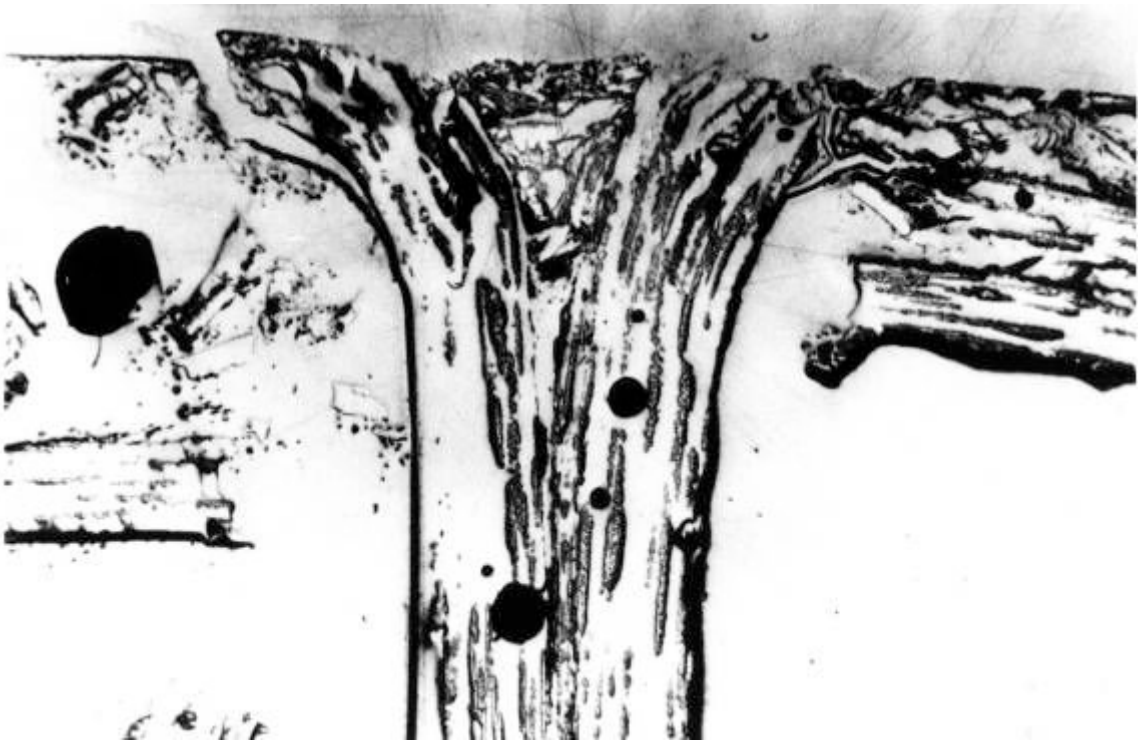

Figure 6.25 Section through the crush zone of a glass mat-polyester tube crushed at room temperature.

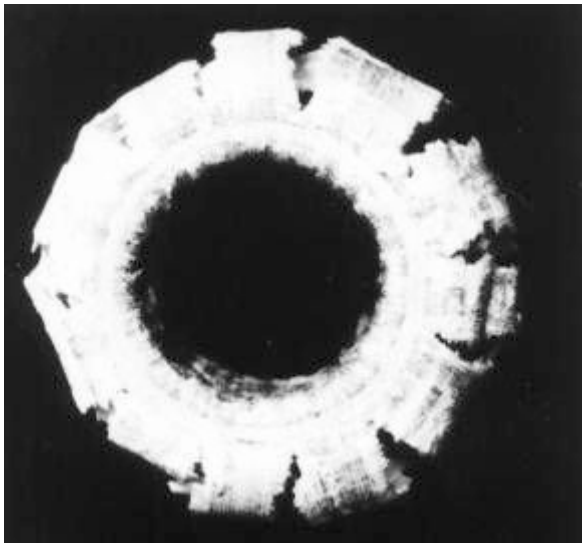

Figure 6.26 Axial macro photograph of the crush zone of a Tufnol tube crushed at room temperature showing eleven fronds.

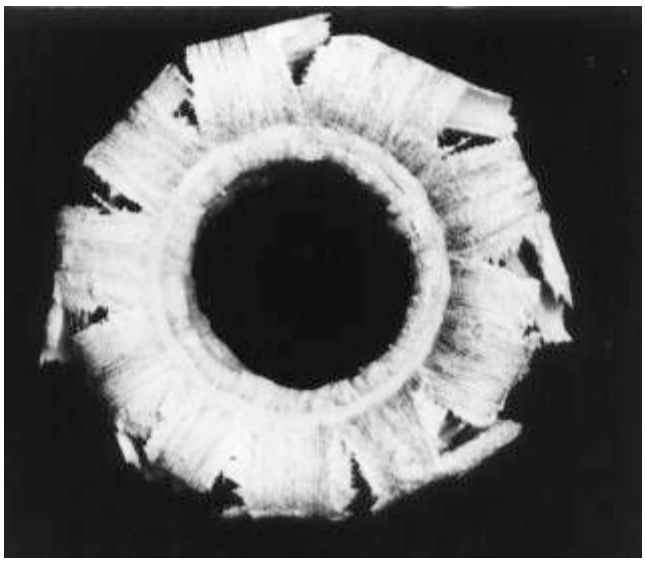

Figure 6.27 Axial macro photograph of the crush zone of a Tufnol tube crushed at 40 °C showing ten fronds.

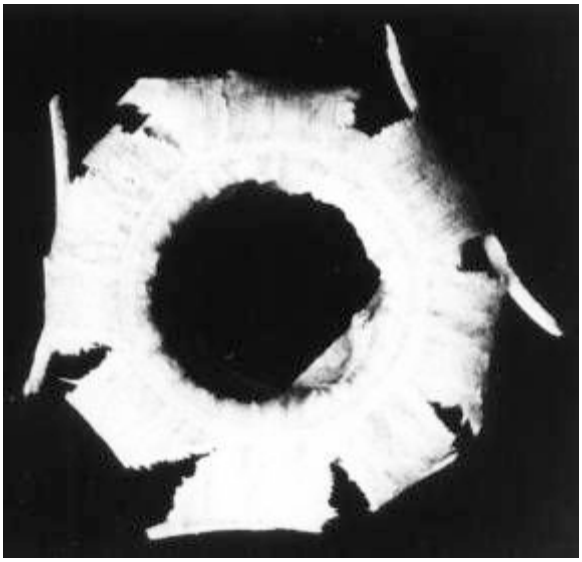

Figure 6.28 Axial macro photograph of the crush zone of a Tufnol tube crushed at 80 °C showing eight fronds.

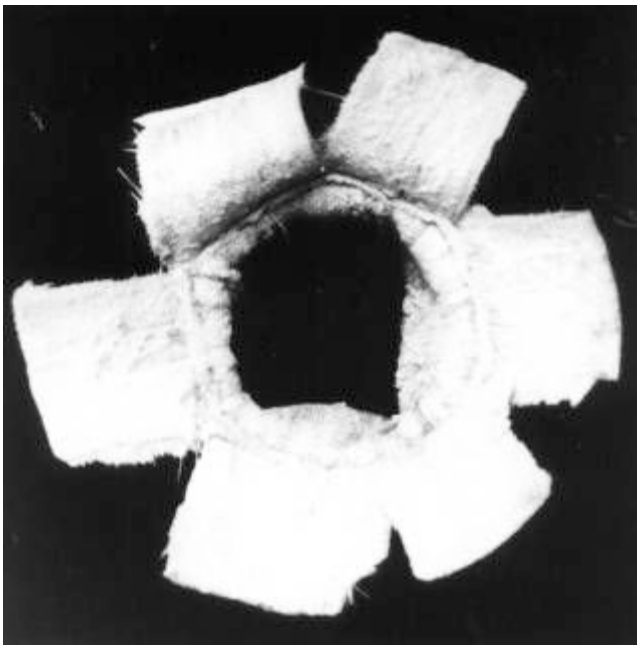

Figure 6.29 Axial macro photograph of the crush zone of a Tufnol tube crushed at 100 °C showing six fronds.

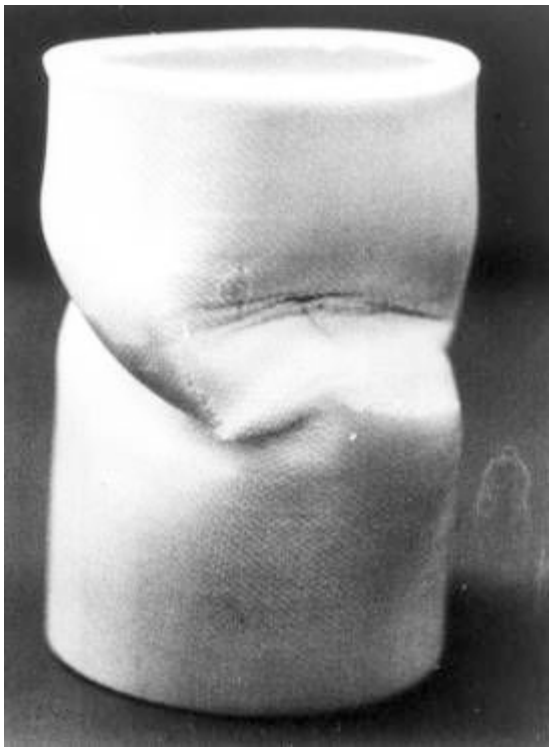

Figure 6.30 Macro photograph of a Tufnol tube crushed at 110 °C showing the buckling mode.

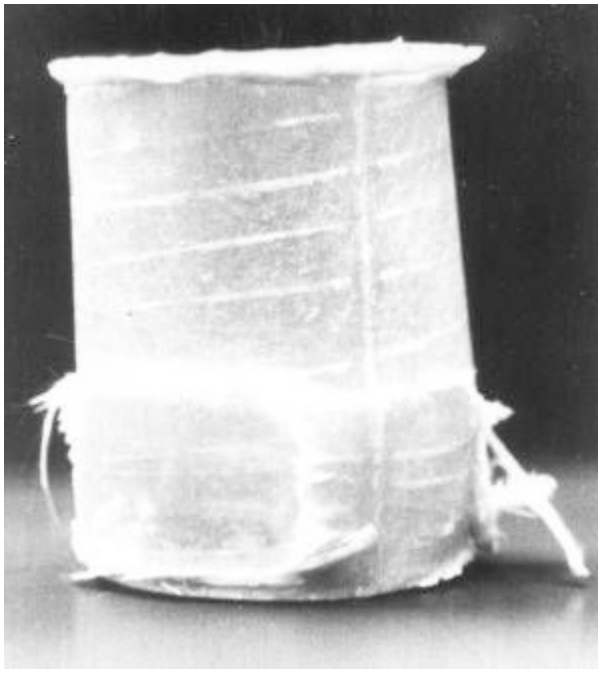

Figure 6.30 Macro photograph of an RJPR tube crushed at 70 °C showing the interpenetration mode.

7 Friction

This chapter is divided into two sections: an analysis of the frictional forces in the crush zone and their effect on the other forces; and temperature rises in the crush zone due to frictional heating.

7.1 Forces Within the Crush Zone

Fairfull [51] identified the various forces that were present in the crush zone of a tube that crushed with a frond-wedge-frond crush mode. This work did not give any magnitudes for the forces apart from the loads supported by the internal and external fronds and the debris wedge. Sufficient information is available from this work, and that published by Fairfull and Hull [63], to enable an estimate to be made of the magnitudes of the various forces within the crush zone. The crush zone forces, as depicted by Fairfull {figure 2.40}, are shown in figure 7.1, with the addition of hoop restraints.

In this analysis, the assumption has been made that the crush zone was quasistatic and that there was no contribution to the forces from the necessity of accelerating material. As the crush zone force measurements were made at a very slow speed (0.33 mm s^{-1}) this assumption was valid.

From this work, P_i was shown to be 13% of the total crush load, P_w 67% and P_e 20%. μ_1 was estimated to be about 0.37, for crushing against a ground steel platen, and μ_2 could be estimated from this work. Observation of crush zone micrographs as in section 6.1.1.1 for room temperature constant speed crushing, showed that, if the

wedge was considered to have had a triangular cross section, then $\theta \approx \phi \approx 33°$[1]. Using these data, the magnitudes of the forces in the crush zone could be estimated.

7.1.1 Force Balance

Resolving horizontally on the wedge:

$$P_1 \cos\theta + \mu_2 P_2 \sin\theta = P_2 \cos\phi + \mu_2 P_1 \sin\phi \qquad (7.1)$$

For $\theta = \phi$, as observed, this was rewritten:

$$(P_1 - P_2) \cos\theta + (P_2 - P_1)\ \mu_2 \sin\theta = 0 \qquad (7.2)$$

which could be solved if $P_1 = P_2$ or $\mu_2 = \cot\theta$. Fairfull [51] concluded that the latter solution was the probable one, but this conclusion must have been incorrect. As the coefficient of friction could vary instantaneously whilst the wedge angle could not, then the latter condition was unlikely, so the probable solution of equation 7.2 was $P_1 = P_2$.

Resolving vertically on the wedge gave:

$$P_1 \sin\theta + \mu_2 P_1 \cos\theta + P_2 \sin\phi + \mu_2 P_2 \cos\phi = P_w \qquad (7.3)$$

For $\theta = \phi$ and $P_1 = P_2$ this was rewritten as:

$$P_w = 2P_1\ (\sin\theta + \mu_2 \cos\theta) \qquad (7.4)$$

Resolving horizontally on the entire crush zone gave:

$$\mu_1 P_i + P_{hi} = \mu_1 P_e + P_{he} \qquad (7.5)$$

which could be rewritten as:

$$P_{he} = P_{hi} + \mu_1 (P_i - P_e) \qquad (7.6)$$

---

[1] This was found to be the mean approximate wedge angle for a large number of observations.

Resolving horizontally on the internal frond:

$$P_{hi} = P_1 \cos\theta - \mu_1 P_i - \mu_2 P_1 \sin\theta \qquad (7.7)$$

which could be rewritten as:

$$P_{hi} = P_1 (\cos\theta - \mu_2 \sin\theta) - \mu_1 P_i \qquad (7.8)$$

From these calculations it was possible to estimate the contribution to the energy absorbed by each of the frictional mechanisms.

7.1.2 Frictional Energy Absorption

Considering a small movement of the crush platen of δx, the energy absorbed by friction at the wedge-frond interface, E_{wf}, was given by the frictional force multiplied by the distance through which that force acted. This distance was given by the resolved distance along the wedge-frond interface of the movement of the platen δx. This was $\delta x \sec\theta$ and $\delta x \sec\phi$, for each side of the wedge, hence E_{wf} was given by:

$$E_{wf} = \mu_2 P_1 \delta x \sec\theta + \mu_2 P_2 \delta x \sec\phi \qquad (7.9)$$

For $P_1 = P_2$ and $\theta = \phi$ equation 7.9 was rewritten:

$$E_{wf} = 2 \mu_2 P_1 \delta x \sec\theta \qquad (7.10)$$

Use of the resolved distance along the wedge-frond interface implied that there was an acceleration of the material relative to the motion of the platen. However, the relative motion was complex so that without knowing the stress system within the crush zone, the distances moved and the relative speeds of all of the material, it was not possible to quantify this effect. It was unlikely that any significant effect occurred at the speeds

under consideration in this part of the work. Material acceleration in the crush zone is discussed later in section 8.2.1.

Fairfull and Hull [63] stated that, for a value of $\mu_1 = 0.37$, the total energy absorption, E_t, was 2.27 times that of the nonfrictional mechanisms E_m. From the figures given, there was an error in this calculation and it should have read 2.5 times. This meant that E_t was given by:

$$E_t = E_f + E_m \tag{7.11}$$

where E_f was the energy absorbed by all frictional mechanisms. As:

$$E_t = 2.5\ E_m \tag{7.12}$$

then:

$$E_f = 1.5\ E_m \tag{7.13}$$

so:

$$E_f = 0.60\ E_t \tag{7.14}$$

From the work carried out by Fairfull and Hull [51,63,108], the external fronds took 20% of the crush load (P_e) and the internal fronds 13% (P_i). If the total crush load was F, then $P_e = 0.2$ F and $P_i = 0.13$ F. Thus the contribution of frond-platen friction, E_{fp}, assuming that the sliding distance was that of the distance of movement of the platen, was given by:

$$E_{fp} = \mu_1 (P_e + P_i)\ \delta x \tag{7.15}$$

then:

$$E_{fp} = \mu_1 (0.2 + 0.13) F \delta x \quad (7.16)$$

so:

$$E_{fp} = \mu_1 0.33 F \delta x \quad (7.17)$$

If, as measured, $\mu_1 = 0.37$ then:

$$E_{fp} = 0.12 F \delta x \quad (7.18)$$

hence:

$$E_{fp} = 0.12 E_t \quad (7.19)$$

Thus frond-platen friction accounted for about 12% of the total energy absorbed. From equation 7.14, the total frictional energy absorption accounted for 60% of the energy absorbed, so the frictional contribution of the other mechanisms, wedge-frond friction and inter-ply sliding, accounted for 48% of the total energy absorbed. From equations 7.4 and 7.10, this proportion was independent of the value of μ_1, provided the crush load distribution and crush zone geometry were unaltered.

Assuming that inter-ply sliding accounted for a negligible amount of frictional energy absorption[1], it was possible to estimate the forces within the crush zone. If friction at the wedge-frond interface accounted for 48% of the total energy, i.e.:

$$E_{wf} = 0.48 E_t \quad (7.20)$$

and the wedge semi-angle was 33° (as observed), then the frictional coefficient at the wedge-frond interface could be calculated.

From equation 7.4, and knowing that the wedge carried 67% of the crush load:

[1]This assumption was reasonable due to the lack of delamination observed in the fronds of these tubes.

$$P_1 = \frac{0.67F}{2(\sin q + m_2 \cos q)} \tag{7.21}$$

From equation 7.20, wedge-frond friction accounted for 48% of the crush load, i.e.

$$E_{wf} = 0.48\ F\ \delta x \tag{7.22}$$

combining this with equation 7.10 gave:

$$2\ \mu_2\ P_1\ \sec\theta = 0.48\ F \tag{7.23}$$

which when rearranged gave:

$$P_1 = \frac{0.24\ F}{\mu_2\ \sec\theta} \tag{7.24}$$

Equating this with equation 7.21 gave:

$$\mu_2\ \sec\theta = 0.716\ (\sin\theta + \mu_2 \cos\theta) \tag{7.25}$$

If $\theta = 33°$ then:

$$\boxed{\mu_2 = 0.66}$$

This was an upper bound value because of the assumption made of inter-ply sliding accounting for a negligible amount of frictional energy absorption. It should be noted that, when applied to equation 7.2, this value of μ_2 would require a wedge angle of greater than 90° for $\mu_2 = \cot\theta$, indicating that the assumption that $P_1 = P_2$ was the correct solution for equation 7.2, although that assumption was used in obtaining this value of μ_2. However, 0.66 is a reasonable value for composite sliding friction [109].

7.1.3 Hoop Restraints

From the above work it was possible to calculate the magnitudes of the hoop restraints in the radial direction, P_{he} and P_{hi}. From equation 7.6, using $P_i = 0.13\ F$, $P_e = 0.2\ F$ and $\mu_1 = 0.37$, as measured:

$$P_{he} = P_{hi} - 0.0259\ F \tag{7.26}$$

From equation 7.8:

$$P_{hi} = P_1\ (\cos\theta - \mu_2 \sin\theta) - 0.37\ P_i \tag{7.27}$$

The value of $\mu_2 = 0.66$ could be used in equation 7.24 to find that:

$$P_1 = 0.305\ F \tag{7.28}$$

as $\theta = 33°$ and $\mu_2 = 0.66$, equation 7.26 became:

$$P_{hi} = 0.146\ F - 0.048\ F \tag{7.29}$$

$$P_{hi} = 0.098\ F \tag{7.30}$$

hence equation 7.26 gave:

$$P_{he} = 0.072\ F \tag{7.31}$$

The relationship between P_{hi} and P_{he} was not in the same proportion as the relationship between the loads on the internal and external fronds as:

$$\frac{P_{hi}}{P_{he}} = 1.36 \tag{7.32}$$

while:

$$\frac{P_e}{P_i} = 1.54 \qquad (7.33)$$

It should be noted that, while the horizontal restraints on the wedge were referred to as hoop restraints, their origin must have included a contribution from rotational moments from the axial loads in the tube wall away from the centre of the wall. Calculation of the ratio of this contribution to the contribution from hoop restraint was outside the scope of this analysis. A possible experimental method of measuring the different contributions would be to use tubes containing flat wall sections. In these sections the restraint will be due to the moments of axial loads only, there being no hoop restraint in this case. However, isolating the effects is potentially very difficult as flat plate sections are known to be very unstable (section 2.1.3.5.6).

7.1.4 Change of μ_1

Fairfull and Hull [63] showed that friction at the frond-platen interface could affect the specific energy absorption that was measured, and that:

$$E_t = \frac{E_m}{1 - (k + \mu_1 c)} \qquad (7.34)$$

where k was the proportion of the total energy absorbed by friction other than at the frond-platen interface and c was the load fraction born by the fronds, given by:

$$c = \frac{(P_i + P_e)}{F} \qquad (7.35)$$

The published figures gave a value for c of 0.33. From equation 7.21, $k = 0.48$[1], so if $\mu_1 = 0.28$, as was reported for rotation against a polished steel platen, from equations

[1] k was derived independently of the value of μ_1. It did however, require the assumption that the crush load distribution was independent of μ_1.

7.11 and 7.34 friction accounted for 57% of the total energy absorbed, hence 57% of the crush load, ie:

$$E'_f = 0.57\, F'\, \delta x \qquad (7.36)$$

where F' was the total load on the crush zone for the lower value of μ_1. In this case $F' = 0.93\, F$. Assumptions made were: that the load distribution across the crush zone and the wedge angle remained the same as for $\mu_1 = 0.37$, and that the energy absorption of the non-frictional mechanisms, E_m, was unaffected by the reduction in frond-platen friction. Thus:

$$E'_{fp} = \mu_1\, 0.33\, F'\, \delta x = 0.0924\, F'\, \delta x \qquad (7.37)$$

Equation 7.28 was derived without reference to μ_1 so: $P'_1 = 0.305\, F'$. From geometry 48% of the total energy absorbed was by wedge-frond friction, thus the total energy absorbed by friction was given by:

$$E'_f = (0.48 + 0.0924)\, F'\, \delta x = 0.57\, F'\, \delta x \qquad (7.38)$$

This value was the same as that obtained from equation 7.36, indicating that the assumption that the crush load distribution was the same as for the case of $\mu_1 = 0.37$ might have been valid. However, the two results obtained for $\mu_1 = 0.28$ were obtained from the same data, albeit through different routes. Both routes assumed that the crush load distribution was independent of the frond-platen friction so any conclusions based on this equality can, at best, be suspect in their validity.

As in section 7.1.3, the hoop restraints were estimated for this situation. From equation 7.28

$$P'_1 = 0.305\, F' \qquad (7.39)$$

Assuming that $\mu_2 = 0.66$ equation 7.27 gave:

$$P'_{hi} = 0.11\,F' \qquad (7.40)$$

hence from equation 7.6:

$$P'_{ho} = 0.09\,F' \qquad (7.41)$$

These were both a higher proportion of the crush load than for the situation with $\mu_1 = 0.37$. This implied that the load distribution in the crush zone was changed by altering the frond-platen friction, hence the assumptions made in this analysis have been invalidated and the hoop restraints probably not as calculated above for $\mu_1 = 0.28$.

7.1.5 Wedge Shape

In this work, the wedge was treated as having been triangular in cross section and described by a wedge angle. Observation has shown that this was, at best, an approximation, as the wedge appeared to consist of a flat top with concave surfaces at the wedge-frond interface, thinning to a point at the apex of the wedge {e.g. figure 6.3}. Thus the above treatment of the wedge must have been inaccurate. However, within the limits of the available experimental data, it was not possible to be any more accurate. The concave surfaces probably led to a non-uniform load distribution at the wedge-frond interface, with a maximum load at the wedge-frond-platen triple point, decreasing as the local wedge angle decreased.

7.1.6 Conclusions of Frictional Forces

This work has shown that friction is an important contributor to energy absorption and that the presence of frond-platen friction means that energy absorption in the crushing of composite tubes is not purely a material property, but is also dependent on the nature of the crush platen. All the above calculations assumed that the non-frictional contribution to crushing remained independent of frond-platen friction. It was shown

that the stress system within the crush zone was changed by altering the frond-platen friction, so this assumption was not entirely valid.

7.2 Temperature Rises in the Crush Zone

As has been discussed in section 7.1, frictional mechanisms accounted for a significant proportion of the energy absorption. It is well known that a large amount of the energy absorbed in a frictional system is dissipated as heat, thus causing localised temperature rises. In the 1930's Bowden and Ridler [110] showed that, for two metals in sliding contact, local interfacial temperatures could reach in excess of 1000 °C, and that the limit to the maximum temperature was the melting point of the lower melting of the two metals. This is the basic principle of the industrial process of friction welding[1] [111].

Temperature rises could be extremely important in the behaviour of composite tubes subjected to axial crushing, as most of the material properties that govern the energy absorption capability of a tube are known to be temperature dependent (see section 2.2). As friction was an important energy absorbing mechanism, the expected associated temperature rises might have been significant in determining the behaviour of the tubes. Thus some insight was required into the magnitude of the temperature rises, and how they varied with the crush speed. The nature of the crushing process meant that experimental measurement of the temperature rises and distribution was difficult, so an analytical modelling approach was adopted to simulate the problem and to predict the behaviour. Some experimental confirmation of the findings was sought by other workers [112].

---

[1] It should be noted that friction welding is essentially a solid state process performed at temperatures close to, but below, the melting points of the metals.

The purpose of this analysis was not so much to predict peak temperatures at the frictional interfaces as to provide an insight into possible temperature distributions within the crush zone, and how these distributions varied with the test variables which were considered, in particular the crush speed. Variation with speed was expected as the fronds underwent heating over a short distance, while flowing past the wedge, so the speed determined the duration of heating, hence the time available for heat to diffuse away from the interface.

7.2.1 Modelling Approach

As discussed in sections 6.1.1.1 and 7.1, the crush zone of these tubes consisted of an annular wedge of fragmented debris, past which flowed fronds of the material from the tube wall {figure 6.5}. From the analysis in section 7.1, it could be calculated that 80% of the frictional energy absorption occurred at the wedge-frond interface; i.e.:

$$E_{wf} = 0.48\, E_t \qquad (7.42)$$

$$E_f = 0.6\, E_t \qquad (7.43)$$

thus:

$$E_{wf} = 0.8\, E_f \qquad (7.44)$$

It was this contribution that was taken as the major source of frictional heating in this model.

Two different treatments were required for the heat dissipation calculations, as the necessary treatment of the conduction of heat through the wedge was different to that for the fronds. During crushing, the wedge remained in a constant position relative to the wedge-frond interface, such that it's temperature rose and heat was conducted away from the heat source and dissipated to the crush platen, which acted as a heat

sink {figure 7.2}. Equilibrium might have been reached in the wedge, and the temperature distribution could be predicted by a process of iteration, employing the concept that, at equilibrium, the heat flowing into any element of material was equal to that flowing out of that element to the surrounding elements. Thus the maximum temperature would be expected to have been found at the furthest distance from the crush platen heat sink, this having been at the apex of the wedge.

The treatment of the heat flow in the fronds was very different from the treatment of the wedge, as the fronds were always in motion relative to the wedge-frond interface. This situation was one of thermal diffusion away from the heat source. The material that formed the fronds was originally situated in the tube wall remote from the crush zone and was thus at ambient temperature. As crushing proceeded, the frond material flowed past the wedge and was subjected to frictional heating over a period of time, equal to that of the time that any element at the wedge-frond interface took to traverse the interfacial distance. In the absence of any other mechanism that might have altered the temperature distribution, the highest temperature was expected to have been found at the element of the frond in contact with both the wedge and the platen, due to that element having undergone the maximum amount of heat input from friction.

While the behaviour of the two constituent parts of the crush zone could be predicted within the assumptions that had to be made, the behaviour of the whole crush zone was somewhat different, the difference being due to the difference in temperature distribution on either side of the wedge-frond interface. If the interface had been a perfect barrier to thermal conduction this would have represented little difficulty. However, as the wedge and fronds were in contact under a high interfacial pressure (about 35 MN m^{-2}), this was not the case and it was probable that the interface

presented no barrier to thermal conduction. The system was thus considered in it's entirety.

The other main effect on heat flow concerned the presence of the crush platen. During the time that the fronds were flowing past the wedge they were remote from the platen but, as they reached the end of the traverse, they came into close proximity with the platen which was able to act as a heat sink, conducting heat away from the fronds. The presence of frond-platen frictional heating was ignored due to the heat sink effect.

7.2.2 Wedge Behaviour

The modelling of the wedge behaviour involved a relaxation method, assuming that the wedge was in thermal equilibrium. In this case, the amount of heat flowing out of the wedge into the platen was equal to that being input to the wedge by friction. This was assumed to have occurred at low speeds, a not unreasonable assumption provided that sufficient crushing had occurred to provide the energy necessary to achieve the temperature rises in the wedge. The assumption of equilibrium was not strictly valid at high crushing speeds, this situation is discussed later in section 7.2.10.

The thermal relaxation in the wedge involved dividing the wedge into a number of elements and using the principle that, at equilibrium, the heat flowing into an element must have been the same as that flowing out of that element. Using square elements this could be written as an equality of temperatures, i.e.:

$$T_{v+1,h} + T_{v-1,h} + T_{v,h+1} + T_{v,h-1} - 4T_{v,h} = 0 \qquad (7.45)$$

where T was the temperature at the position with vertical coordinate v and horizontal coordinate h {figure 7.3} [113]. If equation 7.45 was found at any point not to equate to zero, then the value obtained was referred to as the residual R. This residual represented the deviation from the true equilibrium temperature at that point with

those surrounding temperatures. A better estimate of the true value of $T_{v,h}$ was obtained by adding R/4 to the old value. Once this had been done for all elements, new residuals were calculated and the process repeated. This calculation was continued until the sum of the residuals reached a predetermined value, at which point the improvements in the calculated values by performing further calculation, were less than the desired precision of the temperatures.

This method of calculation presented little difficulty for square elements, but imposed a restriction on the wedge angle 2θ, in that a new mesh was required for every new angle. It was thus desirable to adapt the technique to enable the model to be sufficiently versatile to cope with any desired wedge angle. This was done by dividing the residuals into horizontal and vertical components, R_h and R_v respectively, and adjusting according to the angle. This gave:

$$R_h = (T_{v,h+1} + T_{v,h-1} - 2T_{v,h}) \cot^2\theta \qquad (7.46)$$

$$R_v = (T_{v+1,h} + T_{v-1,h} - 2T_{v,h}) \tan^2\theta \qquad (7.47)$$

Equation 7.45 was modified accordingly to become:

$$(T_{v+1,h} + T_{v-1,h} - 2T_{v,h}) \tan^2\theta +$$

$$(T_{v,h+1} + T_{v,h-1} - 2T_{v,h}) \cot^2\theta = 0 \qquad (7.48)$$

These residuals were then used to calculate the new value of the temperature $T_{v,h(new)}$ as:

$$T_{v,h(new)} = T_{v,h\ (original)} + \frac{(R_v + R_h)}{2\ (\tan^2\theta + \cot^2\theta)} \qquad (7.49)$$

The iterative process was then performed as before. For thermal equilibrium each residual did not necessarily approach zero but the sum of $R_h + R_v$ did, and it was the sum that was used to determine the end of the iterative process.

The treatment of heat input to the wedge at the wedge-frond interface is described in section 7.2.4.

7.2.3 Frond Behaviour

The behaviour of the fronds was modelled by applying the standard linear thermal diffusion equation (7.50) [113] to a set of n bars consisting of a number of elements extending away from the wedge-frond interface, at which point there was a source of heat input due to friction:

$$T_{n,p+1} = Fo\ [\ T_{n+1,p} + T_{n-1,p} + \left(\frac{1}{Fo} - 2\right)\ T_{n,p}\ ] \qquad (7.50)$$

where $T_{n,p}$ was the local temperature at the element x_n at time τ_p {figure 7.4}. Fo was the Fourier number of the system, a dimensionless grouping of the thermal conduction parameters. This was given by:

$$Fo = \frac{\alpha \Delta\tau}{\Delta t^2} \qquad (7.51)$$

where Δt was the linear dimension of an element normal to the direction of heat flow {figure 7.4} [113], $\Delta\tau$ was the time interval considered and α was the thermal diffusivity of the material given by:

$$\alpha = \frac{k}{C_p \rho} \qquad (7.52)$$

where k was the thermal conductivity, C_p the specific heat capacity and ρ the density of the material.

While the actual value of the Fourier number was not in itself important for the modelling, it was required to be less than 0.5 for reasons of conservation of energy [113]. Consequently, the values of Δt and $\Delta\tau$ could not be varied entirely independently. Δt was determined by the desired resolution of the model (see section 7.2.5) so that, according to equation 7.51, the limit on the Fourier number dictated a maximum magnitude of the time element $\Delta\tau$. The values of Δt and $\Delta\tau$ were related by the value of the crushing speed being studied, so that the maximum magnitude of $\Delta\tau$ gave a minimum usable value of v_c due to $\Delta\tau$ being given by:

$$\Delta\tau = \frac{\Delta t}{v_c}\frac{\cos\theta}{\tan\theta} \qquad (7.53)$$

The shape of the bar was taken to be one of constant depth {figure 7.4}. This assumption was not strictly valid as, in the crush zone, the depth decreased as the outside of the wall was approached because of curvature of the material around the wedge-frond interface but the amount of error was insignificant when compared to the difficulties of allowing for this effect .

The assumption was made that there was no heat flow between adjacent bars, this being an assumption that was not strictly valid but was unavoidable for the calculation.

7.2.4 Heat Input

Calculation of the heat flows as outlined in sections 7.2.2 and 7.2.3 was straightforward but the input of heat at the wedge-frond interface presented a more difficult problem. Most worked examples that were available using the thermal diffusion equation [113], involved changing the temperature of one face of a wall and then calculating the temperature profiles as a function of time. This was not an immediately applicable situation, so a method of simulating the heat input needed to

be devised. This was done by calculating what the temperature rise would have been in the first element, over the time interval $\Delta\tau$ for the input of heat from friction at the wedge-frond interface. This temperature rise was denoted by ΔT. The amount of heat flowing into each element at the wedge-frond interface, E_e, was the product of the frictional force at the interface and the distance through which that force acted, being halved to allow for the assumption that half of the heat flowed to the frond and half to the wedge. The frictional force at the interface was the fractional force on each element[1] which was given by:

$$F_f = \frac{\mu_2 P_1}{n} \tag{7.54}$$

The distance moved along the interface was given by:

$$\Delta x = \frac{w}{n} \operatorname{cosec}\theta \tag{7.55}$$

As the energy was the force multiplied by the distance through which that force acted, then combining equations 7.54 and 7.55 with equation 7.4 and halving to allow for the heat distribution to the wedge and frond gave:

$$E_e = \frac{\mu_2 P_w w \operatorname{cosec}\theta}{4 n^2 (\sin\theta + \mu_2 \cos\theta)} \tag{7.56}$$

This assumed that all the frictional energy was dissipated as heat. The assumption that half of the energy flowed into the frond and half into the wedge was probably invalid but unavoidable due to the mathematics of the system. To surmount this problem, the temperature distributions in the wedge and frond would need to have been known, resulting in a problem of circular references in the computer program used in the

[1] Frictional forces are normally independent of the apparent area of contact. However, this was an energy term so that the assumption of the fractional friction force, hence fractional energy, was used.

calculations. Knowing the heat capacity of the element, it was straightforward to calculate ΔT as:

$$\Delta T = \frac{E_e}{C_p V_e \rho} \tag{7.57}$$

where V_e was the volume of an element. The heat in the first element of the frond was given by the total heat input up to that moment, minus the heat conducted away along the bar.

7.2.5 Model Resolution

The size of the elements that were used in the model needed to be determined. Although the choice of element size may be regarded as largely arbitrary, a finer mesh would tend to give more accurate local temperatures, whilst a coarser mesh would simplify calculation. For reasons discussed in section 7.2.3, a coarser mesh enabled slower crushing speeds to be considered. An element size was used that was similar to the thickness of the plies of glass cloth that had been encountered in experimental work. This was because the material for which this model was designed was a glass cloth-epoxy composite. The two constituents had somewhat different thermal conductivities (1 W/m K for glass [113] and 0.1 W/m K for an epoxy resin [40]), so that a finer mesh to improve resolution would have been meaningless. The model was designed to work with a wall thickness of 2.5 mm, consisting of sixteen plies of glass cloth to simulate the Tufnol tubes used in much of the experimental work. Thus the linear dimension of the elements in the fronds was taken to be t/16 {figure 7.4}. The model was however, designed to be usable with other tube wall thicknesses although caution must be employed if used in this way.

7.2.6 Combination of the Wedge and Frond

Once the models had been formulated for the two component parts of the crush zone, it was then required to combine them. The individual models showed very different temperature distributions at the wedge-frond interface, as the maximum temperature found in the frond was near to the frond-platen interface, while that for the wedge was found at it's apex, where the frond temperature was a minimum. If heat was able to flow across the interface, then the temperature distributions would be affected significantly by the presence of the other component. As stated in section 7.2.1, the assumption was made that the interface presented no barrier to thermal conduction. The two models were joined at the interface by incorporating thermal conduction terms in the appropriate equations and adjusting the residual calculations in the wedge accordingly.

For the frond calculations a term was incorporated into the calculation for the first element when in contact with the platen to simulate the heat sink effect. The model was then considered to be sufficiently advanced to provide some insight into what happened in the crush zone.

7.2.7 Variable Values

For the system under consideration there were a large number of variables that had an effect on the final temperature distributions that were calculated. In total there were ten independent variables that were significant. These could be divided into four main sections: material properties, tube geometry, crush zone properties and test variables.

The relevant material properties were the specific heat capacity, thermal conductivity and density. The specific heat capacity of the material was determined using a DSC, as described in section 3.4.4, and found to be about 1300 J/kg K. This value was

consistent with figures given in the literature for a glass-epoxy composite [114]. However, the specific heat capacity of the material was found to decrease with increasing temperature above about 100 °C, as measured on the DSC, although this behaviour was not consistent {see figures 3.13 and 3.14}. For the purpose of this analysis, it was considered to be constant at a mean value. This assumption was required by the limitations of the computer software used. The value of thermal conductivity, k_c, was taken from the literature [114], with a value of about 0.47 W/m K. This figure was largely independent of the temperature. This value was lower than that given by the rule of mixtures for the longitudinal direction of a unidirectional composite (about 0.53 W/m K for a material with a fibre volume fraction of about 48%), and higher than that given by a modified Halpin-Tsai type equation (7.58) [115] for the transverse direction:

$$\frac{k_c}{k_m} = 1 + \frac{1 + v_f}{\left(\frac{1}{k_f - k_m}\right) + \left(\frac{v_m}{k_m}\right)} \qquad (7.58)^1$$

which gave a value for k_c of "0.12 W/m K".

The value of the material density was measured from the Tufnol tubes, being typically 1800 kg m^{-3}.

The tube dimensions were the mean diameter D_m, and the wall thickness t. The mean diameter was given by:

$$D_m = D_i + t \qquad (7.59)^1$$

[1] This version of the Halpin-Tsai equation was taken from the literature. However, it is clearly dimensionally incorrect as the left hand side of the equation is dimensionless while the right hand side, second term, has dimensions of W/m K. Searching for the references given has not clarified where the mistake was so the calculated figure must be ignored.

This diameter was used in all the calculations that required a value for the tube diameter, even though it's universal use was not strictly valid, as the diameter changed with position in the tube wall. However, it's use did not have any seriously deleterious effect on the validity of the final results and considerably simplified calculation. The values of the dimensions used were $t = 2.5$ mm and $D_i = 50$ mm.

The crush zone properties were the wedge angle 2θ, the width of the wedge at the interface with the platen $2w$, the coefficient of friction at the wedge-frond interface μ_2 and the load supported by the wedge alone P_w. The wedge angle was determined from the sections that had been taken through the crush zone and was taken to be 66°. The wedge width was taken to be the same as the wall thickness of 2.5 mm, this being reasonably consistent with observation. The values taken for the coefficient of friction and the load supported by the wedge were based on work carried out by Fairfull and Hull [51,63,108] and the analysis of forces in the crush zone as given in section 7.1. The coefficient of friction was taken to be 0.66. This value might have been speed sensitive [116-118] but no quantitative data was available to make any allowances. The load supported by the wedge was taken to be 30 kN.

The other value that was required for the calculation was the crushing speed which could be varied upwards from 4 mm s^{-1} as discussed in section 7.2.3.

---

[1] This value was different from the value given in the literature review (section 2.1.3.5.2). The difference was due to the heat flow behaviour of the internal and external fronds being considered to be the same in this model.

7.2.8 Summary of Assumptions

In the above description of the frictional temperature modelling many assumptions were made in order to make the model usable. These assumptions are summarised as follows:

1. The force distribution and frictional contributions to energy absorption were as calculated in section 7.1.

2. The platen acted as a perfect heat sink.

3. The wedge was in thermal equilibrium and obeyed equation 7.48.

4. Heat flow in the frond obeyed the thermal diffusion equation 7.50.

5. The wedge-frond interface presented no barrier to thermal conduction.

6. Friction at the frond-platen interface did not contribute to the temperature rises.

7. The thermal diffusivity of the material was not dependent on the temperature.

8. All of the energy absorbed at the wedge-frond interface was dissipated as heat in the crush zone.

9. The wedge was triangular in cross section.

10. The wedge angle was about 66° and the wedge width the same as the tube wall thickness.

11. The interfacial pressure at the wedge-frond interface was constant along it's length.

12. The thermal diffusion bar was of constant depth and did not taper as the outside of the tube was reached.

13. There was no heat transfer between adjacent thermal diffusion bars.

14. The input of heat as described by equation 7.56 was a reasonable representation of the true situation.

15. Frictional heat was initially dissipated equally to the wedge and to the frond.

16. There was no difference between the internal and external frond behaviour.

7.2.9 Use of the Model

The model was used initially to predict the temperature rise distributions at speeds over the range from the lowest possible speed of 4 mm s^{-1}, up to 20 m s^{-1}. The iterations were performed until the sum of the residuals was less than 0.05 °C. All the calculations were performed using a computer spreadsheet package, Microsoft Excel v.1.5, on an Apple Macintosh.

7.2.10 Results from the Model

All the quoted results are temperature rises rather than actual temperatures so they represent the temperatures that the elements experienced above ambient temperature.

Temperature rise distributions in the crush zone are shown for 0.004 m s^{-1} and 20 m s^{-1} in figures 7.5 and 7.6. These figures show clearly the difference in distribution for high and low speed, as at high speed the temperature rises were only significant in the frond close to the wedge-frond interface, while the low speed temperature rises were significant away from the interface.

Five different quantities were identified as being typical of the behaviour of the heat flows as functions of the crush speed. These were: the mean overall temperature rise; the mean temperature rise in the frond; the mean temperature rise in a layer of the frond after it had fully traversed the wedge-frond interface; the maximum temperature recorded and the mean temperature rise in the wedge. Each of these quantities are shown as a function of the log. crush speed in figures 7.7 to 7.11. For all the quantities, the increase in the predicted temperature with speed was rapid at low speeds, but at high speeds they were relatively speed insensitive.

Third order polynomials were found to be a good fit to all of the curves in figures 7.7 to 7.11 over the speed range investigated, although the fit at speeds above about 20 m s^{-1} was poor. Extrapolation of the curves to low speeds gave a value of speed where the temperature rise was predicted to be zero. However, it was unlikely that this situation could have occurred as it would have implied that there were no temperature gradients, thus there would have been nothing to drive the heat transfer and the model would not have represented the true situation. It was probable that, at low speeds, below those that the model could simulate, the temperature rises levelled off. Unfortunately the limits of the model did not allow this hypothesis to be verified but the lack of a fit at high speeds indicated that the extrapolation was not valid. The behaviour of the maximum temperature measured may indicate what would be expected at lower speeds {figure 7.11}. The element where the maximum temperature was found was not always the same, as high speeds gave the maximum temperature rise in the frond element that was in contact with the platen and the wedge-frond interface. Slower speeds gave the maximum temperature as being in the frond element at the wedge-frond interface immediately before the one in contact with the platen. Thus the element of maximum temperature moved down the wedge-frond interface

away from the platen with decreasing crush speed. The position of maximum temperature probably tended to a limit somewhere on the wedge-frond interface due to the difference in behaviour of the wedge and the frond as stated in section 7.2.6.

Further support for the hypothesis that extrapolation to zero temperature rises at low speeds was not valid, can be drawn from the intercepts that were calculated. For the frond mean temperature the intercept at zero temperature rise was at about $0.005\ \text{mm s}^{-1}$ while that for the wedge temperature was at about $0.5\ \text{mm s}^{-1}$. If the extrapolations were valid, then these speeds would be expected to have been the same, rather than two orders of magnitude different. Also, if one temperature rise is plotted against another, then they would be expected to give a good linear agreement with the intercept at 0 °C. While good linear agreements were found in all cases, in none of the permutations did the intercept happen at 0 °C, indicating that any extrapolation to low temperatures must have been invalid. An example of such a plot is given in figure 7.12. Thus the curve fits can only be regarded as having been valid over the speed range for which the calculations were performed, hence there was little benefit to be gained from curve fitting, so they have not been shown in figures 7.7 to 7.11.

As was stated in section 7.2.2, the assumption was made that the wedge was in thermal equilibrium. This assumption was not strictly valid for the higher speeds examined. However, the observation that the speed sensitivity of the temperature distribution decreased with increasing speed may lead to the conclusion that this was an assumption that would not be expected to cause serious deviations from the true state for the temperature distribution in the fronds.

7.2.11 Comparison with Experimental Work

The results obtained from the model have been compared to those measured by experiment. Copolla [112] crushed Tufnol tubes against a platen made from the same glass cloth-epoxy material with a thermocouple imbedded in it. The thermocouple was situated close to the surface of the platen and the tube positioned such that the thermocouple would be near to the frond-wedge-platen triple point, thus the position of greatest predicted temperature rise. Two speeds were examined, being 0.05 mm s^{-1} and the slowest speed that the model could calculate, 4 mm s^{-1}. The 4 mm s^{-1} crush gave a dramatic temperature rise of the order of 120 °C, which was reasonably consistent with the model's prediction of about 100 °C for the frond element in closest contact with the platen. The 0.05 mm s^{-1} crush showed a temperature rise of about 20 °C, this temperature rise reaching an equilibrium level. While it was not possible to compare this directly with a predicted temperature, this low temperature increase was consistent with the observation that bulk temperature rises were considerably lower at slow speeds than at high speeds, as were the peak temperature rises that were predicted.

While this work indicated the validity of the model, the test conditions were not the same as those for which the model was designed. The most significant variation was in the nature of the crush platen. One assumption made in the model, that the platen acted as a good heat sink, was not valid for the tests. The effect of the change in crush platen material will have been to increase the temperatures in the crush zone, this being due to the removal of the heat sink effect. However, these tests did indicate that the temperature rises that were calculated were within the right ballpark, so that it was

probable that the temperature distributions predicted were reasonably consistent with what actually happened in the crush zone.

7.2.12 Consequences

With all the models calculated high local increases in temperature were encountered. These local temperatures could have resulted in some degree of degradation of the polymer matrix which would be consistent with the observation of solvent aromas in the vicinity of a tube immediately after impact testing and with the observation of steam rising from the crush zones of tubes crushed at speed, after they had been subjected to a moisture uptake programme [119]. The speeds for which the model was best suited were however, somewhat lower than the impact speeds used in testing, because of the equilibrium assumption in the wedge. However, the bulk temperature of the wedge was of little importance in determining the energy absorption level as, once established, the wedge did not undergo any significant deformation or fracture. The only consequence of the wedge temperature rise was in the effect it had on the temperature rises within the fronds.

What could be considered to have been of greater importance were the temperature rises in the outer plies of the fronds. This was due to the outer frond elements having undergone greater deformations during crushing than those near to the wedge. A rise in temperature, which will have resulted in a lowering of the strength and stiffness of the material (section 2.2), might have had a deleterious effect on the crush performance and the stability of the crush zone. Consequently, lower crush speeds, which allowed the dissipation of heat to the outer plies, might have been expected to have given lower values of crush stress. This effect would have been in addition to the

viscoelastic effects of the polymer matrix. This is discussed further with regard to the observed crush zones, in section 8.4.

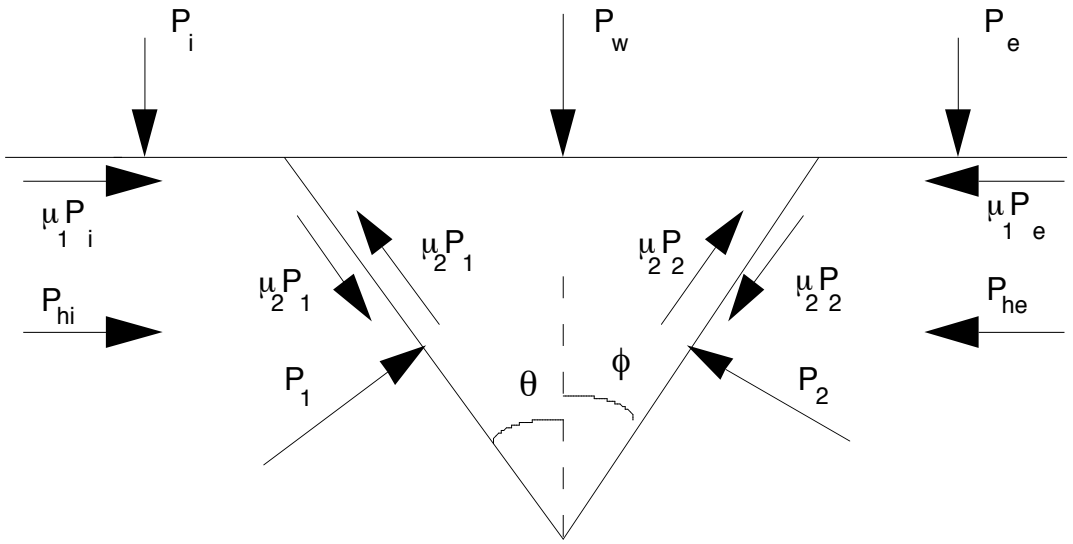

Figure 7.1 Schematic of the forces present in the crush zone of a glass cloth-epoxy tube with t/D of about 0.05. P_i was the load carried by the internal fronds, P_e was the load carried by the external fronds, P_w was the load carried by the debris wedge, $P_{hi,ho}$ are the internal and external hoop restraints, μ_1 was the coefficient of friction between the fronds and the platen and μ_2 was the coefficient of friction between the fronds and the debris wedge. Note: P_1 and P_2 are not shown in the wedge.

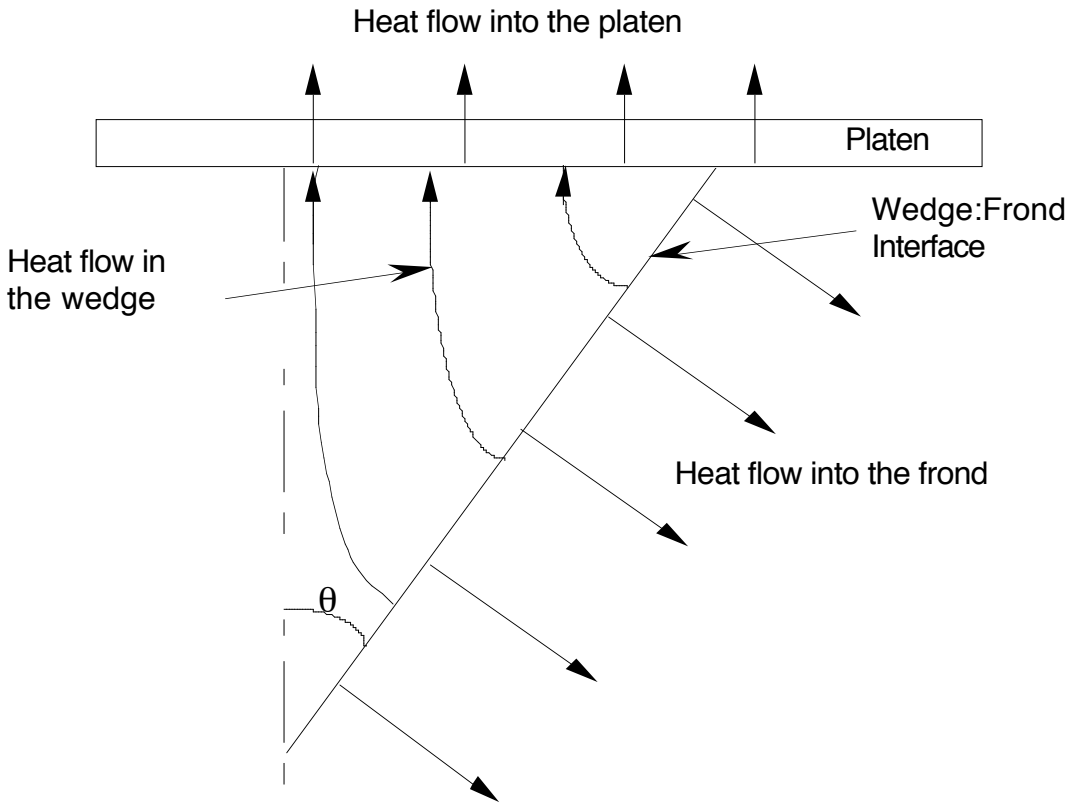

Figure 7.2 Direction of heat flows in the crush zone (schematic).

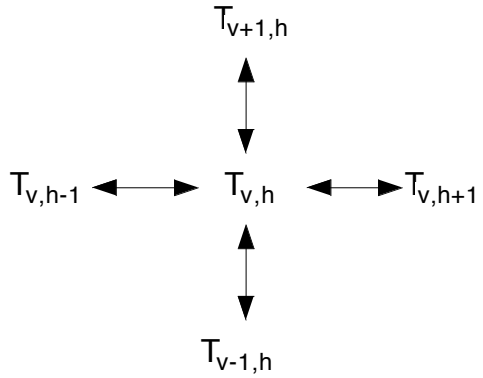

Figure 7.3 Nomenclature of elements in the wedge.

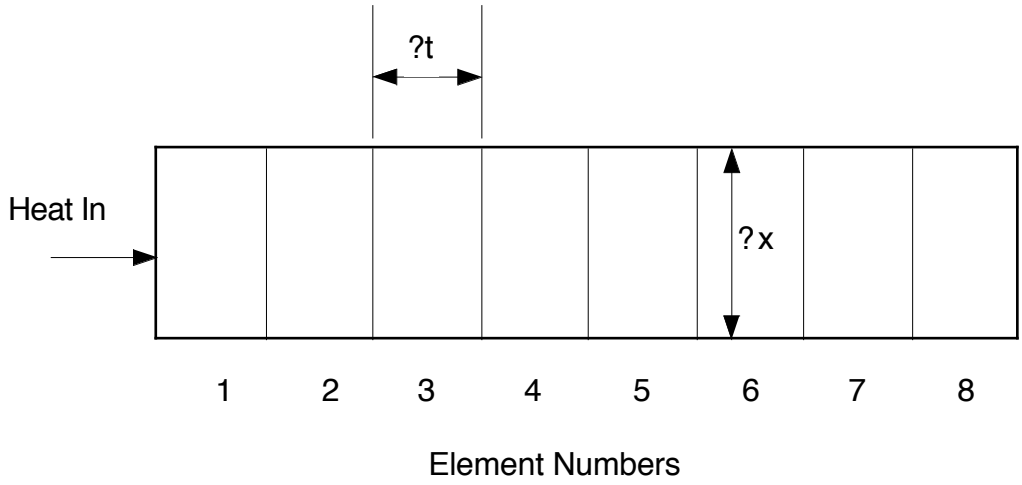

Figure 7.4 Heat flow elements in the fronds.

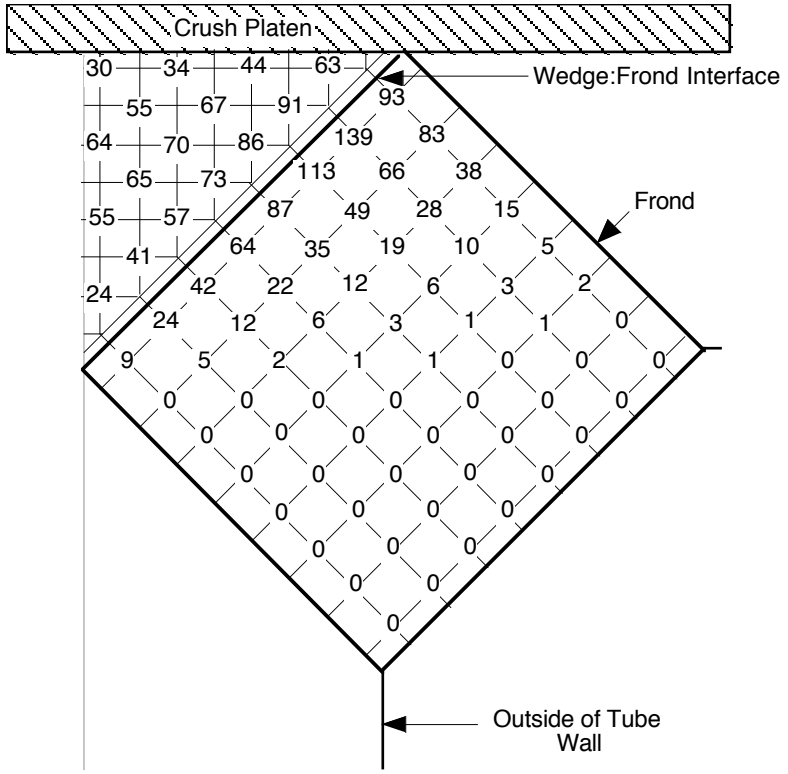

Figure 7.5 Schematic of the predicted temperature distribution in the crush zone for a crush speed of 0.004 m s^{-1}.

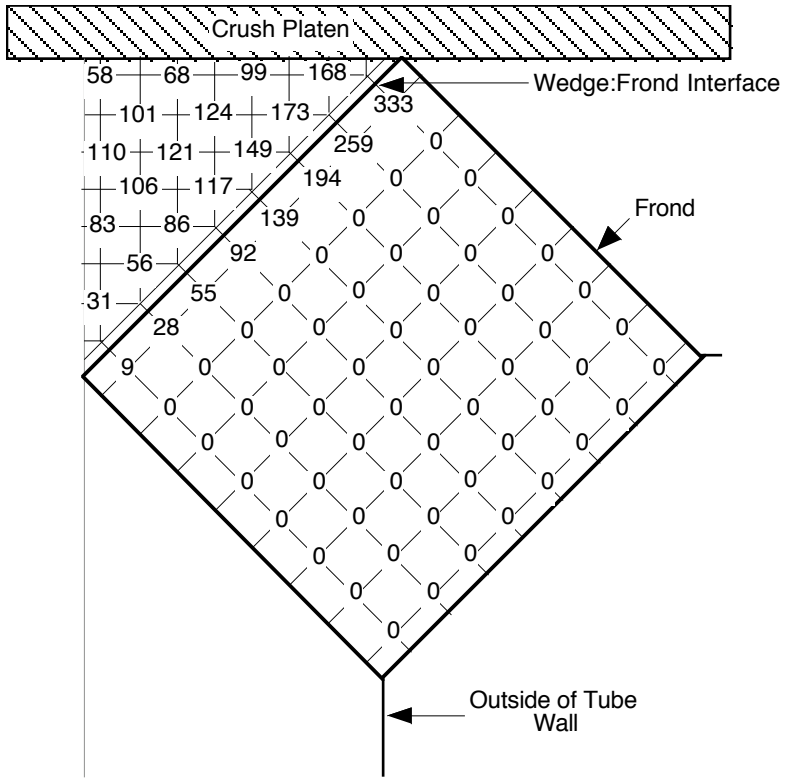

Figure 7.6 Schematic of the predicted temperature distribution in the crush zone for a crush speed of 20 m s^{-1}.

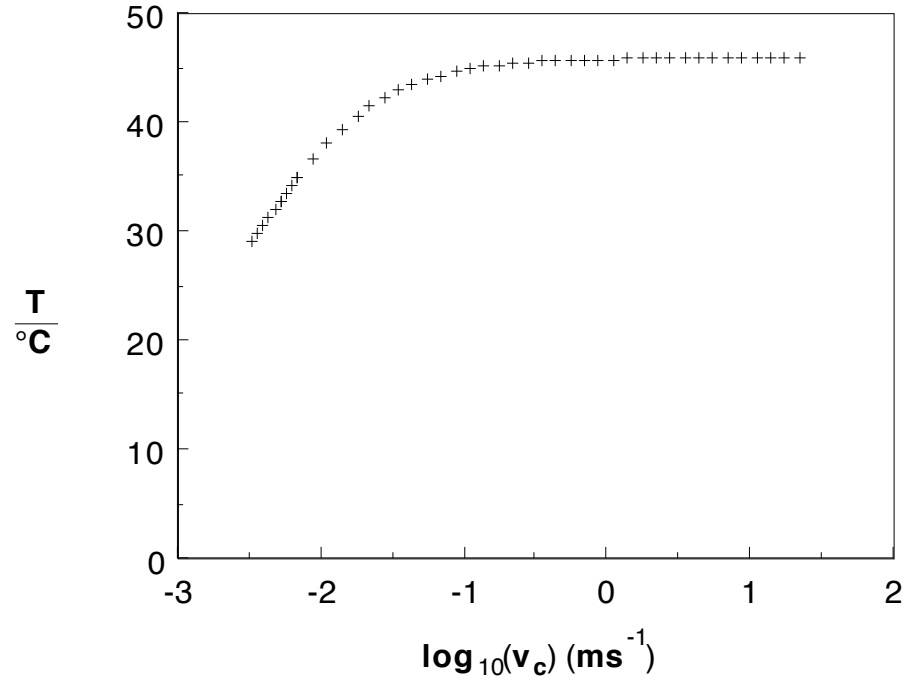

Figure 7.7 Plot of the calculated mean temperature rise of the entire crush zone as a function of the log. crush speed.

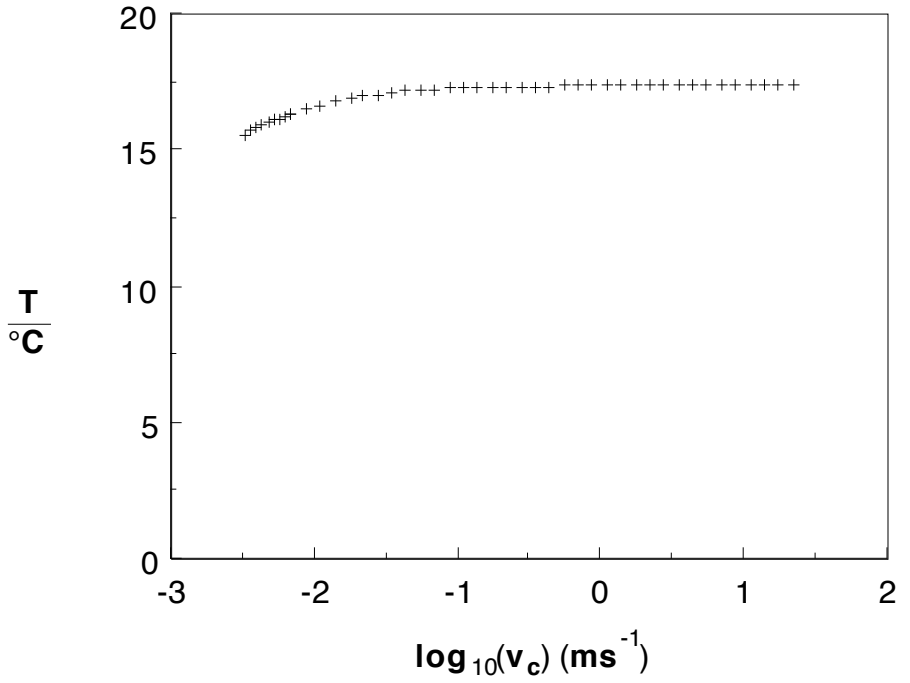

Figure 7.8 Plot of the mean temperature rise in the frond as a function of the log. crush speed.

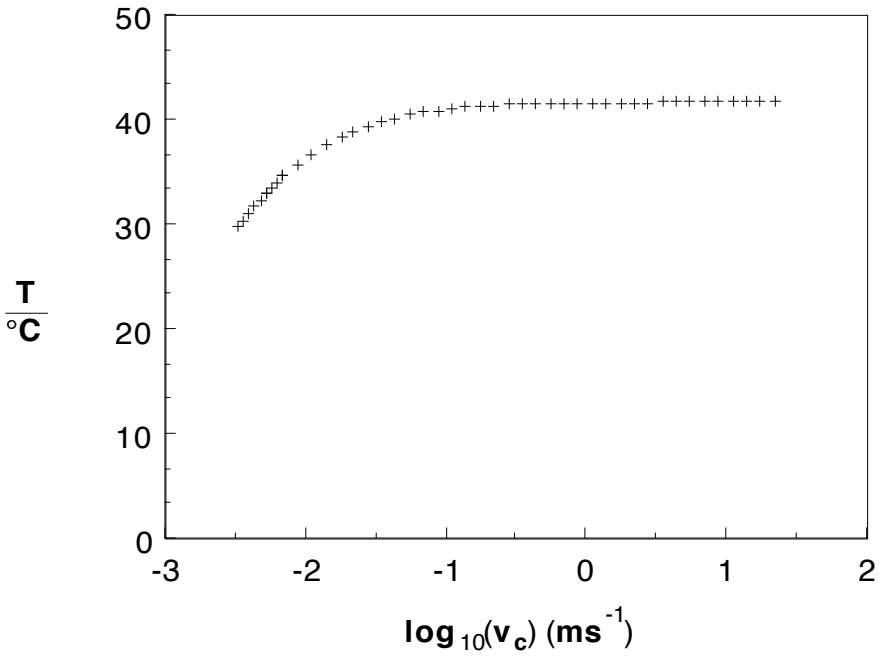

Figure 7.9 Plot of the temperature rise in a layer of the frond after fully traversing the wedge-frond interface, as a function of the log. crush speed.

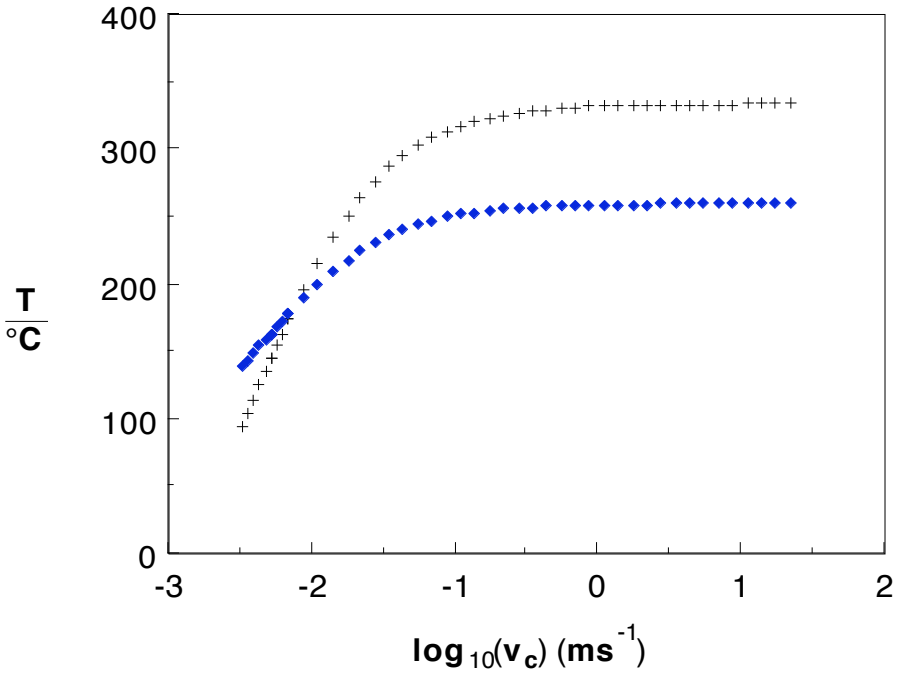

Figure 7.10 Plot of the calculated temperature rises for the two elements at the wedge-frond interface that were + closest to the platen and → one removed from the platen, as a function of the log. crush speed. These were the maximum temperature rises calculated.

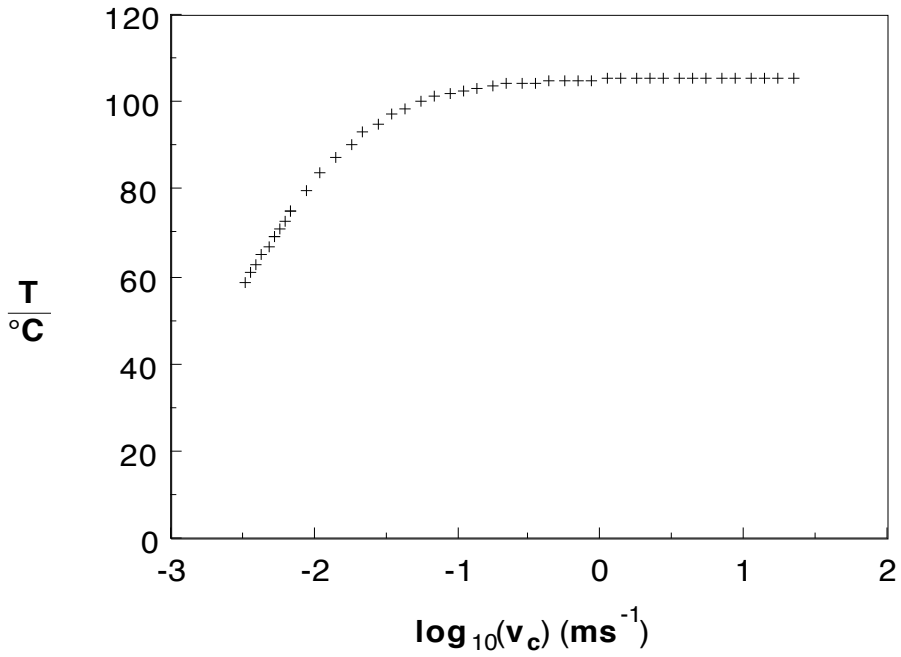

Figure 7.11 Plot of the mean temperature rise in the wedge as a function of the log. crush speed.

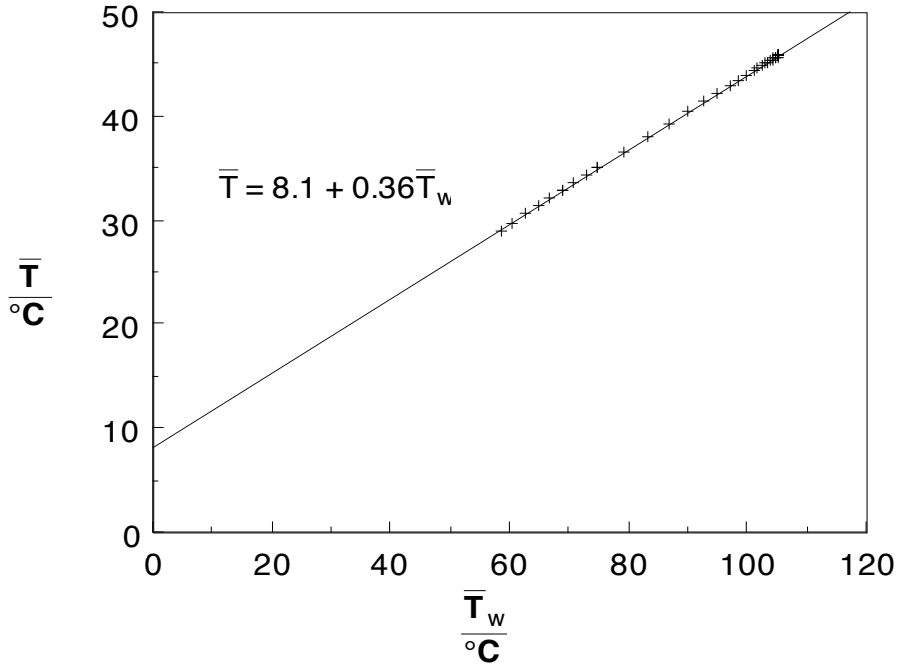

Figure 7.12 Plot of the mean temperature rise in the entire crush zone against the mean temperature rise in the wedge alone, showing that zero temperature rise in one quantity does not correspond to zero temperature rise in the other.

8 Discussion

This chapter has been divided into six main sections. The first section deals with the types of crush test that have been used in this work, the second with speed effects at room temperature in each of the types of tube, the third with the interrelation between the crush speed and the testing temperature, the fourth with the crush mode, the fifth with the effect of residual stresses and the sixth with the effect of tube length on the magnitude of serration of the crush load response.

8.1 Crush Tests

Three types of crush tests were employed in this project. These were: constant speed crushing, constant speed crushing with an instantaneous speed change and impact tests. Little comment is required for the constant speed tests, but the other two types of test differed significantly from them and need explanation.

8.1.1 Instantaneous Speed Change Tests

Many of the data used to calculate the values of speed sensitivity, as given in chapters 4 and 5, were from the series of experiments where the tube was crushed incorporating an instantaneous speed change (see section 3.2.1.1.1).

8.1.1.1 Assumptions

Two major assumptions were made in using these test results for the calculations in Chapter 5; firstly, that the specific crush stress of the tube was independent of whether the speed change was from fast to slow or vice versa, and secondly, that the specific crush stress varied linearly with the logarithm of the crush speed.

The first assumption implied that the crush zone morphology was unaffected by the crush history of the tube, thus the speed sensitivity of the specific crush stress was due

to simple changes in the actual material properties rather than changes in the crush zone morphology. This assumption was not strictly valid, as changes in material properties would be expected to give changes in the crush zone morphology. However, examination of the crush traces obtained from these tests showed that, after the change in speed, the crush load took a short distance, typically 2-3 mm (see also section 8.4.3.1), to equilibriate before a constant mean crush load was reached {figures 4.58 to 4.64}. This observation indicated that there had been a change of crush mode related to the change in speed, and that the initial speed crush zone must have been cleared at the second speed, before the equilibrium crush zone for that speed was established. These observations were further confirmed by the measurements of the crush load, as the equilibrium crush load was independent of whether it was measured before or after a speed change. Thus the first assumption may be considered valid. Changes in the crush mode are discussed later in section 8.4.

The second assumption, that the specific crush stress varied linearly with the logarithm of the crush speed, can be validated by considering the response of the series of tests performed over a wide range of speeds, with each tube crushed at a single speed {e.g. figure 4.1}. Within the degree of scatter in the results, the fit of a straight line to each of the data sets was good, meaning that this assumption was reasonable.

8.1.1.2 Features of the Load Response

A regularly observed feature of the instantaneous speed change tests when the speed change was from slow to fast was a peak load, after which the crush load fell to the equilibrium level {figures 4.59, 4.61 and 4.63}. This peak load was also observed in the impact tests that were performed after the crush zone was established (see section

8.1.2.3). This feature was probably due to the difference between static and dynamic friction within the crush zone, and was analogous to an activation energy that needed to be overcome in order for fast crushing to proceed.

When the speed change was from fast to slow, a sharp drop in the measured load was frequently observed. However, this load drop was accompanied by a reverse movement of the signal from the displacement transducer which was recovered on further crushing, indicating that the load drop was due to a testing machine response rather than a material response and may be disregarded for the purposes of this investigation {figures 4.58, 4.62 and 4.64}.

8.1.2 Impact Tests

While the majority of crush testing performed in this project was carried out at constant speed, some high speed impact tests were performed on the crash rig as described in section 3.2.1.2. The tests performed on the crash rig differed in nature from constant speed crushing, as the speed decreased during the test, from the impact velocity to zero at the end of crushing {figure 8.1}. The change in speed might have affected the crush load and requires consideration.

8.1.2.1 Load Response

The work on instantaneous speed changes for constant speed crushing showed that, on changing the crush speed, the crush load took a short distance to reach a stable equilibrium value of the mean crush load (section 8.1.1). It was deduced that this feature of the crush load was due to the clearing of the initial speed crush zone and the establishment of the equilibrium crush zone for the second speed. A similar situation may be deemed to have occurred during the impact tests. During the impact crush the equilibrium crush zone for the speed at any moment will have been trailing the actual

crush zone as the crush zone was established at the start of crushing, that is for the highest speed of crush for the test. The crush zone will have been constantly changing to try to reach the equilibrium crush zone for the speed at that moment, so the crush zone at any point in time will have been for a higher speed than the actual speed at that moment. Direct evidence for this phenomenon is difficult to find, but the statistical test that was carried out in section 4.2.1 for Tufnol tubes, comparing the crush load measured from the initial impact, with those from the subsequent impacts, might lend some credence to this hypothesis. The initial impact on each tube was performed with a chamfered end, so the crush zone that was set up was one for a high speed. At the end of the initial impact crush, the crush zone will have changed to one for a lower speed, thus a lower crush load as observed for constant speed crushing for these tubes {figure 4.1}. Subsequent impacts on the tubes were commenced with the crush zone already established, being the crush zone from the end of the previous test, thus one for a speed lower than the impact velocity. Due to the lag in the crush zone as observed for instantaneous speed changes (section 8.1.1), the crush zone cannot have reached the form for the impact speed, consequently the crush load was less than for the initial impact. However, this behaviour was not observed for glass mat-polyester tubes although this might have been due to a greater degree of scatter in the results. Trends with respect to speed were different for the glass mat-polyester tubes from those for the Tufnol tubes so this might have masked any crush zone lag effect.

The observation of lower crush loads for subsequent impacts might have been due to micro-damage in the tube ahead of the crush zone. However, this would be expected to give a similar result for the glass mat-polyester tubes, particularly as polyester resins tend to be more brittle than epoxies [74], hence more sensitive to micro-damage. Micro-damage might also have given a decreasing crush load with the accumulated

number of impacts on the tube as damage accumulated. No such decrease was observed. These observations do not eliminate this possibility and some future work in this area might be beneficial.

8.1.2.2 Load Trace Serration

All the impact force-time traces showed a degree of serration, comparable to that observed for constant speed crushing {figures 1.5 and 3.8 (a)}. With the impact tests however, the serration might have been due to ringing in the load cell or in the test piece. Initial observation of the crush traces was inconclusive as to whether the frequency of the serrations remained constant throughout the crush, or decreased as the speed decreased. If the former case were true, the serrations were probably due to ringing in the load cell, whilst the latter case would suggest their being due to a specimen response. When the frequency of the serrations in the crush trace was measured, a figure of 3 kHz was obtained. This figure was compared to the natural frequency of the load cell, as found by striking the crush platen with a copper mallet, of about 20 kHz. The use of a protective steel plate on the load cell reduced the natural frequency to 8 kHz without affecting the crush load response. As this figure was found to be much higher than the frequency of serration in the crush traces, the serrations cannot have been due to ringing in the load cell.

The possibility of the serrations being due to ringing in the sample can be disregarded, as the frequency was found to be independent of the tube length, thus independent of the expected natural frequency of the tube.

8.1.2.3 Initial Peak Load

The other notable feature of most of the impact traces was an initial load peak observed for all impacts performed after the crush zone had been established in a previous test {figure 3.8 (a)}. The load peak was similar to that obtained in the instantaneous speed change tests with the speed change from slow to fast {e.g. figure 4.61} and probably had the same origin in the difference between static and dynamic friction (section 8.1.1.2). The size of the peak was related to the impact velocity as shown in figure 4.3, a plot of the normalised peak height as a function of the impact velocity. If the peak load was due to the difference between static and dynamic friction, figure 4.3 should extrapolate to unity at $v_i = 0$. However, the value of F was known to be speed dependent, from the results presented in figure 4.2[1], so this extrapolation might be invalid. When the extrapolation was carried out on these data, the value of F_i/F did not extrapolate to unity, implying that the conclusion concerning the origin of the peak load might have been incorrect. However, the level of scatter in these data was high, hence conclusions difficult.

8.1.2.4 Impact Force-Time Traces

The traces obtained from the impact tests were force-time traces rather than the force-displacement traces that were obtained from constant speed crushing. Force-velocity traces would have been more use in determining speed related effects, but it was not possible to obtain these with the instrumentation available. However, the force-time traces that were obtained approximated to force-velocity traces. This was due to the crush load approximating to a square wave. As the area under the force-time trace was

[1] This figure was for specific crush stress which was directly related to F as the tubes were all of the same dimensions.

a measure of the momentum of the sled on impact; at any time in the crush, the area under the force-time trace up to that moment represented the momentum that had been "absorbed" by the crushed tube. As momentum scales linearly with velocity, a square wave force-time response will give a linear decrease in velocity with time {figure 8.1}. Thus the force-time traces that were obtained could be approximated to force-velocity traces. It should be possible to integrate the force-time trace on a computer to give an accurate force-velocity response, but it is unlikely that this would give any further insight into crushing under impact conditions.

8.1.2.5 Displacement:Time Traces

Examination of the displacement:time traces, that were used to obtain the impact velocities, showed a reversal of the displacement after the crushing had finished {figure 3.8 (b)}. This feature of the test was due to the sled bouncing back after the energy of the impact had been absorbed. This bounce-back was observed in high speed cinematography of impact tests. It was possible to determine the bounce-back velocity of the sled from the gradient of the displacement-time trace and to relate this to the force-time trace obtained for that tube. The bounce-back was due to elastic unloading of the tube after crushing. By performing a momentum balance on the crush trace, it was possible to determine the point on the force-time trace that corresponded to zero crush velocity. On figure 8.2, a schematic of a typical force-time trace for a glass mat-polyester tube, the point of zero velocity was found to be at point N.

The bounce-back velocity was expected to have been a function of the length of the tube at the end of the impact crush, due to the stored elastic strain energy in the tube increasing linearly with increasing tube length. On relief of the crush load, this energy

was converted to kinetic energy of the sled, so the more strain energy that was released, the higher was the bounce-back velocity. As kinetic energy is proportional to the square of the velocity, the bounce back velocity was expected to be proportional to the square root of the tube length. The degree of error in the measurements for the bounce-back velocity and changes in the bungee pre-tension, meant that this effect could not be shown from the data collected.

The aforementioned high speed cinematography of the tests was unable to offer any insight into the high speed crushing process apart from showing the bounce back of the sled. It has not been described here because it did not form part of this project and was performed before the commencement of the project, by other workers.

8.2 Speed Effects

Figures 4.1 to 4.11 show the room temperature speed sensitivities of the various tubes tested in this investigation. Speed effects in the properties of polymers and polymer composites, are generally related to the viscoelastic response of the material (section 2.2). However, in the case of tube crushing, frictional temperature rises have been shown to be present as an additional speed related effect (section 7.2). One other non viscoelastic contribution to speed effects has been identified, namely inertia of debris.

8.2.1 Inertial Effects

During tube crushing, there was a significant flow of material in various directions away from the crush zone. At high speeds this debris must have been accelerated from rest, relative to the tube, to the velocity of motion away from the crush zone, requiring an accelerating force according to Newtonian physics. This force will have resulted in an increase in the crush load, so it is important to estimate the magnitude of this force and to know whether it is of significance.

Considering the case of constant speed crushing at a velocity v_c, assuming that the inertial effects from the internal debris were the same as those from the external debris, and that the debris moved away from the crush zone at v_c normal to the tube axis (due to conservation of matter), the momentum of the debris could be calculated. Considering an element of tube length δx from a tube with a mass per unit length m/l. The mass, M_e, of the element was:

$$M_e = \frac{m\ \delta x}{l} \tag{8.1}$$

then the mass of the external debris of this length, M_d, was:

$$M_d = \frac{m\ \delta x}{2l} \tag{8.2}$$

The distance over which acceleration, a_d, took place was δx, due to conservation of matter, so the inertial force, F_{in}, was:

$$F_{in} = M_d\ a_d \tag{8.3}$$

using:

$$v_c = u_c + a_d t \tag{8.4}$$

and:

$$x = u_c t + \frac{1}{2}\ a_d\ t^2 \tag{8.5}$$

where $u_c = 0$ gave:

$$a_d = \frac{1}{2}\ \frac{v_c^2}{x} \tag{8.6}$$

combining equations 8.2, 8.3 and 8.6 gave:

$$F_{in} = \frac{m\, v_c^2}{4\, l} \qquad (8.7)$$

For the case of a 20 m s^{-1} crush of a tube with a mass per unit length of 0.8 kg m^{-1}, for instance a Tufnol tube impact tested on the crash rig, a force of 80 N was calculated for the external fronds, or 160 N for both the internal and external fronds combined. As crush loads for these tubes were typically of the order of 50 kN, 160 N was not significant as it was within the error of experimental measurement and less than the observed scatter in the results.

From equation 8.7, the inertial force increased with the square of the crush speed. Thus at higher speeds this force could become significant. Rearranging equation 8.7 gave:

$$v_c = \sqrt{\frac{4F_{in}l}{m}} \qquad (8.8)$$

Setting a significance level at an arbitrary 1 kN[1], from equation 8.8 a speed of about 70 m s^{-1} must be exceeded for this force to become significant. This is shown in figure 8.3. 70 m s^{-1} is considerably above the speed range that was investigated in this project and can be disregarded.

In section 7.1.2 local acceleration of material within the crush zone was mentioned. This acceleration was essential to allow the flow of material to occur past the wedge, acceleration being positive close to the wedge-frond interface and negative close to the outside of the tube wall. The relative distances involved were small and any

[1] 1 kN is approximately the error of measuring the crush load from a typical crush trace with no serration.

effects due to this phenomenon can be disregarded for tests within the speed range considered in this project.

8.2.2 Epoxy Matrix Tubes

All of the tubes used in this project that incorporated epoxy resins as the matrix showed increases in specific crush stress with increasing crush or impact speed {figures 4.1, 4.2, 4.9 to 4.11}. This behaviour was consistent with that observed by other workers [17,60]. The increases reflected increases in the strength and fracture toughness of the material as discussed in section 2.2 and observed in the bend tests that were carried out in this project {figures 4.68 to 4.70}.

The majority of the changes in specific crush stress could be related to simple changes in the mechanical properties, as there were no observed systematic change in the crush zone morphology, although this is discussed further in section 8.4.3[1]. In the case of constant speed crush tests, a good straight line fit was found for the specific crush stress with increasing speed on a logarithmic scale. This behaviour was consistent with the linear increases in yield strength and Young's modulus that have been observed for epoxy resins (see section 2.2.1.1.1).

That the specific crush stress increased linearly with the logarithm of the speed did not mean that the speed sensitivity was due to viscoelastic responses without any contribution from frictional heating (section 7.2). It was not known what the response would have been if there had been no heating, nor was it known what the effect of the heating would have been without any speed dependent response of the matrix, so it

[1] Apart from a greater degree of fracture at high speeds. However, this has not been quantified.

was not possible to be any more definite, although this is discussed further in section 8.4.

The force-time traces from the impact tests on the epoxy matrix tubes were expected to show a decrease in the mean load as the crush progressed. This was because the crush speed decreased during the crush, hence the equilibrium specific crush stress decreased in accordance with the results presented in figures 4.1 and 4.2. This expected decrease was however, not observed. This might have been connected to the crush zone trailing the crush speed, as was discussed in section 8.1.2.1, as the main determinant of the specific crush stress might have been the crush mode. The decrease was expected to be about 6 kN for a 20 m s^{-1} impact. This was the difference in crush load between that measured for a 20 m s^{-1} impact and that for a 0.002 mm s^{-1} crush; this load change might have been masked by the serrations in the crush trace. The lack of a decrease in the crush load might have been significant with respect to the theory of the crush zone trailing the speed and the effect on the crush loads for subsequent impacts. It implied that there was no significant mode change during the impact, thus the subsequent impacts would not have been expected to give a lower crush load than the initial impact.

One aspect of the crush mode that was not carried from one impact to the next was the temperature rise response, as the time between performing an impact and setting up for the next impact allowed the crush zone to cool so the temperature rise response was not dependent on the previous impact. However, the model in section 7.2 showed that the temperature rise response was independent of the crush speed at the speeds encountered in the impact tests so this observation might be of little consequence

apart from requiring the crush zone to reach thermal equilibrium for the subsequent tests.

8.2.3 Polyester Matrix Tubes

Section 4.2.2 showed that there was a significant decrease in specific crush stress with the change from constant, slow speed crushing to high speed impact testing {figure 4.6}. This behaviour was consistent with the differences in specific energy absorption that were quoted in the literature for low and high speed crushing, for tubes with similar matrix materials {e.g. figures 2.22 and 2.26}. Although little information was available concerning the variability of the material properties with the strain rate, reference should be made to the observation in section 2.1.4.1.1.1 of the literature review, that the fracture toughness of these resins increased with increasing strain rate, while the specific energy absorption of polyester resin matrix tubes decreased with increasing matrix fracture toughness. Generally, most of the mechanical properties of polyester resins improve with increasing strain rate (section 2.2.1.2), meaning that the decrease in specific crush stress that was observed must have been due to some mechanism other than deformation or fracture.

The force-time traces obtained from the impact tests on the glass mat-polyester tubes, for instance figure 3.8 (a), showed that the crush load increased with increasing duration of crush, hence decreasing speed. This behaviour was expected for tubes where the crush load decreased with increasing speed. The concept of the crush zone trailing the crush speed as discussed in section 8.1.2.1 will have been applicable to this situation, but it was not clear if there was any change in the actual crush mode during the decrease in crush speed. That there was no significant difference between the specific crush stress for the first impact and subsequent impacts, unlike for the

Tufnol tubes, suggested that there was no difference in crush mode and that the differences in specific crush stress with speed were due to the actual speed at any time.

The change between the results from low speed crush to those from impact tests, might be related to the frictional heating behaviour at the interfaces. Although the modelling that was carried out in section 7.2 was based on the observations for the Tufnol tubes, the modelling could be applied to the glass mat-polyester tubes where the frond-wedge-frond type of crush mode was observed {figures 6.24 and 6.25}. At high speeds, the interfacial temperatures were predicted to be high, typically exceeding 300 °C for these tubes at the resolution used. This might have resulted in polyester decomposition, leading to a decrease in the friction, hence a decrease in the crush load and specific crush stress. This however, does not explain why filament wound tubes with a ±55° lay-up were more sensitive to the crush speed than 0-90° tubes with the same matrix resin {figure 2.21}.

The instantaneous speed change tests for the glass mat-polyester tubes showed a different behaviour from the comparison between the impact tests and the constant speed crush tests. These tests, at room temperature (22 °C), gave no appreciable difference in the crush load for high or low speed. This was consistent with the single, constant speed crush tests, as the latter showed no speed sensitivity over the speed range utilised in the instantaneous speed change tests for the polyester matrix tubes {figure 4.4}. It must be concluded that these tubes behaved differently at impact speeds compared to low speeds.

Unlike for the glass mat-polyester tubes, the constant speed crush test results from the RJPW tubes gave a clear increase in specific crush stress with increasing speed over the range tested, also showing clearly on the instantaneous speed change test traces.

The nature of the reinforcement for these tubes was different, a material variable that is known to have an effect on the speed sensitivity of the specific crush stress (section 2.1.4.1).

8.3 Time-Temperature Superposition

Many of the properties of polymer composites are known to be dependent on both the temperature and the strain-rate. These dependencies can often be related to processes that are thermally activated.

8.3.1 Thermally Activated Processes

It has long been appreciated that the time and temperature dependencies of properties can be approximately related by an Arrhenius type equation. For instance, the rate constant, k, of a chemical reaction can be given by:

$$k = A \exp\left(\frac{-\Delta H}{RT}\right) \qquad (8.9)$$

where the time and temperature dependencies are governed by the activation energy for the reaction, ΔH [120]. In equation 8.9, R is the gas constant, which may be replaced by Boltzmann's constant depending on the units for ΔH; T is the absolute temperature and A is a constant.

For most viscoelastic phenomena such as deformation, values of ΔH relate to a thermal activation barrier that must be overcome for the rate controlling step in the process to proceed, for instance chain rotation or chain sliding. Providing there is no change in the rate controlling mechanism, the value of ΔH would be expected to be independent of the temperature and the strain-rate. However, if there was a change in mode of deformation with different processes becoming rate determining, then ΔH

might not be constant and would only be related to the strain-rate and temperature in question.

The Arrhenius equation, as normally quoted, was derived from the van't Hoff equation (8.10) involving an integration with respect to the temperature:

$$\frac{d \ln k}{dT} = \frac{\Delta H}{RT^2} \qquad (8.10)$$

The integration required the assumption that ΔH was independent of the temperature, hence if ΔH varied with temperature, the integration would have been imprecise and errors could have occurred. The Arrhenius equation was originally derived for chemical reactions but can also be applied to other thermally activated processes. The requirement for the rate constant of a reaction to be proportional to the negative reciprocal of the absolute temperature, is often not obeyed for complex chain reactions, hence the Arrhenius equation is not obeyed [120].

8.3.2 Application to Tube Crushing

The basic principles of thermally activated processes were applied to the crushing of composite tubes at different speeds and temperatures. For this purpose the Arrhenius equation was adapted to deal with tube crushing. This was done by replacing the rate constant with the crush speed, i.e.:

$$v_c = v_{c0} \exp\left(\frac{-\Delta H}{RT}\right) \qquad (8.11)$$

Although the Arrhenius equation was applied and values of the activation energy determined, three different effects were identified that did not allow the Arrhenius equation to describe accurately the interrelation of speed and temperature for crushing. These were: frictional heating in the crush zone, residual strains in the material and

inertial effects of movement of the crush debris away from the crush zone. Frictional heating was speed dependent and has been discussed in depth in section 7.2. Residual strains are discussed in section 8.5 and were only dependent on the temperature of testing, being independent of the crush speed apart from any interaction with the frictional heating which might have occurred. Inertial effects were discussed in section 8.2.1 , being dependent on the crush speed and not the temperature.

Despite the limitations imposed by these factors, values of ΔH were determined for each of the tube types investigated. For the case of tube crushing, there was a distinct change in mechanism between tests performed at high and low temperatures such that the values of ΔH would not necessarily be expected to be the same. Also, there were a large number of individual fracture and deformation processes that occurred in the crush zone so the interaction of these processes determined the crush zone morphology, hence it was unclear as to whether there was only one rate determining mechanism.

Figures 5.1 to 5.8 show some differences in the behaviour of the various tubes tested in this investigation. Figure 5.1 shows that the speed sensitivity of the specific crush stress for Tufnol tubes was largely independent of the temperature between -100 °C and 80 °C, above which temperature it increased rapidly. This behaviour can be related to the trends observed by Pink and Campbell for the temperature sensitivity of the tensile stress for an epoxy resin {figure 2.42}, in particular the rapid increase in the speed sensitivity as the T_g was approached and the decrease just before the rapid increase with increasing temperature. Figure 5.1 shows some features which might have been due to specimen variability but equally, might have been genuine features of the behaviour of the tubes. In particular there was a peak in the speed sensitivity at

about 50 °C[1]. This peak might have been related to features that were observed in the literature for the speed sensitivity of various material properties (section 2.2) [64], and can be likened to a slight peak in the loss tangent at similar temperatures as shown by Egusa *et al.* for glass cloth-epoxy {figure 2.46} [69-71]. That work showed a more dramatic increase in the loss tangent at temperatures in excess of about 90 °C, which might have been reflected in the results presented in figures 5.1 to 5.8. However, the unstable collapse mode encountered in these tests prevented further extrapolation of the results.

The calculated values of activation energy for crushing for the RJPW tubes gave a negative value at -20 °C, relating to a negative speed dependency. This value implied that there was no activation barrier to overcome, hence the crushing process should have occurred without an input of mechanical energy, so the tube should have collapsed spontaneously. The concept of a self-crushing tube is obviously ridiculous, hence the use of the Arrhenius equation to relate speed and temperature effects can be seen to be unreasonable in this case. Thus doubt concerning the value of quoting an activation energy for crushing must be expressed, except to note that it can be regarded as being a quantity that relates speed and temperature sensitivity at that speed and temperature. As discussed in section 8.2.3, the negative speed dependencies of the polyester matrix tubes that were observed at high speeds were probably due to frictional effects at the wedge-frond interface. This was a single mechanism which appeared to dominate the speed dependency which was not so apparent for the other tubes, so that the conclusions regarding the validity of the activation energy might only be valid for the polyester matrix tubes. It should be noted that the observed low

[1] Which was also observed for the other types of tube.

temperature behaviour was similar to that of high speed, so that some form of time-temperature superposition was present in this case.

Three of the λ versus T traces {figures 5.1, 5.3 and 5.7} showed a sudden increase in λ at high temperature, an increase that was preceded by a slight drop. This slight drop might have been due to experimental scatter, but it's appearance in three of the traces suggests that it was a true effect, which might have been related to the drop in the yield strength of epoxy resins that was observed by Pink and Cambell [64]. The lack of a similar drop in figure 5.7 was due to the random filament reinforced tubes collapsing at too low a temperature (70 °C) for this effect to show up.

8.4 Crush Mode

In much of the preceding discussion, the crush mode was taken as an abstract concept and the crush zone treated as an undefined entity into which uncrushed material entered, and from which crushed material emerged, having absorbed energy (a black box). The crush mode was treated as an entity which was appropriate for the test conditions, and changed with any change in those conditions, the changes being sometimes subtle and not directly detectable in form by observation. Evidence of these changes can be taken from the behaviour of the force-displacement traces obtained from the instantaneous speed change tests where the crush load took a distance to equilibriate to a mean value after the speed change (see section 8.1.1). No description of the crush zone has been given so far apart from the observations based on the crush zone micrographs in chapter 6.

8.4.1 Crush Zone Micrographs

The micrographs in chapter 6, showed that the observed hackle size and the degree of interlaminar shear were related, as high temperatures favoured small hackles and a

high degree of interlaminar shear, while low temperatures favoured large hackles and a low degree of shear {compare figures 6.5 and 6.18}. These observations were indicative of a shear stress system at any point within the fronds as material flowed past the wedge {figure 8.4}. Examination of the hackles showed that they were formed by fracture, as there was no notable material deformation within each individual hackle. It was probable that the fracture was a mixed mode type, with components of mode I and mode II being present, although geometrical considerations indicate that the majority of the fracture was mode II. The geometry of the fronds is discussed further in section 8.4.1.4.

Elongation of voids was observed particularly in the material that was close to the wedge-frond interface during it's traverse of the crush zone. This feature was indicative of matrix deformation, as different plies of the glass cloth slid relative to each other. This deformation could be likened to the inter-ply sliding that was observed by Fairfull [51], where the fronds delaminated. In those tests, the tubes had a much higher void content than the Tufnol tubes investigated in this work, so they probably had a much lower interlaminar shear strength (ILSS) [40]. This lower ILSS resulted in Fairfull observing a very different mode of crushing from that which was observed in this investigation, as there will have been a much lower degree of through thickness stress in the fronds of Fairfull's tubes, when compared to the Tufnol tubes. Consequently, there was no formation of hackles in those tubes. In the Tufnol tubes there was an equilibrium situation where the formation of hackles and the matrix shear deformation balanced according to the test conditions. It is known that the strength of epoxy resins decreases with increasing temperature whilst the fracture toughness of composites increases (section 2.2), thus as the test temperature increased, matrix deformation became easier and fracture more difficult, such that the crush

mode tended towards one incorporating a greater degree of matrix deformation with less fracture. This was consistent with the observations that the size of the hackles decreased with increasing temperature and that the degree of void flattening increased (see also section 6.1.1).

Temperature rises in the crush zone were also significant in determining the nature of the crush zone. In section 7.2 frictional temperature rises were shown to be greatest at the wedge-frond interface, this being close to the region where shear deformation of the matrix was observed. As the temperature rose, then this shear deformation will have required less energy. The temperature rise distribution was a function of the testing speed as, at high speeds, the temperature rises were high, but localised close to the wedge-frond interface, while lower speeds gave lower peak temperatures, but the rises were significant away from the wedge-frond interface. Thus it might be expected that the size of the hackles decreased with decreasing speed. Comparison of the high speed impact micrographs with the constant speed crush micrographs was inconclusive in this respect. The impact tested tubes, shown in figures 6.8 to 6.13, did not generally exhibit any clear hackles, rather the fronds formed with a substantial degree of fracture and delamination. The low speed crush micrographs were also inconclusive as the crush zones did not all exhibit hackles.

The observations that have been made on the behaviour of the hackles and the matrix deformation have been based on idealised crush zones for the temperatures in question, and on a combination of several observations. However the actual features in the crush zones often differed significantly from the ideal. Typical deviations that have been observed, were due to interlaminar shear fractures such as those observed by Fairfull as well as other types of fracture. These have been encountered at high

speeds and low temperatures, conditions under which the fracture toughness of the material is known to be low.

One important conclusion that must be reached is that the factors that determine the exact nature of the crush zone are not as yet fully understood. However, it is clear that there are a large number of variables that must be taken into account although they are not all easily controllable, nor are they independent of each other.

8.4.1.1 Hackle to Deformation Transition

As was discussed in section 8.4.1 the formation of the observed hackles was due to through-thickness shear fracture and the size of the hackles was, to some extent, dependent on the ability of the matrix near the platen to deform in shear normal to the shear crack direction. Figure 8.5 shows two other important features connected with the transition from the shear deformation region to the shear fracture, hackle formation region. These were; local buckling failure of the plies of glass that were originally in the axial direction in the tube wall, and matrix and interfacial cracks perpendicular to the hackle shear cracks. The buckling of the axial fibres appears to have happened in only one layer of the cloth, close to the centre of the frond. The buckling was due to the layer being under a compressive load parallel to the axial direction, with the fibres being unable to buckle due to being constrained in the radial direction by the other layers of glass cloth. When the hackle shear crack grew to the extent of reaching this ply, the constraint was relieved and the ply was able to buckle out of plane, thereby blunting the shear crack and determining the size of the hackle. An important consequence of this behaviour was that the size of the hackles must have been dependent on the relative positions of the plies of glass cloth and the outside of the tube wall, in much the same way as the position of the centre wall crack

was determined, as is discussed in section 8.4.1.2. The cracks that have been observed in this region appear to have been formed in connection with the strand buckling. As the strands buckled out of plane, mode I cracks were formed and the hackle shear cracks were blunted.

This behaviour was reflected in the tubes crushed at higher temperatures. With these tubes, the outer plies of glass cloth appeared to have formed local buckles to give a hackle-like effect {figures 6.18 and 6.20}. Plies that were inside of the fronds also appeared to have buckled, the out of plane constraint having been greatly decreased due to the softening of the matrix. However, the inner frond buckles appeared to have been connected with an external buckle in each case for the plies that were near to the outside of the wall, although this was not always shown clearly for the plies at the centre of the frond.

8.4.1.2 Centre Wall Crack

For most of the crush zone sections that have been observed, the mode was one of frond-wedge-frond with a crack propagating down the centre of the wall ahead of the wedge. It was noted in section 6.1.1.1 that the wedge was sometimes displaced to the inside or outside of the wall centre line, although no trends were identified. Some consideration must be given to the position of this wedge and crack relative to the tube wall.

If the wall had consisted of a flat plate, constrained equally on either side and comprising an even number of plies of glass cloth, then the apex of the wedge and the crack ahead of it, would have been located at the centre of the wall, as this was the equilibrium position for a force balance. Also, the crack will have run through the path of least resistance, this having been between the plies of glass cloth. However,

this case was, at best, an idealisation of the true situation. The tubes used in this investigation differed in two important ways from the ideal, even for perfectly manufactured tubes. Firstly, the curvature of the tube wall meant that the restraints on the wedge and crack were not necessarily equal internally and externally if the wedge and crack had been at the centre of the tube wall (see section 7.1). Secondly, the glass cloth in the tube wall was wound helically rather than concentrically, such that the position of the path for easiest crack propagation closest to the centre of the tube wall, varied around the circumference of the tube by ± half a ply thickness {figure 8.6 (a)}.

The latter observation led to a difficulty in defining the wedge position. Assuming that the helical winding of the glass cloth was the only factor affecting the wedge position, the wedge will have been at the centre of the wall at only one point on the tube circumference. Diametrically opposite this point, the wedge was expected to have had two apices, each half a ply thickness either side of the centre line of the tube wall {figure 8.6 (b)}. Determining the positions of the actual centre-wall wedge and the twin-apex wedge was difficult and the latter has not been observed, if it did indeed exist.

The transition between single apex and twin-apex wedge was not expected to have been sudden at the point diametrically opposite the centre-wall wedge, rather a transition from an externally biased to an internally biased wedge might have occurred over an arc of the tube wall. This transition might be expected to be in accordance with catastrophe theory [121] in that, following the inter-ply position round the circumference, a point will be reached when either the present position, or one the other side of the intervening ply, can be the equilibrium one for the centre

wall crack, depending on the direction of approach. However, the crack must be followed further round the circumference in order to find the position at which the crack will only exist on the other side of the centre line. If the crack were to continue indefinitely, then the whole of the crush zone would delaminate and have a much lower degree of integrity. It is possible that this effect might have given rise to some degree of localised delamination in some parts of the crush zone, although none have been observed for the Tufnol tubes. This might have been a contributing factor to the delamination in the fronds of Fairfull's tubes [51]. The transition of the crack position from one side of the wall centre to the other will probably be accompanied by a progressive shortening of the crack, and a reduction in size of the wedge on that side of the tube wall centre line, to zero. It might be possible to show this effect by progressive sectioning of a mounted crush section, from the wedge top downwards, but attempts have proved inconclusive. Consideration of the interfacial forces with a twin apex wedge indicates that it was not likely to have been very stable and that some interaction between the two wedges might have prevented a twin apex wedge from forming due to wedge shortening before the wedges overlapped. Some investigative practical work in this area might be beneficial.

For the reasons outlined above, within the limit of one ply thickness, any variation in the observed position of the centre wall crack was meaningless with regard to any variations in the crush zone morphology. This limit of ± one ply thickness can also be applied to the size of the hackles in the fronds for similar reasons.

8.4.1.3 Number of Fronds

The number of external fronds formed was dependent on the test temperature, this is shown clearly in figures 6.26 to 6.29. Formation of the fronds was due to the presence

of tensile cracks between the fronds, parallel to the radial direction. These cracks consisted of mainly fibre fracture, which was largely independent of the test temperature in the range under investigation, so the behaviour of the fronds must be explained by a different mechanism. This mechanism was the flattening of the tube in the radial direction between the inter-frond cracks. This effect was due to compressive stresses acting in the radial direction, resulting in deformation that was sensitive to the matrix properties, hence the temperature {figure 8.7}. This deformation showed a degree of out of plane buckling that increased with increasing temperature and led to an instability at high temperatures, resulting in the buckling mode of collapse that was observed and is discussed in section 8.4.2.

8.4.1.4 Strains in the Layers

As the layers of glass cloth moved past the wedge-frond interface they were subjected to bending through a radius of curvature. This bending required strains to be set up in and between the layers for the necessary deformation of the material to be achieved.

Figure 8.8 shows a schematic of layers of glass cloth as they moved past the wedge-frond interface. For a constant wall thickness and radius of curvature of the interface[1], the strains that must have been accommodated in the frond material will have been independent of the test speed and temperature except for any out of plane deformation as discussed in section 8.4.1.3. Thus the system may be said to have been a strain controlled system.

[1]This radius was not constant with respect to the temperature but has been considered as such for the purposes of this analysis (see section 6.1.1).

8.4.1.4.1 Tensile or Compressive Strains

This analysis was to provide some insight into the magnitude of the strains involved in the layers. From figure 6.4 the radius of curvature of the wedge-frond interface, r_{ci}, was about 3.2 mm for a Tufnol tube tested at 10 mm s^{-1}. From figure 8.8 the angle through which the material flowed was 90°, so that the length of the arc, l_a, through which each layer flowed was:

$$l_a = \frac{\pi\, r_c}{2} \tag{8.12}$$

From this the mean strain in each layer could be calculated and it was possible to estimate the tensile strain in adjacent layers in the absence of any shear strains. As the strain was given by the change in length divided by the original length:

$$\varepsilon = \frac{\Delta l_a}{l_a} \tag{8.13}$$

If Δl_a was given by:

$$\Delta l_a = (r_n - r_{n+1})\,\frac{\pi}{2} \tag{8.14}$$

where r_n was the radius of curvature of the centre of the nth layer from the wedge-frond interface. For the layer separation of t/N, where t was the wall thickness and N the number of layers of glass cloth, then:

$$r_{n+1} = r_n - \frac{t}{N} \tag{8.15}$$

so Δl_a was given by:

$$\Delta l_a = \frac{\pi}{2}\,\frac{t}{N} \tag{8.16}$$

and l_a was given by:

$$l_a = \left(2r_n - \frac{t}{N}\right)\frac{\pi}{4} \tag{8.17}$$

so:

$$\varepsilon = \frac{t}{n\left(r_n - \frac{t}{2N}\right)} \tag{8.18}$$

Using the values of $t = 2.5$ mm, $r_n = r_1 = 3.12$ mm[1] and $N = 15$:

$$\boxed{\varepsilon = 0.055}$$

This value was greater than the strain to failure in bending of the Tufnol flat plate material as shown in figure 4.70, of about 0.02. However, this difference could be accounted for by the constraints of the glass cloth in the fronds, by sharing the strains in the plies between tension and compression and shear contributions to the deformation.

8.4.1.4.2 Shear Strains

For the purposes of this analysis it was necessary to assume that shear deformation was between the plies of glass cloth, so that the shear strain, γ, between each layer was taken as being the difference in length of the two adjacent plies, divided by the distance between the centres. This was given simply by:

$$\gamma = \frac{\pi}{2} \tag{8.19}$$

[1]This was the mean radius of the first layer of glass cloth starting at the wedge-frond interface.

This was the total shear deformation that would have been required in the absence of any tensile or compressive deformation. Shear deformation was mainly accommodated by shear flow in the matrix, as the matrix shear modulus was much lower than the glass shear modulus.

This analysis showed that the differences in the lengths could be accommodated by elastic tension or compression, by shearing of the matrix material between the plies, or a complex combination of these effects. The relationship between the degrees of shear and tensile deformation were dependent on the relationship between the elastic properties of matrix shear modulus and composite compressive modulus, as well as the energy to cause permanent shear deformation.

8.4.1.4.3 Evidence from the Micrographs

After the material had traversed the wedge-frond interface, if there had been no permanent deformation in the material, then the fronds would have moved along the platen, the deformation having been relieved once the material had moved away from the crush zone. Figures 6.1 to 6.5 show clearly that this was not the case for crushing at room temperature and that some form of permanent deformation must have occurred. Likewise at higher temperatures, the fronds retained a degree of curvature after traversing the wedge-frond interface {figures 6.17 to 6.21}. Any differences between the amount of post crush curvature of the fronds, is not necessarily indicative that some have experienced greater permanent deformation than those tested at other temperatures. This effect could also be masked by the resin being softer at higher temperatures, so that the recovery of elastic tensile strains in the plies on the relief of the crush load, might have resulted in permanent deformation in a direction that was opposite to that experienced during crushing. Had there been no elastic deformation, the frond radii would have remained the same as the wedge-frond interface radii.

However, the radii of curvature of the fronds were all greater than those of the wedge-frond interface, implying that there must have been a degree of elastic deformation in the crush zone. The difference in the curvature between the frond and the wedge-frond interface could give a measure of the relative contributions of elastic and plastic deformations. However, hoop restraint was an important factor that affected the frond curvature, as was the position of the section through the frond, so no attempt was made to quantify this effect.

If the system was considered as a strain controlled system, then the tensile and compressive strains that must have been accommodated in the plies of glass cloth were independent of the test temperature. If the elastic moduli of the glass cloth were independent of the temperature in the range considered[1], then the stresses in the plies for the same strains must have been the same irrespective of the testing temperature. However this does not take into account the degree of inter-ply shearing which might have occurred, the extent of which will have been strongly dependent on the temperature, as the shear strength and strain to failure of the matrix material were known to be strongly temperature dependent (see section 2.2). Thus the expected mechanism of strain accommodation must have changed with any change in the test temperature. The frictional temperature rises, as discussed in section 7.2, also contributed to the complexity of description of the system.

In the plies close to the wedge-frond interface, out of plane deformation was constrained, so that strain accommodation could not be made in this way. However, away from the wedge-frond interface, the constraint was less and the strains could be

[1]This was not a valid assumption as the weave of the glass cloth implied that the tensile and compressive moduli were dependent on the matrix constraining effect.

accommodated by out of plane buckling. This effect was observed in the plies that were close to the shear hackles in the fronds. Load transfer between adjacent layers will have been by shear, this causing some local shear deformation which may be seen in the micrographs as flattening of the voids.

The micrographs in chapter 6 showed that the requirement for through ply shear fracture to form hackles, was not as great at high temperatures compared to low temperatures. The through thickness shear strength of the material was expected to be largely independent of the test temperature, as it was mainly fibre fracture rather than matrix fracture, so at high temperatures, the required strains must have been achieved by shear deformation between the plies.

8.4.1.5 Modelling

It has not been possible to provide a full description of the proportions of energy absorption by different mechanisms as the stress distribution in the crush zone is unknown. Some attempts have been made with the intention of describing the crush zone mathematically [51,122] but so far these have proved unsuccessful.

In the field of composite energy absorption, many variables have been examined and their effect on the crush stress recorded (section 2.1). The crushing process is such that any change in the material or testing variables will change the stress distribution within the crush zone (see section 7.1). This observation means that, to gain a full understanding of the crush process, the energy absorption and stress distributions must be determined for all of the test circumstances. The most promising method of predicting the behaviour of tubes during crushing is finite element modelling (FEM). However, the inherent complexity of the crush process requires a high degree of understanding of the process before any effective modelling can be carried out.

8.4.2 Frond:Buckling Transition

At the higher temperatures that were used in the testing, in the region of 90 °C to 110 °C for Tufnol tubes but lower for the resinjection tubes, a transformation was observed between the frond-wedge-frond collapse mode and one of macro tube buckling {figure 6.30}. The transition at any speed, occurred over a temperature range of less than 10 °C, this being a range in which the mode could not be predicted with any confidence. The actual mean temperature of this transition range was speed dependent as shown in figure 4.25. The transition was taken from the uncertain mode points in figure 4.25, and a good linear agreement was found with temperature and log. speed. An increase in the speed by a factor of ten was equivalent to a decrease in the temperature of about 5 °C. This speed dependence of the transition was also observed in the instantaneous speed change tests where, at 100 °C, the Tufnol tubes crushed progressively at 10 mm s^{-1} but buckled at 0.002 mm s^{-1}. The transition for the impact tested tubes was found to be at a considerably higher temperature than for the slow speed crush tests. There were two basic reasons for this, firstly the speed itself, this being consistent with the observations above, and secondly the heat losses that the tube will have experienced during the transport of the tube from the oven to the crash rig for testing. It was possible to obtain an estimate of the temperature of the tube at the point of impact by extrapolating the line in figure 4.25 to the impact velocity. This gave a temperature of 128 °C for the impact buckling transition, compared to the oven preheat temperature of 170 °C for buckling, indicating a temperature loss of about 42 °C during the test.

Mathematical models of tubes buckling under axial compression have yielded an equation to predict buckling loads [123]. Composite tubes under conditions where the tube is able to buckle, for instance when the matrix is soft enough to allow buckling to

occur before catastrophic centre fracture, might be expected to obey this equation. However, this buckling equation was based on an axisymmetric tube with no irregularities. For tubes crushed at temperatures in the frond-buckling transition region, there were out of plane deformations due to the attempted formation of fronds. These out of plane deformations could have caused buckling to be initiated at lower loads than those predicted by the buckling equation. For tubes crushed at temperatures that were above the upper boundary of the transition region, there was no evidence of frond formation. This means that the same type out of plane deformations will not have been present, although out of plane loading will have been present due to the use of a 45° external chamfer as a trigger. Examination of the chamfered end showed that the chamfer collapsed to form a square end to the tube, but there was no evidence of any significant out of plane deformation. The out of plane loads mean that normal buckling analysis is inappropriate in the case of these tubes.

The frond-buckling transition was reasonably consistent with viscoelastic behaviour. The three mechanisms identified as potentially causing deviations from this situation were insignificant for this transition. The crush zone temperature rises will not have been present in the region of the tube that buckled as it was remote from the debris wedge, assuming that one formed at all. At the speeds in question inertial effects have been shown to have an insignificant effect on the tube behaviour (section 8.2.1), and the material flow was very different from that in the fronds. Residual stresses were probably not present, as the buckling temperatures encountered were above general post cure temperatures of the composites, hence above the stress-free temperature. This was not necessarily true for the Tufnol tubes as they were cured at 135 °C, but it is probable that there were no significant residual strains set up between 100 °C and 135 °C.

The resinjection tubes also displayed a transition at high temperatures. However, the collapse mode at high temperature was not reliably predictable and it was not possible to produce convincing plots such as in figure 4.25, so none were shown. Failure in these tubes was not consistently by buckling at high temperatures as an interpenetration mode was also observed as shown in figure 6.31.

For the resinject tubes the transition to buckling or interpenetration generally happened at lower temperatures than for the Tufnol tubes. There were three important differences between the resinject and the Tufnol tubes, namely the wall thickness, the matrix resin and the nature of the reinforcement. For the resinject tubes reinforced with woven glass cloth, the most important difference from the Tufnol tubes, with regard to buckling, was probably the wall thickness as a thinner walled tube would be expected to be less stable than a thicker walled tube. This difference probably accounted for the change to the interpenetration mode.

The nature of the reinforcement in the resinject tubes also appeared to have an effect on the transition temperature. In general it was found that the transition was at a lower temperature for the random glass mat tubes than for the woven glass cloth tubes. The reason for the difference will have been related to either the fibre volume fraction or the fibre geometry, or more probably, a combination of the two. Section 2.1.3.4 noted the effect of a higher fibre volume fraction favouring greater stability so this must have been an important factor.

8.4.3 Speed Sensitivity of the Crush Mode

The micrographs in chapter 6 showed that any changes in the form of the crush zone with changing speed could be masked by changes in material properties around the circumference of the tube, such as the void content and distribution, and the relative

positions of the different layers and strands of glass cloth. The discussion related to the instantaneous speed change tests and the impact tests was concerned to some degree with the crush mode changes without making any definitions, so what constituted the crush mode must be defined. Each of the mechanisms of energy absorption, as defined by Fairfull [51] and identified in this work, might have been sensitive to the crush speed to some extent, and it was the combination of the responses of these mechanisms, that determined the speed sensitivity of the crush mode of the tube.

The speed sensitivity of the crush mode could be divided into two areas, material variables and responses of form. The former category included the elastic, deformation and fracture properties of the composite and their effect on the crush mode, while the latter included the crush zone morphology and temperature rises in the crush zone. Most of these variables were not independent of each other so their interaction must be considered.

The material variables tended to affect the crush zone morphology and stress distribution, as did the temperature rises, but at present it is not possible to give any numerical description of how the crush stress was affected by each individual variable. However, it is possible to indicate some of the expected and observed trends with respect to the variables.

As was discussed in section 7.2, the temperature rise behaviour was sensitive to the crush speed in the range of speeds that were used in constant speed crushing. However, it was speed insensitive at the impact speeds examined, so this contribution may be disregarded as a contribution to the variation of crush mode during an impact test.

Two mechanisms that were probably sensitive to the crush speed were the formation of hackles in the fronds by shear fracture, and the shear deformation of the matrix, as observed by the flattening of voids in the fronds close to the crush platen. These mechanisms were competitive to some degree, in that a higher occurrence of one mechanism tended to reduce the extent of the other (section 8.4.1.1). This was due to the frond formation being a strain controlled process, in which a certain amount of deformation had to occur in order for the fronds to flow past the debris wedge (section 8.4.1.4). This deformation took three main forms, elastic strains in the plies close to the wedge-frond interface, shear deformation of the matrix to enable adjacent plies to move relative to each other and through ply fracture to reduce the compressive strains in the plies away from the wedge-frond interface. How the two latter mechanisms interacted depended on three main factors, the resistance of the matrix to shear deformation, the through-ply shear fracture toughness of the material and the stress distribution in the crush zone (section 8.4.1). Assuming that the form of the crush zone was dependent on shear fracture to form hackles and matrix deformation, then the speed sensitivity during a test will have been dependent on the speed sensitivity of these two properties. The impact tested tubes did not generally exhibit hackles hence this discussion is only concerned with constant speed crushing where hackles were formed (see figures 6.8 to 6.13 and section 6.1.1.2). In this speed range the temperature rise behaviour was speed dependent, so this was also a contributing factor to the speed dependency.

As the strain rate sensitivity of the properties of the glass was less than that of the matrix, so the predominant mechanism that will have determined the speed sensitivity of the crush stress of the tube was the matrix shear deformation. The strength of the matrix increased with increasing strain rate (section 2.2), so higher crush speeds

should have favoured a lower degree of shear deformation, hence a higher degree of fracture to form larger hackles. As the speed decreased, the shear strength of the matrix decreased and deformation of the matrix became easier than through ply fracture. As the energy that was absorbed was the least that was required for the necessary material flow, so as the shear strength decreased the crush stress decreased. Superimposed on this effect were the temperature rises in the crush zone. As the crush speed decreased, then the temperature rises away from the platen became significant in the formation of the crush zone and shear deformation was favoured rather than fracture.

While the foregoing discussion has deduced that the strain rate dependency of the resin shear strength might be considered to be the major contributor to the speed sensitivity of the crush mode and the crush stress, the actual effect of any change of this property is unknown due to the inherent complexity of the crushing process.

8.4.3.1 Speed Transition

As has been discussed above, the size of the hackles and the degree of matrix shear deformation were dependent on the crush speed. When a speed change occurred, the hackle size and degree of matrix deformation were at the equilibrium level for the initial speed. Some distance had to be covered in order to move these hackles away from the crush zone and for crushing to proceed with the equilibrium crush zone for that speed. Thus the crush distance that was required in order for the crush zone to equilibriate for the new speed was expected to be of the order of the width of two hackles in the axial direction, this distance being that to clear the initial hackle and to form a new one for the new speed. Measurements taken from figure 6.5, a crush zone from a Tufnol tube crushed at 10 mms^{-1} gave a mean hackle width of about 0.43 mm

for this speed, which gave a transition distance of about 0.9 mm. The crush traces in figures 4.58 to 4.64 indicated a transition distance of about 2-3 mm, which was greatly in excess of the distance of two hackles. This difference could be accounted for by changes in the temperature rise behaviour (section 7.2).

So far the discussion about the hackle size has been based on observations at one speed and theoretical predictions as to what might be expected to happen. Observational confirmation of the predictions should be sought. Comparison of figures 6.4 and 6.5, sections through two Tufnol tubes cut from the same original length of tube and tested at different speeds, showed that the predictions might have been reasonable. Figure 6.5 shows a section through a tube tested at 10 mm s^{-1}, the size of the hackles was larger than in figure 6.4 which was from a tube tested at 0.01 mm s^{-1}. The normal variations in crush zone that have been observed between different tubes meant that caution should be exercised when making claims about the significance of these observations, but they were consistent with the predicted behaviour

8.4.4 Fragmentation Crush Mode

The above discussion has been mainly concerned with the frond-wedge-frond type of crush mode. While this was the main general type observed in this work, one other main type of crush zone was observed, namely the fragmentation crush mode. The fragmentation crush mode differed from the frond-wedge-frond crush mode in that the debris after crushing did not exhibit any post crushing integrity.

This type of crush zone was observed in the tubes tested at low temperatures and high speeds, being particularly apparent in the tubes that were impact tested after

immersion in liquid nitrogen {figures 6.14 and 6.15}, and was also observed by Berry and Hull {figure 2.39} [60].

Some mathematical modelling of this type of crush mode has been carried out but the details are beyond the scope of this work [124].

The fragmentation mode has been observed regularly in tubes where the fracture toughness of the resin was low and the strength high, such that the required deformations to move material away from the crush zone could be accomplished by material fracture with little or no matrix deformation. In particular fragmentation was favoured by low temperatures, high speeds and low moisture contents [119].

The fragmentation mode can be likened to the frond-wedge-frond mode where the shear cracks to form the hackles were large enough to extend through the entire frond thickness {figure 6.13}. Thus the frond-wedge-frond crush mode with distinct hackles can be regarded as a transition crush mode between the fragmentation mode and the frond-wedge-frond mode with no distinct hackles, for instance figure 6.20.

8.5 Residual Stress Effects

As has been discussed above, three factors were identified that did not allow the simple interrelation of speed and temperature. The presence of residual stresses was one such factor as, in composite materials, the presence of residual stresses can affect the mechanical response. Residual stresses can be set up in composites due to differential expansion or contraction of the fibres and matrix, in either cooling from a post cure temperature, or due to curing shrinkage of the matrix material. For instance an unbalanced glass-polyester laminate coupon with a 0-90° fibre arrangement will, on cooling from a post cure temperature, bend into an arc with the 90° fibres on the

inside of the arc [125-127]. This is due to the contraction of the matrix, which is unconstrained in the direction perpendicular to the fibres, being much greater than in the direction parallel to the fibres, where the fibres have a constraining effect. If such a laminate is heated, then the radius of curvature of the arc will increase until the temperature is such that the laminate is flat. At this temperature the residual stresses will have been relieved, this temperature being known as the stress-free temperature. Thus residual stresses can be affected by the test temperature of the material but will be independent of the strain rate.

Residual stresses in composites can be divided into two basic categories, although their origins are the same from differential thermal contraction. These are micro-stresses and macro, component stresses. The former category represents stresses between individual fibres or laminae, and may have the effect of altering properties such as fibre pull-out behaviour and interlaminar shear strength [40]. These stresses can also preload the fibres in compression such that buckling can occur at lower applied compressive loads than would be needed in the absence of the stresses. Residual macro-stresses are found on a larger scale, and are generally due to differences in fibre lay up between adjacent laminae, where the individual laminae undergo anisotropic contraction. They may also be set up due to the component geometry such as circular restraint. It is the latter type of stresses that are considered in this section, although micro-stresses will also have been present.

In this section the measured values have been quoted as strains rather than stresses to eliminate any effects from changes in the material's Young's modulus due to material changes, or differences between plane stress and plane strain conditions.

Residual strains were found to be present in the hoop direction of some of the tubes used in this investigation, with strain distributions as shown in figures 4.71 to 4.73 and 5.9 to 5.11. The magnitude of these strains was of the order of 10% of the flexural failure strain for the material (see section 4.6), being in compression. These failure strains were expected to have altered the stress state in the crush zone of the tube. The crush zone force analysis in section 7.1 showed that there were forces on the wedge in the radial direction. The origin of these forces was mainly in the hoop restraint that was present for circular section tubes but these forces were expected to have been affected by the residual hoop strains. It was possible that the residual stresses might have had the effect of moving the apex of the wedge away from the centre line of the tube wall (using the assumption that, in the absence of residual stresses, this case was true[1]). If the compressive loads on the outside plies of the wall were greater than those on the inside plies, as have been measured for the glass-polyester tubes, the apex of the wedge could have been moved towards the inside of the tube. However this situation was unlikely to have been observed as the position of the apex of the wedge had to be between two plies of the glass cloth for the crack to propagate. For the reasons discussed in section 8.4.1.2, the apex of the wedge was not always expected to be at the centre of the tube wall, hence this effect was difficult to quantify.

One effect that might, to some degree have been quantified, was on the radial splits that were present between the external fronds as they moved away from the crush zone. The effect of the residual stresses will have been one of a preload in the hoop direction. As the fronds were formed, mode I splits formed due to hoop tensile stresses. The residual stresses, being compressive, tended to increase the force

[1] An improbable assumption due to the tube wall curvature

required to reach the failure stress by the preload amount. A similar effect will have been encountered on the inside of the tube where the material moved into the tube. As the desired circumference of the material on the inside of the tube was less than that for the undeformed material, the material collapsed in the hoop direction by buckling. Compressive residual stresses tended to reduce the amount of energy needed to achieve this deformation. It was possible that the difference in the observed loads carried by the internal and external fronds (section 7.1) might have been affected by this difference in the effect of the residual strains, although it is not possible to be any more specific.

These considerations imply that it might be possible to achieve an increase in the energy absorption capability by designing the residual hoop stresses such that the outside of the tube was in compression and the inside in tension. At present no quantitative figures can be given for potential increases and it is probable that the processing changes, such as resin type and post-cure, that will be required to achieve this, will mask any residual stress effects.

What effect the residual stresses had on the crush load was uncertain. If it were possible to model the stress system in the crush zone and to determine the effect on the crush load of varying independently each individual stress, then it would be possible to predict the effect of varying the residual stresses on the crush load. The force analysis in section 7.1 indicated that the forces were closely interrelated such that independent modelling of the forces is potentially very difficult, if not impossible. However, if the residual strains as measured are taken to be about 10% of the failure strain of the material, as measured in the three-point-bend tests in section 4.6, then the effect of the residual strains must be limited by this value. Thus it must be concluded

that the maximum magnitude of the effect of residual strains on the specific crush stress must be limited to ±10%.

All the polyester resin matrix tubes tested were post-cured at 80°C. It is known that the residual stresses in this material increase with increasing post-cure temperature [125-127] so that it might be possible to investigate the effect of varying the residual stresses on the crush load. However increasing the post-cure temperature can alter the chemical cross-linking of the matrix, meaning that the effect of the residual stresses cannot be investigated in isolation of other effects. Some polyester resin matrix tubes were treated in a way intended to increase the magnitude of the residual stresses as described in section 3.4.3.3. This treatment was known to increase the residual stresses in unbalanced laminates using this resin [125-127]. When crush tested, these tubes showed no appreciable difference in crush load between the 80 °C post cure and the 120 °C post cure. However, when they were slit and their residual stresses measured, there was found to be no measurable difference between the values obtained. Thus this work must be deemed to have been inconclusive.

8.5.1 Low Temperature Strains

No attempt was made to measure the residual strains at temperatures below room temperature due to inherent experimental difficulties. However, as these strains were generated by differential thermal contraction during cooling from the post cure temperature, cooling the tubes to low temperatures should have generated further strains. The RJPW and RJPR tubes were post cured at 80 °C. Assuming that this was the minimum stress-free temperature, the strains as measured were generated by cooling through 58 °C as the ambient temperature when the strains were measured was 22 °C. If the thermal contraction behaviour was linear with temperature the

strains could be extrapolated to the minimum temperature that was tested for these tubes, namely -40 °C. If the maximum layer strain that was measured at 22 °C was 0.23% {figure 5.10}, then extrapolation to -40 °C would give a predicted maximum layer strain of about 0.48%. No measurement was made of the failure strain of this material at this temperature so it is not possible to state the maximum magnitude of the effect of these strains on the specific crush stress at -40 °C.

Length Effects

Figures 4.65 to 4.67 show that the length of the tube had no measurable effect on the degree of serration of the crush load response for three different crush modes. This situation was not entirely predictable from the current understanding of the nature of the serrations (section 2.1.3.5.5). The nature of the crush zone was known to be independent of the tube length so that, if the serrations had been due to the breaking off of pieces of material with the load being subsequently relieved, the strain relieved by the break off of a piece of material of a set size would have decreased with increasing tube length. Thus the degree of serration would have been expected to have been proportional to the reciprocal of the tube length, i.e.:

$$\Delta F \propto \frac{1}{l} \qquad (8.20)$$

This was not confirmed by experiment. Fairfull [51] went some way to explaining this apparent anomaly by relating the stiffness of the system to the stiffness of the tube and of the crush zone. This explanation however would still require the degree of serration of the crush zone to be length dependent to some extent. One possible explanation is that the serrations were due to stick-slip friction at various positions in the crush zone (section 2.1.5.4). However, this might be expected to give a speed sensitivity of the

degree of serration but none has been observed. That the serrations might be due to stick-slip crack propagation in the matrix is extremely improbable as shown from the behaviour of tubes tested at various temperatures. The degree of serration decreased with increasing temperature, this being contrary to the trends observed for stick-slip crack propagation in epoxy resins (see section 2.2.1.1.2) [67,75-78], where cracks tended to propagate smoothly at low temperatures and by stick-slip at higher temperatures.

Figures 4.65 to 4.67 show a large degree of scatter in the results obtained for $\Delta F/F$. This scatter can be explained partially by the method of measuring ΔF. This was simply done by eye and as such, tended to be a measure of the maximum degree of serration in the crush trace rather than a measure of the mean level of serration. If the relevant equipment was available, a more meaningful measure of ΔF might be found by digitising the crush trace and obtaining a root-mean-square value on a computer. It might be possible to do this by sending the load signal direct from the load cell to a computer and then processing the signal. This approach to data collection would enable a more accurate measurement of the mean crush load with a possible error analysis, and should be considered for future work.

9 Conclusions

Various conclusions have been reached in this work regarding the detail features of the crush behaviour under conditions of varying speed and temperature. This section summarises the main conclusions reached.

1. The specific crush stress of a composite tube when subjected to axial crushing is dependent on the testing speed and the temperature.

2. The temperature and speed dependencies of the specific crush stress are governed by the matrix material.

3. Epoxy resin matrix tubes show an increase in specific crush stress with increasing speed.

4. Polyester resin matrix tubes tested under conditions of high speed impact give lower values of specific crush stress than when crushed at a constant, slow speed.

5. The specific crush stress of both epoxy and polyester resin matrix tubes decreases with increasing temperature over the temperature range -100 °C to 110 °C.

6. The speed dependency of the specific crush stress is a function of the temperature for all the tubes investigated.

7. Although the speed and temperature dependencies of the specific crush stress of any particular type of tube can, within certain restrictions, be interrelated by the use of the Arrhenius equation, activation energies have been shown to vary with temperature meaning that the equation only describes that tube at that temperature and speed.

8. Temperature rises in the crush zone during crushing are strongly dependent on the crush speed at slow speeds but are independent of speed at the higher speeds that were encountered in this project.

9. Inertia of debris in the crush zone is insignificant in affecting the specific crush stress at the speeds encountered.

10. Residual stresses can have a small but significant effect on the specific crush stress that is temperature but not speed dependent.

11. At high temperatures the crush mode of the tube can become one of unstable buckling collapse with a consequently low value of specific crush stress.

12. The transition temperature from progressive crushing to buckling is speed dependent, showing a linear increase with increasing log. crush speed.

13. This transition temperature is also dependent on the tube dimensions and on the fibre architecture, woven cloth reinforcement favouring higher transition temperatures that random continuous filament mat reinforcement.

14. The appearance of the crush zone is dependent on the temperature with low temperatures favouring mainly fracture and high temperatures favouring deformation. These observations also apply to speed as high speeds favour fracture with slow speeds favouring deformation.

15. The forces in the crush zone are dependent on the roughness of the crush platen and are strongly interrelated.

16. Length has no measurable effect on the degree of serration of the crush trace.

17. When performing a test with an instantaneous speed change, providing the crush load is measured after reaching equilibrium for the new speed the values of crush load measured are independent of whether the speed change is from fast to slow or vice versa.

18. The mechanisms of energy absorption are a complex combination of fracture, deformation and friction.

19. Constant speed crushing is not a true simulation of impact testing.

20. The high temperature buckling mode can be replaced by an interpenetration mode in thin walled tubes.

21. Shear deformation is an important aspect of the tube crushing in determining the speed and temperature sensitivity of the specific crush stress.

22. The speed sensitivity of the specific crush stress generally increases with increasing temperature.

23. The frond-wedge-frond and fragmentation crush modes are both effective in absorbing large amounts of energy but the buckling and interpenetration modes are not.

10 Future Work

The literature review in section 2.1 has shown that much of the work on the behaviour of composite tubes during crushing has been carried out, most of the main variables having been examined in some depth.

The main question posed by this project that remains unresolved is why do polyester matrix tubes give lower values of specific crush stress at high speed when most of the mechanical properties of polyesters improve with increasing strain rate. This work has suggested that the reason might be connected with frictional temperature rises and resultant polymer decomposition but experimental evidence has been scarce. Some work on the frictional behaviour of polyester resin matrix composites might prove beneficial, as might some work on polyester degradation at elevated temperatures.

Other aspects of crushing behaviour that could be usefully looked at include:

Tensile or bend testing of the material of which the tubes are made over the same range of speeds and temperatures. This might show some correlation of the features of the speed sensitivity of the specific crush stress over a range of temperatures with those of the strength, strain to failure and stiffness over the same temperature range. Testing machine availability prevented this work being carried out in this project.

The effects of localised heating on buckling collapse, for instance the softening of one side of the tube by heat. This could lead to instabilities at lower temperatures than those at which the tubes have been observed to buckle in this investigation resulting from off-axis loads[1].

[1]Off-axis loading at room temperature is being studied by Mr. D.A.Williams.

Mathematical modelling of the stress distribution in the crush zone. Finite Element Modelling might be able to provide some insight into the mechanisms that are active in the crush zone. The material variables must be defined before this can be carried out, so a suggestion is made here that Tufnol tubes be considered as they form the basis of the experimental work for the Cambridge group. An experimental measurement of the hoop restraint contributions as mentioned in section 7.1.3 might be beneficial.

Experimental verification of the hypotheses regarding the twin apex wedge in section 8.4.1.2. This will be difficult as the length of overlap (if any) will probably be very short, hence difficult to observe.

Accurate measurement of serration of the crush traces leading to a conclusion as to whether this is sensitive to the tube length. This investigation should involve sophisticated instrumentation and computer treatment of the signal from the load cell of the testing machine.

Full experimental verification of the findings of chapter 7 on friction. This might involve the imbedding of thermocouples in tubes at various positions in order to measure the temperature rise distribution. Infrared monitoring of the crush zone by imbedding optical fibres in the material might provide some information and should be considered for future work.

An in-depth investigation into why subsequent impacts for Tufnol tubes give lower values of specific crush stress than the initial impact, in particular the effect of micro-damage.

Possible residual stress effects. Some attempt has been made in this work to measure the effects of residual stresses but without success. These effects are difficult to isolate from other effects from post curing, particularly the degree of matrix cross-linking, but some insight might be possible by using as a matrix material a polyester resin with a high thermal expansion coefficient to maximise the residual stresses.

11 References

1. HULL, D. Energy Absorbing Composite Structures. SCIENCE AND TECHNOLOGY REVIEW; University of Wales; 1988; No.3.

2. HULL, D. Impact Response of Structural Composites. METALS AND MATERIALS; Jan. 1985: 35-38; ISSN 0266/7185.

3. HULL, D. Axial Crushing of Fibre Reinforced Composite Tubes. Jones N. and Werzbicki T., Ed. STRUCTURAL CRASHWORTHINESS: BUTTERWORTHS; 1983: 118-135.

4. U.S. GENERAL SERVICES ADMINISTRATION. 49 Code of Federal Regulations, Standard No. 208; Occupant Crash Protection. (U.S. Government Printing Office, 1985) 357.

5. BUTLER, N. Spin-Offs for Safer Cars. NEW SCIENTIST; 15 July 1989: 56-58.

6. HANAGUD, S., CRAIG, J.I., SRIRAM, P. and ZHOU, W. Energy Absorption Behaviour of Graphite Epoxy Composite Sine Webs. J. COMPOS. MATER.; May 1989; 23: 448-459.

7. THORNTON, P.H., HARWOOD, J.J. and BEARDMORE, P. Fibre-reinforced Plastic Composites for Energy Absorption Purposes. COMPOS. SCI. TECH.; 1985; 24: 275-298; ISSN 0266-3538/85/$03.30.

8. BEARDMORE, P. and JOHNSON, C.F. The Potential for Composites in Structural Automotive Design. ibid.; 1986; 26: 251-281.

9. DAVIES, G. and EASTLOW, R.A. Automotive Design and Materials Selection. METALS AND MATERIALS; Jan. 1985; 1 (1): 20-25; ISSN 0226/7185.

10. PEANUTS. The Daily Mail c.1987.

11. PLASTICS AND RUBBER INTERNATIONAL; April 1987; 12 (2): 2.

12. SCOWEN, G.D. Glass Fibre Composites in the Automotive Industry. METALS AND MATERIALS; Nov. 1987; 3 (11): 639-642; ISSN 0266/7185.

13. BOWEN, D.H. Applications of Polymer Matrix Composites. ibid.; Dec. 1986; 2 (12): 776-779.

14. SAWLEY, K.J. Materials in Railway Engineering. ibid.; April 1989; 5 (4): 210-214.

15. Award for Reinforced Plastic Suspension System. ibid; May 1989; 5 (5): 260.

16. DAUGHERTY, R.L. Composite Leaf Springs in Heavy Truck Applications. COMPOSITE MATERIALS. Proc. Japan-U.S. Conference; 1981; TOKYO: 529-538. (K. Kawata & T. Akasaka).

17. THORNTON, P.H. Energy Absorption in Composite Structures. J. COMPOS. MATER.; July 1979; 13: 247-262.

18. BLEARS, J. Measurement of Specific Energy Absorbed Values. EAC 1047: University of Liverpool; 17th February 1981.

19. KEALE, R., SEDDON, B., BLEARS, J. and HULL, D. (Department of Metallurgy and Materials Science, University of Liverpool). EAC Report. 1 ed.: University of Liverpool; 2nd May 1979.

20. AJIBADE, M.F.A., BERRY, J.P., BLEARS, J., SEDDON, B.C., SNOWDON, P.R. and HULL, D. (Department of Metallurgy and Materials Science, University of Liverpool). EAC Report. 2 ed.: University of Liverpool; 19th September 1979.

21. BERRY, J.P., BLEARS, J., GRUNDY, J.D., KEAL, R., SEDDON, P., SNOWDON, P., WOOSEY, S. and HULL, D. (Department of Metallurgy and Materials Science, University of Liverpool). EAC Report. 3 ed.: University of Liverpool; 8th January 1980.

22. BERRY, J.P., BLEARS, J., GRUNDY, J.D., KEAL, R., SEDDON, P., SNOWDON, P., WOOSEY, S. and HULL, D. (Department of Metallurgy and Materials Science, University of Liverpool). EAC Report. 7 ed.: University of Liverpool; 8th May 1981.

23. VAN DINGENEN, J.L.J. High Performance Dyneema Fibres in Composites. MATERIALS AND DESIGN; 1989; 10: 2.

24. THORNTON, P.H. and EDWARDS, P.J. Energy Absorption in Composite Tubes. J. COMPOS. MATER.; Nov 1982; 16: 521.

25. HULL, D., BLEARS, J., BERRY, J.P., GRUNDY, J.D., KEAL, R., SEDDON, B., SNOWDON, P.R. and WOOSEY, S. (Department of Metallurgy and Materials Science, University of Liverpool). EAC Report. 9 ed.: University of Liverpool; 21st April 1982.

26. FARLEY, G.L. Energy Absorption of Composite Materials. J. COMPOS. MATER.; 1983; 17: 267-279.

27. idem, Effect of Fibre and Matrix Maximum Strain on the Energy Absorption of Composite Materials. ibid.; 1986; 209: 322-333.

28. idem, Energy Absorption in Composite Materials for Crashworthy Structures. I.C.C.M. VI; July 1987; IMPERIAL COLLEGE, London: 3.57-3.66.

29. SCHMUESER, D.W. and WICKLIFF, L.E. Impact Energy Absorption of Continuous Fibre Composite Tubes. Trans. ASME; Jan. 1987; 109: 72-77.

30. BLEARS, J.,BERRY, J.P., GRUNDY, J.D., KEALE, R., SEDDON, B., SNOWDON, R.P. and HULL, D. (Department of Metallurgy and Materials Science, University of Liverpool). EAC Report. 10 ed.: University of Liverpool; 27th September 1982.

31. THORNTON, P.H. (Materials Science Department, Ford Motor Co., Dearborn, Michigan). The Crush Behaviour of Pultruded Tubes at High Strain Rates. COMPOS. SCI. TECH. (to be published).

32. TAO, W.H., ROBERTSON, R.E., AND THORNTON, P.H. Energy Absorption in Crushing Fiber Composite Materials. 4th Annual Conference on Advanced Composites, Dearborn, Mi.; Sept. 1988: 47-52.

33. BLEARS, J., FAIRFULL, A.H., GRUNDY, J.D., KEAL, R., SEDDON, B., SNOWDON, P.R., WOOSEY, S. and HULL, D. (Department of Metallurgy and Materials Science, University of Liverpool). EAC Report. 12 ed.: University of Liverpool; 8th September 1983.

34. BLEARS, J., CADDOCK, B., FAIRFULL, A.H., KEAL, R., SNOWDON, P.R., WOOSEY, S. and HULL, D. (Department of Metallurgy and Materials Science, University of Liverpool). EAC Report. 13 ed.: University of Liverpool; 23rd Febuary 1984.

35. BLEARS, J., BARNES, J.A., FAIRFULL, A.H., PRICE, N., SNOWDON, P.R. and HULL, D. Progress Report No. 1: Departments of Metallurgy and Materials Science, Universities of Cambridge and Liverpool; 12th March 1985. (I.R.S.C.; 1).

36. FARLEY, G.L. (Aerostructures Directorate, USAARTA-AVSCOM). Energy Absorption of Composite Materials and Structures. 43rd American Helicopter Society Annual Forum, St. Louis, Mo.; May 1987.

37. SNOWDON, P.R. Summary of SMC Development: Department of Metallurgy and Materials Science, University of Liverpool; 15th March 1983; EAC 1073. (Energy Absorbing Composites Project).

38. HULL, D. Energy Absorption of Composite Materials Under crash Conditions. I.C.C.M. IV; Tokyo. New York: Met. Soc. AIME; 1982: 861.

39. BERRY, J.P. Ph.D. Thesis, England: University of Liverpool; 1984

40. HULL, D. An Introduction to Composite Materials: Cambridge University Press; 1981; ISBN 0 521 28392 2.

41. THORNTON, P.H. The Crush Behaviour of Glass Fibre Reinforced Plastic Sections. COMPOS. SCI. TECH.; 1986; 27: 199-223.

42. FARLEY, G.L. Personal Communication; July 1987.

43. PRICE, J.N. Report on Crush Testing of Square Section Resinject Glass/Polyester Tubes. Department of Materials Science and Metallurgy: University of Cambridge; September 1987. (I.R.S.C. Group).

44. FAIRFULL, A.H. and HULL, D. (Department of Materials Science and Metallurgy, University of Cambridge). Effects of Specimen Dimensions on the Specific Energy Absorption of Fibre Composite Tubes. I.C.C.M. VI; July 1987; IMPERIAL COLLEGE, London: 3.36-3.45.

45. FARLEY, G.L. Effect of Specimen Geometry on the Energy Absorption of Composite Materials. J. COMPOS. MATER.; 1986; 20: 390-400.

46. BLEARS, J., BERRY, J.P., FAIRFULL, A.H., GRUNDY, J.D., KEAL, R., SEDDON, B., SNOWDON, P.R. and HULL, D. (Department of Metallurgy and Materials Science, University of Liverpool). EAC Report. 11 ed.: University of Liverpool; 3rd March 1983.

47. FAIRFULL, A.H. Personal Communication; 1986.

48. FARLEY, G.L. (Aerostructures Directorate, USAARTA-AVSCOM, NASA). A Method of Predicting the Energy Absorption Capability of Composite Subfloor Beams. AIAA; 1987.

49. SEN, J.K. and DREMANN, C.C. Design Development Tests for Composite Crashworthy Helicopter Fuselage. SAMPE QUATERLY; 1985; 17 (1): 29-39.

50. SMALL, G.D. and ANSELL, M.P. The Energy-Absorbing Properties of a Novel Cellular Structure. J. MATER. SCI.; 1987; 22: 2717-2722; ISSN 0022-2461/87.

51. FAIRFULL, A.H. Scaling Effects in the Energy Absorption of Axially Crushed Composite Tubes. Ph.D. Thesis, England: University of Liverpool; 1986.

52. idem, Mechanics of Load-Displacement Curve Serrations. Department of Metallurgy and Materials Science: University of Cambridge; March 1986. (I.R.S.C.; 4).

53. PRICE, J.N. The Crush Performance of Tube Sections and Slotted Tubes: Department of Metallurgy and Materials Science, University of Cambridge; Oct.1985; IRSC Sub-Programme 16.

54. THORNTON, P.H. Effect of Trigger Geometry on Energy Absorption in Composite Tubes. Harrigan W.C., Strife J. and Dhingra A.K., Ed. Fifth I.C.C.M.; July 1985; San Diago, California: The Metallurgical Society: 1183-1199.

55. CZAPLICKI, M.J., THORNTON, P.H. and ROBERTSON, R.E. Collapse Triggering of Polymer Composite Energy Absorbing Structures. 4th Annual Conference on Advanced Composites, Dearborn, Mi.; Sept. 1988: 39-46.

56. PRICE, J.N. Effect of Trigger Geometry on Crush Initiation. Department of Materials Science and Metallurgy: University of Cambridge; 4th November 1986. (I.R.S.C.).

57. SIGALIS, I., KUMOSA, M. and HULL, D. Trigger Mechanisms in Energy Absorbing Glasscloth Epoxy Tubes. COMPOS. SCI. TECH. (To be published).

58. CZAPLICKI, M.J., ROBERTSON, R.E. and THORNTON, P.H. Comparison of Bevel and Tulip Triggered Pultruded Tubes for Energy Absorption. (To be published).

59. HULL, D., BLEARS, J., CLOUGH, A., GRUNDY, J.D., KEAL, R., SEDDON, B., SNOWDON, P.R. and WOOSEY, S. (Department of Metallurgy and Materials Science, University of Liverpool). EAC Report. 5 ed.: University of Liverpool; 6th October 1980.

60. BERRY, J. and HULL, D. Effect of Speed on Progressive Crushing of Epoxy-Glass cloth Tubes. Harding J., Ed. MECHANICAL PROPERTIES AT HIGH RATES OF STRAIN; 1984; Oxford. London: Inst. Phys. Conf. Ser.; No. 70: 463-470.

61. BURTIN, C. and HAMELIN, P. Crash-Impact Behaviour of Tubular Composite Structures, IMPACT LOADING AND DYNAMIC BEHAVIOUR OF MATERIALS, 1 (1986).

62. THORNTON, P.H. and JERYN, R.A. Crash Energy Management in Composite Automotive Structures. INT. J. IMPACT ENGIN.; 1988; 7 (2): 167-180.

63. FAIRFULL, A.H. and HULL, D. Energy Absorption of Polymer Matrix Composite Structures: Frictional Effects. STRUCTURAL FAILURE, International Symposium on Structural Failure; MIT; June 1988.

64. PINK, E. and CAMPBELL, J.D. The Low-temperature Macro Deformation of an Epoxide Resin. MATER. SCI. ENG.; 1974; 15: 187-194.

65. YAMINI, S. and YOUNG, R.J. Crack Propagation in and Fractography of Epoxy Resins. J. MATER. SCI.; 1979; 14: 1609-1618.

66. idem, The Mechanical Properties of Epoxy Resins: Part 1 Mechanisms of Plastic Deformation. ibid.; 1980; 15: 1814-1822.

67. idem: Part 2 Effect of Plastic Deformation Upon Crack Propagation. ibid.: 1823-1831.

68. KINLOCH, A.J., SHAW, S.J. and HUNSTON, D.L. Deformation and Fracture Behaviour of a Rubber-toughened Epoxy: 2. Failure Criteria. POLYMER; 1983; 24: 1355-1983.

69. EGUSA, S., SEGUCHI, T. and SUGIUCHI, K. Relationship Between the 77K Mechanical Properties of Glass/Epoxy Composite and the Glass Transition Temperature of the Matrix Resin. J. MATER. SCI. LETT.; 1988; 7: 973-975; ISSN 0261-8028/88.

70. EGUSA, S., UDAGAWA, A., HASHIMOTO, O., ONO, T., YAMAMOTO, Y. and SONODA, K. Preparation and Radiation-Resistance Evaluation of Glass Fibre Composites Having Various Epoxy Matrices. ibid: 503-505; ISSN 0261-8028/88

71. EGUSA, S. Mechanism of Radiation-Induced Degradation in Mechanical Properties of Polymer Matrix Composites. J. MATER. SCI.; 1988; 23: 2753-2760.

72. MIKOLAJCZAK, G., CAVAILLE, J.Y. and JOHARI, G.P. Dynamic Mechanical Behaviour and its Dependence on Preparation Method of Structural Epoxied Resin. POLYMER; 1987; 28: 2023-2031.

73. KINLOCH, A.J., SHAW, S.J., TOD, D.A. and HUNSTON, D.L. Deformation and Fracture Behaviour of a Rubber-toughened Epoxy: 1. Microstructure and fracture studies. ibid.; Oct. 1983; 24: 1341-1354; ISSN 0032-3861/83/101341-14$03.00.

74. YOUNG. R.J. Fracture of Thermosetting Resins. DEVELOPMENTS IN POLYMER FRACTURE-1. Andrews, E.H.: Applied Science Publishers: 183-222.

75. PHILLIPS, D.C., SCOTT, J.M. and JONES,M. Crack Propagation in an Amine Cured Epoxied Resin. J. MATER. SCI.; 1978; 13: 311-322; ISSN 0022-2461/78.

76. SCOTT, J.M., WELLS, G.M. and PHILLIPS, D.C. Low temperature Crack Propagation in an Epoxide Resin. ibid.; 1980; 15: 1436-1448.

77. YOUNG, R.J. and BEAUMONT, P.W.R. Crack Propagation and Arrest in Epoxy Resins. ibid.; 1976; 11: 776-779.

78. PHILLIPS, D.C. and SCOTT, J.M. Determination of the K, v Diagram of Epoxied Resins. ibid.; 1974; 9: 1202-1205.

79. KING, N.E. and ANDREWS, E.H. Fracture Energy of Epoxy Resins Above T_g. ibid.; 1978; 13: 1291-1302.

80. LOW, I-M, and MAI, Y-W. Rate and Temperature Effects on Crack Blunting Mechanisms in Pure and Modified Epoxies. ibid.; 1989; 24: 1634-1644.

81. OCHI, M., SHIBA, T., TAKEUCHI, H., YOSHIZUMI, M. and SHIMBO, M. Effect of the Introduction of Methoxy Branches on Low-Temperature Relaxations and Fracture Toughness of Epoxied Resins. POLYMER; 1989; 30: 1079-1084.

82. MIZUTANI, K. and YOSHI, M. Temperature Dependence of Fracture Toughness of Epoxy Resins Cured with Diamines. J. MATER. SCI.; 1988; 23: 3501-3504; ISSN 0022-2461/88 $03.00 + .12.

83. HARDING, J. Effect of Strain Rate on Material Properties. MATERIALS AT HIGH STRAIN RATES. Blazynski, T. Z.: ELSEVIER APPLIED SCIENCE: 159-186.

84. PRICHARD, G., RHOADES, G.V. and ROSE, R.G. Synthesis Procedure and the Fracture Toughness of Highly Cross-linked Resins. J. MATER. SCI.; 1980; 15: 1635-1639; ISSN 0022-2461/80/071635-05$0.25.

85. CHRISTIANSEN, A. and SHORTALL, J.B. The Fracture Toughness and Fracture Morphology of Polyester Resins. ibid.; 1976; 11: 1113-1124.

86. PRICHARD, G. and RHOADES, G.V. The Fracture of Highly Crosslinked Resins. An Invited Review. MATER. SCI. ENG.; 1976; 26: 1-11.

87. OWEN, M.J. and ROSE, R.G. The Fracture Toughness and Crack Propagation Properties of Polyester Resin Casts and Laminates. J. PHYS. D: APPL. PHYS.; 1973; 6: 42-53.

88. SHEN, C-H. and SPRINGER, G.C. Effects of Moisture and temperature on the Tensile Strength of Composite Materials. Springer, G.S. (ed). ENVIRONMENTAL EFFECTS ON COMPOSITE MATERIALS. U.S.A.: Technomic: Chapter 7; ISBN 087762-300-7.

89. PRICHARD, G., ROSE, R,G, and TANEJA, N. The Effect of Water on the Critical Stress Intensity Factor of Unsaturated Polyester Resins. J. MATER. SCI.; 1976; 11: 718-722.

90. PINK, E. and CAMPBELL, J.D. Deformation Characteristics of Reinforced Epoxy Resin: Part 1 The mechanical properties. ibid.; 1974; 9: 659-664 .

91. idem: Part 2 An analysis of thermally activated deformation. ibid.; 1974; 9 (665-672).

92. DANIEL, I.M. Testing of Fiber Composites at High Strain Rates. I.C.C.M. II; 1978; Toronto, Canada: 1003-1018.

93. SPRINGER, G.S. Effects of Temperature and Moisture on Sheet Moulding Compounds. ENVIRONMENTAL EFFECTS ON COMPOSITE MATERIALS. 2 ed.: 59-78.

94. JOHNSON, A.E. and LYNSKEY, B.M. Variation with Temperature of the Impact Behaviour of SMC. FIBRE REINFORCED COMPOSITES '84; 1984.

95. SMILEY, A.J. and PIPES, R.B. Rate Effects on Mode I Interlaminar Fracture Toughness in Composite Materials. J. COMPOS. MATER.; July 1987; 21: 670-687; ISSN 0021-9983/87/07 0670-18 $4.50/0.

96. FRIEDRICH, K., WALTER, R., CARLSSON, L.A., SMILEY, A.J. and GILLESPIE, J.W. Jr. Mechanisms for Rate Effects on Interlaminar Fracture Toughness of Carbon/Epoxy and Carbon/PEEK Composites. ibid.; 1989; 24: 3387-3398.

97. HARDING, J. and WELSH, L.M. A Tensile Testing Technique for Fibre-Reinforced Composites at Impact Rates of Strain. J. MATER. SCI.; 1983; 18: 1810-1826.

98. WELSH, L.M. and HARDING, J. Effect of Strain Rate on the Tensile Failure of Woven Polyester Resin Composites. INST. PHYS. CONF. SER. No. 70; 1984: 343-344.

99. TUFNOL Ltd. Composite Laminates, Technical Information Sheet. Perry Barr, Birmingham; November 1988.

100. BS 6182 pt 8. Industural Laminated Rods and Tubes Based on Thermosetting Resins: BRITISH STANDARDS INSTITUTION; 1982.

101. CIBA-GEIGY Ltd. Epoxy Resin 7065N75. Duxford, Cambridgeshire.

102. FIBREGLAS Ltd. Chopped-Strand-Mats, Technical Information Sheet; FPL 461 January 1980.

103. SCOTT BADER Ltd. Crystic 272, Technical Leaflet No. 107; July 1986.

104. VETROTEX (UK) Ltd. Unifilo U750, Technical Information Sheet.

105. CIBA-GEIGY Ltd. CY219/HY219, Instruction Sheet No. T64a. Duxford, Cambridgeshire; September 1981.

106. CURTIS, P.T. CRAG Test Methods for the Measurement of the Engineering Properties of Fibre Reinforced Plastics. Technical Report 85099. Royal Aircraft Establishment: HMSO; November 1985.

107. POLAKOWSKI, N.H. and RIPLING, E.J. Strength and Structure of Engineering Materials Ch. 17: Prentice-Hall Inc.

108. FAIRFULL, A.H. Internal Report. Department of Materials Science and Metallurgy, University of Cambridge; 1987.

109. LHYMN C., TEMPELMEYER K.E. and DAVIS P.K. The Abrasive Wear of Short Fibre Composites. COMPOSITES; 1985; 16: 127-136.

110. BOWDEN, F.P. and RIDLER, K.E.W. The Physical Properties of Surfaces, III-The Surface Temperature of Sliding Metals, The Temperature of Lubricated Surfaces. PROC. ROY. SOC. (LONDON), Series A; May 1936; 154 (883): 640-657.

111. METALS HANDBOOK; 8th Edition, Vol. 6. Welding and Brazing. 507-518: A.S.M.; 1971.

112. COPOLLA, J.C. Personal communication. 1989.

113. ROGERS, G.F.C. and MAYHEW, Y.R. Engineering Thermodynamics Work and Heat Transfer: Longman; 1967; ISBN 0 582 44727 5.

114. MAGUIRE, D.M. and KULACKI, F.A. Thermophysical Properties of Composite Materials: a State-of-the-Art Assessment. I.C.C.M. V. San Diego, Calif. 1985.

115. DAVIDSON, R. Performance Characteristics of Composite Materials. METALS and MATERIALS; October 1986; 2 (10): 651-655; ISSN 0266/7185.

116. RAMESH R., KISHORE and RAO R.M.V.G.K. Dry Wear Studies on Glass-Fibre-Reinforced Epoxy Composites. WEAR; 1983; 89: 131-136.

117. McLAREN K.G. and TABOR D. Friction of Polymers: Influence of Speed and Temperature. NATURE; March 2, 1963; 197:856-858.

118. CLERICO M. and PATIERNO V. Sliding Wear of Polymeric Composites. WEAR; 1979; 53: 279-301.

119. PAFITIS, D.G. Personal communication. 1989.

120. GLASSTONE, S. Textbook of Physical Chemistry: Macmillian; 1956.

121. McGRAW-HILL ENCYCLOPEADIA OF SCIENCE AND TECHNOLOGY, 6th Ed. 3 BOR-CLE, 286-288. 1987. ISBN 0-07-07929292-5 [SET].

122. IBE, M.S. Energy Absorption and Failure in Composite Tubes, M.Sc. Thesis, England: University of Liverpool; June 1987.

123. TIMOSHENKO, S.P. Theory of Elastic Stability, McGRAW-HILL, New York, 1961.

124. KOMOSA, M.K. Personal communication. 1989.

125. JONES, F.R., MULHERON, M. and BAILEY, J.E. Generation of Thermal Strains in GRP. Part 1 Effect of water on the expansion behaviour of unidirectional glass fibre-reinforced laminates. J. MATER. SCI.; 1983; 18: 1522-1532; ISSN 0022-2461/83.

126. idem. Part 2 The origin of thermal strains in polyester cross-ply laminates. ibid: 1533-1539.

127. FONTANA, Q.P.V. Unpublished work, University of Surrey, 1980.